Dissertation zur Erlangung des Doktorgrades

der Fakultät für Biologie

der Ludwig-Maximilians-Universität München

Conditionally cytotoxic and drug-controllable non-cytotoxic rabies viruses

Verena Pfaffinger

aus

München, Deutschland

2022

Erklärung

Diese Dissertation wurde im Sinne von §12 (3) der Promotionsordnung vom 27. November 1991 von Herrn Professor Dr. Conzelmann betreut und von Herrn Professor Dr. Grothe vor der Fakultät für Biologie vertreten.

Hiermit erkläre ich, Verena Pfaffinger, dass die Dissertation zu keinem Zeitpunkt ganz oder in wesentlichen Teilen einer anderen Prüfungskommission vorgelegt worden ist. Ich habe noch zu keinem früheren Zeitpunkt versucht, eine Dissertation einzureichen oder an einer Doktorprüfung teilzunehmen.

München, den 27.06.2022 ....Verena Pfaffinger

(Datum)   *(Unterschrift)*

Eidesstattliche Versicherung

Ich, Verena Pfaffinger, versichere hiermit an Eides statt, dass die vorgelegte Dissertation von mir selbständig und ohne unerlaubte Hilfe angefertigt ist.

München, den 27.06.2022 ....Verena Pfaffinger

(Datum)   *(Unterschrift)*

„The science of today is the technology of tomorrow "

Edward Teller

Danksagung

An dieser Stelle möchte ich mich bei allen bedanken, die mich auf dem Weg während der gesamten Doktorarbeit begleitet haben.

Als allererstes gilt mein Dank meinem Doktorvater, Prof. Dr. Karl-Klaus Conzelmann, der mir diese Arbeit, so wie sie hier ist, erst ermöglicht hat, mich trotz baldiger Rente als letzte Doktorandin in sein Labor aufgenommen hat und mir dieses spannende Thema an die Hand gegeben hat. Vielen Dank vor allem auch, dass ich an sämtlichen Konferenzen teilnehmen durfte! Zudem gilt mein Dank Prof. Dr. Benedikt Grothe, der meine Betreuung innerhalb der Fakultät für Biologie übernommen hat und daher Erstgutachter dieser Arbeit ist. Weiterhin möchte ich noch einmal gesonderten Dank an alle Mitglieder des TAC meiner Arbeit aussprechen: Vielen Dank an Prof. Dr. Benedikt Grothe, Prof. Dr. Angelika Böttger und Prof. Dr. Karl-Klaus Conzelmann. Danke für die interessanten Meetings, die spannenden Fragen und Diskussionen und natürlich das Feedback.

Selbstverständlich möchte ich mich bei allen Arbeitskollegen bedanken: Besonderer Dank gilt hier Alex, der mich schon während meiner Masterarbeit betreut hat, mir den Weg in die Doktorarbeit geebnet hat und vor allem auch immer für Fragen und Diskussionen bereitstand! Vielen Dank auch an Martina, Anika, Dominic, Doro, und Kathi, die sowohl in guten als auch in schwierigeren Zeiten für mich da waren. Danke natürlich auch an Max, Blex und Marwa. Besondere Erwähnung gebührt auch Johanna und Chloé, die nicht nur ehemals Kollegen waren, sondern auch längst Freunde geworden sind. Danke an alle Viro Runners, insbesondere Stephi, ohne die auch sonst vieles sicherlich so nicht zustande gekommen wäre. Natürlich auch ein herzliches Dankeschön an alle Studenten, allen voran Ursula, die mich als HiWi sehr unterstützt hat.

Zu guter Letzt möchte ich einen großen Dank an meine Familie aussprechen: Danke an meine Mama und meinen Papa, denn nur durch ihre Unterstützung habe ich diesen Weg überhaupt so gehen können. Danke an meinen Bruder Stefan und meine Schwägerin Sarah, mit denen man alle Sorgen kurz vergessen und einfach die Zeit genießen kann. Und am Ende gilt mit der größte Dank meinem Freund Maxi, der während dieser gesamten Zeiten immer für mich da war.

Table of Content

Summary

The SMASh system is a commonly used tool for targeted degradation of proteins. Thereby, a protein of interest is fused to the SMASh-tag consisting of the Hepatitis C virus (HCV) NS3 protease and a degron. In absence of a NS3 protease inhibitor, the SMASh-tag cleaves itself off and releases the protein of interest. However, the cleavage is prevented in presence of the inhibitor leading to the degradation of the whole newly synthesized fusion protein.

Previously, we have observed a high cytotoxicity induced by SMASh upon addition of the inhibitor in protein shutoff experiments. The aim of this work was to characterize this cytotoxicity. To this end, three different approaches were pursued: Firstly, various cells were tested in killing assays to find a resistant cell line or cell type. Secondly, apoptosis induced by SMASh inhibition was investigated regarding killing kinetics, caspase activation, diverse SMASh fusion proteins, and expression systems. Additionally, different apoptosis-related knockout cells were generated to gain insights on the pathway triggered by SMASh. As a third approach, the SMASh-tag itself was modified and analyzed for cytotoxic components within the SMASh-tag.

In fact, all cell lines tested here could be killed by expression of SMASh-tagged proteins and inhibitor treatment, including cells from different hosts such as mouse, hamster, monkey, and human. Of note, not only were all cell lines killed by SMASh inhibition, we also were able to prove that SMASh is toxic when fused to a wide variety of proteins. The fate of cells appeared to be independent of SMASh expression from viruses or plasmids. Moreover, we have demonstrated that SMASh induces apoptosis instantly after addition of the NS3 protease inhibitor with detectable Annexin V binding and PARP cleavage already at one hour post drug treatment. Thereby, the involvement of the initiator caspase-8, -9 and -10 as well as the effector caspases -3/-7 could be proven. Moreover, various cell lines carrying a knockout of apoptosis related genes were generated and could be killed indicating a minor or irrelevant role of PKR and FADD, single caspase-8 and caspase-10 during apoptosis.

Another aim of this thesis was to analyze the SMASh-tag itself in regard of cytotoxic components. For this purpose, various mutations, alterations, and truncations were introduced into the SMASh-tag. Thereby, we could show that minor changes did not prevent cytotoxicity, whereas larger alterations of the SMASh-tag, as shown by different truncated versions of the SMASh-tag, resulted in a loss of the ability to induce cell death. All in all, these finding led us to the final model that NS3 inhibitor such as DNV or ASV binding

to the SMASh-tag trigger a conformational change. This could expose the SMASh-tag to the binding of cellular apoptotic factors such as various caspases, which in turn are drivers of the apoptotic fate.

The second main goal of this thesis was to provide a controllable virus for neurotracing approaches enabling long term studies in mice. For this reason, a non-cytotoxic tag was generated with the aim to control RABV replication and spread, even after infection of cells. This so called tt1-tag lacks the NS3 helicase but contains an additional PEST sequence for degradation at the C-terminus. We could successfully show that the tt1-tag is not toxic, even two days post inhibitor treatment. We demonstrated that virus control is possible, if tt1-tag is fused to a viral protein like the RABV N or P. In consequence, this virus could be used for long term neurotracing experiments in the future.

1 Introduction

1.1 Rabies virus

1.1.1 Overview

Rabies is a zoonotic disease causing acute, highly lethal encephalitis. The name rabies originates from Latin meaning madness or rage, whereas the ancient Greeks called rabies "lyssa" which can be translated with rage as well. These names reflect the association of rabies with mad dogs that are furious and bite. Already around 2300 B.C. rabies was mentioned in the Mesopotamian law of Eshnunna, which is so far the first known annotation of the disease (Baer 2007). In addition to that, other ancient cultures around the world like Greece, Rome, Egypt, but also China have documented the disease (Velasco-Villa et al. 2017). Today it is a proven fact that the causative agent of the disease is a virus of the *Lyssavirus* genus. Although other lyssaviruses can induce rabies-like encephalitis, rabies in particular is caused by rabies virus (RABV), the prototype of this genus. RABV belongs to the order of Mononegavirales, which is characterized by a single stranded negative-sense RNA genome. Although the order is named non-segmented negative strand RNA viruses (NNSV), it includes also bi-segmented plant viruses (Dietzgen et al. 2017). As a member of the *Rhabdoviridae* family it displays a bullet- or rod-like shape. Of note, the rhabdovirus family is constantly extended and includes among others the genus of *Vesiculovirus* with Vesicular stomatitis virus (VSV) as a prominent member and the *Lyssavirus* genus including RABV.

Moreover, RABVs are classified into two types of strains: street strains and fixed strains. In contrast to street strains that are directly isolated from an infected animal or human, fixed strains are obtained from passaging in cell culture or animals. Street Alabama Dufferin (SAD) was originally isolated from a rabid dog in Alabama 1935 and named SAD B19 after serial passaging in baby hamster kidney (BHK) cells. Due to the thereby emerged attenuation, it was widely used as vaccine strain to immunize wildlife populations (Schneider 1995; Vos et al. 1999). In addition, recombinant cDNA derived from SAD B19 has been successfully used for the first production of infectious virus particles by reverse genetics. The thereby generated strain was named SAD L16 (Schnell et al. 1994). In this thesis, SAD L16 strain was used as "wildtype" strain and served as basis for all further constructs.

1.1.2   Epidemiology and pathogenicity

Every year, rabies causes approximately 59 000 deaths. More than 95 % of these occur in Asia and Africa, predominantly in rural areas within poor and vulnerable populations who live remotely and have no access to medical care. In contrast, the disease displays no problem in big cities or developed countries, where either preventive vaccine or fast post-exposure treatment is available (Knobel et al. 2005; WHO 2021). Thus, it is estimated that hundreds of thousands of deaths are prevented through the post-exposure treatment and vaccination, that more than 29 million people receive each year (WHO 2021).

The causative agent of the disease is rabies virus (RABV), which is in 99 % transmitted by dogs. Usually, primary infection of a muscle cell occurs after a bite or scratch of the rabid animal. Then, the virus replicates in the muscle cells before it reaches primary motor neurons via neuromuscular junctions. Once in the peripheral nervous system, RABV spreads towards the central nervous system (CNS) in exclusively retrograde manner (Figure 1). The subsequent invasion of the CNS is accompanied by the onset of symptoms. The appearance of symptoms indicates the stage at which the infection is no longer curable but in almost 100 % cases fatal (Koyuncu et al. 2013; Davis et al. 2015). So far, only one single case is known in which a patient survived rabies after the onset of symptoms (Willoughby et al. 2005).
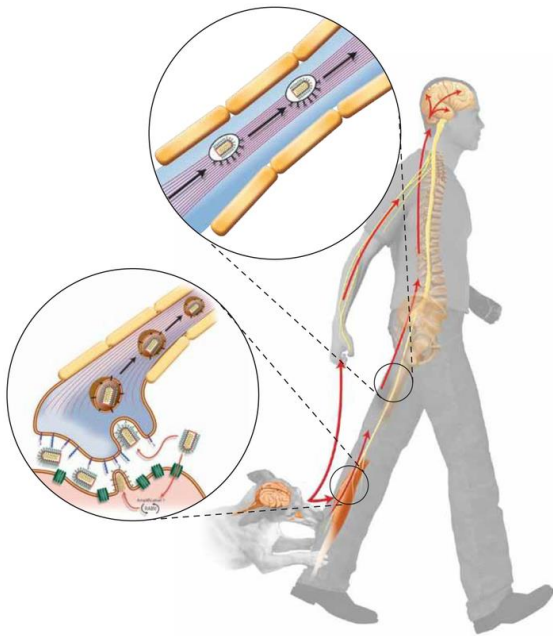
Figure 1: Rabies virus route of infection.
After the bite of a rabid animal in the peripheral muscle tissue, RABV enters the peripheral nervous system via neuromuscular junctions. By retrograde transport along axons, RABV spreads towards the CNS. Infection of the brain displays the last step of infection, which is associated with a start of clinical symptoms leading to death (adapted from (Davis et al. 2015)).

After initial flu-like symptoms, the disease progresses either in the form of encephalitic rabies or in the form of paralytic rabies, dependent on the development during the acute neurological phase. In most cases, encephalitic form occurs including hyperactivity followed by fluctuating consciousness and phobic spasms. Within a week, the patient falls into a coma and dies due to cardiac arrest. In contrast to the classical encephalitis, around 20 % of the patients develop the paralytic form of rabies, which is less dramatic, but takes longer. Often, limb and muscle weakness progress into a gradual paralysis, which is later followed by coma and death (Jackson 2013). Thereby, incubation time of the disease is not only dependent on the location of the bite, but also on the transmitted viral load and the RABV strain. Hence, typical incubation period is between two and three months. However, it can vary from 7 days up to more than 6 years (Hemachudha et al. 2002). Interestingly, pathological changes within the CNS are relatively mild despite the extensive clinical signs. Indeed, RABV has developed various mechanisms to evade the host immunity to maintain the integrity of the neuronal network (Lafon 2008; Ito et al. 2016).

So far, there is no natural transmission between humans known. However, one case of rabies was reported after organ transplantation from an infected donor (Vora et al. 2013). In fact, most cases are transmitted by dogs, but RABV has a wide host range including other carnivorous land mammals such as raccoons and skunks, but also bats. New hosts are infected at late stage of the disease when rabid animals are hyperactive and exhibit hypersalivation combined with a high load of RABV particles in the saliva (Jackson 2013; Fooks et al. 2017).

Until now, it is not possible to cure the disease after the outbreak of clinical symptoms. However, active immunization with rabies vaccines can be administered to prevent rabies before any exposure. Furthermore, effective post-exposure prophylaxis (PEP), which involves cleansing of the wound, passive immunization with rabies immune globulin (RIG) and additional vaccination is available (Manning et al. 2008; Zhu and Guo 2016). In addition to pre- and post-exposure prophylaxis in humans, the risk of rabies exposure can be reduced by vaccination of domestic animals and wildlife populations. For this purpose, attenuated rabies virus strains such as SAD B19 or recombinant viruses like vaccinia virus or adenoviruses expressing the rabies virus glycoprotein are used for oral immunization in vaccine baits. With this strategy, the risk of RABV could be eliminated in North America, large areas of Latin America, Western Europe, and Japan. Nevertheless, rabies is still endemic in more than 150 countries and therefore an important global health concern (Rosatte 2013; Hampson et al. 2015; Taylor et al. 2021). For this reason, rabies is included in the WHO's new 2021-2030 road aiming to reduce dog-mediated rabies death to zero by 2030 (WHO 2018, 2020).

1.1.3 Organization of virus particles

RABV is a non-segmented negative strand RNA virus, that is composed of five different structural proteins: the nucleoprotein (N), the phosphoprotein (P), the matrix protein (M), the glycoprotein (G) and the large protein (L).

RABV N encapsidates the viral genome in a ratio of one N protein per nine ribonucleotides (Iseni et al. 1998). Thereby, a helical structure called nucleocapsid is built protecting the viral RNA from being recognized by the host innate immune system. Moreover, the nucleocapsid serves as the template for replication and transcription by the viral RNA-dependent RNA polymerase L (Albertini et al. 2006; Albertini et al. 2008).

The phosphoprotein has received its name due to a number of serine phosphorylations at the N- and C-terminus and forms, together with L and the nucleocapsid, the so-called ribonucleoprotein (RNP). Within the RNP, the highly phosphorylated P serves as a cofactor for the polymerase L (Mavrakis et al. 2004). Moreover, it functions as chaperone for newly made N. In consequence, oligomerization of N, as well as binding to cellular RNA is prevented, whereas binding to newly synthesized viral RNA is promoted by P (Albertini et al. 2008; Wunner and Conzelmann 2013). Moreover, RABV P plays a crucial role in evasion of the innate immune system by counteracting type I Interferon (IFN) induction as well as IFN-mediated JAK/STAT response thus limiting expression of interferon-stimulated genes (ISGs), many of which have antiviral activity (Brzózka et al. 2005; Ito et al. 2010; Rieder et al. 2011; Wiltzer et al. 2014).

The matrix protein M is the smallest structural protein with a molecular weight of about 25 kDa and connects the viral RNP with the envelope. By condensing the RNP it is responsible for the bullet-shape of the virus particle (Mebatsion et al. 1999). Besides its important role in virus assembly and budding, M is further relevant for balancing replication and transcription (Finke et al. 2003; Okumura and Harty 2011).

As the name suggests the RABV glycoprotein is highly glycosylated. Thus, N-glycosylation is involved in the transport to the cell surface as well as virus assembly and budding (Okumura and Harty 2011; Hamamoto et al. 2015). As a type I transmembrane protein, RABV G is the only viral protein that is exposed to the outside. For this reason, cell tropism is determined by G. Virus entry is mediated by interaction of trimeric G with a cellular receptor like the nicotinic acetylcholine receptor (nAChR), neuronal cell adhesion molecule (NCAM), p75 neurotrophin receptor (p75NTR) or the newly discovered RABV receptor metabotropic glutamate receptor subtype 2 (mGluR2) (Lafon 2005; Wang et al. 2018). Hence, RABV G plays an essential role in regard to the transsynaptic spread in neurons and determines the axonal

transport of viral particles in retrograde direction (Etessami et al. 2000; Mazarakis et al. 2001; Wunner and Conzelmann 2013).
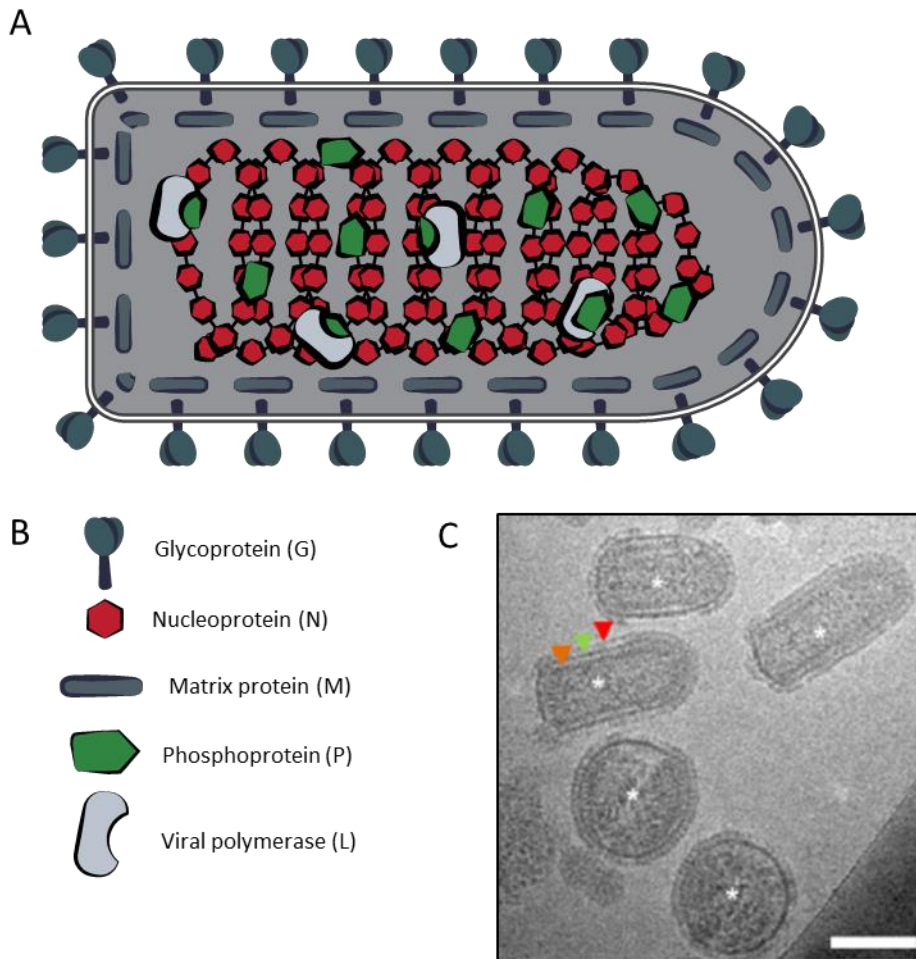
Figure 2: Organization of rabies virus particles.
A) Schematic representation of a RABV particle including RNA genome, five structural proteins and envelope. B) Legend for the viral proteins shown in A). C) Cryo-electron microscopy picture of a RABV particle. Orange arrow: M/N protein; red arrow: G protein; green arrow: membrane (Guichard et al. 2011);(adapted from dissertation (Wachowius 2016)).

Those five proteins are encoded within the approximately 12 kb single stranded RNA of negative-sense in the following, highly conserved order: 3'-N-P-M-G-L-5'. The RNA genome together with the five proteins form the viral particle, that is typically bullet shaped measuring approximately 75 nm × 180 nm (Figure 2; (Willoughby 2012).

1.1.4   Life cycle

All members of the rhabdovirus family show a similar life cycle, which can be categorized into three different phases including virus entry, transcription and replication and finally virus assembly and budding. Most of the insights of the rhabdovirus life cycle were initially gained by analyzing VSV.

During the first phase, the virion attaches to the cell surface, where it binds a cellular receptor via the ectodomain of the G protein. For RABV four receptors are described so far: nAChR, NCAM, p75NTR and mGluR2 (Lafon 2005; Wang et al. 2018). Thus, the recognition of mainly neuronal receptors determines the neurotropic character of RABV with nAChR playing an important role for entering the neuronal system from a muscle cell. The interaction between G and the receptor triggers endocytosis of the viral particle which is then transported within the endosomes along the axons towards the neuronal cell body in a retrograde manner. Decreasing pH forces G to change the conformation which leads to the fusion of the viral envelope with the endosome, and subsequently to the release of RNPs into the cytoplasm. With this the phase of transcription and replication begins.

The nucleocapsid changes in the cytoplasm into a more relaxed conformation and is available for transcription by the RNA-dependent RNA polymerase L and its cofactor P within liquid-like inclusion bodies (Lahaye et al. 2009; Nikolic et al. 2017; Nevers et al. 2020; Su et al. 2021). Due to the negative sense of the RNA genome, transcription of mRNAs is immediately possible by N, P, and L proteins of the input RNP (so called primary transcription). The RABV genome contains five monocistronic genes, which are separated by non-coding, intergenic regions (IGRs). Each gene starts with a transcription initiation signal (TIS) and ends with transcription termination and polyadenylation signal (TTP). Additionally, the genome is flanked by non-coding 3'-leader and 5'-trailer regions and has a triphosphate modification at the 5'-end. First of all, transcription is initiated at a genomic promoter in the 3'-end of the leader. Then, the leader sequence and the five genes N, P, M, G, and L are transcribed in a sequential manner. After each gene, transcription is stopped by the TTP, but reinitiates with a certain chance due to the TIS of the following gene depending on the IGR. This stop-start mechanism naturally creates a transcriptional gradient, with most copies of N-mRNA and few copies of L-mRNA (Whelan et al. 2004; Albertini et al. 2011; Fodor 2020). The strength of this gradient differs across rhabdoviruses and is dependent on the length of intergenic regions. RABV exhibits a steep mRNA gradient, whereas only two nucleotides in each IGR in VSV cause a relatively flat gradient. At the end, the non-coding leader mRNA contains a 5'-triphosphate, but each coding mRNA is provided with a 5'-cap-1 structure and a 3'-poly(A) tail and is therefore recognized and translated by the host's translational machinery.
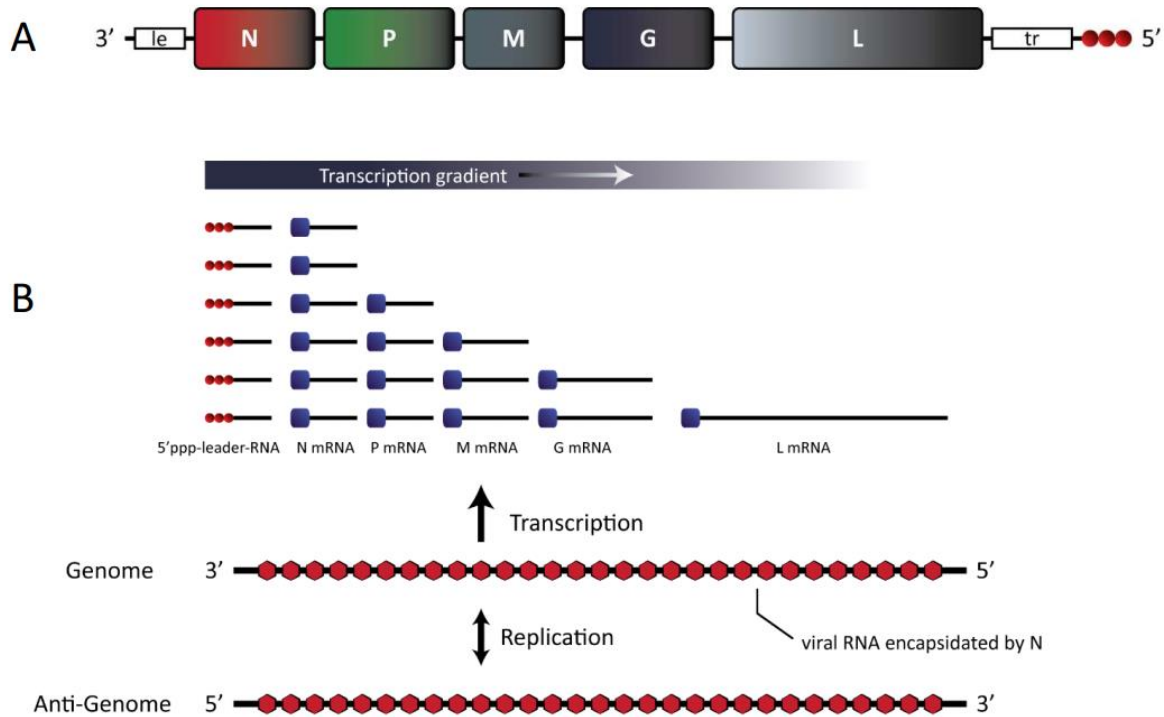
Figure 3: Replication of rabies virus.
A) Schematic representation of RABV genome including the five monocistronic genes, 3'-leader and 5'-trailer regions, as well as the triphosphate modification at the 5' end. B) Illustration of RABV transcription and replication. The encapsidated RNA genome serves as template for transcription and translation. Transcription is initiated at the 3' end of the genome. Each coding mRNA is 5´-end capped and 3´-end polyadenylated. The stop-start mechanism leads to a transcriptional gradient with N as most abundant and L as less abundant mRNA. After primary transcription, replication begins with encapsidation of the nascent leader RNA, followed by generation of a complete antigenome. This serves as template for production of a new RNA genome (adapted from dissertation (Wachowius 2016)).

Primary transcription and protein translation must take place before replication can begin, because N is indispensable for the encapsidation of the new RNA. For this reason, the N levels are crucial for replication. As soon as enough N protein is produced, it binds the nascent leader RNA. With that replication starts (Ogino and Green 2019). TTP and IGR sequences, as well as intergenic regions are ignored and a whole positive sense RNA antigenome is generated. As an essential element, the antigenome RNP serves as template for the new genome RNP. Importantly, the 3'-end of the antigenome carries the antigenomic promoter within the trailer region. From that, the trailer is generated, which contains an encapsidation signal. With that encapsidation of nascent RNA and elongation of the trailer is initiated resulting in an identical copy of the original genome (Albertini et al. 2011; Hudacek and Schnell 2014). Thereby, P ensures the encapsidation of exclusively viral RNA by N acting therefore as a chaperone for N. Interestingly, the strong activity of the replicative antigenome promoter leads to a 49:1 ratio between genomic and

antigenomic RNA (Finke and Conzelmann 1997). Newly made nucleocapsids can then be used for secondary transcription or as template for the production of further genomic RNAs (Figure 3) (Whelan et al. 2004). Once enough RNP copies are produced, the phase of virus assembly and budding can start.

Viral proteins are independently produced by the host cell. As a transmembrane protein, G is synthesized by ribosomes associated to the endoplasmic reticulum. After association to trimeric complexes, G is transported to the cell surface via the Golgi apparatus, where it is organized in clusters. M plays a crucial role in virus assembly and budding, since is serves as hub between the RNP and G. Thus, it is able to bind newly formed RNPs and recruit them to the cell surface (Mebatsion et al. 1996; Mebatsion et al. 1999). There, M interacts with the cytoplasmic tail of trimeric G. During this interaction, the RNP is condensed into a supercoiled structure triggering exocytosis of the viral particle in a process called budding. With the separation of the budding virion from the cell, the virus is ready to infect a new cell (Jayakar et al. 2004; Okumura and Harty 2011).

1.1.5   RABV as transsynaptic tracer

Rabies virus is unique among neurotropic viruses, since, once in a neuron, RABV spreads from neuron to another neuron exclusively via chemical synapses. In natural infections, which in most cases result from bites or scratches, the virus enters the first neuron via neuromuscular junctions. The glycoprotein is then responsible for the retrograde transport along the axons. After replication, new viruses are transported to dendrites and transferred at synapses to presynaptic neurons. While the exact mechanisms involved are not known, RABV obviously can be used as a natural polysynaptic tracer. By using full-length viruses expressing eGFP, the tracing signal is amplified through viral replication and can be followed along neuronal connections. However, since infection of neurons is not synchronous, differentiation between infected primary, second- and further order neurons is difficult (Figure 4A) (Astic et al. 1993; Ugolini 1995; Ugolini 2011). Moreover, infection of starter cell by conventional RABV is not specific since experimental brain infection allows initial access to various neuronal cell types. Thus, even when replication is restricted like in case RABV ΔG eGFP (SAD-G), a recombinant RABV which does not encode the glycoprotein but pseudotyped with it, single neurons can be infected without later spreading, but specific starter cells cannot be defined (Figure 4B) (Wickersham et al. 2007a).

RABV transsynaptic transmission and spread in the brain requires the presence of G, as first illustrated by experiments with SAD ΔG viruses "pseudotyped" with the homologous SAD G (Etessami et al. 2000). This was exploited in 2007 for establishment of the first monosynaptic tracing system. Specifically, this

approach provides G only in an initially infected cells, allowing transfer of a G-deficient virus to presynaptic neurons only. The system developed by Wickersham and colleagues does not only allow to specifically analyse direct neuron-neuron connections but to select and identify specific starter neuron cells. For this approach, SAD ΔG eGFP (EnvA), a recombinant RABV lacking the glycoprotein is used that is pseudotyped with the avian sarcoma leukosis virus (ASLV) envelope EnvA. Of note, as EnvA originates from ASLV, it is not able to bind receptors of mammalian neurons. In consequence, SAD ΔG eGFP (EnvA) is not able to infect neurons from mammals. Therefore, expression of the EnvA receptor TVA has to be established in the starter cell in order to allow infection. Moreover, a red fluorescent protein such as DsRed2 can be expressed in these cells to label them as starter cells. Lastly, the transcomplementation with RABV G is required to allow further spread to the monosynaptically connected neurons. With those three proteins, which can be delivered for example by a helper virus with a cell-type-specific promoter, starter cells can be specifically infected and direct synaptically connected neurons stained. Of note, SAD ΔG eGFP (EnvA) is not able to spread further due to the lack of RABV G in secondary infected cells (Figure 4C). In consequence, the system displays exclusively monosynaptic tracing (Wickersham et al. 2007b; Ghanem and Conzelmann 2016).
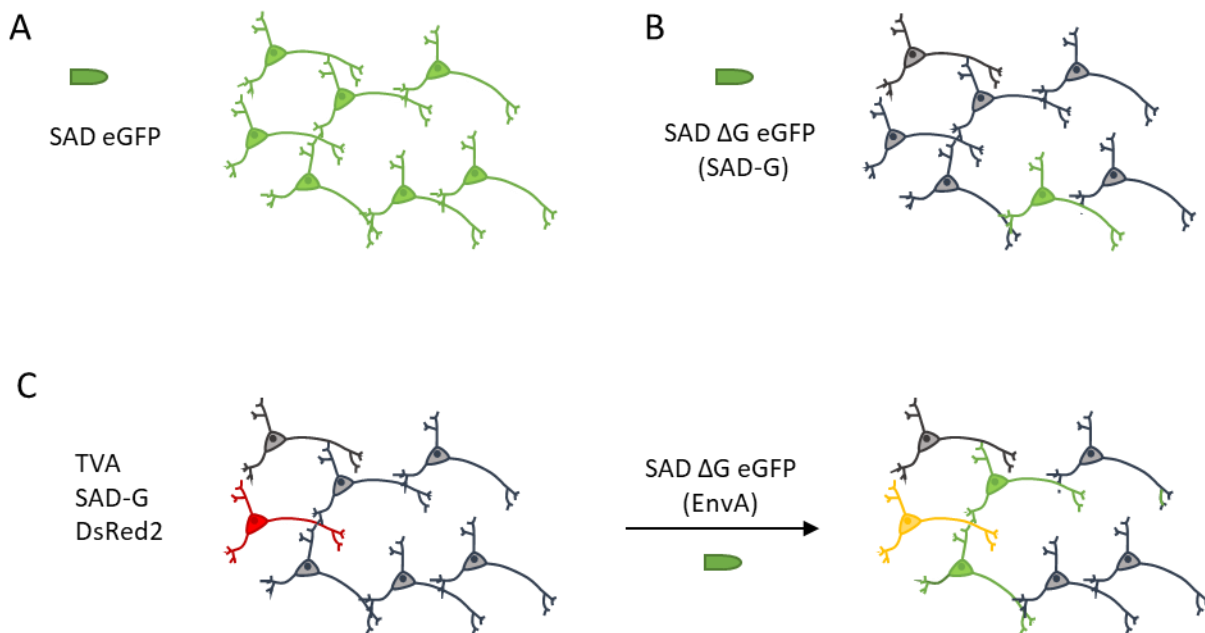
Figure 4: Neuronal tracing with rabies virus.
A) Spread of full-length SAD eGFP virus resulting in staining of several neurons. B) Infection of neurons with G deleted and SAD-pesudotyped SAD ΔG eGFP (SAD-G) virus is limited to a random starter cell. C) After providing the TVA receptor, SAD-G and a red fluorescent protein in a selected starter cell, for example by recombinant AAV, it can be infected with SAD ΔG eGFP (EnvA). SAD-G enables viral spread one additional round. As a result, starter cell and monosynaptically connected neurons are stained.

1.2   Apoptosis

Viruses exploit host cells for their transcription and replication. In order to prevent the spread of pathogens various host cell defense mechanisms have evolved. One strategy is the depletion of invaded cells by regulated cell death. Different forms of cell death could thereby occur. Traditionally, cell death is categorized in different groups due to morphological changes: type I cell death or apoptosis, type II or autophagy and type III cell death or necrosis. Necrosis is characterized by cell swelling, followed by membrane disruption and lysis, whereas autophagy involves the formation of autophagosomes and lysosomal degradation of respective content (Galluzzi et al. 2007; Nagata and Tanaka 2017; Galluzzi et al. 2018; D'Arcy 2019; Tang et al. 2019). In contrast, apoptotic hallmarks are cell shrinkage and chromatin condensation in first place, followed by nuclear fragmentation. Then, the membrane starts to bleb leading to the release of so-called apoptotic bodies. These apoptotic bodies are tightly packed with cellular material and usually phagocytosed by other cells such as macrophages, parenchymal or neoplastic cells (Kerr et al. 1972; Saraste 2000; Häcker 2000). Phagocytic recognition is mediated by translocation of phosphatidylserine (PS) residues from the inner to the outer leaflet of the plasma membrane. In contrast, healthy cells display an asymmetric lipid composition with PS only in appearing the inner leaflet of the membrane (Chaurio et al. 2009). In consequence, apoptosis is usually considered to be not immunogenic, but silent. However, in cell culture for example apoptosis can be followed by secondary necrosis (Silva 2010; Pasparakis and Vandenabeele 2015).

Apoptosis is tightly regulated by caspases. Caspases are evolutionarily conserved aspartate-specific cysteine proteases and exist in precursor form of an inactive procaspase which becomes active upon cleavage. Apart from inflammatory caspases, apoptotic caspases can be divided into initiator and effector or executioner caspases. Thus, initiator caspases contain either a DED domain such as caspase-8 and -10 or a CARD domain like in case of caspase-9 (Riley et al. 2015; Huber et al. 2018). Proteins with those domains belong to the so-called death domain superfamily which also contains proteins with a death domain (DD) or a Pyrin domain. These domains are responsible for mediating protein interaction of different stress signal components (Ferrao and Wu 2012). In contrast to initiator caspases that need this motif to become activated in multi protein complexes, effector caspases do not contain such a domain but are activated by other caspases. As the name suggests executioner caspases carry out the final death by hydrolyzing a wide range of substrates. One of them is the Poly(ADP-ribose)-Polymerase 1 (PARP) which plays an important role in DNA repair within a healthy cell (Hengartner 2000; Morales et al. 2014). Usually,

apoptosis is distinguished between two major forms: extrinsic and intrinsic apoptosis. An overview of these both pathways is illustrated in Figure 5.
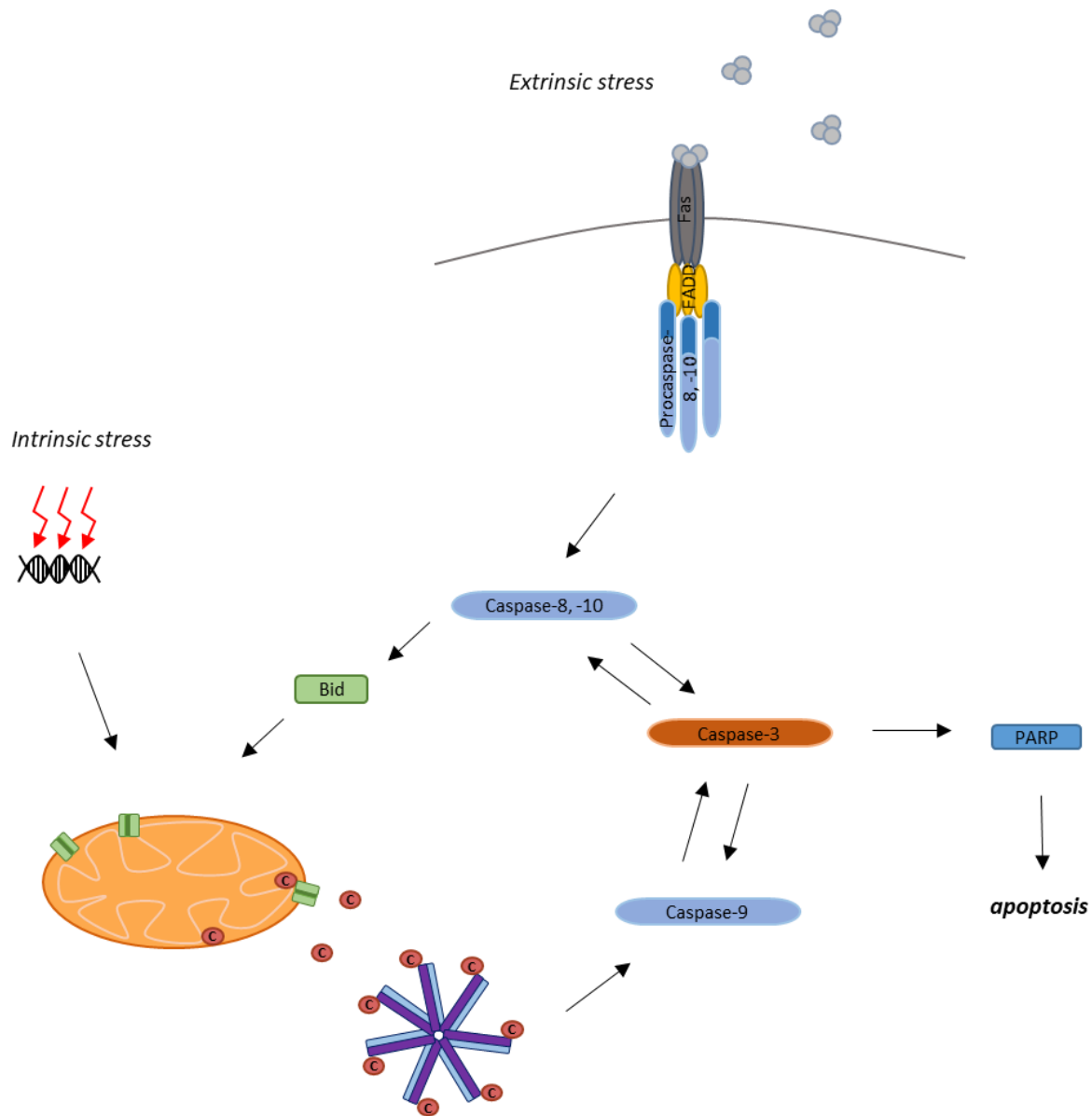
Figure 5: Overview of extrinsic and intrinsic apoptosis pathways.
Extrinsic apoptosis is mediated upon ligand binding to a death receptor such as Fas. Trimerization of death receptor leads to recruitment of the adaptor protein FADD. Subsequent recruitment of procaspase-8 or -10 results in their autocatalytic activation within the DISC. Then, initiator caspases are able to further activate effector caspases such as caspase-3, which in turn cleaves remaining procaspases and further substrates like PARP resulting in final apoptotic outcome. Intrinsic apoptosis is mediated via pro-apoptotic BCL-2 proteins such as Bak and Bax forming a pore within the mitochondrial membrane. Subsequent mitochondrial outer membrane permeabilization results in cytochrome c release, which is the key event leading to formation of the apoptosome including procaspase-9, which is then activated within this complex. Further activation of the effector caspase-3 leads to apoptosis. Crosstalk between extrinsic and intrinsic pathways are possible through cleavage of Bid by Caspase-8, leading to oligomerization of Bak and Bax within the mitochondria.

1.2.1   Extrinsic apoptosis

Extrinsic apoptosis is initiated by extracellular binding of a so-called death ligand to a death receptor. Currently, there are six known apoptotic death receptors with the most extensively studied interactions between FasL/FasR, TRAIL/TRAILR1/TRAILR2 and TNFα/TNFR (Daniel et al. 2001). Death ligands are usually expressed on the surface of activated T lymphocytes, NK cells and macrophages, but appear also on epithelial cells, or immature dendritic cells (Falschlehner et al. 2009). Thus, Fas or TRAIL act as cytokine like molecule forcing the aggregation of death receptors upon their binding. Sharing a characteristic DD, the trimerized death receptors subsequently are able to recruit adaptor proteins such as the Fas-associated protein with death domain (FADD). Those proteins contain a DD as well interacting with the one of the receptors, and also a DED allowing to bind the respective DED of procaspase-8 or procaspase-10 (Wu and Lo 2009). With the receptor, FADD and procaspase-8 the death-inducing signaling complex (DISC) is assembled (Guicciardi and Gores 2009). In contrast to the Fas and TRAIL induced pathway, TNFα binding to TNFR leads to the formation of the complex I. In complex I the TNF receptor type 1-associated death domain protein (TRADD) serves as hub for the TNF receptor associated factor 2 (TRAF2) and RIPK1 with the TNFR. Only if complex I dissociates from the receptor, it is converted into complex II by binding of FADD to the available DDs and subsequent recruitment of procaspase-8 or -10. Otherwise, the pro-survival NF-κB pathway is promoted (Micheau and Tschopp 2003).

In any case FADD is the essential adaptor protein to execute extrinsic apoptosis. After binding of the procaspase-8 to the DISC or complex II, more procaspase-8 molecules are recruited allowing their homodimerization and subsequent auto-catalytical activation (Fu et al. 2016). This process is enhanced or inhibited depending on low or high levels of the large isoform of the cellular FLICE-like inhibitory protein (cFLIP$_L$). As catalytical inactive homolog of caspase-8 it can bind to the DISC and be incorporated into caspase-8 filaments (Micheau et al. 2002; Pop et al. 2011). In contrast, the short isoform of cFLIP (cFLIP$_S$) exclusively counteracts apoptosis initiation (Krueger et al. 2001).

The active initiator caspase-8 cleaves and thereby activates downstream effector caspases such as caspase -3, -6 or -7 which then hydrolyzes various other target molecules and amplify the signal via further cleavage of procaspases-8, -9 and -10. Moreover, the signal can be amplified via the mitochondrial pathway. Thereby, Bid serves as substrate for caspase-8. After cleavage, the truncated version tBid translocates to the mitochondria and subsequently initiates oligomerization of Bax or Bak leading to pores within the mitochondrial outer membrane (MOM). In consequence cytochrome c is released into the

cytosol where it binds to APAF-1 activating the intrinsic pathway (Korsmeyer et al. 2000; Degli Esposti 2002; Kantari and Walczak 2011).

Of note, rodents express caspase-8 but lack caspase-10. Hence, most studies focused on caspase-8. In humans caspase-10 and caspase-8 are very close homologs sharing the same gene locus. Although caspase-10 was considered as apoptotic initiator caspase, its role is discussed controversially. Thus, it was shown to be assembled in the DISC and processed during Fas and TRAIL induced apoptosis. Thereby, some studies observed that caspase-10 is able to functionally substitute caspase-8 within the DISC (Kischkel et al. 2001; Wang et al. 2001) whereas others do not (Sprick et al. 2002). Moreover, Horn and colleagues discovered caspase-10 to counteract caspase-8 mediated cell death (Horn et al. 2017).

1.2.2   Intrinsic apoptosis

Intrinsic apoptosis is usually triggered by an intracellular stress stimulus such as DNA damage, UV and γ-irradiation, or reactive oxygen species (ROS). The following stress signaling is strictly regulated by members of the BCL-2 family, which function in either pro- or anti-apoptotic favor. BCL-2 proteins share at least one conserved BCL-2 homology (BH) domain allowing interactions with each other. Thus, anti-apoptotic proteins such as BCL-2 inhibit pro-apoptotic family members like Bax and Bak by binding their BH3 domain, which is essential for apoptotic signaling (Kale et al. 2018). This inhibition is in turn counteracted by the pro-apoptotic Noxa and Puma. Many BCL-2 proteins are under the control of the tumor suppressor protein p53 transcription factor, which was shown to upregulate pro-apoptotic genes, whereas transcription of anti-apoptotic proteins is downregulated (Aubrey et al. 2018).

Bak and Bax, activated in response to a stress stimulus, oligomerize to pore-forming complexes that lead to mitochondrial outer membrane permeabilization (MOMP). Loss of mitochondrial outer membrane integrity via MOMP is a crucial event during intrinsic apoptosis, allowing pro-apoptotic factors from the intermembrane space to enter the cytosol (Westphal et al. 2011). One factor is cytochrome c which usually functions as electron carrier protein during ATP synthesis. Once translocated in the cytosol, cytochrome c binds to APAF-1 promoting its heptamerization (Hüttemann et al. 2011). Moreover, procaspase-9 is recruited and binds to the CARD domain of APAF-1. The thereby formed complex involving cytochrome c, APAF-1 and procaspase-9 is called apoptosome. Within the apoptosome, procaspase-9 is able to dimerize resulting in autocatalytic cleavage and in consequence activated caspase-9. Then, caspase-9 dissociates from the complex leaving space for further procaspase-9 molecules. Furthermore, free caspase-9 activates

effector caspases like caspase-3, -6 and -7, which in turn hydrolyze further downstream proteins (Hengartner 2000; Fulda and Debatin 2006).

1.2.3 Apoptosis induction by PKR

Protein kinase R (PKR) is an important stress sensor in mammalian cells that is activated during viral or cellular stress. Nevertheless, apoptosis mediated by PKR is typically not described within the previously mentioned categories of extrinsic or intrinsic apoptosis.
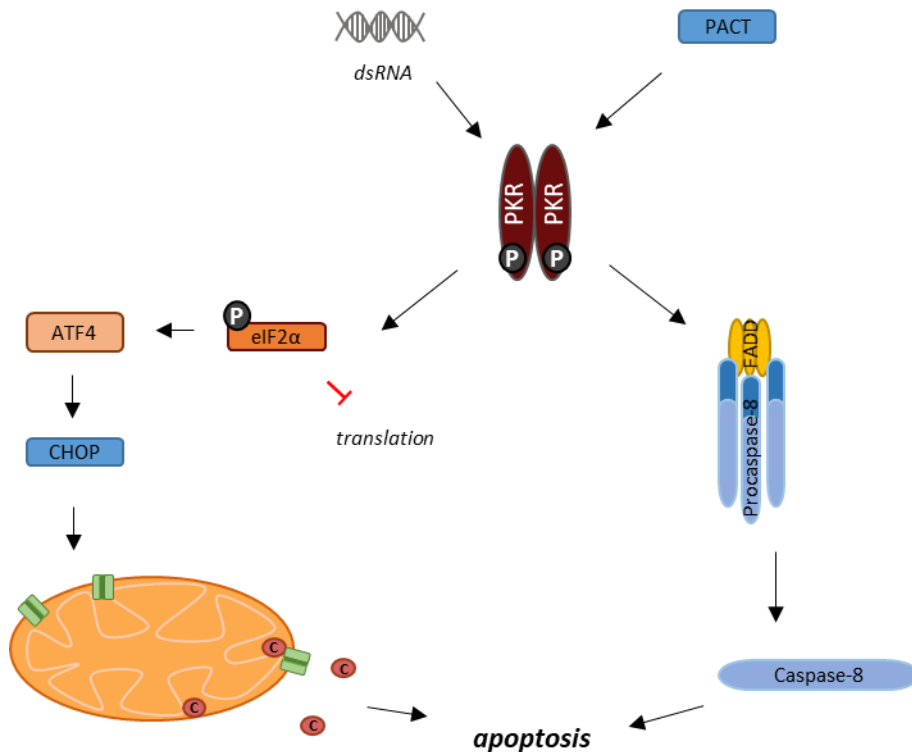
Figure 6: Overview of PKR mediated apoptosis.
PKR is activated either by PACT or double stranded RNA, leading to its dimerization and subsequent autophosphorylation. Following phosphorylation of eIF2α results in shutdown of general translation, whereas translation of ATF4 is upregulated. This results in activation of CHOP, initiates pore-formation by Bak and Bax resulting in apoptosis. In addition, PKR activation is associated with FADD activation of caspase-8 leading to apoptosis.

The serine/threonine kinase consists of two domains: the N-terminal dsRNA binding domain which in turn contains two dsRNA binding motifs and the C-terminal kinase domain. In healthy cells, PKR is usually constitutively expressed, but upregulated upon IFN induction (Gal-Ben-Ari et al. 2019). PKR can be activated for example by ER stress or growth factors via PACT (Marques et al. 2008). However, most prominent PKR activator is intracellular viral dsRNA originating for example from influenza. Moreover, endogenous microRNAs are also able to initiate PKR activation (Lee et al. 2007). Thus, dsRNA binding to

the dsRNA binding domain induces formation of PKR dimers. In consequence, PKR is able to auto-phosphorylate and thereby activate itself. Once activated, PKR is able to phosphorylate its most characterized substrate, the eukaryotic initiation factor-2α (eIF2α) (Gal-Ben-Ari et al. 2019). EIF2α is a key factor during mRNA translation. Phosphorylation leads to its suppression and thereby inhibition of general translation which also implies blocking of virus protein production. In contrast, translation of specific mRNAs like the activating transcription factor 4 (ATF4) is upregulated. ATF4 in turn upregulates transcription of CHOP, which then regulates apoptosis by acting as transcription activator of pro-apoptotic gene or repressor in regard of anti-apoptotic genes (Figure 6) (Scheuner et al. 2006; Hu et al. 2018).

Moreover, PKR mediated induction of apoptosis is associated with activation caspase-8 by FADD. Although FADD is typically associated within death receptor mediated apoptosis, it has been shown that death receptors and DISC formation is not needed for FADD activation during PKR signaling. Instead upregulation of FADD expression might cause caspase-8 activation (Balachandran et al. 1998; Gil and Esteban 2000a, 2000b).

Beside initiation of apoptosis fate, PKR activates the NF-κB pathway in order to counteract infection while maintaining cell homeostasis. Whether the cell finally undergoes cell death or survives is dependent on the extent and duration of the stress stimuli (García et al. 2007; Garcia-Ortega et al. 2017; Xu et al. 2018).

1.3   The small molecule–assisted shutoff (SMASh) system

In the last decade, CRISPR/Cas9 genome editing has revolutionized the possibilities for studying protein function. Although this system is easy to utilize and cost-effective, there are some disadvantages. First, a genetic knockout does not only lead to a complete but also irreversible depletion of the protein. In consequence, the system is not suitable for studies on essential proteins. Moreover, unwanted off-target mutations might be introduced into the genome. Besides that, the use of the CRIPSR/Cas9 system is restricted to application at the DNA level, while control at the RNA or protein level is not possible. For control at RNA levels, RNA interference (RNAi) systems are used (Wilson and Doudna 2013; Neumeier and Meister 2020), and CRISPR/Cas approaches are being developed (Wessels et al. 2020).

For proteins, other methods are necessary and available, most of which, however, required genetic engineering of cells. Examples include Auxin-inducible degron (AiD), Conditionally-stable FKBP12 and UnaG tag degrons, TRIM away, Affinity-directed PROtein Missile system (AdPROM), DeGradFP and ZIF1 proteolytic systems Hydrophobic tagging (HyT) PROteolysis-TArgeting Chimeras (PROTACs) MDM2-based PROTACs, Cereblon (CRBN)-based PROTACs VHL c-IAP PROTACs and specific and non-genetic IAP-

dependent protein erasers (SNIPERs), Keap1-based PROTACs, HALO and dTAG PROTACs (Natsume and Kanemaki 2017; Röth et al. 2019).

In 2015 Chung and colleagues invented the small molecule–assisted shutoff (SMASh) system, a novel degradation system allowing targeted proteolysis of a protein of interest (POI) by addition of a small molecule (Chung et al. 2015).

1.3.1 Regulation of protein levels by SMASh

The SMASh-tag contains the hepatitis C virus (HCV) NS3 protease, a degron-like sequence and a linker followed by the NS3 cleavage site, where the POI is fused to. In absence of any drug, the SMASh-tag cleaves itself off and releases an untagged and functional protein, whereas the tag itself is degraded. However, in presence of a specific NS3 inhibitor such as asunaprevir (ASV) or danoprevir (DNV) cleavage is blocked resulting in the instant degradation of the whole newly made fusion protein (Figure 7). This process is reversible by drug removal through washing. Thereby, protein production increases again very rapidly to normal levels.

This targeted protein degradation has many advantages. Thus, it allows study of essential proteins or viral proteins from non-DNA viruses like RABV. Furthermore, regulation of protein levels is not only reversible, but can be adjusted by inhibitor dosage. Of note, the SMASh-tag can be fused either N-terminally or C-terminally to a POI and is therefore suitable for various targets. Overall, the SMASh system represents an efficient tool for protein control that requires only minimal genetic modification (Chung et al. 2015; Hannah and Zhou 2015).
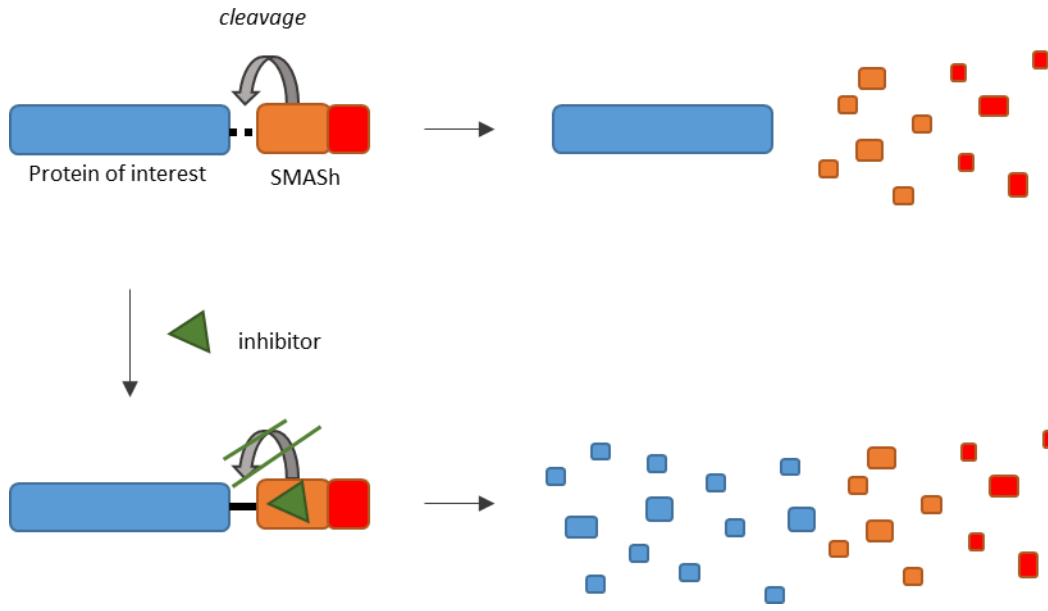
Figure 7: Protein control by SMASh.
The protein of interest is fused to the SMASh-tag containing an HCV NS3 protease and a degron. Usually, the degron is cleaved off and degraded. However, in presence of an HCV NS3 protease inhibitor cleavage is blocked, and newly generated proteins degraded. Blue: Protein of interest; Orange: NS3 protease; Red: degron; Green: NS3 inhibitor.

1.3.2   SMASh-tag sequence

As mentioned above, the SMASh-tag consists of a serine protease, a degron-like sequence, and a linker with the protease cleavage site at its free terminus. All in all, the SMASh-tag is derived from the HCV NS3/NS4A protease. HCV belongs to the *Flaviviridae* family and exhibits therefore a positive single strand RNA genome which is translated into a polyprotein precursor (Rabaan et al. 2020). The polyprotein is processed by host and viral proteases into structural and non-structural proteins. One key player in this process is the bifunctional NS3 serine protease. Beside the protease within the N-terminal region, it contains a helicase in the C-terminal region. RNA helicase of NS3 is particularly essential for HCV replication due to its task to bind the HCV RNA genome, but is not required for NS3 protease function (Lin 2006). Nevertheless, it might affect the efficiency. For an optimal protease activity, the NS3 cofactor NS4A is required forming a non-covalent complex with the NS3 serine protease (Bartenschlager et al. 1995). Furthermore, at least the first 180 amino acids of the NS3 N-terminus are necessary for protease activity containing the catalytic triad with His57, Asp81, and Ser139 (His1083, Asp1107, and Ser1165 of the polyprotein). Beside self-cleavage of NS3/NS4A, NS4A/NS4B, NS4B/NS5A, and NS5A/NS5B serve as viral substrate for the NS3/4A serine protease (Manns et al. 2017; Morozov and Lagaye 2018; Chong et al. 2019).

The HCV NS3 protease activity serves as the basis for the SMASh-tag. In Figure 8 the amino acid sequence of a C-terminal SMASh-tag is presented. The NS4A/4B cleavage site serves as substrate for the SMASh NS3 protease and is connected via a linker to the protease. The SMASh-tag protease domain consists of 185 amino acids of the N-terminal original HCV NS3 protease, whereas most of the helicase domain is depleted. Of note, Chung and colleagues inserted four additional amino acids KIDT within the remaining helicase domain, which cannot be found in the original HCV sequence and is not commented within their publication (Chung et al. 2015). Nevertheless, since the SMASh-tag lacks most parts of the helicase domain, KIDT might serve as linker to ensure efficient support of NS4A.

In HCV, NS4A consists of three different domains: the N-terminal membrane anchor domain, a central domain which is responsible for the NS3 cofactor function of NS4A, and a C-terminal domain including a kink-region containing the amino acids PAIIP and an acidic region with a high number of acidic amino acids (Roder et al. 2019). Within the SMASh-tag the membrane anchor domain with its transmembrane domain as well as the central domain are present, whereas the C-terminus of the acidic region is deleted. Thus, the original function for assembly end envelopment should be impaired (Roder et al. 2019). Together with the SMASh helicase domain, NS4A functions like a degron. Chung and colleagues indicated the involvement of proteasome and autophagosomes in degradation process (Chung et al. 2015). However, the exact mechanism of how the degron-like sequence functions is not yet understood (Röth et al. 2019).

Figure 8: Sequence of the SMASh-tag.
SMASh-tag consists of an HCV NS4A/4B cleavage site (green), a linker including a flag-tag (black), the NS3-protease (orange), parts of the NS3 helicase (grey) and NS4A (red). Black asterisks indicate the catalytic triad of the NS3 protease (modified from (Chung et al. 2015)).

1.3.3 SMASh induced cytotoxicity

Chung and colleagues invented the SMASh system as tool for targeted protein degradation. Although they performed drug-inducible protein shutoff experiments, no cytotoxic effect was reported (Chung et al. 2015).

Prior to this thesis, SMASh controllable RABV viruses were generated with SMASh fused either to the P or to the N protein. In fact, a cytotoxic effect of the SMASh-tag was determined upon drug addition in a shutoff experiment. Thus, viruses including the SMASh-tag fused to the RABV P protein turned toxic when the inhibitor was added 8 hours or later post infection with a high MOI. Figure 9 represents microscopic pictures of ASV or DMSO control treatment 4 hours after treatment, which was performed 24 hours post infection with SAD P-SMASh. Similar outcome was observed with fusion to RABV N or to non-viral YFP-SMASh. In addition, first experiments suggested a slight cytotoxic effect even after transfection with a non-viral SMASh-tagged protein.
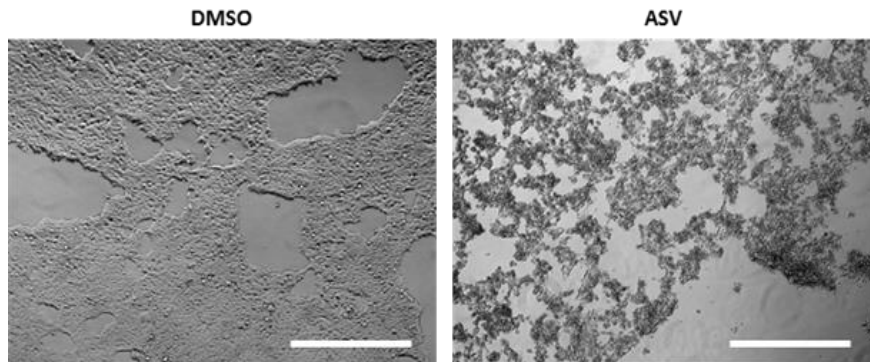
Figure 9: Induction of cell death by SMASh and ASV.
DMSO control treatment has no effect on cells, whereas ASV treatment after established SAD P-SMASh infection for 24 hours causes cell death within 4 hours. Size bar: 500 µm (adapted from master thesis (Masterthesis V. Pfaffinger 2016)).

Although MAVS is a natural cellular substrate of the NS3 protease and cleaved also by SMASh, experiments with MAVS knockout cells revealed that MAVS is not important for cell death induction. Moreover, IFN-α and –β were not induced upon SMASh. In contrast, processing of the initiator caspase-8, -9 and -10 as well as the effector caspase-3 could be shown by Western blot analysis. PARP, which serves as marker for apoptosis, was cleaved suggesting an apoptotic cell death. Involvement of RIPK1, which functions as a decision maker towards apoptosis or necroptosis, a form of programmed necrosis, was observed. Thus, degradation of RIPK1 could be observed in Western blot supporting an apoptotic outcome for the cell. As

an essential element in TNF mediated apoptosis, the adaptor protein TRADD did not play an important role in SMASh induced apoptosis, as indicated of SMASh induced cell death in TRADD knockout cells (Masterthesis V. Pfaffinger 2016). All in all, why and how SMASh induces apoptosis after drug addition remains unclear.

1.4 Aim of the thesis

The SMASh system is widely used as a tool for targeted protein degradation, and most studies have used SMASh in a protein switch-off approach (Fay et al. 2018; Zhu et al. 2019; Wu et al. 2020). Previously, we observed a high cytotoxicity induced by SMASh upon addition of the inhibitor in protein shutoff experiments. First analysis indicated the activation of apoptosis including different caspases and PARP. Within this thesis, induction of apoptosis will be confirmed by additional experiments including measurement of caspase activity and Annexin V binding to apoptotic cells. In addition, the cytotoxicity of SMASh is further characterized using various time course experiments to determine the kinetics of cell death.

It is not yet understood what exactly is needed for SMASh-mediated cell death and which pathway is triggered in particular. To gain more insights in this regards, different cell lines as well as various cell lines with knockout of apoptosis related genes will be generated and analyzed with respect to SMASh and inhibitor induced cell death. In addition, the SMASh-tag itself will be investigated to identify essential toxic components. Therefore, various deletion or truncation constructs will be generated and tested in regard of toxicity.

Based on the thereby gained results, a non-toxic controllable SMASh-tag derived tag will be designed, generated, and characterized. Moreover, the ability of virus control will be investigated. With the aim to provide an improved tool for neurotracing approaches, controllable non-toxic Cre-expressing ΔG viruses will be analyzed.

2 Materials and Methods

2.1 Materials

2.1.1 Chemicals

Table 1: List of chemicals used in this thesis.

Chemical	Manufacturer
Acetic acid, 100 %	Roth
Acetone, Rotipuran 99.8 %	Roth
Acrylamide Rotiphorese® Gel 30 (37.5 : 1)	Roth
Agar	BD
Agarose, UltraPure	Invitrogen
alamarBlue™ HS Cell Viability Reagent	Thermo Fisher Scientific
Albumin Fraction V (BSA)	Roth
Ammonium persulfate	Sigma-Aldrich
Ampicillin sodium salt (Amp)	Roth
Asunaprevir	MedChem tromica
Bis-Tris	Santa Cruz Biotech
Blasdicidin	Invivogen
Bovine Serum Albumin (BSA)	Roth
Bromophenole blue	Sigma-Aldrich
Danoprevir	MedChem tromica
Dimethyl sulfoxide (DMSO)	Roth
Dimethylformamide	Merck
Ethanol	Merck
Ethidium bromide solution 1 %	Roth
Ethylenediamine tetraacetic acid (EDTA)	Sigma
G418	Roth
Glycerol, Rotipuran 99.5 %	Roth
HEPES	Roth
Hydrochloric acid, Rotipuran 37 %	Merck
Hygromycin B	Invivogen
Isopropanol	Merck
Kanamycin monofulfate	Sigma-Aldrich
Magnesium chloride hexahydrate (MgCl2 • 6H2O)	Fluka
Magnesium sulfate heptahydrate (MgSO4 • 7H2O)	Merck
Methanol	Roth
Milk powder, blotting grade	Roth
MOPS (3-(N-morpholino)propanesulfonic acid)	Roth
Orange G	Fluka
Paraformaldehyde (PFA)	Merck
Poly-D-lysine hydrobromide	Sigma-Aldrich
Potassium chloride (KCl)	Merck
Potassium dihydrogen phosphate	Merck

Chemical	Manufacturer
Puromycin	Invivogen
Sodium bisulfite (NaHSO3)	Sigma
Sodium chloride (NaCl)	Merck
Sodium dihydrogen phosphate	Merck
Sodium dodecyl sulfate (SDS)	Serva
Sodium hydroxide	VWR Chemicals
Tetramethylethylenediamine (TEMED)	Roth
Tris, Pufferan 99.9 %	Roth
Triton X-100	Merck
Tryptone	BD
Tween-20	Roth
Yeast Extract	BD
β-Mercaptoethanol	Sigma-Aldrich
Zeocin	Invivogen
z-AEVD-fmk	Selleck Chemicals
z-IETD-fmk	Selleck Chemicals
z-LEHD-fmk	Selleck Chemicals
z-VAD-fmk	Selleck Chemicals

2.1.2 Buffers and solutions

Table 2: List of buffers and solutions used in this thesis.

Agarose gel electrophoresis	
10 x TAE	2 M Tris-HCl, (pH 7.8) 0.25 M Sodium acetate trihydrate 0.25 M EDTA
10 x TEN	50 mM Tris-HCl (pH 7.4) 1 mM EDTA 150 mM NaCl
1 x TAE + EtBr	200 mL 10 x TAE 1800 mL ddH2O 120 µL Ethidium bromide solution (1%)
OG loading buffer	50 % (v/v) 10x TAE 15 % (w/v) Ficoll 400 0.125 % (w/v) Orange G Store at -20°C, after thawing 4 °C
Mini preparation	
Flexi I	100 mM Tris-HCl pH 7.5 10 mM EDTA 200 µg/mL RNase Stored at 4 °C
Flexi II	200 mM NaOH 1 % (w/v) SDS
Flexi III	3 M potassium acetate 2 M acetic acid, pH 5.75

SDS-PAGE	
APS	10 % APS (w/v) Appropriate volume ddH2O Store at -20 °C, after thawing at 4 °C
3.5 x Bis-Tris	1.25 M Bis-Tris HCl pH 6.8
20 x MOPS buffer	1 M Tris 1 M MOPS 20 mM EDTA 2 % SDS
1 x MOPS buffer (running buffer)	50 mL 20 x MOPS 2 mL 2.5 M Sodium Bisulfite
SDS sample buffer	62 nm Tris/HCl pH 6.8 10 % SDS 15 % β-mercaptoethanol 30 % Glycerol 0.012 % Bromophenol blue
Separation gel mix (10 %)	1 x Bis-Tris 10 % acrylamide/bisacrylamide 37.5:1 ddH$_2$O appropriate volume
Separation gel	Separating gel mix (10 %) 1 % APS (v/v) 0.4 % TEMED (v/v)
Stacking gel mix (6 %)	1 x Bis-Tris 6 % acrylamide/bisacrylamide 37.5:1 ddH$_2$O appropriate volume
Stacking gel	Stacking gel mix (6 %) 1 % APS 0.1 % TEMED
Western blotting	
Extra-Dry blotting buffer	48 mM Tris 20 mM Hepes 1 mM EDTA 1.3 mM Sodium Bisulfite 1.3 mM Dimethylformamide
TBS	50 mM Tris 150 mM NaCl pH 7.4 (adjusted with HCl)
TBS-T	TBS 0.05 % Tween-20
5 % milk in TBS	1x TBS 5 % (w/v) milk powder
10 % BSA in TBS	1x TBS 10 % (w/v) BSA powder
Flow cytometry	
3 % PFA	1 x PBS 3 % (w/v) Paraformaldehyd

2.1.3   Media and cell culture additives

Table 3: List of media and cell culture additives used in this thesis.

Components of cell culture medium	Manufacturer
D-MEM (L-Glutamine, high glucose)	Gibco
G-MEM (L-Glutamine, high glucose)	Gibco
DPBS (no calcium, no magnesium)	Gibco
L-Glutamine	Gibco
MEM Amino Acids	Gibco
Neurobasal medium (no Aspartic Acid, no Glutamic Acid, serum free)	Gibco
Tryptose Phosphate Broth	Gibco
Penicillin-Streptomycin	Gibco
Trypsin-EDTA 0.25 %	Gibco
GlutaMAX	Gibco
Gentamicin (50mg/mL)	Gibco
B27 supplement serum free (50x)	Gibco

Table 4: Media compositions for cultivation of mammalian cell lines.

Cell culture medium	Composition of media
DMEM 3+	450 mL D-MEM 50 mL FCS 5 mL L-Glutamine 2 mL Pen-Strep *Stored at 4 °C*
GMEM 4+	450 mL G-MEM 50 mL FCS 4.5 mL Tryptose phosphate 10 mL MEM amino acids 2 mL Pen-Strep *Stored at 4 °C*
Neuron medium	97 mL Neurobasal medium 2 mL B27 1 mL GlutaMAX 1µL Gentamicin (50 mg/mL) *Stored at 4 °C*
LV-medium	500 mL DMEM 50 mL FCS 10 mL HEPES 5 mL Sodium Pyruvat 2.5 mL Pen-Strep *Stored at 4 °C*

Table 5: Media for *E. coli* bacteria cultivation used in this thesis.

LB	85 mM NaCl 0.5 % (w/v) Bacto yeast extract 1 % (w/v) Bactotryptone 1 mM MgSO4 Stored at 4 °C
LB Amp	1 x LB 25 mg/mL Ampicillin Stored at 4 °C
LB ++	1 x LB 20 mM MgSO4 10 mM KCl

2.1.4   Kits

Table 6: List of kits used in this thesis.

Kit	Manufacturer
NucleoBond Xtra Midi	Macherey-Nagel
QIAquick Gel Extraction Kit	Qiagen
QIAquick PCR Purification Kit	Qiagen
Mammalian Transfection Kit	Stratagene
QuantiNova SYBR Green PCR kit	Qiagen
PureLink Genomic DNA Mini Kit	Thermo Fisher Scientific
RealTime-Glo MT Cell Viability Assay System	Promega
RealTime-Glo Annexin V Apoptosis Assay Sytem	Promega
Annexin V-FITC Apoptosis Staining / Detection Kit	Abcam
LIVE/DEAD Fixable Far Red Dead Cell Stain Kit	Thermo Fisher Scientific
LDH release Pierce LDH Cytotoxicity Assay Kit	Thermo Fisher Scientific
Caspase-Glo3/7 Assay System	Promega
Caspase-Glo 8 Assay System	Promega
Caspase-Glo 9 Assay System	Promega

2.1.5   Enzymes

Table 7: List of enzymes used in this thesis

Enzyme	Manufacturer
Restriction Enzymes	New England Biolabs
Q5 DNA Polymerase	New England Biolabs
T4 DNA ligase	New England Biolabs
Alkaline Phosphatase, Calf Intestinal (CIAP)	New England Biolabs
Instant Sticky-End Ligase Master Mix	New England Biolabs
RNase	Macherey-Nagel

2.1.6 Oligonucleotides

All DNA oligonucleotides that were used in this thesis are listed in the appendix and were ordered from Eurofins Genomics.

2.1.7 gRNAs

For generation of knockout cells target sites were selected as followed:

Table 8. List of target sites for gRNAs used in this thesis.

Target gene	gRNA name	Target sequence	Source
PKR	014	GCAACCTACCTCCTATCATG	(Sanjana et al. 2014)
	018	TAATACATACCGTCAGAAGC	(Sanjana et al. 2014)
	019	ATTCAGGACCTCCACATGAT	(Schmidt et al. 2015)
FADD	036	GAGCAGCTCGCGCAGGAGCT	(Schmidt et al. 2015)
CASP8	032	GCTCTTCCGAATTAATAGAC	(Sanjana et al. 2014; Horn et al. 2017)
	033	AGTCGTTGATTATCTTCAGC	(Sanjana et al. 2014)
	034	TCCTTTGCGGAATGTAGTCC	(Sanjana et al. 2014)
CASP10	035	GGGGGTCCAAGATGTGGAGA	(Horn et al. 2017)
	041	GACTGCTGCCCACCCGACAA	(Sanjana et al. 2014)
	042	TCTTCTGCCGTATGATATAG	(Sanjana et al. 2014)
	043	GTAGACCTCCCTAAGTTTCC	(Sanjana et al. 2014)

2.1.8 Cell lines

Table 9: List of Cell lines mentioned in this thesis.

Cell line	Description	Medium	Source
HEK 293T	Human embryonic kidney cells expressing SV40 T-antigen	DMEM 3+	ATTC
HEK 293T Cas9 cl. 5	HEK 293T expressing Cas9	DMEM 3+	Alexander Ghanem
HEK 293T FADD -/-	HEK 293T containing FADD Knockout	DMEM 3+	This work
HEK 293T Casp8 -/-	HEK 293T containing Caspase-8 Knockout	DMEM 3+	This work
HEK 293T Casp8/Casp10 -/-	HEK 293T containing Caspase-8/-10 double Knockout (including in-frame mutations)	DMEM 3+	This work
HeLa	Human cervix carcinoma cells	DMEM 3+	Martin Leverkus Lab, RWTH Aachen
HeLa Casp8 -/-	HeLa containing Caspase-8 Knockout	DMEM 3+	Martin Leverkus Lab, RWTH Aachen
HeLa Casp10 -/-	HeLa containing Caspase-10 Knockout	DMEM 3+	Martin Leverkus Lab, RWTH Aachen
hIPSC derived astrocytes	Human induced pluripotent stem cell derived astrocytes	Astrocyte Medium	Magdalena Götz, LMU
U-87 MG	Human glioblastoma cells	DMEM 3+	Oliver Keppler, LMU

Cell line	Description	Medium	Source
U-251 MG	Human glioblastoma cells	DMEM 3+	Oliver Keppler, LMU
HFF	Human foreskin fibroblasts (primary isolate)	DMEM 3+	Barbara Adler, LMU
N2A	Mouse neuroblastoma cell line	DMEM 3+	ATTC
MEF	Mouse embryonic fibroblasts	DMEM 3+	Christian Wahl-Schott
mESC derived neurons	Mouse embryonic stem cell derived neurons	Neuron medium	Maximilian Eizinger
GL261 new	Mouse glioblastoma cells	DMEM 3+	Christine Engeland, NCT and DKFZ
GL261 moko	Mouse glioblastoma cells	DMEM 3+	Christine Engeland, NCT and DKFZ
B16	Mouse melanoma cells	DMEM 3+	David Anz
MC38	Mouse colon carcinoma cells	DMEM 3+	David Anz
BHK-21	Baby hamster kidney cells	GMEM 4+	ATCC
BSR T7	BHK-21-derived cells expressing T7-pol	GMEM 4+	(Buchholz et al. 1999)
Vero	African green monkey cells	DMEM 3+	ATCC

2.1.9 Antibodies

Table 10: List of primary and secondary antibodies used in this thesis.

Epitope	Host	Dilution	Manufacturer	Order number
Actin (20-33)	Rabbit	1/1000	Sigma-Aldrich	A5060
RABV P (160-5)	Rabbit	1/50000	In house	-
RABV N (S50)	Rabbit	1/25000	In house	-
GFP (D5.1)	Rabbit	1/1000	Cell signaling	2956
PARP	Rabbit	1/1000	Cell signaling	9542
Caspase-9	Rabbit	1/1000	Cell signaling	9502
Caspase-10	Rabbit	1/1000	Cell signaling	9752
Caspase-8 (1C12)	Mouse	1/500	Cell signaling	9746
pPKR (pT446) [E120]	Rabbit	1/1000	Abcam	ab32036
FADD	Rabbit	1/1000	Cell signaling	2782
Rabbit HRP	Goat	1/20000	Jackson ImmunoResearch Laboratories	111-035-045
Mouse HPR	Goat	1/20000	Jackson ImmunoResearch Laboratories	115-1035-003

2.1.10 Plasmids

Table 11: List of Plasmids used in this thesis.

Plasmid	Description	Source
pCS6_YFP-SMASh	Expression plasmid for pCR3 promoter controlled YFP-SMASh	(Chung et al. 2015)
pLV_guide_hyg	Plasmid for Lentivirus containing hygromycin resistance	Alexander Ghanem
pLV_guide_zeo	Plasmid for Lentivirus containing zeocin resistance	Alexander Ghanem
pLV_guide_Hyg_032	Plasmid for Lentivirus containing guide RNA for CASP8 (032), hygromycin resistance integrated	This work
pLV_guide_Hyg_033	Plasmid for Lentivirus containing guide RNA for CASP8 (033), hygromycin resistance integrated	This work
pLV_guide_Hyg_034	Plasmid for Lentivirus containing guide RNA for CASP8 (034), hygromycin resistance integrated	This work
pLV_guide_Hyg_041	Plasmid for Lentivirus containing guide RNA for CASP10 (041), hygromycin resistance integrated	This work
pLV_guide_Hyg_042	Plasmid for Lentivirus containing guide RNA for CASP10 (042), hygromycin resistance integrated	This work
pLV_guide_Hyg_043	Plasmid for Lentivirus containing guide RNA for CASP10 (034), hygromycin resistance integrated	This work
pLV_guide_Zeo_035	Plasmid for Lentivirus containing guide RNA for CASP10 (043), zeocin resistance integrated	This work
pLV_guide_Zeo_036	Plasmid for Lentivirus containing guide RNA for FADD (036), zeocin resistance integrated	This work
pΔ8.9	lentiviral packaging plasmid	A. Lepier, LMU
pMD2-VSV-G	Expression plasmid for VSV G	Alexander Ghanem
pTIT-G	T7-Pol and EMCV IRES dependent expression of RABV G	(Finke et al. 2003)
pTIT-L	T7-Pol and EMCV IRES dependent expression of RABV L	(Buchholz et al. 1999)
pTIT-M	T7-Pol and EMCV IRES dependent expression of RABV M	(Finke et al. 2003)
pTIT-N	T7-Pol and EMCV IRES dependent expression of RABV N	(Buchholz et al. 1999)
pTIT-P	T7-Pol and EMCV IRES dependent expression of RABV P	(Buchholz et al. 1999)
pCAGGS	Eukaryotic expression vector with chicken-β-actin promoter	(Niwa et al. 1991)
pCAGGS SMASh-P	Expression plasmid for SMASh-P	This work
pCAGGS YFP-SMASh	Expression plasmid for SMASh-YFP	This work
pCAGGS YFP-SMASh prot stop	Expression plasmid for YFP-SMASh containing a stop codon after protease domain	This work

Plasmid	Description	Source
pCAGGS YFP-SMASh heli stop	Expression plasmid for YFP-SMASh containing a stop codon after helicase domain	This work
pCAGGS YFP-SMASh-PEST dheli	Expression plasmid for YFP-tt1	This work
pCAGGS YFP-SMASH-PEST delta heli NS4A1-20	Expression plasmid for YFP-tt2	This work
pCAGGS_YFP-SMASh_TautzNS3-180-PEST	Expression plasmid for YFP-tt4	This work
pCAGGS_YFP-SMASh_TautzNS3-213-PEST	Expression plasmid for YFP-tt3	This work
pSAD-T7-HH-L16-SC	Full-length L16 cDNA rescue construct	(Ghanem et al. 2012)
pSAD-T7-HH-G-eGFP-SC	Full-length L16 cDNA rescue construct containing an extra transcription unit in between G and L with an N/P gene border followed by eGFP	(Ghanem et al. 2012)
pSAD_T7-HH_P SMASh_G_eGFP_SC	Full-length SAD eGFP cDNA rescue construct containing a C-terminal SMASh-tag at the P gene	(Masterthes is V. Pfaffinger 2016)
pSAD T7-HH_YFP-SMASh_SC	Rescue plasmid for SAD YFP-SMASh	(Masterthes is V. Pfaffinger 2016)
pSAD T7-HH_YFP-SMASh S139A_SC	SAD YFP-SMASh rescue construct containing indicated mutation	This work
pSAD_T7-HHRz_YFP-SMASh-LTHP-AAAA_SC	SAD YFP-SMASh rescue construct with LTHP motif replaced by AAAA	This work
pSAD_T7-HHRz_YFP-SMASh-LTHP-AAHP_SC	SAD YFP-SMASh rescue construct with LTHP motif replaced by AAHP	This work
pSAD_T7-HHRz_YFP-SMASh-LTHP-LTAA_SC	SAD YFP-SMASh rescue construct with LTHP motif replaced by LTAA	This work
pSAD_T7-HHRz_YFP-SMASh-LTHP-LTHA_SC	SAD YFP-SMASh rescue construct with LTHP motif replaced by LTHA	This work
pSAD_T7-HHRz_YFP-SMASh-KIDT-AAAA_SC	SAD YFP-SMASh rescue construct with KIDT replaced by AAAA	This work
pSAD_T7-HH_dG_eGFP_L-SMASh_SC	SAD ΔG eGFP rescue construct containing C-terminally SMASh-tagged L	This work
pSAD_T7-HH_eGFP_P-tt1_SC	SAD eGFP rescue constructs containing C-terminally tt1-tagged P	This work
pSAD_T7-HH_N-tt1_SC	SAD L16 rescue construct containing C-terminally SMASh-tagged N	This work
pSAD_T7-HHRz_DG_eGFP-T2A-NLS-CRE_N-tt1_SC	SAD ΔG eGFP-Cre rescue construct containing C-terminally tt1-tagged N	This work

2.1.11 Recombinant viruses

The following recombinant viruses were generated from cDNA by reverse genetics (Ghanem et al. 2012).

Table 12: List of recombinant viruses used in this thesis.

Virus	If not rescued in this thesis, kindly provided by
LV guide_Hyg_014	Alexander Ghanem
LV guide_Hyg_018	Alexander Ghanem
LV guide_Hyg_019	Alexander Ghanem
LV guide_Hyg_032	
LV guide_Hyg_033	
LV guide_Hyg_034	
LV guide_Hyg_041	
LV guide_Hyg_042	
LV guide_Hyg_043	
LV guide_Zeo_035	
LV guide_Zeo_036	
SAD eGFP	
SAD P-SMASh	
SAD eGFP P-SMASh	
SAD N-SMASh	
SAD YFP-SMASh	
SAD YFP-SMASh S139A	
SAD SMASh	Yassine Haddad
SAD SMASh-ΔCS	Yassine Haddad
SAD SMASh-YFP	Yassine Haddad
SAD YFP-SMASh-LTHP-AAAA	
SAD YFP-SMASh-LTHP-AAHP	
SAD YFP-SMASh-LTHP-LTAA	
SAD YFP-SMASh-LTHP-LTHA	
SAD YFP-SMASh-KIDT-AAAA	
SAD ΔG eGFP L-SMASh	
SAD eGFP P-tt1	
SAD N-tt1	
SAD ΔG eGFP-T2A-CRE N-tt1	
SAD L16 high DI	Alexander Ghanem
SAD TR high DI	Alexander Ghanem
SAD ΔG eGFP N-SMASh	
SAD ΔG eGFP SMASh-L	

2.1.12 Laboratory equipment

Table 13: List of laboratory equipment used in this thesis.

Equipment	Name	Manufacturer
Incubators	Certomat BS-1	Sartorius
	Cell culture incubator	Sanyo
	37 °C incubator	Heraeus
Centrifuges	Centrifuge 5417 R	Eppendorf
	Centrifuge 5804 R	Eppendorf
	Centrifuge 5418	Eppendorf
	Varifuge 3.0R	Heraeus
	Table centrifuge Z160-M	Hermle
Microscopes	Light micoscrope TMS	Nikon
	UV-Light microscope IX71	Olympus
Freezers	Premium No Frost	Liebherr
	-80 °C II Shin	Nunc
	Forma ULT deep freezer	Thermo Scientific
Miscellaneous	BD FACS Lyrics	BD Bioscience
	Chemiluminescence developing system (Fusion FX7)	Vilber-Lourmat
	Luminometer Centro LB 960	Berthold
	Magnetic stirrer/heater	VELP Scientifica
	pH-meter	VWR International
	PIPETBOY acu	IBS
	Pipettes (2/10/200/1000 µL)	Eppendorf; Gilson
	Polyacrylamid gel electrophoresis system	Peqlab
	Agarose gel electrophoresis system	Peqlab
	Roller mixer SRT2	Stuart
	Semi-Dry blotting system	Peqlab
	Spectrophotometer Nanodrop ND-1000	Peqlab
	Thermocycler T3	Biometra
	Thermomixer 5436	Eppendorf
	Thermostated hot-block 5320	Eppendorf
	Semi-Dry-Blotter	Peqlab

2.1.13 Laboratory consumables and miscellaneous

Table 14: Laboratory consumables and miscellaneous used in this thesis.

Consumables	Manufacturer
Lipofectamine® 2000	Thermo Fisher Scientific
FITC Anti-Rabies Monoclonal Globulin (#800-092)	Fujirebio Diagnostics
WesternBright ECL Spray	Advansta
Nitrocellulose membrane (0.45 µm)	BioRad
Cell culture plates (6-well, 24-well, 48-well, 96-well)	Sarstedt
1.5/2.0 mL reaction tubes	Eppendorf

Consumables	Manufacturer
15/50 mL falcons	Sarstedt
Cell culture flasks (T25/T75)	Falcon
Pierce™ Centrifuge Columns, 10 mL	Thermo Fisher Scientific
Precision Plus Protein™ Standard	Biorad
1 kb DNA ladder	New England Biolabs
PCR Marker	New England Biolabs
LIVE/DEAD™ Fixable Far Red Dead Cell Stain Kit	Thermo Fisher Scientific
Annexin V Pacific Blue™ Ready Flow Conjugate	Thermo Fisher Scientific

2.2 Methods

2.2.1 Plasmid construction

2.2.1.1 Polymerase Chain Reaction (PCR)

As a first step of the generation of a new plasmid, specific DNA sequences were amplified *in vitro* by performing a Polymerase Chain Reaction (PCR). Thereby, multiple amplification cycles were carried out with a heat resistant DNA polymerase. After denaturation of the dsDNA at 98 °C, annealing of specific primers to the free 3'-OH-end of the DNA template was conducted at primer dependent temperatures (usually 50-60 °C), followed by elongation at 72°C. Using those steps, the complementary strand of the original template DNA was synthesized.

The standard PCR reaction was prepared in 50 µL total volume as follows:

Table 15: Components of standard PCR reaction.

Component	volume
Template DNA	1 µL (1pg-10 ng)
Forward Primer (10 µM)	2.5 µL
Reverse Primer (10 µM)	2.5 µL
dNTPs (19 mM)	1 µL
Q5 buffer (5x)	10 µL
Q5 high GC buffer (5x)	10 µL
Q5 High-Fidelity DNA Polymerase	0.5 µL
ddH20	22.5

The reactions were carried out in a thermocycler with heated lid. Standard PCR program was conducted as follows:

Table 16: Standard PCR settings.

Step	Time	Temperature	Cycles
Initiation	30 sec	98°C	1
Denaturation of dsDNA Template	30 sec	98°C	
Primer annealing	30 sec	55 °C	35
Elongation/Synthesis of complementary DNA	20 sec/kb	72 °C	
Final Extension	2 min	72 °C	1
Cooling	∞	4 °C	

If two fragments had to be combined and inserted into the vector, an overlap extension PCR was performed. Therefore, both fragments were amplified individually. The reverse primer of the first fragment, as well as the forward primer of the second fragment contain overlapping sequences. In the following overlap extension PCR both fragments were used as template in equimolar proportion and outer primer for annealing. In order to allow annealing of both fragments in first place, five initial cycles were conducted at the beginning with an annealing temperature 5°C above the determined melting temperature of the primers. This was followed by 25 cycles with standard temperatures as described in the standard PCR.

Table 17: PCR settings for overlap extension PCR.

Step	Time	Temperature	Cycles
Initiation	30 sec	98°C	1
Denaturation of dsDNA Template	30 sec	98°C	5
Primer annealing	30 sec	55 °C + 5 °C	
Elongation/Synthesis of complementary DNA	20 sec/kb	72 °C	
Denaturation of dsDNA Template	30 sec	98°C	25
Primer annealing	30 sec	55 °C	
Elongation/Synthesis of complementary DNA	20 sec/kb	72 °C	
Final Extension	2 min	72 °C	1
Cooling	∞	4 °C	

At the end, amplificated PCR products were validated by agarose gel electrophoresis and purified using the QIAquick® PCR Purification Kit according to the supplier´s manual. Final elution was done in 35 µL ddH2O.

2.2.1.2 Agarose gel electrophoresis

For validation of the correct PCR product, or to separate DNA bands after digestion with restriction enzymes, an agarose gel electrophoresis was performed. Therefore, a 1 % (w/v) agarose gel was prepared using 1 x TAE buffer. In case of DNA products < 500 bp, a 2 % agarose gel was prepared. DNA was mixed with Gel Loading Dye (6X) and loaded into the pocket of the gel. For determination of the size, either 1 kb marker or PCR marker was loaded in a separate pocket. Electrophoresis was conducted at 120 V for 30-60 min in a chamber with 1 TAE and 0.075 % ethidium bromide as running buffer. Subsequently, ethidium bromide-stained DNA was visualized by UV-light, and images acquired using the BioRad GelDoc

system. If DNA fragments were needed further for ligation, fragments were excised from the gel and purified by the QIAquick Gel according to the supplier´s manual.

2.2.1.3 Restriction enzyme digestion

After amplification of the specific DNA sequence, the purified PCR product and the respective vector plasmid were separately digested by restriction endonucleases from New England Biolabs (NEB) according to the manufacturer's protocol. Incubation time and temperature were dependent on each enzyme. For each digest, 5- 10 µg of the product or 2 µg of vector DNA was used. After digestion the vector was further incubated with 1 µL of the alkaline phosphatase Calf intestine phosphatase (CIP) for 20 min at 37 °C to circumvent re-ligation events. Then, digested DNA was separated and purified via agarose gel electrophoresis.

In order to validate successful cloning, analytical check digest was performed. Therefore, 1 µL of the DNA of a midi preparation was incubated with 0.1 µL of respective enzymes and buffer at corresponding temperature for one hour. Then, digest pattern was analyzed by agarose gel electrophoresis.

2.2.1.4 Ligation of DNA fragments

Restriction enzyme digestion of DNA insert and vector was followed by ligation of the respective fragments. In a 10 µL standard reaction, 1 µL of the T4 DNA Ligase from NEB was mixed with 2 µL Ligase Buffer (10x), 7 µL digested and purified insert and 1 µL linearized and purified vector DNA. Then, the reaction mix was incubated 2 hours at RT or overnight at 4 °C. In a next step, the complete ligation mix was used for transformation into chemical competent *E. coli* bacteria. Due to the resistant gene within the plasmid, bacteria were plated on LB plates containing the corresponding antibiotic and incubated over night at 37 °C. Then, single colonies were picked, cultivated, and analyzed in regard of correct insertion and DNA sequence.

2.2.1.5 Transformation of plasmid DNA into competent bacteria

For transformation of a ligation mix or plasmid, 50 µL of chemically competent *E. coli XL-1 blue* were thawed on ice. Then, either the whole ligation mix or 1 µL of a purified plasmid was added and incubated for 20 min on ice. After the subsequent heat shock at 42 °C for 2 min, bacterial cells were chilled on ice for 2 min and supplemented with 300 µL LB++ medium for shaking at 37 °C for 30 min. After this step, bacteria suspension was plated on selective LB plated containing the respective antibiotic. For SAD rescue plasmids and pCAGGS expression plasmids, 100 µg/mL ampicillin was used. LB plates were then incubated over night at 37 °C.

2.2.1.6   Mini preparation of plasmid DNA from bacteria

Mini preparation of plasmid DNA was performed in order to analyze different plasmid clones in regard of correct ligation of vector and insert. Therefore, single colonies were picked from the LB plate and transferred into 1 mL selective LB medium. After overnight shaking at 37 °C with 800 rpm, bacterial cells were harvested by centrifugation (14 000 rpm, 1 min). Then, the pellet was resuspended in 200 µL Flexi I, followed by 5 min incubation with 200 µL Flexi II to lyse the bacterial cells. In a third step, 200 µL Flexi III was added and suspension was incubated for 5 min on ice for neutralization. After this, centrifugation of the suspension was conducted for 7 min at 14000 rpm to separate plasmid DNA and cell debris as well as denatured proteins. The supernatant, which contains the plasmid DNA, was supplemented with 400 µL isopropanol for DNA precipitation. After an additional centrifugation step for 7 min at 14000 rpm, the supernatant was discarded, whereas the pellet with the plasmid DNA was dried at RT and solubilized in 50 µL ddH$_2$O. Then, plasmids were validated by check digest and agarose gel electrophoresis. Clones with correct digest pattern were used for midi preparation.

2.2.1.7   Midi preparation of plasmid DNA from bacteria

For midi preparation single colonies were picked from the selective LB plate and transferred into 50-100 mL LB medium containing the according antibiotic. After shaking at 37 °C overnight, bacterial cell suspension was harvested by centrifugation for 20 min at 3500 rpm at 4 °C. After discarding the supernatant, the DNA was extracted from the bacteria in the pellet using the NucleoBond® Xtra Midi/Maxi Kit. All steps were performed according to the manufacturer's protocol. In brief, bacterial cells were resuspended in the resuspension buffer containing RNAse. After incubation with lysis buffer, the neutralization buffer was added. Then, the suspension was transferred in a column containing a filter, which was earlier equilibrated using the equilibration buffer. Columns and filters were included in the kit. After loading with the suspension, the column with filter was washed with the equilibration buffer. Then, the filter was removed and discarded and an additional washing step using the washing buffer conducted. DNA was eluted from the column and precipitated. After a further washing step with 70 % ethanol, the DNA was dissolved in 200-400 µL ddH$_2$0 and DNA concentration was determined using UV-Vis Spectrophotometer Nanodrop ND-1000.

2.2.1.8   Sequencing of DNA

Plasmids were sequenced by Sanger Sequencing, which was conducted by GATC Biotech. Therefore, sequence specific primers and the plasmid DNA or purified DNA fragments were diluted according to the GATC Biotech guidelines. Sequence was analyzed with SnapGene 2.6.2.

2.2.2 Cell culture

If not otherwise mentioned, adherent mammalian cell lines were cultivated at 37 °C and 5 % CO_2 in a T25 or T75 flask with appropriate growth media. Cells were monitored every 3-4 days and split depending on their growth using Trypsin with 0.25 % EDTA. The standard splitting ratio was 1:10 but could vary between 1:4 to 1:15. If required, antibiotics were added every second passage for selection.

For experiments, cells within a flask showing a confluent monolayer were detached with Trypsin/EDTA, resuspended in growth media, and seeded into wells. Thereby, the cell number was calculated based on the estimated cell number per flask: T25 flask: 3.1×10^6; T75 flask: 9.4×10^6.

If not otherwise mentioned cells were seeded as followed:

Table 18: Estimated cell number per well.

Well	Number of cells	Volume of medium
6 well	1.2×10^6	2 mL
12 well	5×10^5	1 mL
24 well	2.5×10^5	500 µL
48 well	1.3×10^5	200 µL
96 well	4.5×10^4	100 µL

Wells with seeded cells were incubated at 37 °C and 5 % CO_2 overnight.

2.2.3 Freezing and thawing of cells

All cells were stored for long term purposes in liquid Nitrogen. Therefore, a confluent T25 flask was trypsinized and resuspended in 5 mL media containing 10 % DMSO. Suspension was aliquoted in cryotubes and frozen to –80 °C in NALGENE Mr. Frosty freezing container, which was filled with isopropanol to slowly freeze the cells by a rate of -1 °C /min. After a minimum of 24 hours, the cryotubes were transferred to a N_2-storange tank. To ensure proper freezing, one aliquot was thawed as control the next day. For large-scale freezing of cells, confluent T75 flasks were taken for freezing accordingly.

For thawing, cells were thawed at RT, mixed with 9 mL of fresh media in a 50 mL falcon. DMSO was removed by a centrifugation step at 4°C and 1000 rpm for 10 minutes. Subsequently, the cell pellet was resuspended in fresh media and transferred to a T25 flask or respective dish.

2.2.4 Microscopic analysis

Cells were analyzed with UV- or transmission light using a fluorescence microscope (Olympus IX 71). Thereby, equal settings were applied for acquiring images within each experiment.

2.2.5 Transfection and infection

For transfection of mammalian cells, cells were grown overnight to a confluence of 60 %. Transfection was performed with 2.5 µL Lipofectamine 2000 per µg DNA. Both, transfection reagent and plasmid DNA were individually incubated in respective media without supplements for 5 min at RT. After subsequent pooling, solution was incubated further for 20 minutes, before it was dropped on seeded cells.

For infection experiments, cells were grown overnight to a confluence of 60-80 %. Virus preparation was diluted in growth media and dropped on cells with a specific multiplicity of infection (MOI). Thereby, the required volume of the virus preparation was calculated as follows:

$$volume\ (virus) = \frac{MOI\ x\ cell\ number}{concentration\ (virus)}.$$

2.2.6 Generation of recombinant rabies viruses

2.2.6.1 Virus rescue

For generation or recombinant RABVs BSR T7 cells were used as standard cells. Cells were seeded in 6 well plates and incubated overnight at standard conditions. Then, cells were transfected with 10 µg viral cDNA, together with the helper plasmids pTIT-N (5 µg), pTIT-P (2.5 µg) and pTIT-L (2.5 µg). Thereby, transfection was performed with calcium phosphate using the Mammalian Transfection $Ca_3(PO_4)_2$ Kit. Transfection was carried out according to the manufacturer's protocol. Therefore, medium was changed one hour before transfection to DMEM without supplements and again changed 3.5 hours post transfection to GMEM 4+ media. After three days, supernatant was transferred to fresh cells, whereas fresh medium was added to transfected cells. Cells were incubated for three additional days. Then, transfected cells were fixed with 80 % acetone and stained with Centocor, a FITC-conjugated antibody against the RABV nucleoprotein, whereas cells with the passaged supernatant were transferred in a T25 flask and incubated for additional three days. This step was followed by harvest of the rescue supernatant by centrifugation at 1800 rpm for 10 min at 4 °C to remove the cell debris. Rescue supernatant aliquots were stored at -80 °C and titrated the next day.

In case of recombinant SAD ΔG eGFP (SAD-G) viruses, BSR T7 derived $MG_{on}139$ cells were used and transfected as described above with the viral cDNA and the helper plasmids N, P and L. However, the helper plasmid pTIT-G (2 µg) was included in first place and additional transfection of pTIT-G was done after day one and two post $Ca_3(PO_4)_2$ transfection using the FuGENE HD transfection kit. Thereby, a similar protocol was applied as for Lipofectamine 2000. Moreover, expression of RABV M and G was induced by

addition of 1 μL doxycycline per mL media. Cells were monitored each day via fluorescence microscopy and harvested as described above as soon as cells were infected. Then, virus rescue was titrated on BSR T7 cells.

2.2.6.2   Virus stock production

For virus stock production a confluent T25 flask of BSR T7 cell was split 1:3 and infected with virus rescue at a MOI of 0.01. First harvest was taken 3 days after infection including the addition of fresh media onto cells, whereas a second harvest was conducted after additional four days. During each harvest, the whole supernatant was collected, centrifuged at 1800 rpm for 10 min at 4 °C to get rid of the cell debris, aliquoted and stored at –80°C. After a minimum storage of one night, virus titer was determined by titration.

For production of SAD ΔG eGFP (SAD-G) virus stocks, $MG_{on}139$ cells were infected with a MOI of 0.1. Six hours later medium was replaced by fresh one supplemented with 1 μL doxycycline per mL media. Supernatant was harvested at day 3 and day 7 post infection, cleared of cell debris and subjected to ultracentrifugation for further enrichment of viral particles. For this purpose, TEN buffer containing 20 % sucrose was first provided in ultracentrifugation tubes, onto which the supernatant was then carefully layered. Viral particles were pelleted by centrifugation for 2 hours at 24000 rpm and 4°C. Then, supernatant was discarded and the pellet resuspended in OptiMem overnight at 4°C while constantly shaking, followed by aliquoting, and storing at -80°C. The next day virus stocks were titrated on BSR T7 cells.

2.2.6.3   Titration of virus preparations

The concentration of viral particles in a virus preparation or supernatant was determined by titration. If not otherwise mentioned BSR T7 cells were used for this purpose. A confluent T25 flask of cells was resuspended in 30 mL fresh media, seeded in a 96 well plate and incubated for at least 2 h at standard conditions. Virus preparations or supernatants, that were stored at -80 °C, were thawed, followed by preparation of a serial dilutions with seven 1:10 dilutions in GMEM media without supplements. Then, 100 μL of each dilution was added to the 96 well plate in duplicates. After allowing virus spread for 2 days at 37 °C and 5 % CO_2, cells were stained with Centocore. Therefore, media was removed, cells were washed with PBS, fixed with 70 % acetone at 4 C for 20 min and incubated with a PBS suspension containing Centocore for 2 h at 37 °C. Of note, in case of RABV viruses lacking the G (SAD ΔG), virus spread was allowed for three days. After an additional washing step with PBS, fluorescent foci were counted using the UV microscopy Olympus IX71. Based on those counts, focus forming units per mL (ffu/mL) were calculated and served as viral titer.

2.2.7 Virus growth curve

Growth curves were done on BSR T7 cells. Therefore, a confluent T25 flask was split 1:3 into a new T25 flask and allowed to attach for at least 2 hours at 37 °C and 5 % CO_2. For multistep growth analysis cells were infected with the respective recombinant and wildtype viruses using a MOI of 0.01 and incubated for 3 - 5 hours, followed by supernatant replacement with fresh GMEM 4+ media. After additional 30 minutes, the first 100 µL sample was harvested and stored at −80 °C. Additional harvests followed at 24 h, 48 h, 72 h and 96 h post infection or indicated timepoints. Then, all samples were titrated on BSR T7 cells in a 96 well plate to determine the virus concentration at each timepoint.

2.2.8 Killing assay

Standard killing assay was performed in HEK 293T cells. Therefore, cells were seeded into 24 well plate, and infected the following day with an MOI of 3 with respective SMASh viruses. Mock treated cells served as well as cells infected with SAD eGFP or SAD L16 were used as negative controls. After 24 hours, 3 µM of the HCV NS3 inhibitor asunaprevir (ASV) or danoprevir (DNV) was added. If not otherwise mentioned, cells were analyzed additional 24 hours later via microscopy and lysed for further Western blot analysis.

2.2.9 Generation of Knockout cells

2.2.9.1 Generation of lentiviral particles

Knockout cells were generated by using lentiviruses as vector for gRNA delivering. For lentiviral vector production, a lentivirus vector plasmid containing the corresponding gRNA was generated. Therefore, respective forward and reverse primers were annealed at 95 °C, digested with BsmBI and inserted into the pLV_guide_hyg or pLV_guide_zeo vector containing an antibiotic resistance. As standard plasmid, the vector with hygromycin resistance was used. For double knockout, different vectors were taken for each gene. Then, selection was conducted accordingly. After validation of correct gRNA insertion, 1.25 µg of each plasmid was transfected with Lipofectamine 2000 in HEK 293T cells in a 6 well plate together with 0.5 µg of the envelope plasmid pMD2-VSV-G and 1.5µg of pΔ8.9, which is needed for virus packaging. Six hours post transfection, medium was replaced by LV-medium. After incubation for three days at standard conditions, lentiviral particles were harvested. Therefore, supernatant was cleared of cell debris by centrifugation at 4 °C and 1800 rpm for 5 min. Then, supernatant was filtered through a 0.45 µm filter to allow the diffusion of lentivirus particles, aliquoted and stored at -80 °C. Of note, for the following transduction the concentration of viral particles was not determined.

2.2.9.2 Lentiviral transduction of mammalian cells

For the generation of knockout cells HEK 293T Cas9 cells were used as parental cells in this thesis. This cell line was established and validated in regard of functional Cas9 expression previously by Alexander Ghanem. Cells were seeded in 24 wells and infected with 500 µL or 50 µL Lentivirus suspension. Additionally, a negative control without any lentiviruses was included. Twenty-four hours post transduction cells were diluted in a 1:20 ratio and transferred into a 6 well, where they were treated with 10 µL hygromycin per mL media to select for successful transduction. Cells were incubated for 6 days with selective media under standard conditions.

2.2.9.3 Selection of monoclonal cells

To obtain monoclonal knockout cells, a single cell dilution was conducted. Therefore, cells were serially diluted to reach an estimated concentration of 10^1, 10^0 and 10^{-1} cells per well. Again, cells were grown in selective media containing hygromycin. Every day, wells were screened for single colonies using a light microscopy. Approximately after 20 days, or when cells grew to confluency, colonies were transferred into 24 wells. Thereby, fresh media was supplemented again with hygromycin. Four days later, cells were transferred further into 12 wells, whereby 10 % were lysed and used for Western blot analysis to check the expression pattern for respective knockout. After gaining confluent 12 or 6 wells, one part of the cells was frozen and stored at -80 °C for validation. The other part was used for extraction of genomic DNA.

2.2.9.4 Validation of Knockout cells

As mentioned before, knockout cells were checked for absence of respective protein by Western blot analysis. Moreover, knockout cells were validated by illumina sequencing, which was conducted by the group of Veit Hornung. For this purpose, genomic DNA was extracted from each knockout clone using the Genomic DNA Purification Kit in accordance with the manufacturer's instructions. Then, genomic regions containing the knockout were amplified by two different PCRs. For the first PCR a primer pair (indicated in blue as P1 in Figure 10) containing an overlapping sequence to the genomic DNA as well as an additional sequence that overlap partially with a barcode primer sequence was used. For the second PCR, primers (indicated in green as P2 in Figure 10) of the barcode sequencing set 1 (as defined by AG Hornung) were used. Those Primer sequences were provided by AG Hornung. Each primer of the primer set contains a specific barcode sequence. Due to the individual combination of barcode primer pairs for each genomic DNA, sequence could be assigned to specific knockout clones during analysis.

For each clone and each locus, a unique combination of specific forward and reverse barcode primer (P2) were used. Then, correct product size was validated by agarose gel electrophoresis using 3 µL of the PCR

product. Ten µL of each barcode PCR was used without further purification and pooled for sequencing. At the end, sequencing results were analyzed using the webtool OutKnocker 1.31.

Figure 10: Schematic illustration of sequencing primer pairs
P1: Primer pair 1 (indicated in blue), that is used for first PCR binding to genomic DNA (indicated in black) and containing overlapping sequence with P2. P2: Primer pair 2 (indicated in green), that is used for second PCR binding to P1. Those primers contain an individual barcode at the non-overlapping end indicated by an asterisk. For each knockout clone, a unique combination of P2 is used.

2.2.10 Flow cytometry analysis

For analyzation of apoptotic cells, flow cytometry analysis was done. Therefore, HEK 293T cells were seeded in 24 well and directly infected with SAD eGFP or SAD eGFP P-SMASh with a MOI of 3. Mock treated cells served as negative control, whereas cells treated with 1 µM staurosporine at timepoint of infection were used as positive control. Twenty-four hours later, cells were treated with 3 µM DNV or DMSO for 4 hours.

Then, cells from the supernatant were harvested by centrifugation of 3000 rpm for 5 minutes at RT and pooled with trypsinized cells in the well. Cells were washed with PBS, followed by another centrifugation step and resuspended in 500 µL Annexin V buffer. In parallel, a dead cell control was prepared by boiling PBS cell solution at 60 °C for 10 minutes. After respective centrifugation, cells were resuspended as well in 500 µL Annexin V buffer. For staining 0.5 µL of freshly prepared live/dead staining solution was added to the cells and incubated for 15 minutes without light. Then, one drop of pacific blue coupled Annexin V dye was added and incubated for further 15 minutes in the dark at 25 °C in accordance with the manufacturer's instructions. Additionally, single staining controls were performed. This was followed by a centrifugation step at 3000 rpm, cells were fixed by 4 % PFA in PBS overnight at 4 °C. At the end, cells were subjected to the BD FACS Lyrics for analyzation. Results were evaluated later by the software FlowJo 10.6.2.

2.2.11 Western blot analysis

For Western blot analysis, the procedures described in the following were carried out.

2.2.11.1 Denaturing polyacrylamide gel electrophoresis (SDS-PAGE)

Sodium dodecyl sulfate polyacrylamide gel electrophoresis (SDS-PAGE) was used for separation of proteins according to their molecular weight. Therefore, cells in culture dishes were lysed in an appropriate volume of SDS sample buffer which was dependent on the culture dish (Table 19).

Table 19: Volume of SDS sample buffer per well.

Culture dish	Volume of SDS sample buffer
6 well plate	1 mL
12 well plate	750 µL
24 well plate	500 µL
48 well plate	250 µL
96 well plate	100 µL

Before loaded in separate pockets on a Bis-Tris polyacrylamide gel, which was prepared in advance, samples were heated for 10 minutes at 95 °C. The Bis-Tris polyacrylamide gel is composed of a 6 % stacking gel in the upper part and a 10 % separating gel below. SDS-PAGE was conducted at 35 V overnight or at 130 V for 3 hours at constant cooling. Thereby, MOPS was used as running buffer. At the end, the gel was immediately used for Western blotting.

2.2.11.2 Western blotting

After separation of proteins by gel electrophoresis, proteins were transferred from the gel to a nitrocellulose membrane by Western blotting. For this purpose, the Peqlab semi-dry blotting system having the cathode at the bottom and the anode at the lid and the Xtra-dry blotting buffer was used. Three layers of Whatman paper on the bottom, followed by the nitrocellulose membrane above, the Bis-Tris gel with the separated proteins and finally three more layers of Whatman paper as the top layer were placed in the blotting system. All components have previously been soaked or washed in Xtra-dry buffer. Then, electroblotting was conducted at 400 A per gel for 1 hour. Subsequently, the membrane was blocked with 5 % milk in TBS-t or 2.5 % BSA in TBS-T for another hour in order to circumvent unspecific antibody binding. This step was followed by membrane washing and incubation with the in TBS-T diluted primary antibody at 4 °C over night. After three 10 minutes washing steps with TBS-T, the membrane was incubated with the secondary antibody TBS-T suspension at RT for 2 hours. Again, three 10 minutes washing steps were applied, before the blot was subjected to immunodetection.

2.2.11.3 Immunodetection

Due to the conjugation of the secondary antibody to a horseradish peroxidase, immunodetection was done by incubation of the membrane with the Clarity Western ECL Blotting Substrates. The chemiluminescent signal was subsequently monitored by the Fusion FX7 system (Viber Lourmat). Thereby, exposure time was automatically applied by the system. If not suitable, additional images of the Western blot with adjusted exposure time were acquired. If needed, the membrane was washed and incubated with an additional primary antibody as described above.

2.2.12 Caspase activity assay

In order to determine relative caspase activity, Promega Caspase-Glo 3/7, Caspase-Glo 8, and Caspase-Glo 9 assay system respectively, was used according to the manufacturer's protocol. A killing assay was conducted in advance: HEK 293T cells were seeded in a white-walled 96 well plate and infected with SAD P-SMASh with a MOI of 3. Mock treated cells as well as SAD L16 infected cells served as control. Moreover, a control without any cells, but only medium was included. Twenty-four hours later 3 µM DNV or DMSO was added to the cells and incubated for another 2 hours. Then, substrate for measuring caspase activity was added in a 1:1 ratio and incubated at RT for 45 min. Subsequently, luminescence of each sample was measured by a Berthold Luminometer Centro LB 960. In order to obtain the relative caspase activity, the measured value was normalized to mock undergoing DMSO treatment.

2.2.13 Real time Annexin V assay

In order to analyze kinetic of apoptosis upon SMASh and inhibitor binding, RealTime-Glo Annexin V Apoptosis assay from Promega was used according to the manufacturer's protocol. In brief, HEK 293T cells were previously seeded in a white-walled 96 well plate and infected with SAD L16 and SAD P-SMASh at a MOI of 3. Mock cells were used as negative control, whereas staurosporine served as positive control and was added at the same time as the HCV NS3 inhibitor at 24 hours post infection. At this timepoint, the reaction reagent containing the Annexin V NanoBiT Substrate, Annexin V-SmBiT and Annexin V-LgBiT was added to the cells in a 1:1 ratio. In case of a cell undergoing apoptosis, phosphatidyl serine is exposed to its surface, allowing Annexin V binding, and therefore colocalization and functioning of the NanoLuc Luciferase components SmBiT and LgBiT. Luminescence was measured at indicated timepoints using the Berthold Luminometer Centro LB 960. Then, relative Annexin binding was calculated for each timepoint by normalizing to DMSO treated mock cells.

2.2.14 Real time viability assay

RealTime-Glo MT Cell Viability assay from Promega was used to determine cell viability over time. Therefore, HEK 293T cells were previously seeded in a white-walled 96 well plate and infected with indicated viruses at MOI of 3. The HCV NS3 inhibitor DNV was either added directly at infection or 24 hours post infection. At the same time as inhibitor was given, reaction reagent containing the NanoLuc Luciferase and its substrate was added in a 1:1 ratio to the cells. Then, luminescence was monitored at indicated timepoints by Berthold Luminometer Centro LB 960. The relative cell viability was calculated by normalization to mock cells, that were treated with DMSO.

2.2.15 Resazurin assay

For determination of cell viability at one single timepoint, AlamarBlue HS Cell Viability Reagent was used. Therefore, 10 % of the ready-to-use resazurin-based solution was added to the supernatant of the cells and incubated at 37 °C until change of color could be notified (usually 10-30 minutes). Medium without cells served as control. In case the resazurin assay was not conducted in 96 well plate, 100 μL of the supernatant was transferred into a 96 well plate. Then, fluorescence was measured using the Berthold Luminometer Centro LB 960 with an excitation wavelength of 560 nm and an emission of 590 nm. To obtain the relative viability, the medium control value was first subtracted and then normalized to mock treated with DMSO. If mentioned in respective experiment, cells were lysed in SDS sample buffer and subjected to Western blot analysis afterwards.

2.2.16 Lactate dehydrogenase (LDH) assay

In order to validate whether cells undergo a lytic cell death, a LDH assay was performed according to the manufacturer's instructions using the Pierce LDH cytotoxicity assay kit. As a standard, experiment was conducted in 96 well plate. At desired timepoint, 50 μL of the supernatant was taken and mixed in 1:1 ratio with LDH bottom in a new 96 well plate. Thereby, a positive control containing 100 % dead cells was included, which was previously generated by addition of 10 x lysis buffer. After a 30 min incubation in the dark at RT, absorbance was measured at 490 nm and 680 nm by Berthold Luminometer Centro LB 960. At the end, relative LDH release was calculated as follows:

$$LDH\ release\ [\%] = \frac{value - mock}{positiv\ control - mock}\ x\ 100.$$

2.2.17 Statistical analysis

For statistical analysis GraphPad Prism 8.3.0 was used. Statistical significance of the data was determined using a two-way ANOVA test with Sidak's correction for multiple comparison if results were influenced by two factors (virus construct and treatment). For comparison of only two independent samples, unpaired t-test was performed. If not otherwise mentioned, data are represented as mean and standard deviation of three technical replicates of a representative experiment. P values are differentiated as followed:

$p > 0.05$: n. s. (not significant); $p \leq 0.05$: *; $p \leq 0.01$: **; $p \leq 0.001$: ***; $p \leq 0,0001$: ****.

3 Results

3.1 Induction of apoptosis by SMASh

With the goal to generate a drug-controllable RABV, the SMASh-tag was previously fused to the C-terminus of the nucleoprotein and the phosphoprotein, respectively. However, first studies displayed a high cytotoxic effect, when an inhibitor was applied after establishment of infection. Western blot analysis of PARP and various caspases revealed evidence of apoptosis activation. Thus, the effector caspase-3, as well as the initiator caspases-8, -9, -10 could be shown to be involved (Masterthesis V. Pfaffinger 2016). In the first part of this thesis, induction of cell death by SMASh was further characterized by analyzing various cells and virus constructs with different immunological experiments.

### 3.1.1 SMASh viruses can be inhibited in viral growth

Before characterizing the cytotoxicity induced by SMASh, we aimed to know whether the SMASh-tag has an impact on viral growth in absence of the inhibitor. Therefore, multistep growth curves were conducted with SAD P-SMASh and SAD N-SMASh on BSR T7 cells. Wildtype SAD L16 served as control. In addition, SAD YFP-SMASh containing the SMASh-tag fused to a non-viral protein was included (Figure 11A). In the first approach, growth kinetics were determined in absence of the NS3 inhibitor. Wildtype virus revealed fastest growth kinetics and yielded highest infectious titers at all time points. Growth of SAD P-SMASh and SAD YFP-SMASh was only slightly attenuated, and viral titers at late stages (96 h) of infection were reduced by approximately 10-fold. This indicated that the functions of the viral P protein retaining the few amino acids DEMMEC at the C-terminus after cleavage were largely unaffected. Growth of SAD N-SMASh however, was more severely attenuated, as evidenced by slower accumulation, although at late stages final virus reached 10^7 ffu/mL (Figure 11B). The extra C-terminal amino acid residues derived from the SMASh-tag or insufficient cleavage of tagged N could be responsible for this attenuation.

Next step was to evaluate the effect of the inhibitor in regard to viral growth. Multistep growth curves were performed and 3 µM DNV was added at media exchange 4 h. p. i.. The presence of the inhibitor did not have apparent effects on the growth and titers of wildtype SAD L16 or SAD YFP-SMASh, carrying the tag at a non-essential protein, in contrast to SAD P-SMASh or SAD N-SMASh. Although viral growth could not be blocked completely, viral titers of SAD P-SMASh were reduced by more than 4 logs at 96 hours post infection by the inhibitor. In case of SAD N-SMASh no viral amplification was detected until 48 h post

infection and titers reached only 10^2 ffu/mL at 96 h post infection, which is a 5 log/100000-fold decrease. (Figure 11C).

All in all, these results suggest that it is possible to diminish amplification of viruses carrying SMASh-tags at essential proteins, and most effectively by fusion to the nucleoprotein. As it was not possible to completely block replication, we assumed that protein production by input virus four hours prior inhibitor treatment might be sufficient to allow further replication.
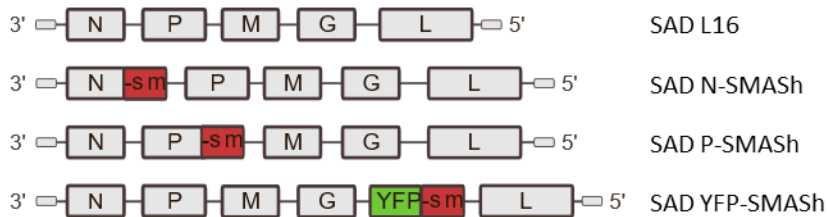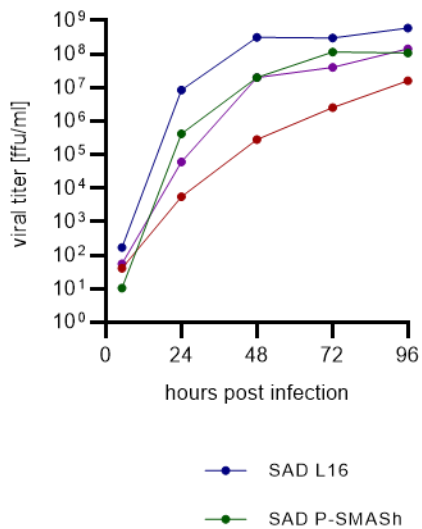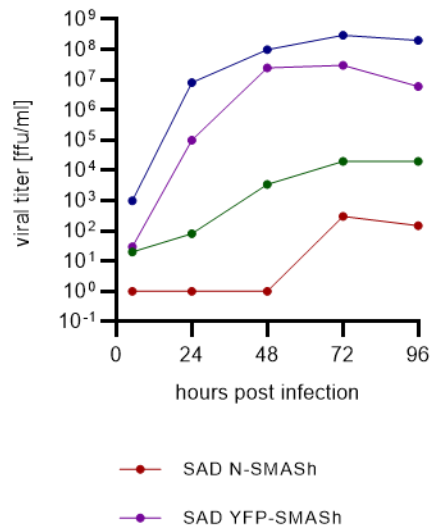

Figure 11: Viral growth of SMASh viruses in presence and absence of NS3 inhibitor.
(A) Schematic representation of RABV SMASh viruses. (B, C) Multistep growth curve on BSR T7 cells of SAD L16, SAD P-SMASh, SAD N-SMASh and SAD YFP-SMASh in absence of inhibitor (B) and in presence of 3 μM DNV after media exchange at 4 hours post infection (C). Samples were taken at indicated time points and titrated on BSR T7 cells.

### 3.1.2 Cell death is induced by diverse SMASh viruses upon drug treatment

Different SMASh viruses cause cell death upon inhibitor treatment. These include SAD P-SMASh, SAD N-SMASh as well as SAD YFP-SMASh. It could be shown that SMASh-toxicity correlates with the expression levels of SMASh-tagged proteins (Masterthesis V. Pfaffinger 2016). To underpin those findings, we performed killing assays in HEK 293T cells with those viruses and quantified cell death via real time viability assays after addition of DNV 24 h. p. i.. Interestingly, already the control virus SAD L16 affected cell viability compared to mock, but inhibitor treatment of SAD L16 had no further impact. In contrast to this, viability of SMASh virus infected cells was dropping few hours when treated with DNV. The strongest and fastest effect was observed in SAD P-SMASh infected cells, where viability was reduced within five hours by more than 50 %. Of note, SAD P-SMASh infection caused lower viability in control treated cells as well, although levels were comparable with those of the SAD L16 control. In case of SAD YFP-SMASh, viability was significantly reduced 24 h post DNV treatment. Cytotoxicity of SAD N-SMASh could be ranked in the middle, causing low but significant cell death five hours post infection (Figure 12).
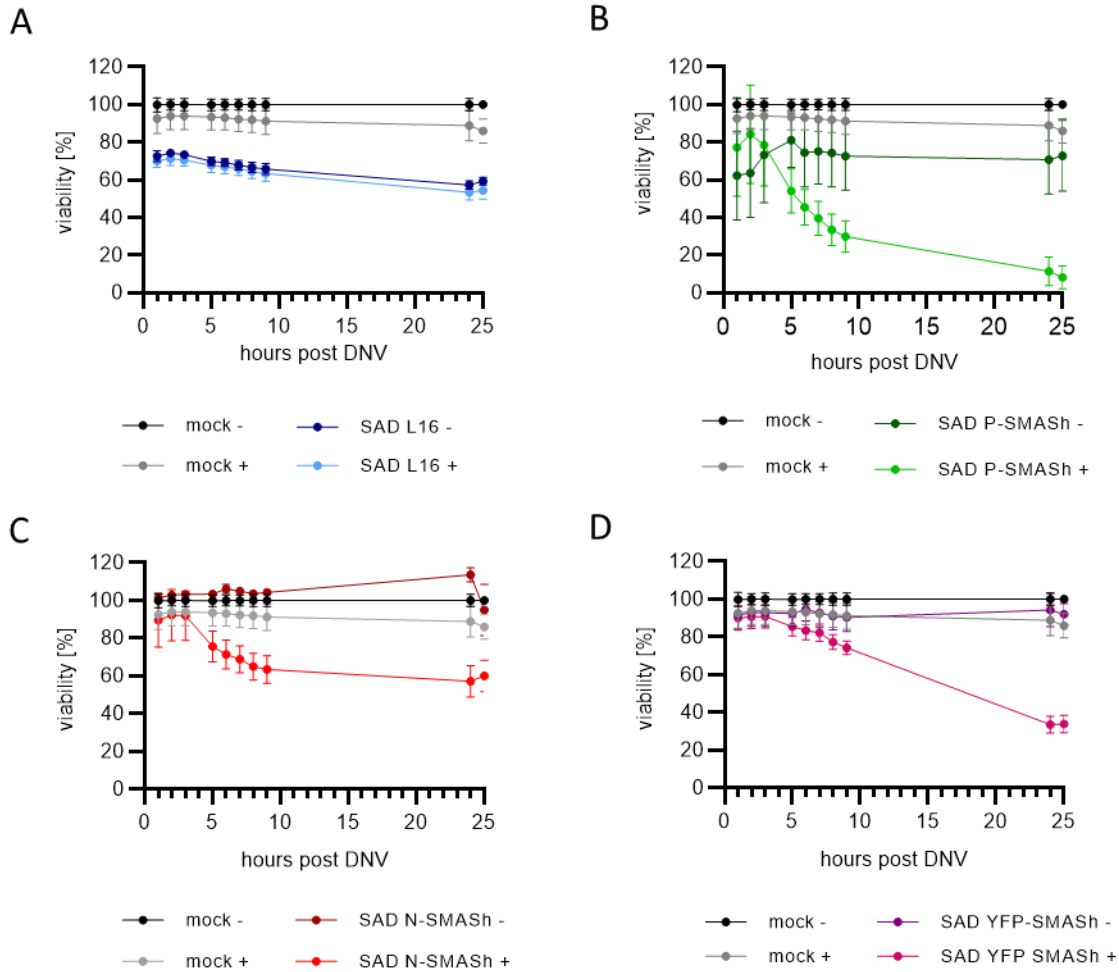
Figure 12: Diverse SMASh viruses induce cell death after DNV addition 24 h. p. i..
HEK 293T cells in 96 wells were mock-infected or infected with either SAD L16, SAD P-SMASh, SAD N-SMASh, SAD YFP-SMASh (MOI=3). Twenty-four hours later cells were treated with 3 µM DNV (+) or DMSO (-) and real time viability measured between 0 and 24 h. p. DNV.. Dots and error bars represent mean + SD of technical triplicates normalized to mock and DMSO samples of each timepoint. (A) mock + SAD L16; (B) mock + SAD P-SMASh; (C) mock + SAD N-SMASh; (D) mock + SAD YFP-SMASh.

For control, a similar experiment was performed, but this time DNV or DMSO was added at the timepoint of infection. As before, cells infected with SAD L16 displayed a reduced viability 24 h post infection, which was independent of treatment. Neither SAD P-SMASh nor SAD N-SMASh in treated or non-treated cell cultures showed cytotoxicity, reflecting inhibition of virus replication, and accumulation of SMASh-tagged fusion proteins. In striking contrast, SAD YFP-SMASh became progressively cytotoxic after 24 hours post infection and DNV underlying the hypothesis that a certain amount of SMASh-tagged protein is necessary for a conditional cytotoxic outcome (Figure 13).
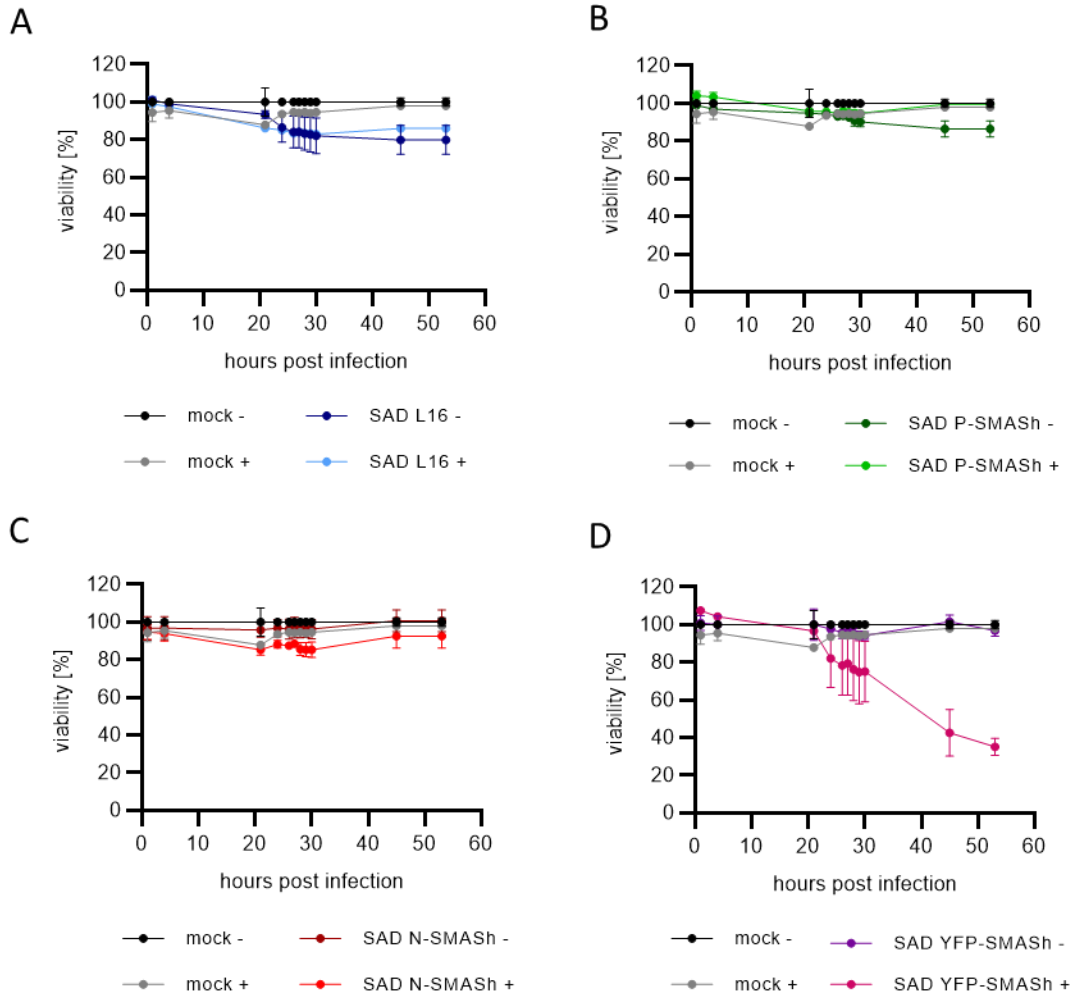
Figure 13: SMASh fusion to non-viral YFP allows induction of cell death after DNV treatment at infection.
HEK 293T cells in 96 wells were mock infected or infected with either SAD L16, SAD P-SMASh, SAD N-SMASh, SAD YFP-SMASh (MOI=3). Directly at infection cells were treated with 3 µM DNV (+) or DMSO (-) and real time viability measured between 0 and 53 h. p. i.. Dots and error bars represent mean + SD of technical triplicates normalized to mock and DMSO samples of each timepoint. (A) mock + SAD L16; (B) mock + SAD P-SMASh; (C) mock + SAD N-SMASh; (D) mock + SAD YFP-SMASh.

3.1.3   Apoptosis is induced by plasmids expression of SMASh

First experiments from master thesis of V. Pfaffinger (2016) indicated that SMASh-tags expressed from transfected plasmids have a conditional cytotoxic effect. However, effects were very small and not comparable to the cytotoxicity observed after viral infection. Thus, we aimed to further evaluate the extent of SMASh killing dependent of protein expression after plasmid transfection or viral infection. For comparison we used N-SMASh provided either in form of SAD N-SMASh or pCAGGS N-SMASh.

SAD YFP-SMASh and pCAGGS YFP-SMASh were taken to examine YFP-SMASh cytotoxicity in parallel. HEK 293T cells were either transfected with the respective plasmid (500 ng/24 well) or infected with viral stock (MOI=3) to reach a transfection or infection of the complete cell culture. Twenty-four hours later, cells were treated with the inhibitor DNV or DMSO, lysed 6 hours later and subjected to Western blot analysis. As confirmed by WB, SMASh-tagged proteins were expressed to comparable levels. In both expression systems SMASh showed induction of cell death upon DNV treatment. PARP was cleaved to a similar extent after plasmid and viral expression (Figure 14A).

Additionally, we compared P-SMASh cytotoxicity in regard of transfection and infection (Figure 14B). Therefore, HEK 293T cells were transfected with pCAGGS P-SMASh. Six hours later, infection with SAD eGFP of transfected cells was performed, as well as individual infection SAD eGFP P-SMASh (MOI=3) of non-transfected cells. Cells were treated with DNV 26 h. p. i. and lysed 16 hours post DNV treatment. Though to different degrees, PARP cleavage was observed in all cultures treated with DNV, irrespective of transfection or infection. Differences regarding PARP cleavage after inhibitor treatment between plasmid and virus expressed P-SMASh apparently correlated with P expression levels, which was lower in pCAGGS P-SMASh transfected cells. Moreover, in plasmid-transfected and virus-infected cells, a low PARP cleavage was observed. In this case, however, correlation with the P-SMASh expression level was not possible, as the virus additionally expresses wildtype P (Figure 14B). Overall, we concluded that SMASh proteins expressed from viruses and plasmids are equally toxic. Contrary to findings from the master thesis, no enhancement by additional viral infection to transfected cells was observed. Generally, cytotoxicity seems to be indeed related to expression levels, which also fits to previous findings.
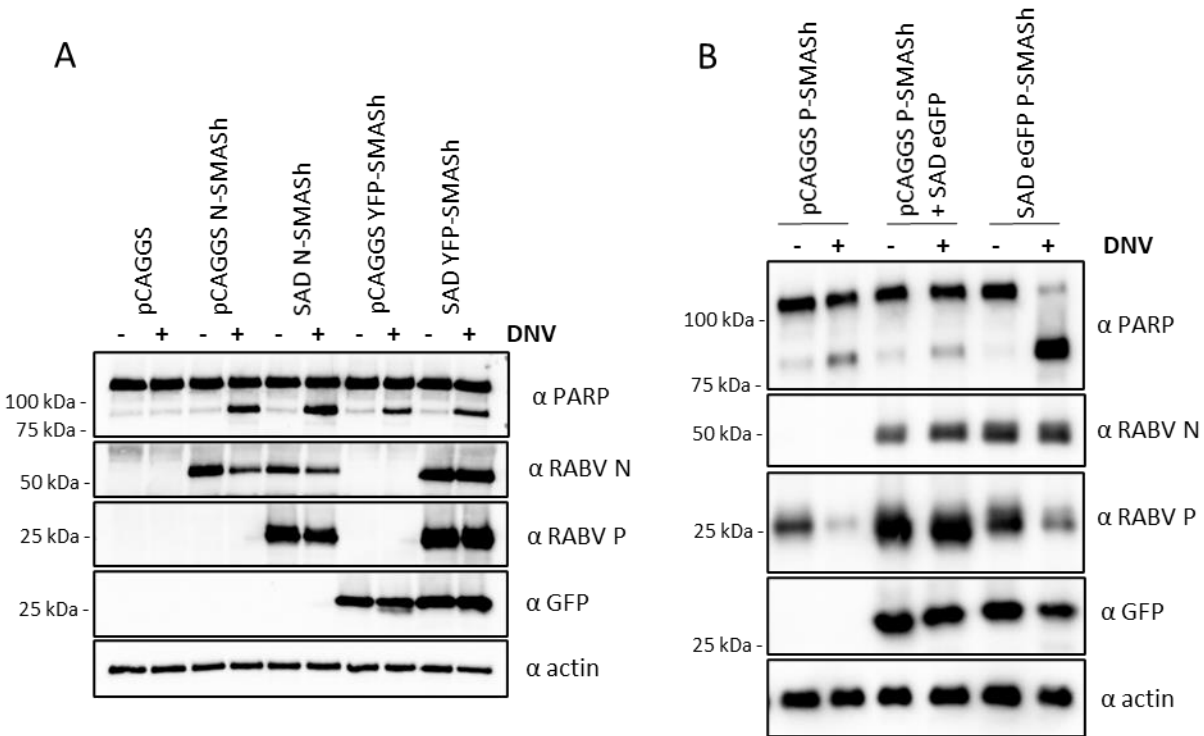
Figure 14: SMASh induces cell death upon inhibitor independent of expression by virus or plasmid.
(A) HEK 293T cells in 24 wells were transfected with 500 ng pCAGGS, pCAGGS N-SMASh, pCAGGS YFP-SMASh, or infected with SAD N-SMASh or SAD YFP-SMASh (MOI=3). Twenty-four hours later 3 μM DNV (+) or DMSO (-) was added, followed by lysing the cells for Western blot analysis at 6 h. p. DNV. (B) HEK 293T cells in 24 wells were transfected with 500 ng pCAGGS P-SMASh or not. 6 hours later, infection with SAD eGFP of transfected cells or SAD eGFP P-SMASh (MOI=3) of mock-transfected cells was performed. After additional 26 hours 3 μM of DNV (+) or DMSO (-) was added to the cells, before they were lysed 16 h. p. DNV for Western blot analysis.

3.1.4   Instant induction of apoptosis after drug addition

Apoptosis is a highly regulated process of programmed cell death. It includes activation of a signaling cascade of initiator and effector caspases leading to physiological changes of the cell.

One hallmark of apoptosis is the loss of membrane asymmetry by translocation of cytosolic phosphatidylserine (PS) to the outer leaflet of the plasma membrane with its integrity remaining intact (Chaurio et al. 2009). This process is usually followed by the autolytic process of secondary necrosis in immortalized cell culture (Wu et al. 2001; Vanden Berghe et al. 2010). When translocated to the outer leaflet or the membrane is disrupted as in the case of necrosis, phosphatidylserine is accessible for Annexin V to bind. To study the timing of apoptosis we used this distinctive feature and performed a real time Annexin V binding assay. In this assay, Annexin V is fused to subunits of NanoBiT® luciferase (Annexin V-LgBiT and Annexin V-SmBiT) which complement in close proximity leading to a luminescence signal.

Because SAD P-SMASh has killed the cells at the highest rate (Figure 12), this virus was used for analyzing SMASh induced toxicity in this and following other experiments. Killing assay was carried out as before: cells were infected with a high MOI of 3. After infection was established, cells were treated with 3 µM DNV 24 h. p. i. and analyzed at indicated timepoints (Figure 15A). As positive control, cell death was induced by the apoptosis inducer staurosporine. Strikingly, already one hour post DNV treatment Annexin V bound to PS in SAD P-SMASh infected cells, whereas in staurosporine treated cells Annexin V binding occurred only after 24 h of induction. Annexin V binding was also detectable in SAD P-SMASh non-treated control cells as well as in SAD L16 infected cells at 24 h. p. DNV (Figure 15A).

To ensure that Annexin V binding did not occur due to necrosis or other lytic cell death events, we further determined LDH release after drug treatment. Therefore, independent killing assays were carried out with SAD eGFP and SAD eGFP P-SMASh in similar manner as before and stopped for analysis after 4 and 24 h. p. DNV., respectively (LDH release analysis at 24 h. p. DNV was performed by Franz Bauernschmitt). Except in the positive direct lysis control, LDH release was only basal after 4 hours of inhibitor treatment. In contrast, 24 h. p. DNV a significant LDH release in staurosporine treated cells could be detected which was similar to the positive control. However, in SAD P-SMASh eGFP and DNV treated cells only minor, non-significant LDH release was measured (Figure 15C). Overall, the appearance of Annexin V binding but no evidence of LDH in the supernatant shortly after cell death induction is a great indication of apoptotic cell death.
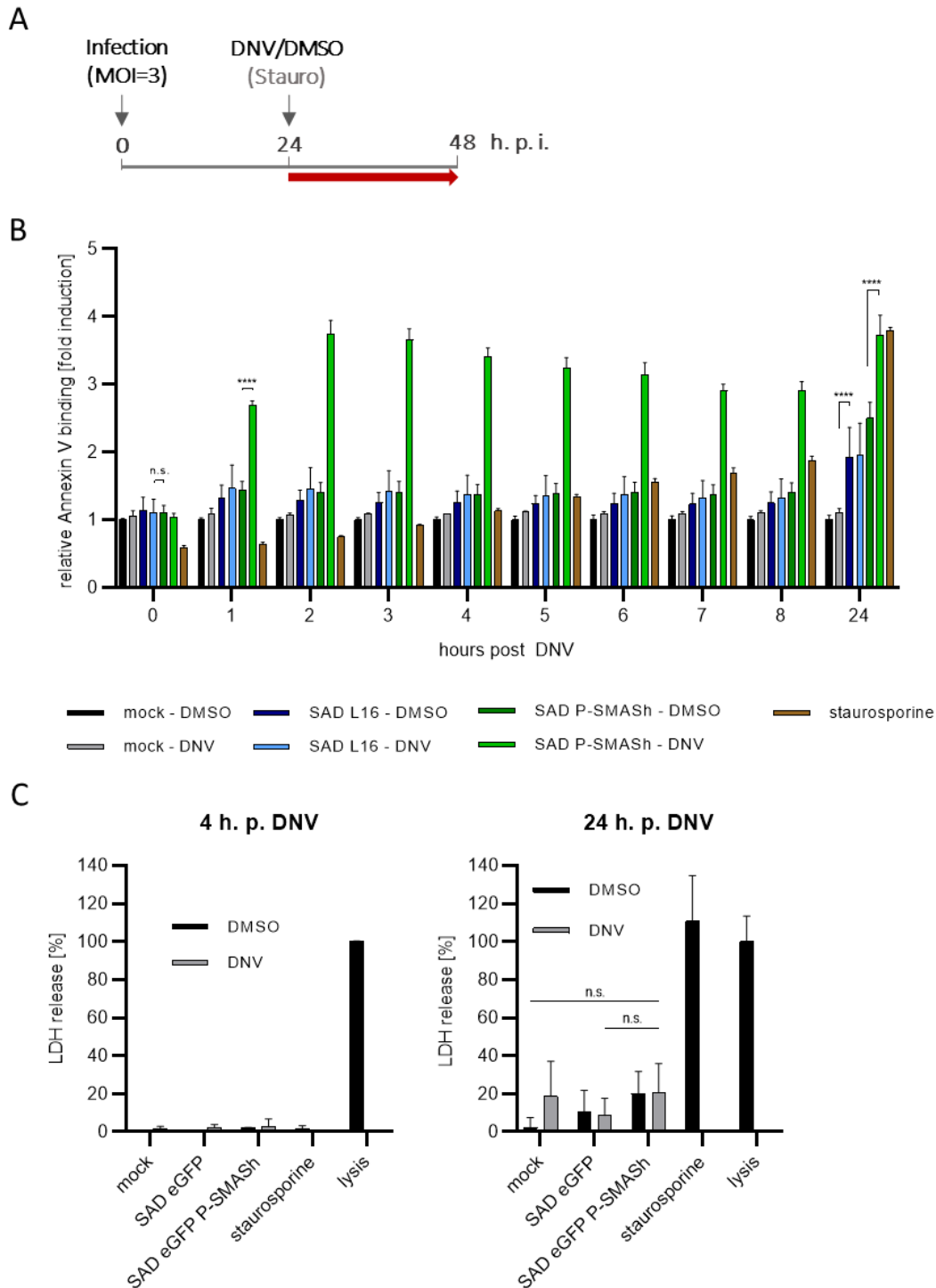
Figure 15: Annexin V binding detectable at one hour post DNV addition.
(A) Schematic representation of experimental setup. (B) HEK 293T cells in 96 wells were infected with either SAD L16, SAD P-SMASh (MOI=3) or left uninfected. Twenty-four h. p. i. cells were treated with 3 µM DNV or DMSO and real time Annexin V binding measured between 0 and 24 h. p. DNV.. As positive control 1 µM staurosporine was added to cells at timepoint of DNV/DMSO treatment. Bars and error bars represent mean + SD of technical triplicates normalized to mock and DMSO samples of each timepoint. (C; D) Killing assay was performed as above with SAD eGFP and SAD eGFP P-SMASh and LDH release measured either at 4 or at 24 h. p. DNV, respectively.

In order to confirm these results, we next conducted an experiment analyzing Annexin V binding via flow cytometry. Hence, killing assay with SAD eGFP P-SMASh was performed and cells harvested 4 hours post treatment. SAD eGFP as well as the apoptosis inducers staurosporine and Raptinal served as controls. In addition to Annexin V staining, a live-dead staining was done.

To analyze the results, cell debris were excluded and only counts reflecting single cells were selected. Thereby, more than 90 % of all counts in negative control treated cells (mock, SAD eGFP and SAD eGFP P-SMASh + DMSO) were selected. However, in SAD eGFP and DNV treated samples, likewise the positive control samples (Raptinal, Staurosporine), only approximately 60 % of all counts displayed single cells, whereas almost 40 % revealed a very low granularity and size indicating cell debris (Figure 16B).

Furthermore, selected cells were analyzed for viability (Figure 16C) and Annexin V positivity (Figure 16D). The respective gating strategy represented in Figure 16A. Approximately 20 % of SAD eGFP P-SMASh and DNV treated cells could be determined as dead and more than 75 % of selected single cells were Annexin V positive. Notably, staurosporine revealed significantly less dead and Annexin V-positive cells and also treatment with the rapid apoptosis inducer Raptinal resulted in similar amounts of dead cells, but only 19 % showed positive Annexin V staining. These results corroborate the instant induction of apoptosis upon SAD eGFP P-SMASh infection and DNV treatment.
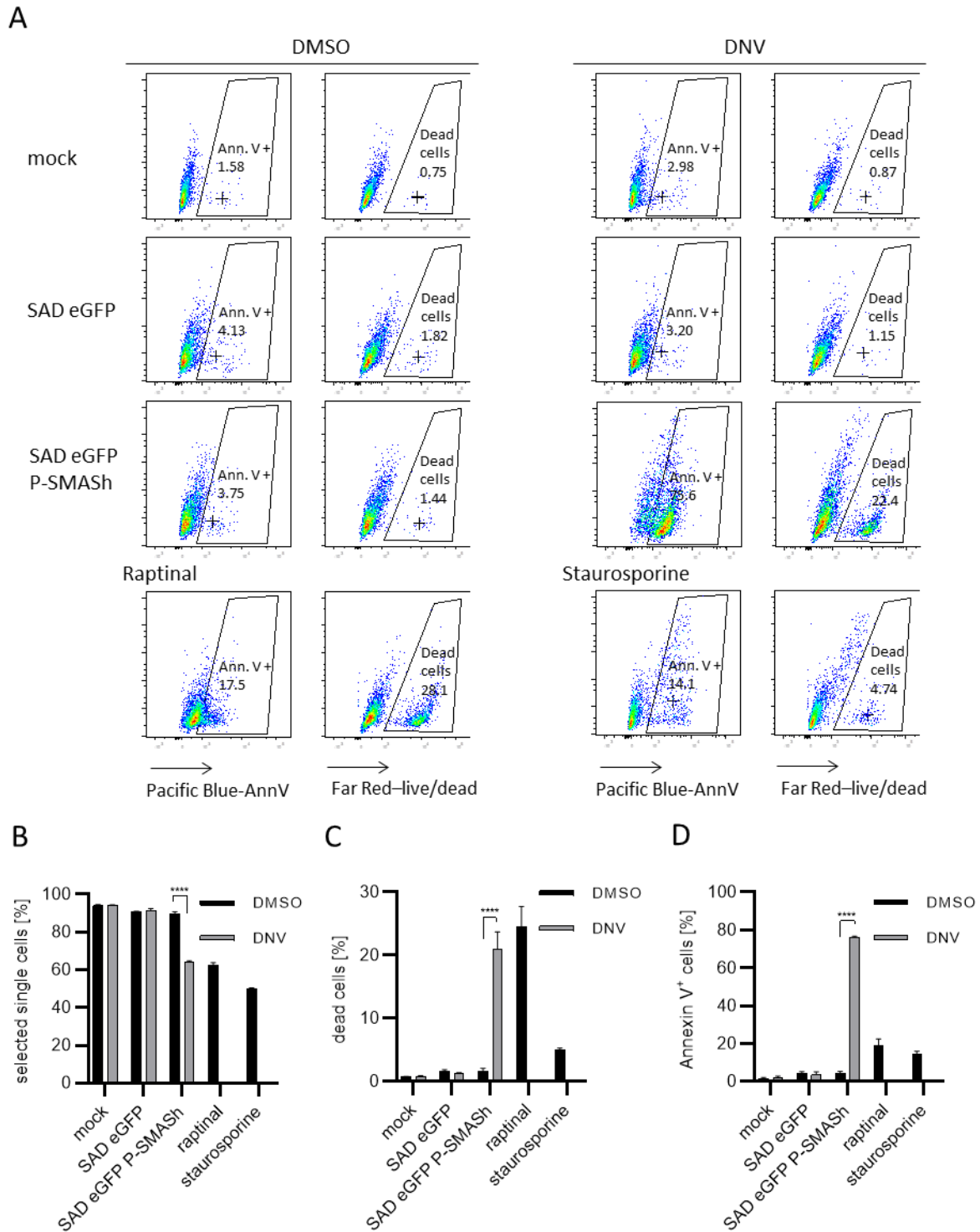
Figure 16: Annexin V positive cells after 4 hours post DNV addition.
HEK 293T cells in 24 wells were mock-infected or infected with either SAD eGFP, SAD P-SMASh (MOI=3). Twenty-four hours later 3 µM DNV or DMSO was added to the cells. Treatment with 1 µM staurosporine or 10 µM Raptinal served as positive control. Four h. p. DNV cells were harvested and subjected to FACS analysis. Staining was done for Annexin V (pacific blue) and live/dead (far red). (A) overview gating strategy, (B) selected living single cells, (C) dead cells and (D) Annexin V positive cells.

In addition to Annexin V binding we analyzed the kinetics of PARP cleavage during SMASh-tag induced cell death. We again conducted a killing kinetic, infected HEK 293T cells with SAD eGFP P-SMASh and treated cells with 3 µM DNV. Then, cells were lysed at different timepoint and investigated via Western blot. PARP was cleaved only in SAD eGFP P-SMASh infected cells that were treated with the inhibitor and, notably, PARP cleavage could be detected already one hour after induction (Figure 17). This is consistent with the previous assays. In conclusion, these results illustrate the rapid killing process induced by SMASh.
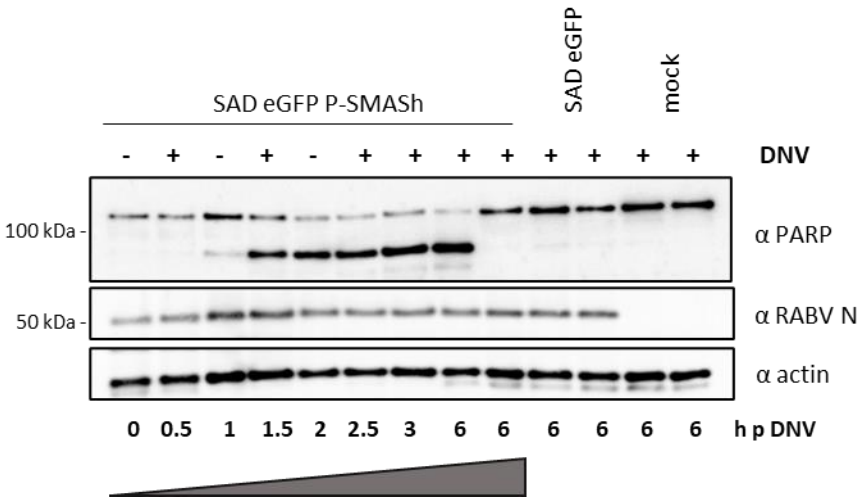

Figure 17: PARP cleavage is detectable as early as one hour post DNV addition.
HEK 293T cells in 24 well were infected with the indicated viruses (MOI=3) and treated with 3 µM DNV at 24 h. p. i.. SAD eGFP P-SMASh infected and DNV treated cells were lysed at 0, 0.5, 1, 1.5, 2, 2.5, 3 or 6 hours post treatment, respectively. At latest timepoint (6 h. p. DNV) control cells were lysed as well and analyzed via Western blot.

3.1.5 Activation of intrinsic and extrinsic apoptotic Caspases

SMASh triggered apoptosis involves activation of several caspases. Specifically, the intrinsic initiator caspase-9, the extrinsic initiator caspases-8 and -10 as well as the effector caspase-3 were found to be activated upon NS3 inhibitor treatment (Masterthesis V. Pfaffinger 2016). To confirm these findings, we performed a Caspase-Glo activation assay. Thereby, a luciferase becomes active after its substrate is released upon cleavage by corresponding caspase. A killing assay was carried out in HEK 293T cells. Cells were infected with SAD L16 or SAD P-SMASh (MOI=3) and treated with DNV 24 h. p. i.. Then, luciferase components were added 2 h post DNV treatment and luminescence measured 45 minutes later. As expected, Caspase-8, Caspase-9 as well as Caspase-3/-7 were significantly activated in SAD P-SMASh and DNV treated cells (Figure 18). This is coherent with the results from Western blot analysis in the master

thesis showing cleaved caspase-8 and -9 as well as the loss of full-length caspase-10 and -3, which indicates respective activation (Masterthesis V. Pfaffinger 2016).
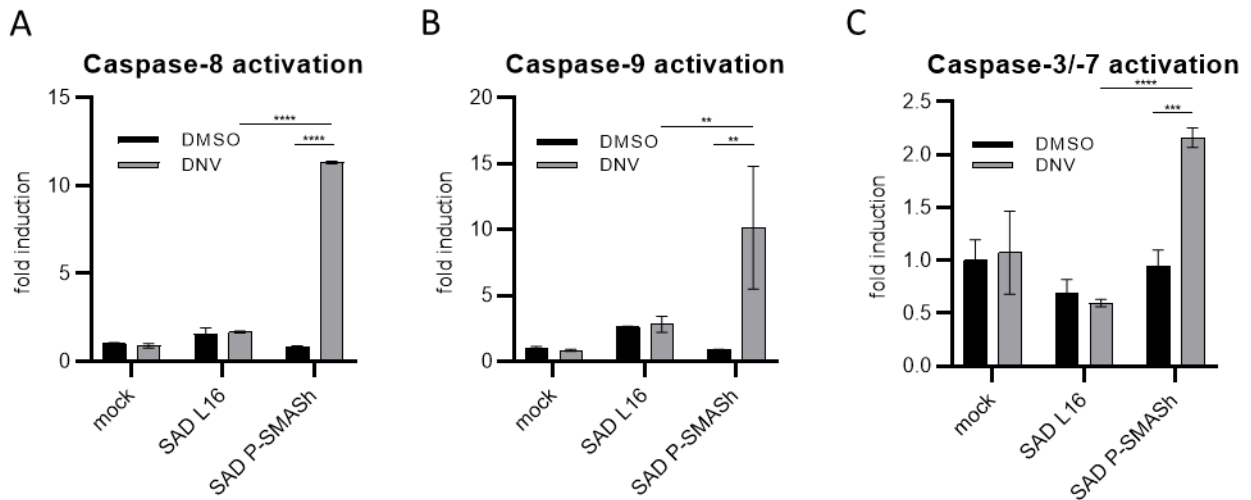

Figure 18: Caspase activation during SMASh induced apoptosis.
HEK 293T cells in 96 well were infected with SAD L16, SAD P-SMASh (MOI=3) or not and treated with 3 µM DNV or DMSO at 24 h. p. i.. Substrate for measuring caspase activity was added two hours post DNV treatment and activity determined 45 min later. (A) Increase of Luciferase reflecting caspase-8 activity, (B) caspase-9 activity and (C) caspase-3/-7 activity. Mean + SD represent results of technical triplicates.

Nevertheless, it is still not clear which caspase is activated in first place. To address this question experiments with direct caspase inhibitors were carried out. Therefore, inhibitors of the initiator caspases-8, -9 and -10 (z-IETD-fmk, z-LEHD-fmk and z-AEVD-fmk, respectively) were used. First, a killing assay in HEK 293T cells with SAD eGFP P-SMASh (MOI=3) was conducted, and the cells were treated with the respective inhibitor or combinations 30 min before DNV addition. PARP cleavage was determined and used for correlation with toxicity level 16 hours post DNV. Without caspase inhibitor, full-length PARP is almost completely processed leading to a strong band of the cleaved 89 kDa fragment. This cleavage could be partially prevented by the pre-treatment with caspase-9 inhibitor, and even more with caspase-8 inhibitor. Strongest effect, however, was observed with caspase-10 inhibitor z-AEVD-fmk, which almost completely obstructed PARP cleavage. Cell death was almost fully prevented when treated with a combination of two or all three caspase inhibitors. Additionally, full-length caspase-10 protein levels were investigated. In presence of DNV and absence of any caspase inhibitor, pro-caspase-10 could not be detected indicating its full cleavage and thus activation. In contrast, pro-caspase-10 could be detected in presence of the caspase-10 inhibitor, but also in presence of the other caspase inhibitors z-IETD-fmk and

z-LEHD-fmk suggesting that either caspase inhibitors or the caspase-10 antibody might be unspecific (see Discussion) (Figure 19A).

We further investigated the influence of different caspase inhibitors in HeLa cells to see whether SMASh and caspase inhibitors have a similar effect in other human cells. Cells were treated 26 h. p. i. with DNV and respective inhibitors for 25 h. Processing of pro-caspase-10 appeared to be fully abrogated upon z-AEVD-fmk and pan-caspase inhibitor treatment, respectively. PARP cleavage was reduced in all inhibitor conditions. However, again Z-IETD-fmk and z-AEVD-fmk seemed to have a bigger effect on PARP-cleavage than z-LEHD-fmk (Figure 19B).
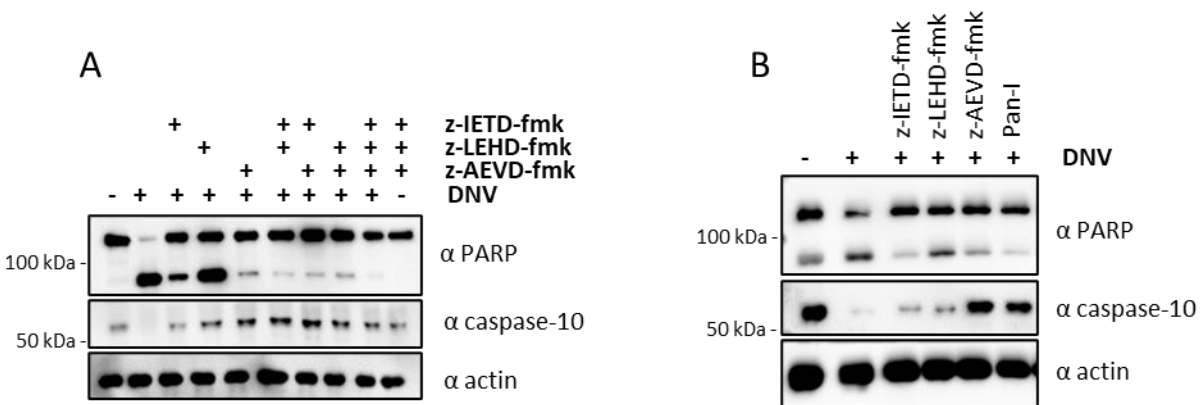
**Figure 19: Reduction of apoptosis by caspase inhibitors.**
(A) HEK 293T cells in 24 well were infected with SAD eGFP P-SMASh (MOI=3) and treated with 3 µM DNV (+) or DMSO (-) at 26 h. p. i.. At the same time either 70 µM z-IETD-fmk, 70 µM z-LEHD-fmk, 50 µM z-AEVD-fmk or combination of inhibitors was added to the cells. Cells were lysed 16 h. p. drug and inhibitor addition for Western blot analysis. (B) Infection of HeLa cells was done in 24 well with SAD eGFP P-SMASh (MOI=3) and 3 µM DNV (+) or caspase inhibitors added as above at 26 h. p. i.. Lysis of cells was performed 25 hours later for Western blot analysis.

Because caspase-8 and -10 inhibitor had the biggest impact on cell death in HEK 293T and HeLa cells, we assumed that those are the main caspases triggered directly by SMASh, and caspase-9 is only activated in downstream steps. This would also fit to the fact that caspase-8 can activate the mitochondrial pathway and thus caspase-9 via Bid (Luo et al. 1998; Li et al. 1998; Schug et al. 2011).

Moreover, experiments with single-round viruses lacking the glycoprotein showed cell death only in infected cells whereas non-infected cells were not affected (Masterthesis V. Pfaffinger 2016). To confirm this, we infected BSR T7 cells with SAD ΔG eGFP P-SMASh (SAD-G) with an MOI of 1 leading to the infection of approximately 75 % of the cell culture. After 24 hours cells were treated with the alternative NS3 inhibitor ASV and analyzed via microscope 20 hours later. ASV and DNV have been compared in previous

work and no difference in conditional cytotoxic effect was found (Masterthesis V. Pfaffinger 2016). Indeed, infected cells underwent cell death displaying typical morphological features of apoptosis such as fragmentation into membrane-bound bodies. In contrast, non-infected cells stayed healthy (Figure 20). This corresponds well to the findings from previous master thesis and led to the conclusion that, although caspases are activated which can mediate apoptosis after extrinsic stimuli, there is no extracellular trigger in case of SMASh-mediated apoptosis.
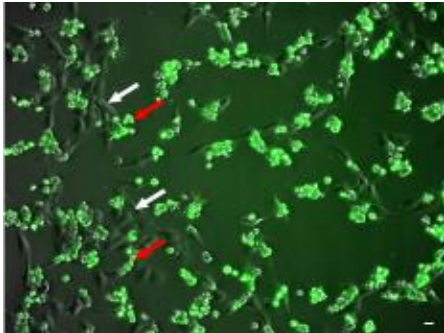
Figure 20: Inhibitor induced cell death occurs exclusively in infected cells.
BSR T7 cells in 24 well were infected with SAD ΔG eGFP P-SMASh (SAD-G) (MOI=1) and treated with 3 µM ASV 24 hours later. After additional 20 hours, cells were analyzed via microscopy. Red arrows indicate infected, dead cells. White arrows mark non-infected, healthy cells. Scale bar: 100 µm.

3.1.6 Various apoptosis related gene knockout cell lines can be killed by SMASh-tag inhibition

So far the trigger of apoptosis is still unknown. In order to gain further insights on the induced pathway, cell lines in which genes involved in apoptotic functions or signaling were used or specifically generated with CRISPR/Cas9 and analyzed in regard of SMASh-induced cell death.
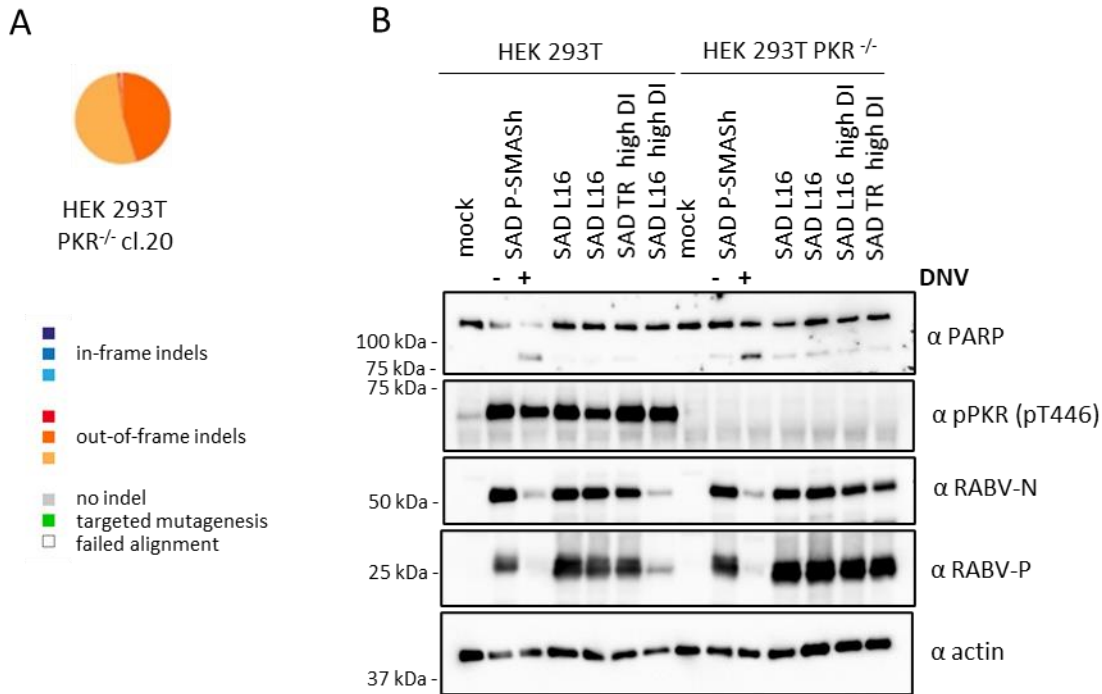
3.1.6.1 SMASh related apoptosis is not induced via PKR

Protein kinase R (PKR) is a key player in cellular defense and regulates several biological processes keeping thereby the balance between cell growth and cell death. Intracellular viral dsRNA generated for example by Influenza is the most described PKR activator. However, a number of other stimuli such as heat shock proteins, growth factors, bacterial lipopolysaccharide and amyloid-β (Aβ) peptide accumulation are able to activate the serine-threonine kinase as well leading to a shutdown of cellular und viral protein synthesis. Depending on the stimuli and its threshold, either pro-survival pathways like NF-κB or anti-survival apoptosis are subsequently initiated. The latter involves the formation of a FADD/Caspase-8 complex but is also triggered by transcription of the pro-apoptotic factors such as p53. (Kumar et al. 1994; Yoneyama

et al. 1998; Gil and Esteban 2000a; García et al. 2007; Garcia-Ortega et al. 2017; Xu et al. 2018; Gal-Ben-Ari et al. 2019).

To investigate whether PKR plays an essential role in SMASh-induced apoptosis, we generated HEK 293T PKR$^{-/-}$ cells. The knockout was first validated by Illumina sequencing (Figure 21A). Successful knockout on functional protein level was obtained by the observation that a virus causing PKR-dependent cell death in wildtype cells, namely SAD TR high DI, could not kill HEK 293T PKR$^{-/-}$ cells (Alexander Ghanem, unpublished results). A SMASh-dependent killing assay was performed in knockout and wildtype HEK 293T cells with SAD P-SMASh and analyzed via Western blot with a phospho-PKR (T446) antibody. Interestingly, infection with various viruses led to phosphorylation of PKR-T446 in HEK 293T wildtype cells, whereas no proteins were detected with respective antibody in PKR$^{-/-}$ cells further confirming PKR-KO identity of those cells.

Interestingly, PARP cleavage was detectable due to SAD P-SMASh infection and DNV treatment in PKR knockout cells in a similar manner as in HEK 293T wildtype cells (Figure 21B). In consequence, we concluded that PKR has no major effect on SMASh induced apoptosis and neither on the mild apoptosis observed in HEK cells by RABV infection alone.

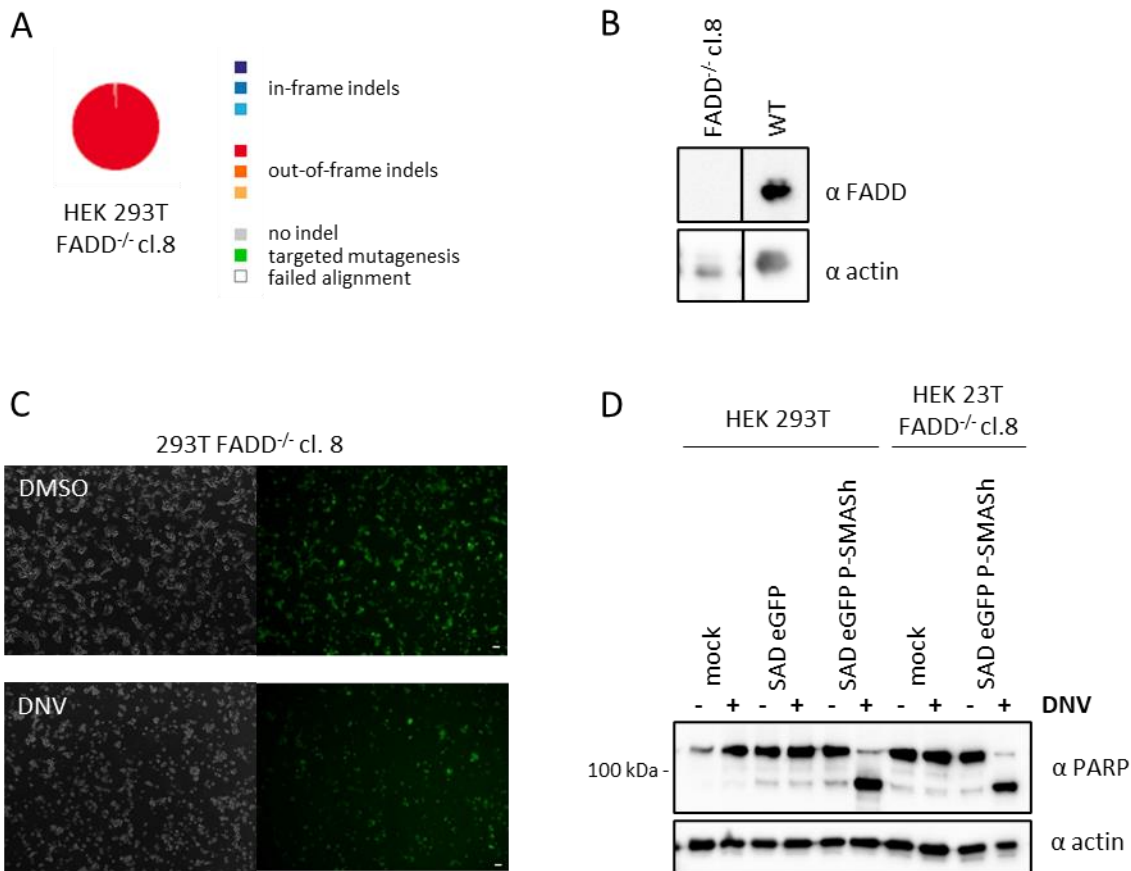**Figure 21: SMASh related apoptosis is induced in HEK 293T PKR$^{-/-}$ cells.**
(A) Schematic representation of Illumina sequencing results of HEK 293T PKR$^{-/-}$ clone 20. (B) HEK 293T and HEK 293T PKR$^{-/-}$ cl. 20 cells in 24 well were infected with two different stocks of SAD L16, SAD TR high DI, SAD L16 high DI, SAD P-SMASh (MOI=3) and treated with 3 µM DNV (+) or DMSO (-) at 24 h. p. i.. After additional 24 hours cells were lysed and subjected to Western blot analysis. Note that PARP is cleaved in PKR-KO cells in the presence of DNV.

3.1.6.2 FADD does not play an essential role for SMASh induced killing

Since PKR seems to be not important for SMASh induced apoptosis, we further aimed to know whether FADD is responsible for this particular mode of cell death. Although FADD stands for FAS-associated protein with death domain, the protein is responsible for apoptotic signal transmission at all known death receptors. The extrinsic apoptosis pathway is usually triggered by extracellular binding of death ligands such as TRAIL or Fas to the respective death receptor. This subsequently leads to the formation of a death-inducing signaling complex (DISC) with FADD as hub between the death receptor and caspase-8/-10. In consequence, FADD is essential for Caspase-8/-10 activation in the context of extrinsic apoptosis (Bodmer et al. 2000; Kuang et al. 2000; Sprick et al. 2000). However, FADD is also able to activate caspase-8 independently of ligand binding to a death receptor. This is for example the case when FADD is overexpressed (Perez and White 1998; Siegel et al. 1998) or in PKR mediated apoptosis (Gil and Esteban 2000b). To answer the question whether FADD is important during SMASh induced apoptosis,

HEK 293T FADD^{-/-} cells were generated. With the aim to completely disrupt the genetic code, we used a guideRNA targeting an exon close to a downstream intron (see Table 8) (Schmidt et al. 2015).

Identity of the cell clones was subsequently verified on a genetic level via Illumina sequencing. In addition, Western blot analysis was done to confirm the FADD knockout identity on protein levels. Clone nr. 8 contained only out of frame, but no in-frame mutations and showed no detectable FADD protein levels (Figure 22A, B). We used this clone to carry out a killing assay with SAD P-SMASh. Therefore, wildtype and FADD knockout cells were infected with a MOI of 3 and treated with DNV 24 h. p. i.. After additional 24 h cells, microscopic pictures were taken, and cells were lysed and subjected to Western blot analysis.

Figure 22: SMASh related apoptosis is induced in HEK 293T FADD^{-/-} cells.
(A) Schematic representation of Illumina sequencing results of HEK 293T FADD^{-/-} clone 8. (B) Western blot analysis of lysed HEK 293T and HEK 293T FADD^{-/-} cl. 8 cells. (C, D) HEK 293T and HEK 293T FADD^{-/-} cl. 8 cells in 24 well were infected with SAD eGFP, SAD eGFP P-SMASh or not (MOI=3) and treated with 3 µM DNV or DMSO at 24 h. p. i.. After additional 24 hours cells analyzed via microscopy and lysed for Western blot analysis. (C) Microscopic images of HEK 293T FADD^{-/-} cl. 8 with after SAD eGFP P-SMASh infection and DNV (+) or DMSO (-) treatment. Scale bar 250 µm. (D) Western blot of cell lysates.

HEK 293T FADD^{-/-} cells underwent same apoptotic fate after SMASh virus infection and DNV treatment as HEK 293T wildtype cells. Thus, DNV addition after SAD P-SMASh infection led to cell death in HEK 293T FADD^{-/-} cells (Figure 22C). Furthermore, an 89 kDA band could be detected with PARP antibody in Western blot, which was specific for this treatment and did not occur in controls (Figure 22D). In conclusion, these results suggested that FADD is not required in SMASh induced apoptosis.

3.1.6.3 Caspase-8 and -10 are not required for killing

FADD is obviously not needed for caspase activation. Next, the question raised whether those proteins themselves are the key components for SMASh induced apoptosis. Previous reports show the ability of the authentic HCV NS3 protein to directly bind caspase-8 and active it (Prikhod'ko et al. 2004). In consequence, it might be possible to block cell death by depletion of the initiator caspase-8 and/or the homologous caspase-10. To test this hypothesis, HeLa CASP8^{-/-} and HeLa CASP10^{-/-}, respectively, as well as the parental HeLa wildtype cells were kindly provided by the Leverkus group (Horn et al. 2017). First step was to sequence respective clones. Therefore, genomic DNA was isolated and sequenced via illumina sequencing (Figure 23A). We were able to confirm the identity of caspase-10 knockout having only out of frame indels. Nevertheless, protein bands of approximately 60 kDa corresponding to the size of caspase-10, were detected with a polyclonal caspase-10 antibody (Figure 23B), which might be caused by cross reaction with the closely related caspase-8. Furthermore, HeLa caspase-8^{-/-} reveal not exclusively out of frame mutations, but also in-frame indels. In order to obtain clones carrying exclusively out of frame mutations single cell dilution was carried out and monoclonal knockout cells were isolated. After gDNA isolation of each clone, mutations were analyzed again by Illumina sequencing (Figure 23A).

Next step was to find out, whether those knockout cells were killable. Hence, killing assay was conducted with HeLa parental cells, HeLa CASP10^{-/-} and HeLa CASP8^{-/-} subclone 2 and analyzed via microscopic and Western blot analysis. Cell death was observed not only in parental HeLa, but also in cells containing caspase-8 or caspase-10 knockout upon SAD eGFP P-SMASh infection and DNV treatment. Furthermore, PARP cleavage could be observed in cells with respective treatment suggesting the induction of apoptosis (Figure 23C). In addition, cell viability was determined in independent experiments by resazurin assay 4 hours post DNV. Thereby, a reduction of viability upon drug treatment after SAD eGFP P-SMASh infection could be determined in all three cell lines. Notably, the absence of caspase-8 led to reduced viability even in SAD eGFP-infected and untreated (DMSO) cells. In contrast, the absence of caspase-10 seemed to have no effect on viability (Figure 23D).
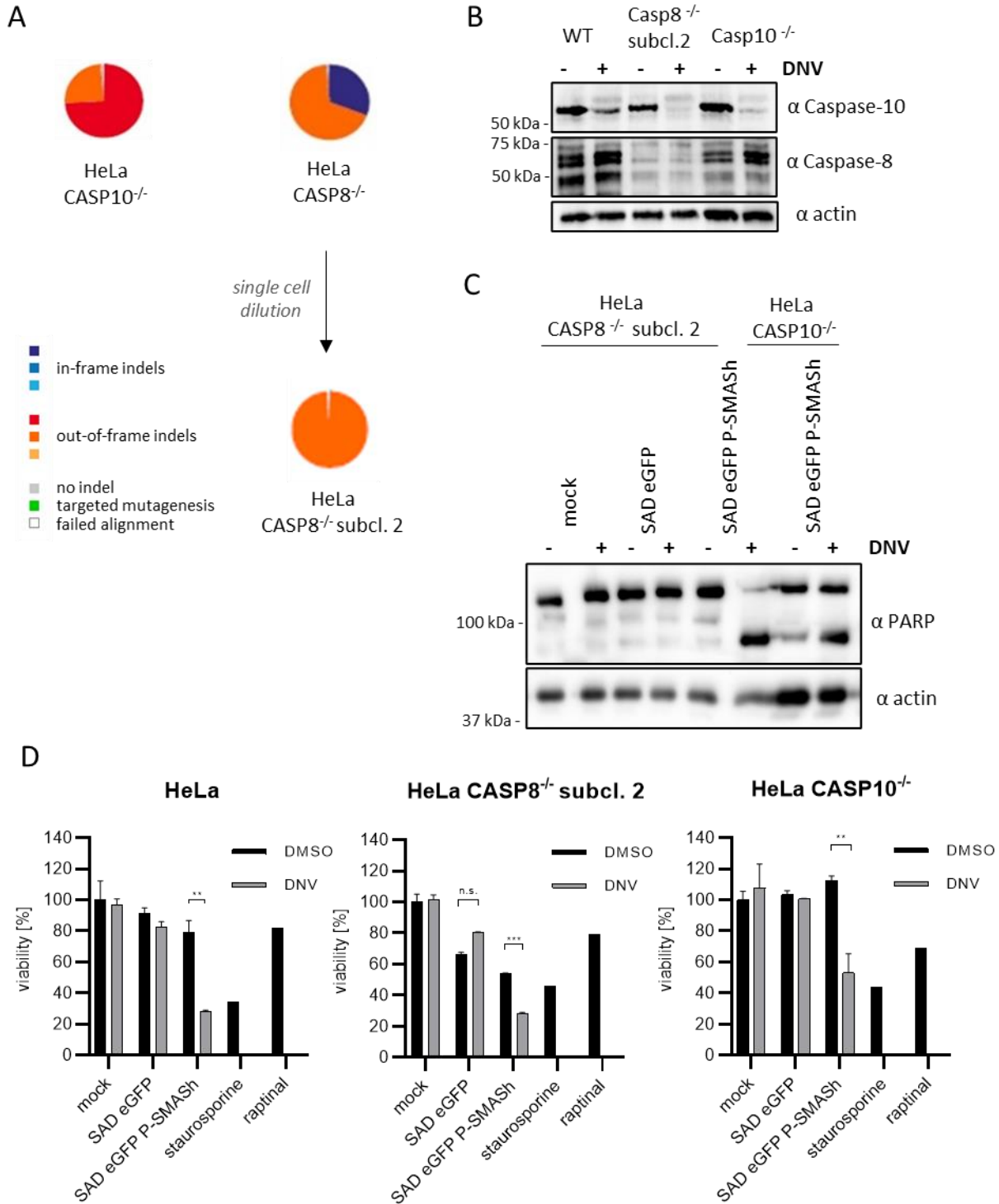
Figure 23: Caspase-8 and -10 is not needed for SMASh related killing.
(A) Schematic representation of Illumina sequencing results of HeLa CASP10^{-/-} and CASP8^{-/-} before and after subcloning. (B) HeLa cells, HeLa CASP8^{-/-} subcl. 2 and HeLa CASP10^{-/-} in 24 wells were infected with SAD eGFP P-SMASh (MOI=3) and treated with 3 µM DNV (+) or DMSO (-) at 24 h. p. i.. Cells were lysed 24 hours later for Western blot analysis. Note that caspase-10 Antibody is not specific. (C) Killing assay as before with HeLa CASP8^{-/-} subcl. 2 and HeLa CASP10^{-/-} cells. (D) Killing assay as before in 96 wells with SAD eGFP, SAD eGFP P-SMASh (MOI=3). Three µM

DNV was added 24 hours post infection and viability was determined 4 hours later via resazurin assay. Staurosporine and Raptinal controls were not done in replicates, other bars and error bar represents mean + SD of technical duplicates.

As pathway studies were so far carried out in HEK 293T cells, we generated HEK 293T CASP8 knockout cells. Furthermore, HEK 293T CASP10$^{-/-}$ were planned, but all 28 clones showed parental sequence with no mutation (data not shown). Caspase-8 single knockout cells were validated by Illumina sequencing revealing exclusively out of frame mutations (Figure 24A). Then, cells were compared to wildtype HEK 293T cells in a killing assay. Twenty-four hours post infection with SAD eGFP or SAD eGFP P-SMASh, cells were treated with the NS3 inhibitor and cell viability was analyzed via resazurin assay additional 24 hours later. The apoptosis inducer Raptinal and Staurosporine served as control. Of note, equal cell number was seeded in 96 wells. However, HEK 293T CASP8$^{-/-}$ cells grew remarkably slower than HEK 293T wildtype cells. For this reason, direct comparison of viability of those two cell lines is not possible. As observed already in other experiments, infection with wildtype or SMASh-tagged RABV caused already substantial reduction of cell viability in HEK 293T wildtype cells. Interestingly, and in striking contrast to the findings in HeLa cells, HEK 293T CASP8$^{-/-}$ cells were more resistant to killing in all conditions. Nevertheless, significant drops in cell viability were measured in SAD eGFP P-SMASh infected cells upon DNV treatment in both cases (Figure 24B).
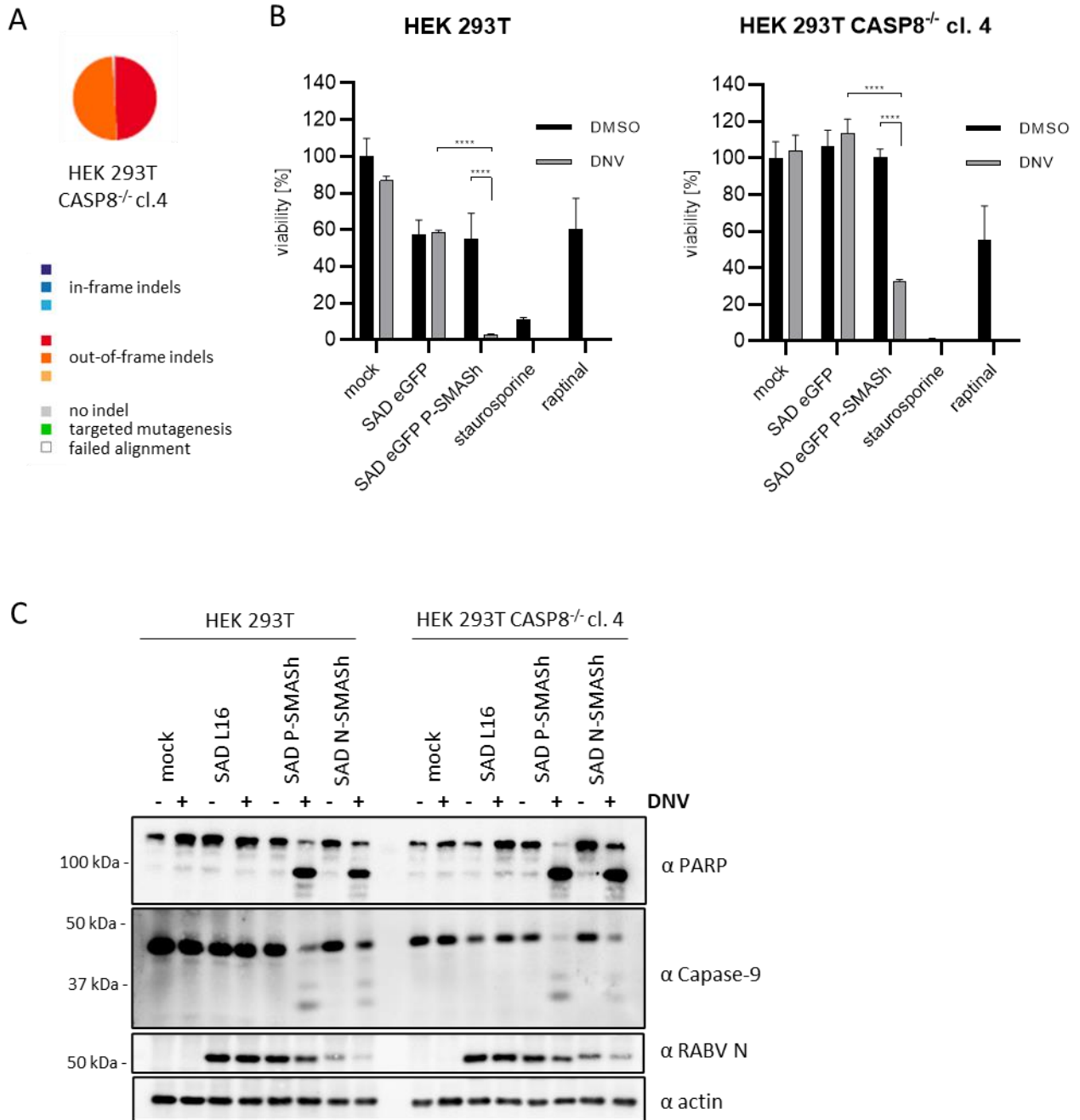
Figure 24: Caspase-8 is not needed for SMASh-related killing.
(A) Schematic representation of Illumina sequencing results of HEK 293T CASP8$^{-/-}$ clone 4. (B) HEK 293T cells and HEK 293T CASP8$^{-/-}$ cl. 4 in 96 wells were infected with SAD eGFP or SAD eGFP P-SMASh (MOI=3) and treated with 3 μM DNV (+) or DMSO (-) at 24 h. p. i.. Cells were analyzed 24 hours later via resazurin assay. One μM Staurosporine and 10 μM Raptinal served as control and were added to cells at same time as inhibitor treatment. Each bar and error bar represents mean + SD of technical replicates. (C) Similar experiment was performed with SAD L16, SAD P-SMASh and SAD N-SMASh in 24 well and cells were lysed 24 h. p. DNV. for Western blot analysis.

To confirm these results a similar killing assay was performed with SAD L16, SAD P-SMASh or SAD N-SMASh, and cells were lysed 24 hours post drug treatment for Western blot analysis. In contrast to resazurin assays, Western blot analysis did not reveal differences in viability between HEK 293T parental and CASP8$^{-/-}$ cells as a comparable pattern of PARP cleavage upon infection and DNV treatment was observed. In addition, we could also detect caspase-9 cleavage in cells with cleaved PARP indicating respective activation (Figure 24C). Taken together, SAD P-SMASh and SAD eGFP P-SMASh, respectively, caused cell death upon DNV addition with typical apoptotic PARP cleavage regardless of caspase-8 deficiency. Consequently, we concluded that Caspase-8 is not essential for SMASh related killing.

To assure, that apoptosis is induced in HEK 293T CASP8$^{-/-}$ cells as well, rather than necroptosis or pyroptosis, LDH release was measured. Again, killing assay with SAD eGFP and SAD P-SMASh was performed as before. Indeed, we did not detect significant increase of LDH in the supernatant supporting the evidence of apoptosis induction in HEK 293T CASP8$^{-/-}$ cells (Figure 25).
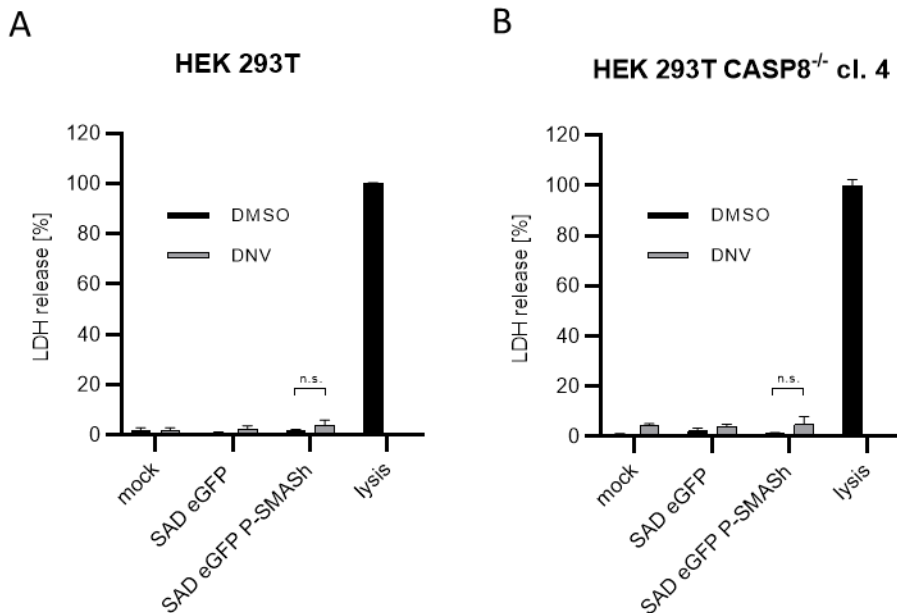
Figure 25: LDH release in HEK 293T and HEK 293T CASP8-/- cells.
HEK 293T and HEK 293T CASP8$^{-/-}$ cl. 4 in 96 wells were infected with SAD eGFP or SAD eGFP P-SMASh (MOI=3) and treated with 3 µM DNV or DMSO at 24 h. p. i.. LDH release was measured 24 h. p. DNV. Means of technical triplicates are represented by bars with respective standard deviations indicated by error bars (A) LDH release in HEK 293T cells. (B) LDH release in HEK 293T CASP8$^{-/-}$ cl. 4 cells. n. s.: not significant.

Moreover, CASP8/CASP10 double knockout mutants were generated in HEK 293T cells. We were not able to sequence the double knockout clones via Illumina sequencing. Instead, we used sanger sequencing for characterization of the isolated gDNA. Within 46 clones, we found one clone containing mainly out of

frame mutations in both, caspase-8 and caspase-10, genes. Although we cannot ensure complete genomic knockout, we might gain evidence of how important caspase 8 and 10 during SMASh induced apoptosis are.

Again, killing assays were performed as beforehand mentioned and cell viability determined 24 hours post DNV via resazurin assay. Staurosporine and Raptinal were used as apoptosis inducing controls. Notably, similar to HEK 293T CASP$^{-/-}$cells, HEK 293T CASP8/CASP10$^{-/-}$ cells grew slower than wildtype cells and RABV infection had no remarkable effect on cell viability. Nevertheless, infection with SAD eGFP P-SMASh in combination with inhibitor treatment reduced cell viability significantly. Equal effect was observed with the apoptosis inducer Raptinal, but not with Staurosporine in this experiment (Figure 26A, B).

For Western blot analysis, same experiment was performed. We could detect a clear band of cleaved PARP in SAD eGFP P-SMASh and DNV lysates as well as in the Raptinal control in wildtype and HEK 293T CASP8/CASP10$^{-/-}$ cells. However, in both cell lines Staurosporine did not lead to major PARP cleavage. Although the detected band was very weak, we could observe caspase-9 cleavage after SAD eGFP P-SMASh infection and drug treatment (Figure 26B). These results may suggest that neither caspase-8 nor -10, are essential for the SMASh-dependent cell death.

Figure 26: Cell death induction by SMASh in HEK 293T CASP8/CASP10$^{-/-}$.
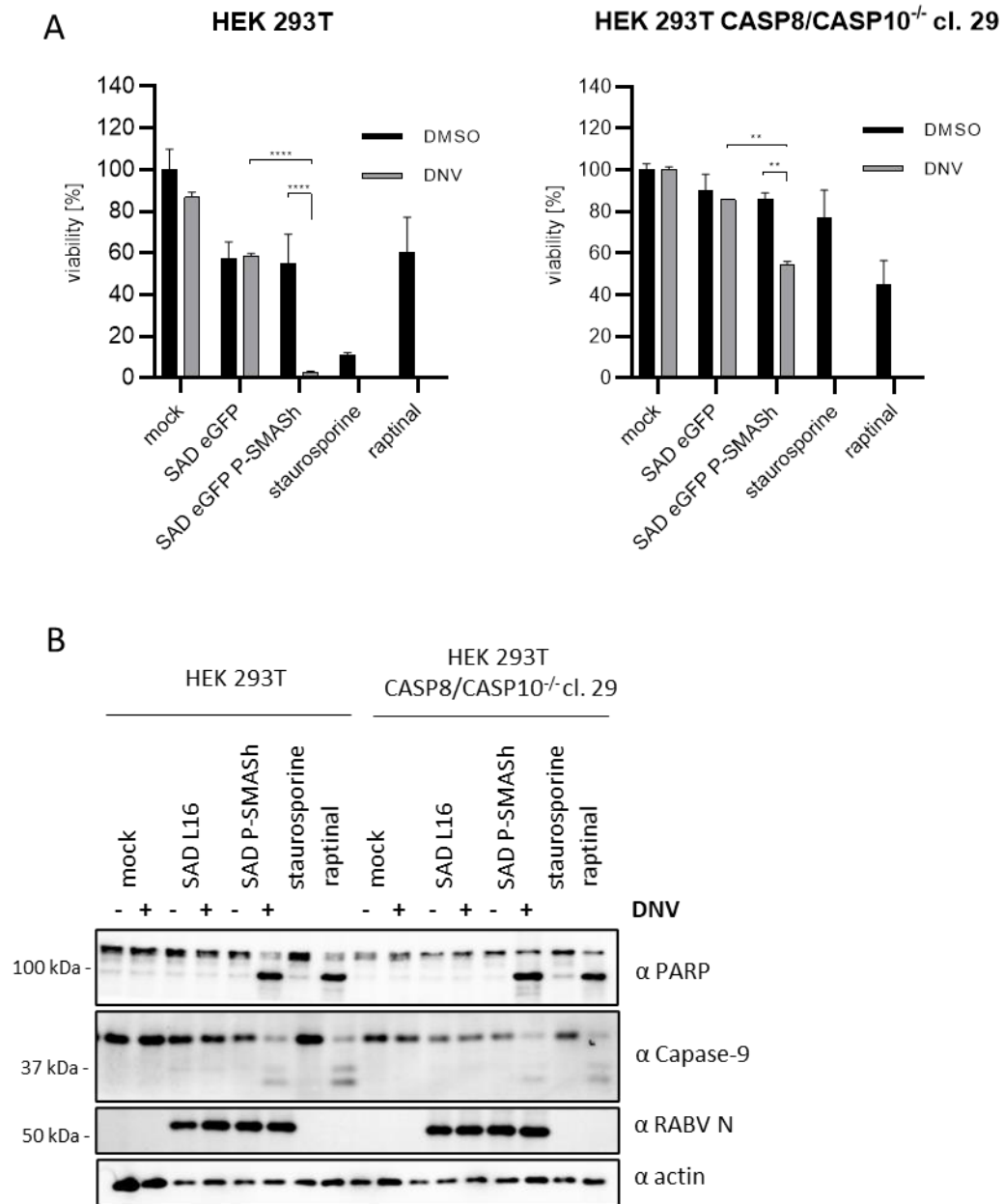(A) HEK 293T cells and HEK 293T CASP8/CASP10$^{-/-}$ cl. 29 in 96 wells were infected with SAD eGFP or SAD eGFP P-SMASh (MOI=3) and treated with 3 µM DNV (+) or DMSO (-) at 24 h. p. i.. Cells were analyzed 24 hours later via resazurin assay. One µM staurosporine and 10 µM raptinal served as control and were added to cells at same time as inhibitor treatment. Each bar and error bar represents mean + SD of technical replicates. (B) Similar experiment was performed with SAD L16 and SAD P-SMASh in 24 well and cells were lysed 24 h. p. DNV. for Western blot analysis.

3.1.6.4 Whole genome knockout screen revealed no survivors

So far, no individual gene knockout mutant cell line was found resisting SMASh induced cell death. To

receive a deeper insight of how exactly respective cell death is executed, we aimed to find a SMASh-killing

resistant knockout mutant. Therefore, a whole genome knockout screen was carried out. A pool of HEK 293T cells containing single knockouts of the whole genome was generated by lentiviral transduction and verified by deep sequencing (whole genome knockout pool and sequencing was carried out by Alexander Ghanem). Subsequently, a killing assay with SAD eGFP P-SMASh was performed with the aim to analyze the genetic sequence of potentially surviving cells. However, all cells died after inhibitor treatment (data not shown). It has to be mentioned, that we were not able not exclude the possibility that virus infection has already stressed and killed some cells independently of SMASh (see Figure 26). Nevertheless, the fact that no survivors were found in the screen goes along with the fact that neither PKR, FADD, CASP8 nor CASP10 knockout cells are resistant to SMASh-related killing. There is a possibility that a single knockout is not sufficient to stop killing by SMASh and depletion of multiple proteins is necessary to do so. Hence, it could be that not only caspase-8/-10 is primarily initiated, but also intrinsic apoptosis, perhaps even together with the executor caspase-3, is triggered simultaneously. The activation of multiple pathways would also fit to the speed of executed cell death.

3.1.7   Drug-dependent killing of cell lines from various hosts

Previous studies revealed high cytotoxicity of SAD P-SMASh post inhibitor treatment not only in HEK 293T cells, but also in HeLa, N2A, MEF, Huh7 and Huh7.5 cells (Masterthesis V. Pfaffinger 2016). Investigation of non-killable cell lines might give insights in how exactly SMASh related cell death is triggered. In order to find a cell line where SMASh and inhibitor addition has no cytotoxic effect, we performed a killing assay in various cell lines from different species. All tested cells were infected with SAD P-SMASh and treated with an inhibitor one day later. A list of the tested cells within this thesis is shown in Table 20. Strikingly, cell death occurred in all cells including cells lines from various hosts such as human, mouse, hamster, and monkey. Even primary isolated HFF cells died due to SMASh and inhibitor treatment (Table 20).

Table 20: Cell lines undergoing cell death upon SAD P-SMASh and NS3 inhibitor

| Species	Cell line	Description
Homo sapiens	HEK 293T	Human embryonic kidney cells expressing SV40 T-antigen
	HEK 293T FADD -/-	HEK 293T containing FADD Knockout
	HEK 293T CASP8 -/-	HEK 293T containing Caspase-8 Knockout
	HEK 293T CASP8/10 -/-	HEK 293T containing Caspase-8/-10 double Knockout *
	HeLa	Human cervix carcinoma cells
	HeLa CASP8 -/-	HeLa containing Caspase-8 Knockout
	HeLa CASP10 -/-	HeLa containing Caspase-10 Knockout
	hIPSC derived astrocytes	Human induced pluripotent stem cell derived astrocytes
	U-87 MG	Human glioblastoma cells
	U-251 MG	Human glioblastoma cells
	HFF	Human foreskin fibroblasts (primary isolate)
Mus musculus	N2A	Mouse neuroblastoma cell line
	MEF	Mouse embryonic fibroblasts
	mESC derived neurons	Mouse embryonic stem cell derived neurons
	GL261 new	Mouse glioblastoma cells
	GL261 moko	Mouse glioblastoma cells
	B16	Mouse melanoma cells
	MC38	Mouse colon carcinoma cells
Mesocricetus auratus	BHK21	Baby hamster kidney cells
	BSR T7/5	BHK-21-derived cells expressing T7-RNA pol
Cercopithecus aethiops	Vero	African green monkey cells

*in-frame deletions in caspase 8 and caspase 10

3.1.8   Cell death in cancer cells can be enhanced by SMASh

Many cancer cells are resistant to apoptosis due to dysregulation of pro- and anti-apoptotic factors. For example, disrupted pro-apoptotic transcription factor p53 is associated with various cancers resulting in a lack of expression of anti-survival Bax, Noxa and Puma (Kandoth et al. 2013; Aubrey et al. 2018). In contrast, anti-apoptotic members of the BCL-2 family are often overexpressed in tumors (Roberts and Huang 2017). Moreover, studies with a human colon cancer cell line MC38 revealed resistance to TRAIL induced apoptosis due to accelerated degradation of caspase-8 (Zhang et al. 2005). Consequently, there might be cancer cells that are resistant to SMASh-induced apoptosis. To evaluate whether SMASh is able to induce cell death in those cells as well killing assay with different cancer cell lines was applied.

In a first approach, we infected human glioblastoma U87-MG cells with a high MOI (MOI=3) in order to infect all cells in culture and treated them with 3 µM DNV 24 h post infection. Cell viability and LDH release was evaluated via resazurin assay and LDH-assay, respectively, additional 24 h later to look for

immunogenic cell death. Interestingly, infection alone already led to viability decrease of approximately 50 %. DNV treatment of SAD eGFP P-SMASh infected cells slightly enhanced cytotoxicity. This effect was significant, when evaluated by single comparison within a t-test (p = 0,0452) but not by 2-way ANOVA. Of note, the rapid apoptosis inducer Raptinal had no significant effect on cell viability (Figure 27A). LDH was not released in any sample but the direct lysis control indicating the induction of a non-lytic cell death like apoptosis (Figure 27B). To receive more insights on cell killing in these specific cancer cells, a similar experiment was carried out and cells were lysed for analyzing PARP cleavage in Western blot. PARP is specifically cleaved in 89 and 24 kDa fragments during apoptosis. As this cleavage pattern is characteristic for apoptosis it is used as marker for apoptotic cell death (Gobeil et al. 2001). In all experiments in this dissertation, an antibody that detects full-length PARP as well as the cleaved 89 kDA fragment was used. In consistency with viability analysis, PARP was cleaved in all infected samples. Full-length PARP was completely gone SAD eGFP P-SMASh and DNV treated cells whereas a faint band was detected in the other infected samples (Figure 27C).
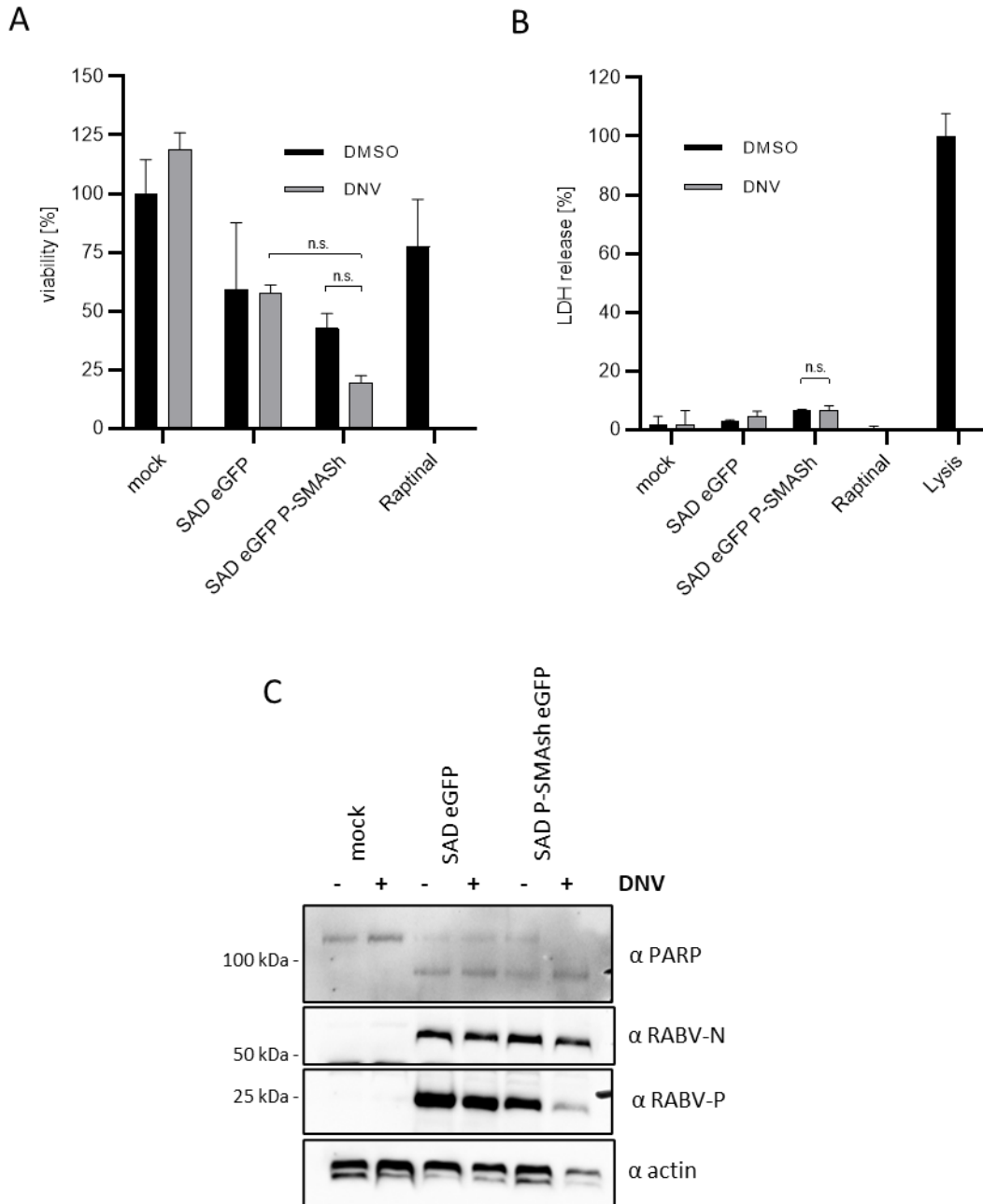
Figure 27: Killing of U87-MG by RABV and SMASh and DNV.
U87-MG cells in 96 wells were infected with SAD eGFP or SAD eGFP P-SMASh (MOI=3) and treated with 3 μM DNV (+) or DMSO (-) at 24 h. p. i.. At time point of inhibitor treatment additional cells were treated with 10 μM Raptinal for control. Cells were analyzed 24 h. p. DNV by resazurin assay (A) or LDH release assay (B). mean + SD of each condition is represented by bars and error bars. Additional experiment was performed in 24 well and cells subjected to Western blot analysis (C). n.s.: not significant.

Next, killing assay was performed with mouse melanoma B16 cells as above. As before, a cytotoxic effect of RABV infection alone was visible, which could be enhanced by addition of DNV in case of SAD eGFP P-SMASh infection (Figure 28A). However, this time we could not detect cleaved PARP in

Western blot, although the band of full-length PARP was very faint. Moreover, the full-length caspase-10 level appears to be slightly reduced, but only in SAD eGFP P-SMASh and DNV treated cells (Figure 28B). Measuring LDH in an independent experiment revealed a significant increase within the supernatant upon SAD eGFP P-SMASh and infection DNV treatment (LDH assay was performed by Franz Bauernschmitt; Figure 28C). In consequence, we assumed that beside the cytotoxicity of RABV infection, SMASh and inhibitor treatment could induce a lytic cell death in B16 cells.
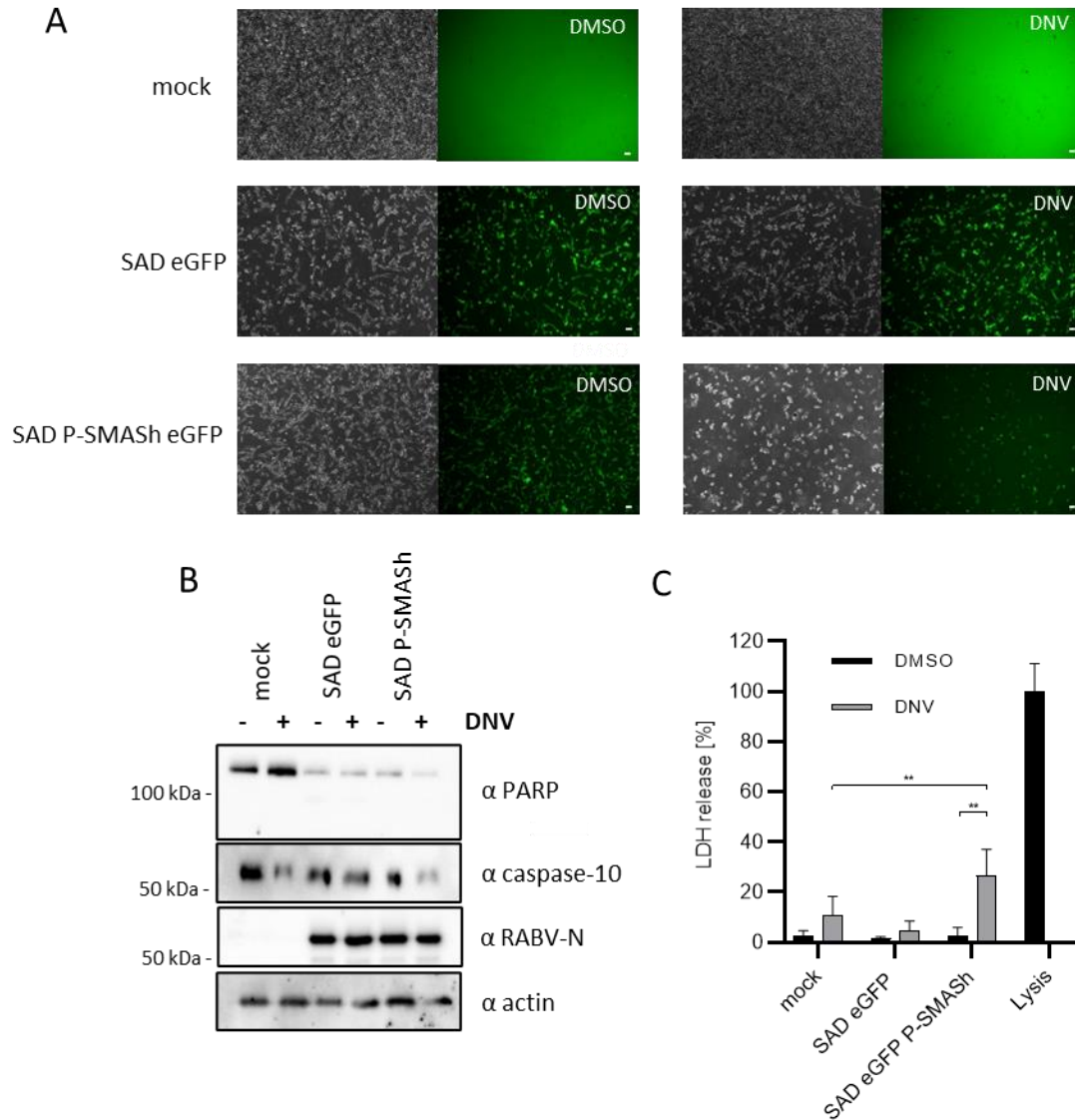

Figure 28: Killing of B16 by RABV and SMASh.
B16 cells in 24 wells were infected with SAD eGFP or SAD eGFP P-SMASh (MOI=3) and treated with 3 µM DNV (+) or DMSO (-) at 24 h. p. i.. Cells were analyzed 24 h. p. DNV via microscope (A) and lysed for Western blot analysis (B). Similar killing assay was performed in 96 well and LDH release measured at 24 h. p. DNV. Means of technical triplicates are represented by bars with respective standard deviations indicated by error bars (C). Scale bar 250 µm.

The phenomenon of killing by RABV and enhancement by SMASh was observed in various other cancer cell lines such as human glioblastoma cells (U-251 MG), mouse glioblastoma cells (GL261 new and moko) and mouse colon carcinoma cells (MC38; Table 20).

Taken together, RABV reveals a pronounced cytotoxicity already without expression of the SMASh-tag in different cancer cell lines. This phenomenon can be enhanced by addition of the NS3 inhibitor after infection with SAD eGFP P-SMASh.

3.1.9 LTHP and KIDT motif of the SMASh-tag are not essential for killing

To understand the initiated pathway, cellular responses after SAD P-SMASh infection and DNV treatment were so far analyzed and, activation of apoptosis involving numerous caspases could be shown. However, it was not possible to identify a single protein that is activated in first place, which might be a hint for numerous activated proteins instead. To receive more insights on the initiation of cell death, we next addressed the question what part of SMASh is necessary for killing. Previously, Prikhod'ko et al. reported that HCV NS3 protease is able to bind and activate caspase-8 by the LTHP motif (Prikhod'ko et al. 2004). Interestingly, the LTHP motif is also included in the SMASh-tag (see Figure 29). Although caspase-8 was not the only activated caspase, the LTHP motif might be necessary for apoptosis activation allowing caspase binding and activation. To address this question SAD YFP-SMASh viruses carrying different mutations within the LTHP motif were generated. Those viruses were named dependent on their mutation SAD YFP-SMASh LTHP-LTHA, SAD YFP-SMASh LTHP-LTAA, SAD YFP-SMASh LTHP-AAHP and SAD YFP-SMASh LTHP-AAAA.

Of note, the LTHP motif appears within the NS3 helicase domain, although the main part of NS3 helicase is deleted within the SMASh-tag with only the parts necessary for degradation left (Chung et al. 2015). Furthermore, four additional non-HCV related amino acids, KIDT, appear within the SMASh helicase domain (see Figure 29). This sequence was not further described by the inventors of the SMASh-tag but might serve as linker. To investigate the role of the KIDT motif in context of conditional cell death, we generated SAD YFP-SMASh KIDT-AAAA with the KIDT motif replaced by four alanine residues.
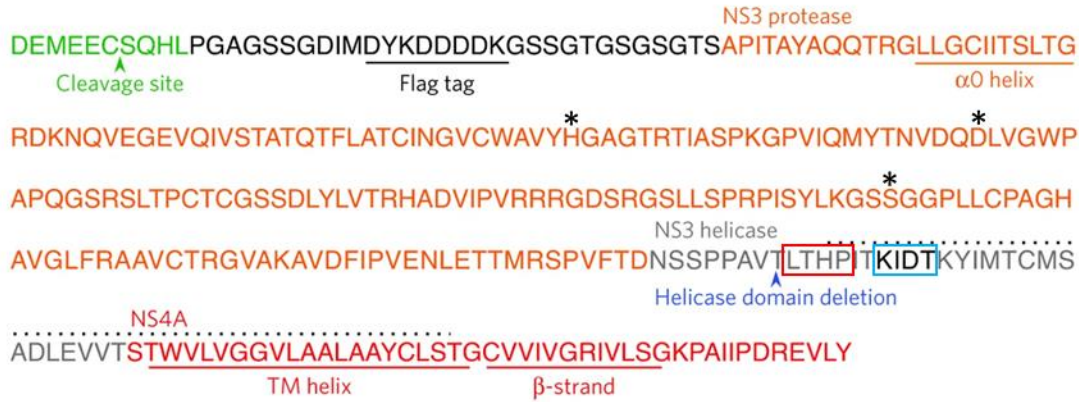
Figure 29: Sequence of SMASh-tag including the LTHP and KIDT motif
LTHP is highlighted within the SMASh sequence by red box. KIDT motif is highlighted by blue box. Black asterisks indicate catalytic triad of the NS3 protease

All respective viruses were used for killing assays. Hence, HEK 293T cells were infected with a MOI of 3 and treated with DNV or DMSO 24 hours later. After additional 24 hours cells were lysed for Western blot analysis. Furthermore, viability was measured in an additional resazurin experiment which was conducted similarly. All samples with viruses containing mutations in the LTHP motif showed similar PARP cleavage to the SAD YFP-SMASh control, when treated with DNV. Also, mutations in the KIDT sequence resulted in PARP cleavage when treated with DNV. However, substantial levels of cleaved PARP could be already detected in the control treatment of KIDT-AAAA (Figure 30A). Higher constitutive toxicity of this mutant was also indicated in the viability assay. Mutations within the LTHP motif showed viability similar to the SAD YFP-control and were also able to conditionally induce cell death. Conditional decrease of viability was also seen in SAD YFP-SMASh KIDT-AAAA infected cells. Reflecting the results from Western blot analysis above, a direct comparison of SAD YFP-SMASh and SAD YFP-SMASh KIDT-AAAA DMSO controls revealed significant reduced cell viability for the latter (unpaired t-test; p = 0.0338). However, significance was not given by two-way ANOVA test and there is no significant difference regarding viability after DNV treatment in those cells (Figure 30B).

Taken together, LTHP motif does not play an obvious role in SMASh related killing, whereas the KIDT motif seems to reduce intrinsic constitutive toxicity of the SMASh-tag.
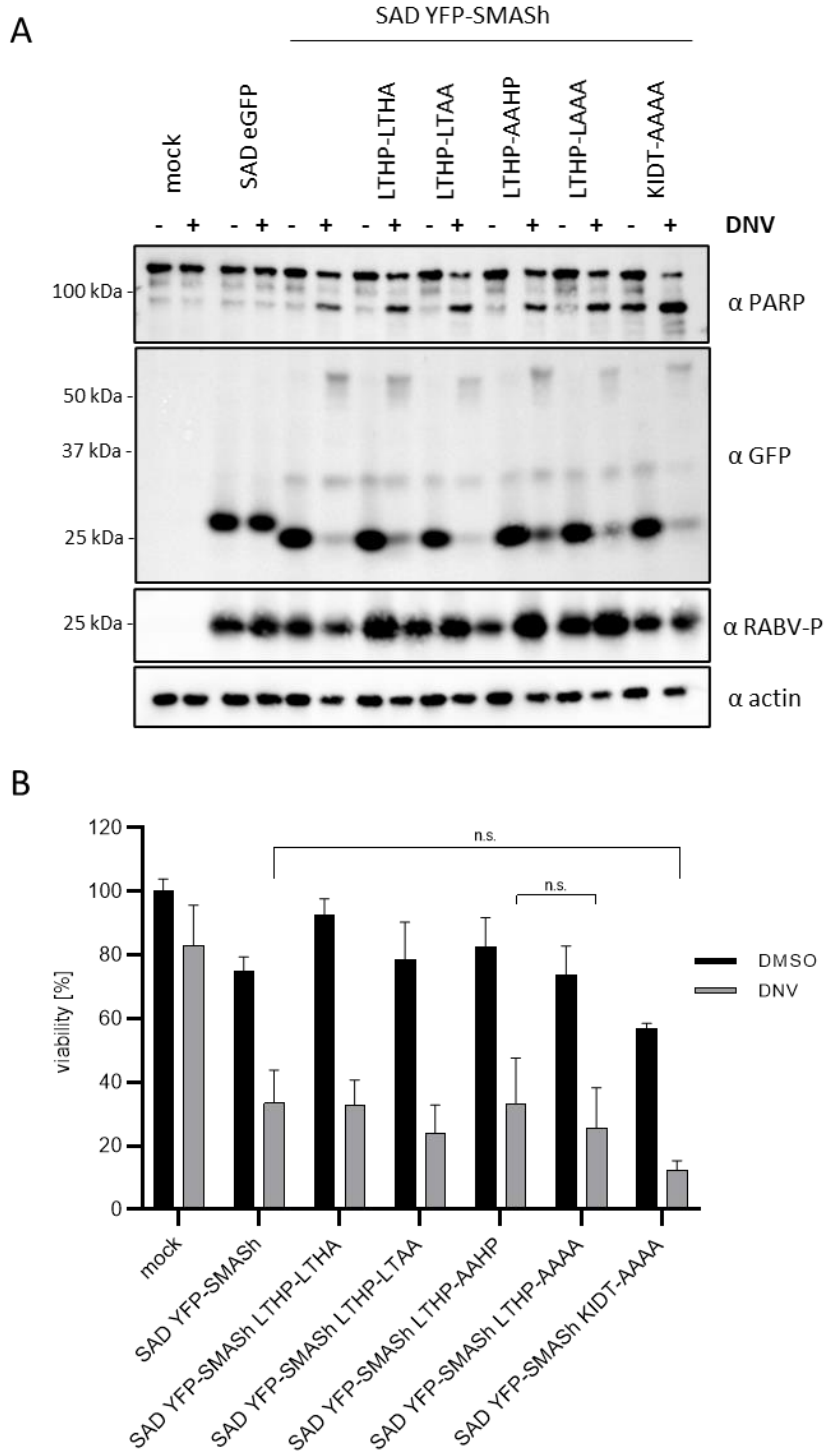
Figure 30: LTHP and KIDT motifs are not essential for killing.
(A) HEK 293T cells in 24 wells were infected with SAD eGFP, SAD YFP-SMASh, SAD YFP-SMASh LTHP-LTHA, SAD YFP-SMASh LTHP-LTAA, SAD YFP-SMASh LTHP-AAHP, SAD YFP-SMASh LTHP-AAAA or SAD YFP-SMASh KIDT-AAAA (MOI=3) and treated with 3 µM DNV (+) or DMSO (-) at 24 h. p. i.. Cells were lysed 24 hours later for Western blot analysis. (B) Similar experiment was performed as above in 96 wells. LDH release was measured 24 h. p. DNV.. Each bar and error bar represent mean + SD of technical triplicates.

3.1.10 SMASh-tag alone provides for conditional cytotoxicity

Next, we wanted to see whether the SMASh-tag by itself is toxic, or able to conditionally induce cytotoxicity, respectively. Therefore, viruses expressing the original C-terminal SMASh-tag separately, without any fusion protein, were generated (SAD SMASh). In addition, we engineered viruses with the tag lacking the complete cleavage site motif, SAD SMASh ΔCS. This was cloned, rescued, and produced by Yassine Haddad (Figure 31A). The new viruses were subjected to a killing assay, followed by Western blot analysis. As indicated by PARP cleavage, SAD SMASh appeared to conditionally induce apoptosis also without fusion to another protein. Nevertheless, it was slightly less toxic under DNV condition despite a similar expression of RABV P and RABV N proteins in infected cells. In contrast to other SMASh-tag containing viruses SAD SMASh ΔCS revealed high constitutive cytotoxicity as indicated by very low actin levels (microscopic data not available), which was not further stimulated by DNV addition. Surprisingly, typical PARP cleavage could not be detected suggesting that this cytotoxic effect is not related to apoptosis. Of note, SAD eGFP served as control and led to slight PARP cleavage as well, independent of DNV or DMSO treatment (Figure 31B).

Additionally, cell viability was determined in an independent experiment with resazurin. As before, the control (here SAD L16 infected) cells show already a reduced viability, whereas SAD YFP-SMASh and SAD SMASh appeared to be less toxic in DMSO treatment. When treated with DNV, cells infected with SAD YFP-SMASh as well as SAD SMASh showed reduced viability. Furthermore, SAD SMASh ΔCS infection resulted in viability of approximately 40 % after both, DMSO and DNV treatment (44 % in DMSO treatment, 40 % in DNV treatment; Figure 31C). Thus, this data corroborates data from Western blot analysis before (Figure 31B).
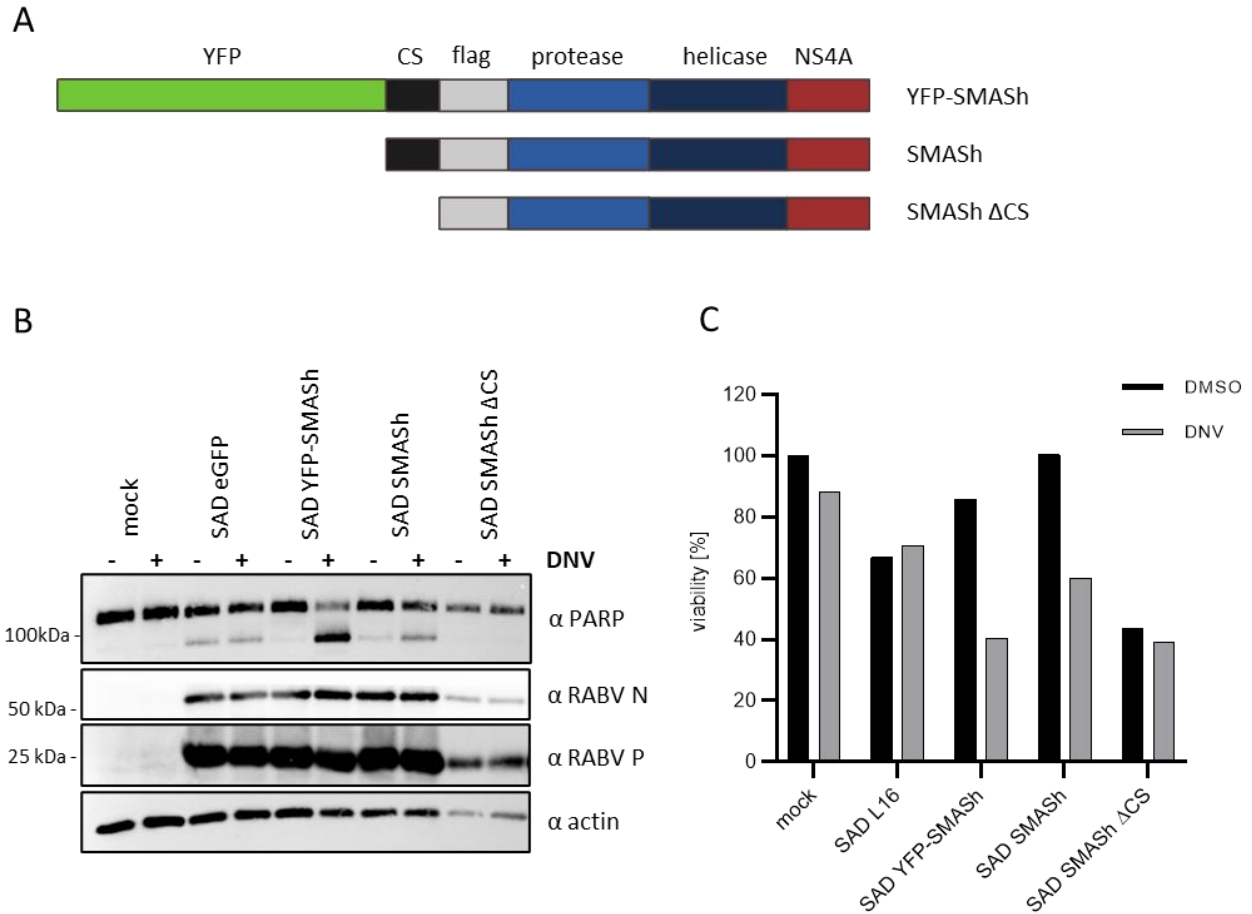
**Figure 31: NS3 cleavage site is important for conditional cytotoxicity of SMASh.**
(A) Schematic representation of YFP-SMASh, SMASh and SMASh ΔCS. (B) HEK 293T cells in 24 wells were infected with SAD eGFP, SAD YFP-SMASh, SAD SMASh or SAD SMASh ΔCS (MOI=3) and treated with 3 μM DNV or DMSO at 24 h. p. i.. Cells were lysed 24 hours later for Western blot analysis. (C) For Quantification of cell death similar experiment was performed with SAD L16 as control. Resazurin assay was conducted 24 h. p. DNV.

3.1.11 NS3/4A protease activity does not play a role in SMASh related killing

In context of HCV, the serine protease NS3/4A is essential for viral replication processing the polyprotein at various junctions and releasing thereby other non-structural proteins. In addition to that it plays an important role combating host cell defense mechanisms. Thus, NS3/4A counteracts innate immunity by hydrolyzing two key adaptors for innate antiviral signaling pathways, the mitochondrial antiviral signaling protein MAVS ((Li et al. 2005b; Meylan et al. 2005) and TIRF (TIR domain containing adaptor inducing IFN-β) (Li et al. 2005a). Furthermore, TC-PTP (T-cell protein tyrosine phosphatase) is downregulated by its cleaving leading to enhancement of EGF-signaling (Brenndörfer et al. 2009).

Since the NS3/4A protease sequence is slightly altered in the SMASh-tag, there might be other substrates that become accessible for the protease. The three residues His57, Asp81 and Ser139 (referring to the original HCV NS3 sequence) form the catalytic triad. Mutation of any residue results in disruption of the catalytic activity. To address the question, whether the NS3 protease hydrolyzes a cellular protein causing apoptosis, we produced SAD YFP-SMASh S139A containing an inactive NS3 protease and compared it with the original SAD YFP-SMASh. It has to be mentioned that the residue 139 refers thereby to the original HCV NS3.
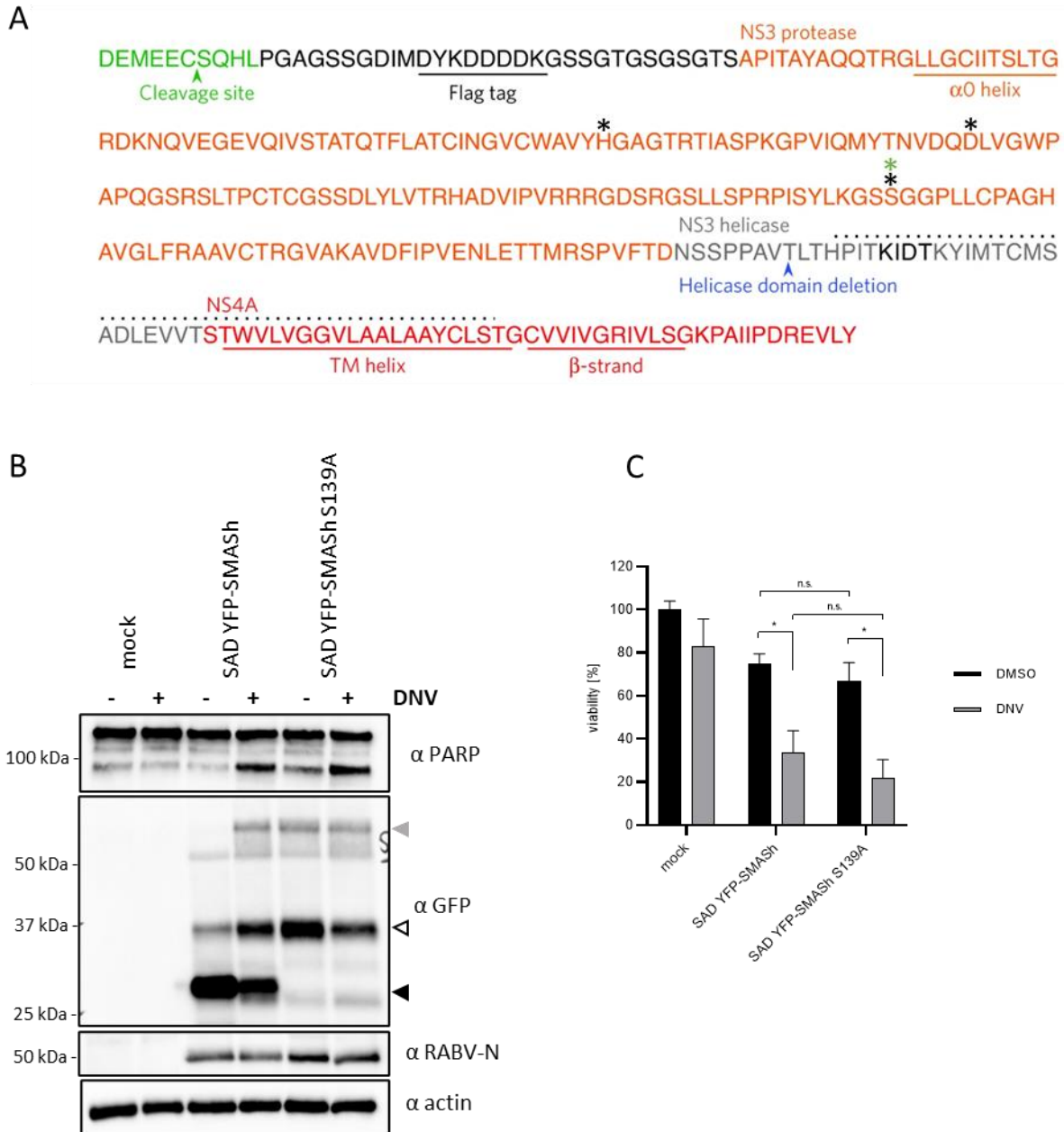
Figure 32: NS3 protease activity is not important for SMASh related killing.
(A) Representation of the SMASh-tag sequence. Black asterisks indicate the catalytic triad of the NS3 protease. The mutated HCV NS3 S139 residue is highlighted by an additional green asterisk. (B) HEK 293T cells in 24 wells were infected with SAD eGFP, SAD YFP-SMASh or SAD YFP-SMASh S139A or SAD SMASh ΔCS (MOI=3) and treated with 3 µM DNV (+) or DMSO (-) at 24 h. p. i.. Cells were lysed 24 hours later for Western blot analysis. Note that S139A has lost the ability to (auto)cleave the YFP fusion protein. Black arrow indicates size of cleaved YFP, grey arrow of respective fusion protein; white arrow indicates additional band (C) Similar experiment was performed in 96 well in triplicates followed by resazurin assay at 24 h. p. DNV. Each bar and error bar represents mean + SD of technical replicates. n.s.: not significant.

By probing with a GFP antibody recognizing YFP as well, cleavage of YFP and inhibition of cleavage by the inhibitor could be analyzed. SAD YFP-SMASh S139A did not cleave the SMASh-tag resulting in full-length fusion protein with the size of approximately 59 kDa (grey arrow), also in the absence of inhibitor. Surprisingly, an additional protein band of approximately 37 kDa (white arrow) in SAD YFP-SMASh and SAD YFP-SMASh S139A samples differing in thickness in DMSO and DNV treated samples could be detected. As it appears in S139A, this indicates NS3/4A independent processing of the YFP-SMASh fusion protein within the SMASh-tag, which was not further followed. Importantly, drug treatment resulted in comparable toxicity of protease competent and incompetent constructs. A slight PARP cleavage was also detected in DMSO treatment and in mock treatment (Figure 32B). However, independent viability assay with resazurin could reveal no significant difference compared to SAD YFP-SMASh (Figure 32C). To further compare SAD YFP-SMASh and SAD YFP-SMASh S139A, a real time viability assay was applied. In a first experiment, we measured viability after inhibitor treatment at 24 hours post infection (Figure 33A). In a second experiment, DNV was added directly at timepoint of infection, followed by viability monitoring (Figure 33B). In both cases the S139A mutant behaved like SAD YFP-SMASh. For this reason, we concluded that the NS3/4A protease activity is not important for killing. Instead, these results indicate that binding of the inhibitor to the active or inactive protease is required for apoptosis, and cleavage is not required. For this reason, we assumed that the NS3 inhibitor might trigger a conformational change leading to the initiation of apoptosis.
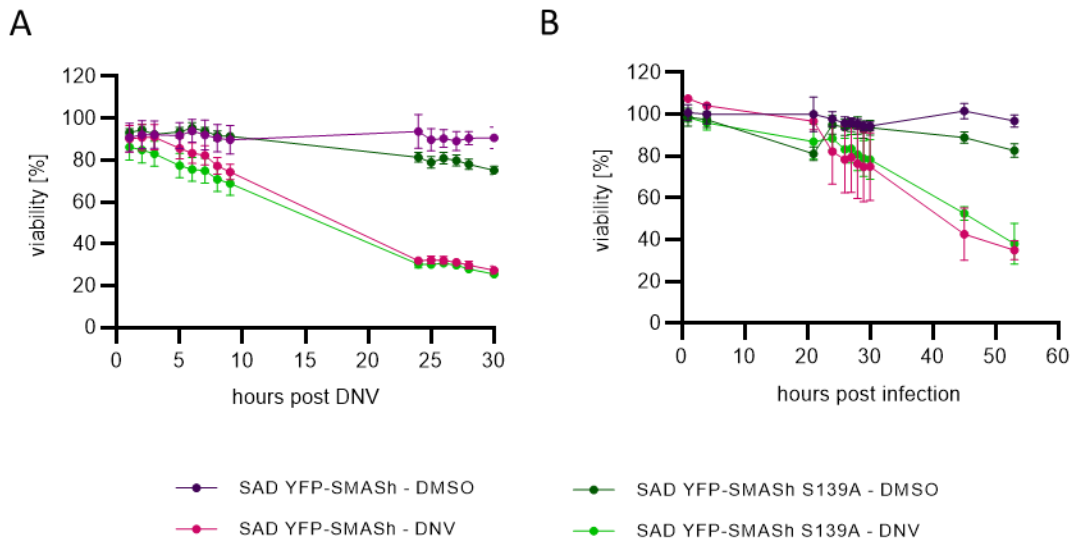
**Figure 33: Mutation within the catalytic triad of NS3 protease has no effect on killing kinetic.**
(A) HEK 293T cells in 96 wells were infected with SAD YFP-SMASh or SAD YFP-SMASh S139A (MOI=3) and treated with 3 µM DNV or DMSO either at 24 h. p. i.. (A) or directly at timepoint of infection (B). Then, real time viability was determined at various timepoints. Dots and error bars represent mean + SD of technical triplicates.

3.1.12 Truncated SMASh is not toxic upon inhibitor treatment

Previous experiments displayed that the NS3 protease catalytic activity does not play a role in killing letting the question of the cytotoxic component within SMASh open. With the aim to gain more insights in how apoptosis is triggered, we generated plasmids expressing differently truncated YFP-SMASh constructs. Thus, the original YFP-SMASh was compared with YFP-SMASh-heli-stop and YFP-SMASh-prot-stop, having a stop codon after the helicase domain or the protease domain, respectively (Figure 34A). All constructs were subjected to a killing assay. Twenty-four hours post transfection 3 µM DNV was added, and cells were lysed 28 hours later for Western blot analysis. Additional to the determination of cytotoxicity by PARP cleavage, we examined the ability of the protease to cleave or degrade the YFP fusion protein, respectively, by using a GFP antibody. Interestingly, we could detect conditional cytotoxicity only in the original YFP-SMASh samples. Both truncated versions, YFP-SMASh-heli-stop and YFP-SMASh-prot-stop, did not induce apoptosis after inhibitor treatment.

DNV should block cleavage leading to the retainment of the fusion protein, which is usually directly degraded. Hence, in pCAGGS YFP-SMASh transfected cells, almost no fusion protein was detected in inhibitor condition. In contrast, truncations resulted in impaired degradation ability indicated by clearly detectable full-length fusion protein of DNV treated cells. This was expected because NS4A served also as part of the degron. In case of YFP-SMASh-heli-stop YFP-SMASh fusion protein was also present in DMSO control treatment suggesting that the cleavage between the SMASh-tag and YFP was compromised as well. This was not observed in YFP-SMASh-prot-stop samples, although it has to be mentioned that expression levels were lower as well (Figure 34B). Taken together, larger modification of the SMASh-tag, which are made by truncations, led to the loss of conditional cytotoxicity, but also affected degradation and cleavage of the fusion protein. All in all, these data support the hypothesis that inhibitor binding induces a conformational change of the SMASh-tag which is then able to initiate apoptosis.
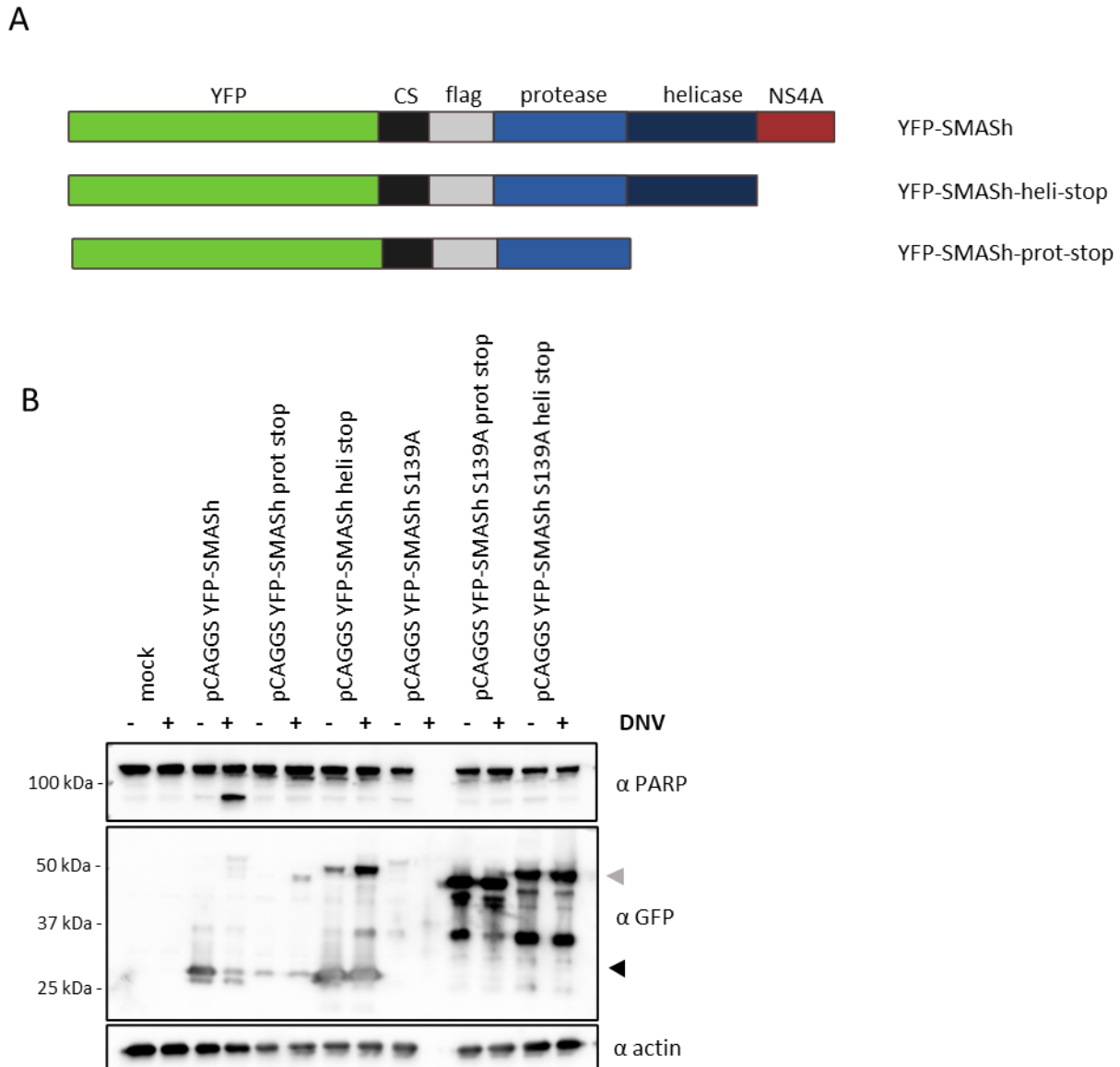
Figure 34: Truncated SMASh is not able to induce cell death.
(A) Schematic representation of YFP-SMASh, YFP-SMASh-heli-stop and YFP-SMASh-prot-stop (B) HEK 293T cells in 24 wells were transfected with 500 ng pCAGGS YFP-SMASh, pCAGGS YFP-SMASh-heli-stop and pCAGGS YFP-SMASh-prot-stop and treated with 3 µM DNV (+) or DMSO (-) at 24 h. p. t.. Cells were lysed 28 hours later for Western blot analysis. Black arrow indicates size of cleaved YFP, grey arrow of respective fusion protein.

3.1.13 N-terminal fusion of SMASh is slightly toxic without inhibitor

Previous experiments displayed a high cytotoxicity of the authentic SMASh-tag upon inhibitor treatment. However, studies concentrated on C-terminal fusion of the SMASh-tag. The SMASh-tag can also be fused N-terminally on a protein of interest. For this approach, Chung and colleagues optimized the tag by

inserting a 6-aa linker within NS4A. Furthermore, the NS4A domain has three additional amino acids at its C-terminus (Chung et al. 2015). To evaluate whether N-terminal fusion of SMASh to a protein leads to apoptosis as well, we compared YFP-SMASh and SMASh-YFP after 6 hours post DNV, which was added 24 hours post transfection. Similar cytotoxic effect was observed in pC6 SMASh-YFP and pCAGGS YFP-SMASh transfected cells after DNV treatment. Interestingly, SMASh-YFP slightly induced apoptosis in the non-drug control as well. It has to be mentioned that different vectors were used in this experiment (Figure 35A). To exclude the vector as reason for cytotoxicity, we generated pCAGGS SMASh-P and compared it to pCAGGS P-SMASh within a killing assay in HEK 293T cells as before. Again, SMASh-P had not only a toxic effect in DNV treated cells, but also within the DMSO control. Thus, PARP was cleaved equally after inhibitor and non-inhibitor treatment (Figure 35B).

In order to confirm these results SAD SMASh-YFP was generated. Killing assay with SAD SMASh-YFP and SAD YFP-SMASh was conducted, and cell viability determined 24 hours post DNV. After that, cells were lysed for Western blot analysis. Again, apoptosis was induced after DNV treatment in both, SAD YFP-SMASh and SMASh-YFP samples. A slight band of cleaved PARP could also be detected in SAD SMASh-YFP control cells, which corresponds to the drop in cell viability measured via resazurin assay. Of note, also in SAD L16 control a reduction of cell viability was determined, although no major PARP cleavage was detectable (Figure 35C, D).

All in all, these results correspond well to findings of previous mentioned experiments. Together, these data provide evidence that the N-terminally fused SMASh-tag is toxic even in the absence of inhibitor, although not to a comparable extent as after addition of DNV.
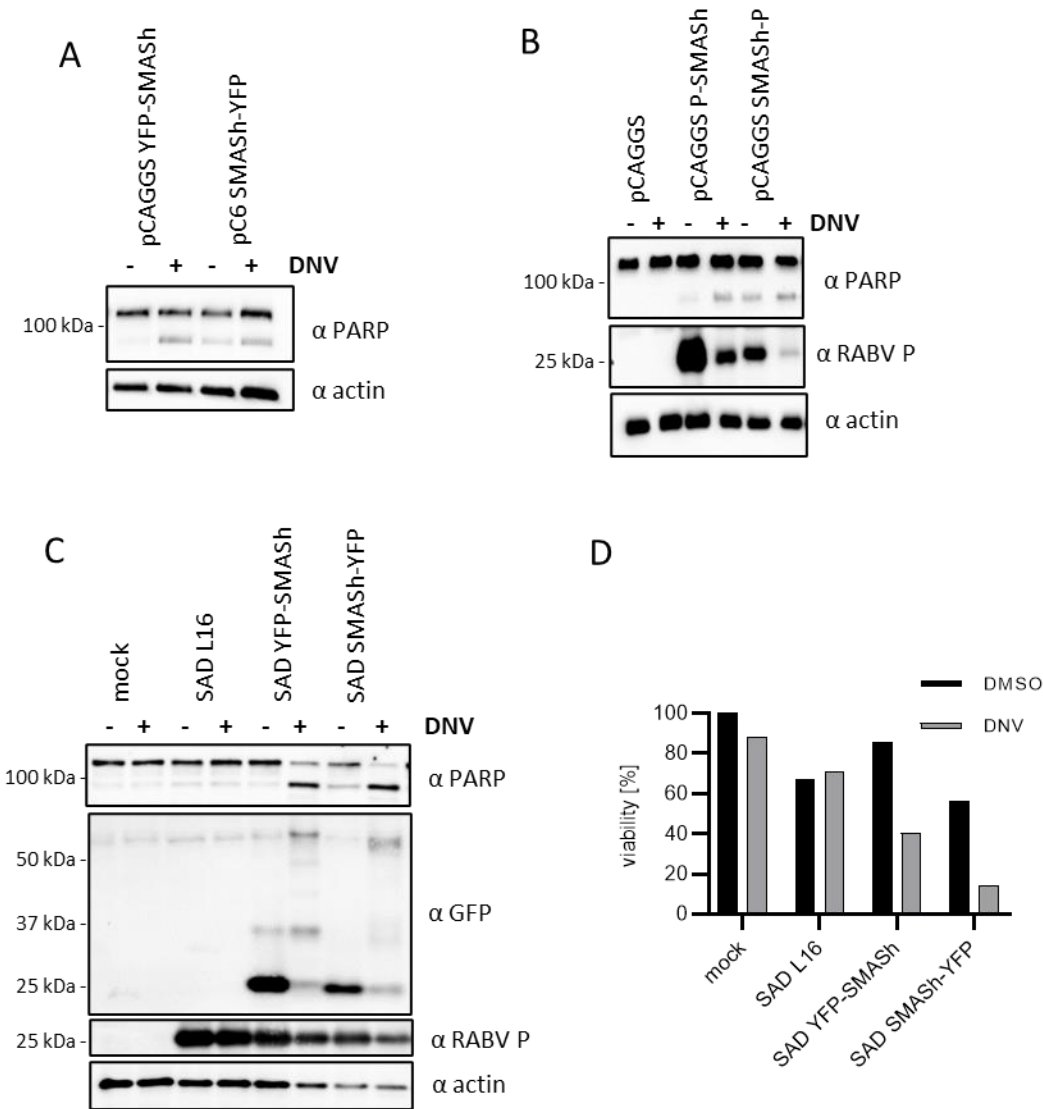
Figure 35: N-terminal SMASh induces cell death already without inhibitor.
(A) HEK 293T cells in 24 wells were transfected with 500 ng pCAGGS YFP-SMASh or pC6 SMASh-YFP and treated 24 hours later with 3 μM DNV (+) or DMSO (-) followed by lysing the cells for Western blot analysis at 6 h. p. DNV. (B) Killing assay with pCAGGS P-SMASh and pCAGGS SMASh-P with same kinetic as before. Transfection was done with 500 ng of pCAGGS P-SMASh or pCAGGS SMASh-P. (C, D) HEK 293T cells were infected with SAD L16, SAD YFP-SMASh or SAD SMASh-YFP (MOI=3) and treated with 3 μM DNV (+) or DMSO (-) 24 h. p. i.. Additional 24 hours later cells were lysed for Western blot analysis (C) after cell viability was determined via resazurin (D).

3.2   Non-toxic controllable RABV viruses

RABV is a neurotropic virus that spreads from neuron to neuron in exclusively retrograde manner. This feature was harnessed already decades ago and non-recombinant RABV used as neuronal tracer e.g. for mapping multiple neurons within a pathway or disease (Astic et al. 1993; Ugolini 1995). In order to map

direct neuronal connections a recombinant single-round RABV ΔG virus is commonly used. Thereby, a starter neuron that expresses not only the RABV glycoprotein but also the EnvA receptor (TVA), is infected with RABV ΔG (EnvA) pseudotyped with the avian viral EnvA envelope protein. Viral spread is supported by RABV G expression in starter cells but limited to one single round staining thereby only direct connected neurons. Nowadays, this technique represents the gold standard for monosynaptic tracing and brought insights on neural connectivity and brain circuitry. However, RABV is to some degree cytopathic, leading to degeneration of neurons after approximately two weeks. In consequence long term studies are so far not possible. To overcome this limitation a controllable RABV might be helpful. This could allow a regulated on-switch of the tracer or shut down before a cytopathic effect.

3.2.1   SAD ΔG eGFP L-SMASh and SAD ΔG eGFP SMASh-L are not suitable for virus control

SMASh fused to the RABV P or N induced cell death when the NS3 inhibitor was applied to an established infection. In contrast, fusion to the RNA-dependent RNA polymerase L had no cytotoxic effect, possibly because of low expression levels (Masterthesis V. Pfaffinger 2016). Hence, we aimed to clarify whether viruses containing SMASh-L or L-SMASh are suitable as controllable viruses. Since single-round viruses lacking the glycoprotein are usually taken for neuronal tracing approaches, experiments were performed with SAD ΔG eGFP viruses on mESC derived neurons (mESC derived neurons were kindly provided by Chloé Scordel and Maximilian Eizinger). In addition to SAD ΔG eGFP L-SMASh and SAD ΔG eGFP SMASh-L we used SAD ΔG eGFP N-SMASh and SAD ΔG eGFP as controls. In this experiment, cells were infected with a MOI of 1 and treated at the same time with DNV or DMSO. In accordance with the standard procedure of handling mESC derived neurons, two days later half of the media was replaced by fresh one supplemented with the NS3 inhibitor or DMSO. Four days post infection neurons infected with control viruses began to degenerate. Neurons lost their pyramidal shape and started to aggregate. In consequence, microscopic pictures were taken, and lysed cells subjected to Western blot analysis.

Interestingly, DNV had almost no effect in SAD ΔG eGFP L-SMASh infected cells, showing green cells in microscopic analysis and similar levels as DMSO treated cells of RABV N and P. In contrast, SAD ΔG eGFP SMASh-L was affected by DNV treatment showing only little GFP signal (Figure 36A) and reduced N and P levels 4 days post treatment (Figure 36B). However, infection was not completely inhibited, possibly because small amounts of functional L proteins are sufficient for viral transcription and replication (see Discussion). In consequence, the non-toxic SAD ΔG eGFP SMASh-L and SAD ΔG eGFP L-SMASh are not suitable for neuronal tracing approaches since establishment of infection was in both cases possible, at least to a certain degree, despite drug treatment.
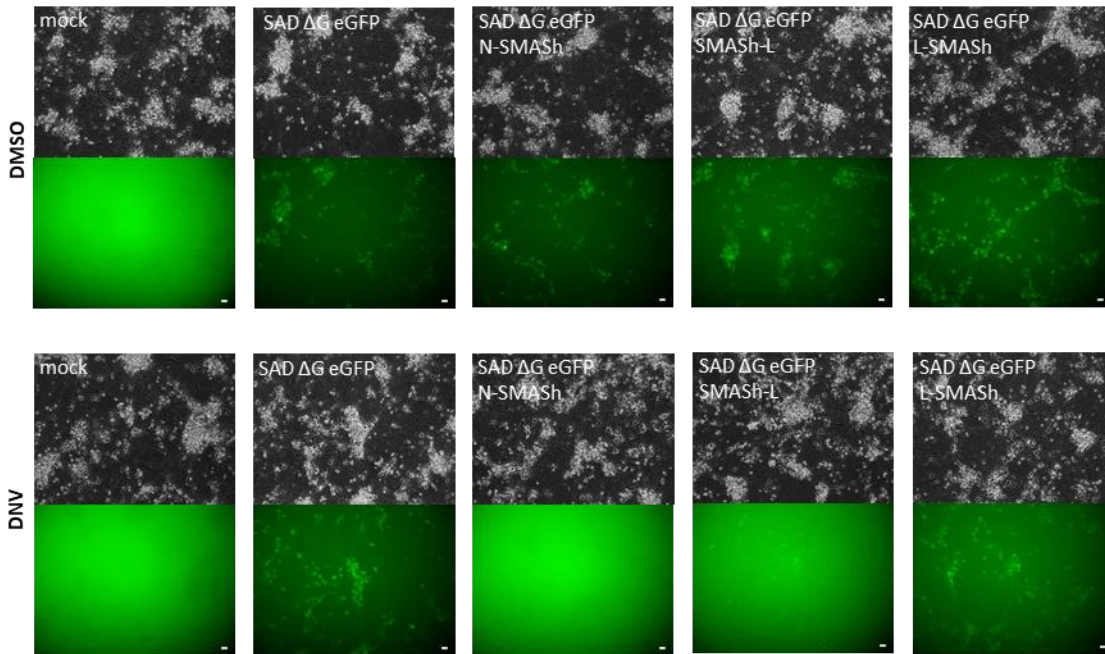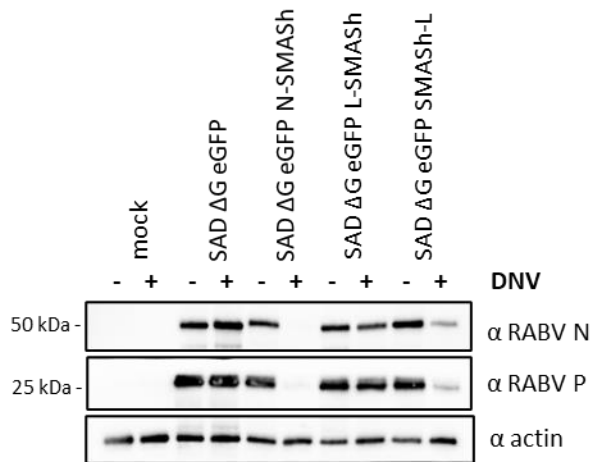
Figure 36: The NS3 inhibitor does not prevent infection of mESC derived neurons with SAD ΔG eGFP L-SMASh and SAD ΔG eGFP SMASh-L.
mESC derived neurons were infected with SAD ΔG eGFP, SAD ΔG eGFP N-SMASh, SAD ΔG eGFP L-SMASh; SAD ΔG eGFP SMASh-L (MOI=1) and simultaneously treated with 3 µM DNV or DMSO. After two days half of the media was exchanged, and fresh media was supplemented with 3 µM DNV (+) or DMSO (-). Four days post infection microscopic pictures were taken (A) and cells were lysed for Western blot analysis (B). Scale bar: 250 µm.

3.2.2 Generation of a non-toxic tag

Previous experiments showed that SMASh fusion to the polymerase L is not suitable for complete control

of viral growth. A fusion to the nucleoprotein might be interesting for virus switch-off/on but leads to cell

death when drug treatment occurs after establishment of infection. In fact, a non-cytotoxic tag that would allow virus control post infection is of great interest. For example, virus vectors encoding Cre recombinase for switching on cellular Cre-dependent reporters or indicators could be silenced after Cre delivery and imaged on long term. For this reason, we aimed to generate a non-toxic SMASh-derived tag.

Experiments with truncated SMASh-tags suggested that major changes within the tag can abolish cytotoxicity (Figure 34). Although the NS3 protease is enzymatically active without NS4A, this cofactor enhances cleavage ability by stabilizing the catalytic triad (Butkiewicz et al. 1996; Kramer et al. 2014; Hamad et al. 2016). In HCV the NS3 helicase is important for RNA binding and unwinding, whereas in context of SMASh, the major part of the helicase domain is deleted and extant parts serve together with NS4A as degron. Thus, we decided to remove the remaining SMASh helicase domain and compensate the impaired degradation ability with a PEST sequence at the C-terminus. PEST sequences are proline (P), glutamic acid (E), serine (S), and threonine (T) rich motifs that functions as signal for rapid intracellular degradation (Rogers et al. 1986; Rechsteiner and Rogers 1996). The new tag is called terminator-tag1 (tt1). In an additional construct (terminator-tag2; tt2), we further modified NS4A and depleted its membrane anchor domain. Another tag was designed similarly to the terminator-tag2, but the minimalized NS4A was moved to a position upstream of the NS3 protease and connected with a linker (terminator tag4; tt4). Moreover, we included a construct with the minimalized NS4A N-terminal upstream of the minimal NS3 protease that consists of the first 180 amino acids of NS3 (terminator tag 3; tt3). Plasmids with NS4A-NS3 fusion cDNAs were kindly provided by Norbert Tautz. New plasmids were created by replacing the SMASh-tag of pCAGGS YFP-SMASh with each of the terminator tags (Figure 37A).

Then, all constructs were compared to the original pCAGGS YFP-SMASh and evaluated with respect to cytotoxicity, cleavage, degradation, and virus inhibition. Therefore, HEK 293T cells were transfected and treated with DNV or DMSO 24 hours later. After additional 23 hours cells were lysed and analyzed via Western blot. As indicated by PARP cleavage only YFP-SMASh was conditionally cytotoxic, whereas all four terminator-tags did not induce cell death. Notably, similar levels of YFP could be observed in DMSO and DNV treated cells, and the full-length proteins were not detectable. This suggests that the protease was not inhibitable by DNV in tt3 and tt4, although the catalytic domain of NS3 was not altered. In case of YFP-tt2, protein bands corresponding to the uncleaved fusion protein as well as cleaved YFP were clearly detected after DNV treatment. As consequence, we concluded that inhibition as well as degradation of terminator-tag2 was impaired. Interestingly, only pCAGGS YFP-tt1 transfected samples displayed no cleaved YFP after drug treatment suggesting a complete inhibition comparable to the authentic SMASh-tag

(Figure 37B). However, degradation of the full-length protein by the PEST sequence was less effective compared to the SMASh-tag. We therefore decided to continue with tt1 for further analysis.
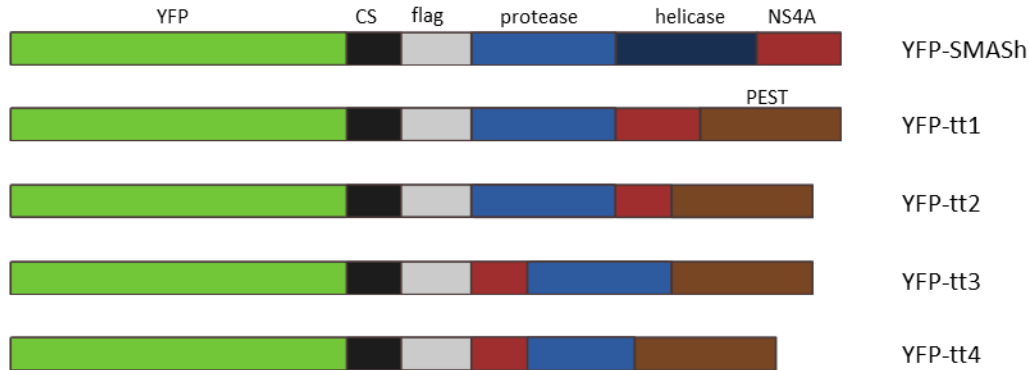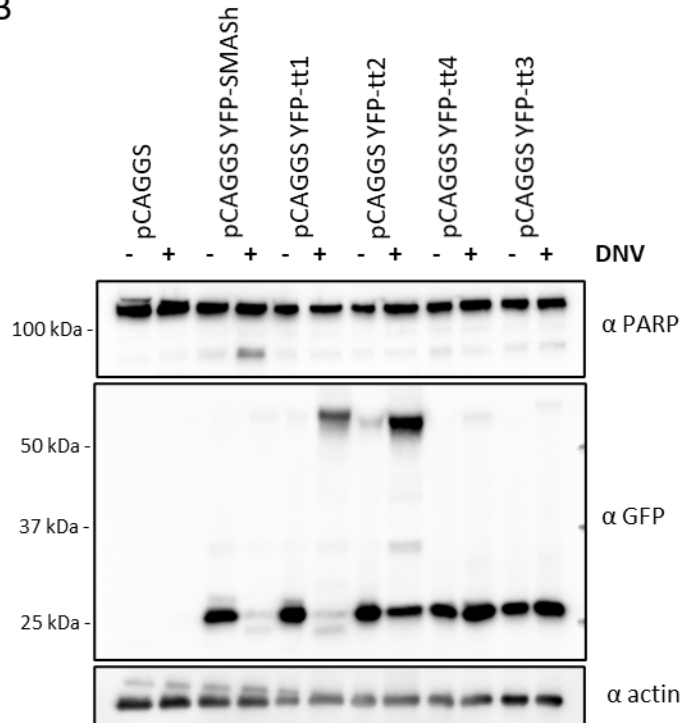
Figure 37: pCAGGS YFP-tt1 is not cytotoxic upon inhibitor treatment.
(A) Schematic representation of SMASh-tag and terminator-tag (tt) 1-4 fused to YFP (B) HEK 293T cells in 24 wells were transfected with 500 ng pCAGGS, pCAGGS YFP-SMASh, pCAGGS YFP-tt1, pCAGGS YFP-tt2, pCAGGS YFP-tt3 or pCAGGS YFP-tt4. After 24 h. p. t. cells were treated with 3 µM DNV (+) or DMSO (-). Additional 23 hours later cell lysis was done for Western Blot analysis. Note that only YFP-tt1 is susceptible to DNV inhibition.

Thus, viruses with tt1 fused to the nucleoprotein and phosphoprotein, respectively, were generated. In order to confirm the loss of cytotoxicity, SAD N-tt1 and SAD eGFP P-tt1 were compared to SAD N-SMASh and SAD eGFP P-SMASh in a killing assay. Therefore, HEK 293T cells were infected with respective viruses and DNV or DMSO added 24 hours later. To determine any cytotoxic effect, cells were analyzed 48 hours after DNV treatment. Indeed, tt1 did not cause cell death regardless of the fusion protein and DNV or DMSO treatment (Figure 38A). This corresponds to Western blot results showing no cleaved PARP in SAD N-tt1 and SAD eGFP P-tt1 infected cells. Furthermore, substantial reduction of RABV N levels in SAD N-tt1 and of RABV P in SAD eGFP P-tt1 could be observed upon inhibitor treatment indicating a functional, but non-toxic tag (Figure 38B). While non-degraded P fusion proteins are expected to retain some functionality, this is not expected for N fusion protein (see Discussion) is still functional.
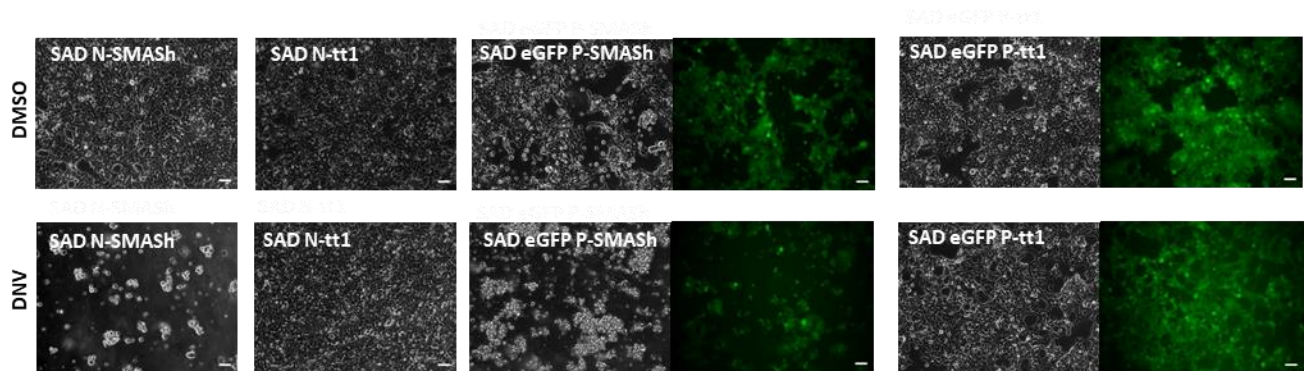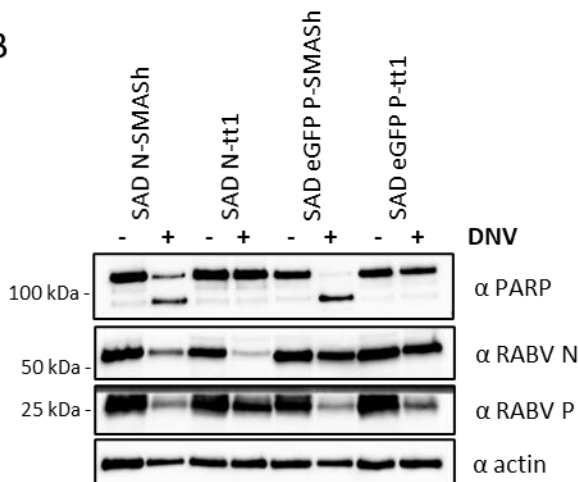
Figure 38: SAD N-tt1 and SAD P-tt1 are not toxic upon inhibitor treatment and can be regulated.
HEK 293T cells were infected with SAD N-tt1, SAD eGFP P-tt1 (MOI=3). As control infection was done with SAD N-SMASh or SAD eGFP P-SMASh. After 24 hours cells were treated with 3 µM DNV (+) or DMSO (-) and analyzed 48 h. p. DNV in regard to cytotoxicity via microscope (A) and Western blot (B). Scale bar: 100 µm.

3.2.3 Viral growth of Terminator-tag1 viruses is similar to SMASh viruses

In order to investigate if the slightly impaired ability to degrade N- and P- fusion proteins affects viral replication and inhibition respectively, we compared growth kinetics of tt1 and SMASh viruses. Therefore, multistep growth curves of SAD N-tt1 and SAD N-SMASh as well as SAD eGFP P-tt1 and SAD eGFP P-SMASh were determined in BSR T7 cells. For control SAD L16 and SAD eGFP were included. First, growth analysis was conducted in the absence of DNV. SAD eGFP P-tt1 showed similar growth kinetics as SAD eGFP P-SMASh and the control viruses reaching viral titers of approximately 10^8 ffu/mL after 48 hours. Growth of SAD N-tt1 as well as SAD N-SMASh was slightly attenuated and showed about 1 log lower titers at any measured timepoint compared to the control viruses (Figure 39A, B).

Next, we conducted the same experiment in presence of the inhibitor. Initial infection was done without inhibition, and DNV was supplied after media exchange at 5 h. p. i.. Addition of DNV led to similarly reduced viral growth in SAD eGFP P-tt1 and SAD eGFP P-SMASh, reaching a plateau at around 10^4 ffu/mL between 48 and 72 hours p.i.. In case of SAD N-tt1 reduction of viral titers was even stronger and was even slightly decreasing after 72 hours. Same was observed with SAD N-SMASh (Figure 39C, D). We assumed that 5 hours of initial infection were enough to allow viral release of tt1 viruses into the supernatant for at least 2 days.

All in all, viruses with tt1 fusion to RABV N or P show identical growth as viruses with SMASh fusion to respective proteins in presence or absence of the inhibitor. Therefore, we concluded that the tt1-tag is as functional as the SMASh-tag, but not toxic. Furthermore, non-degraded fusion protein seems to have no impact.
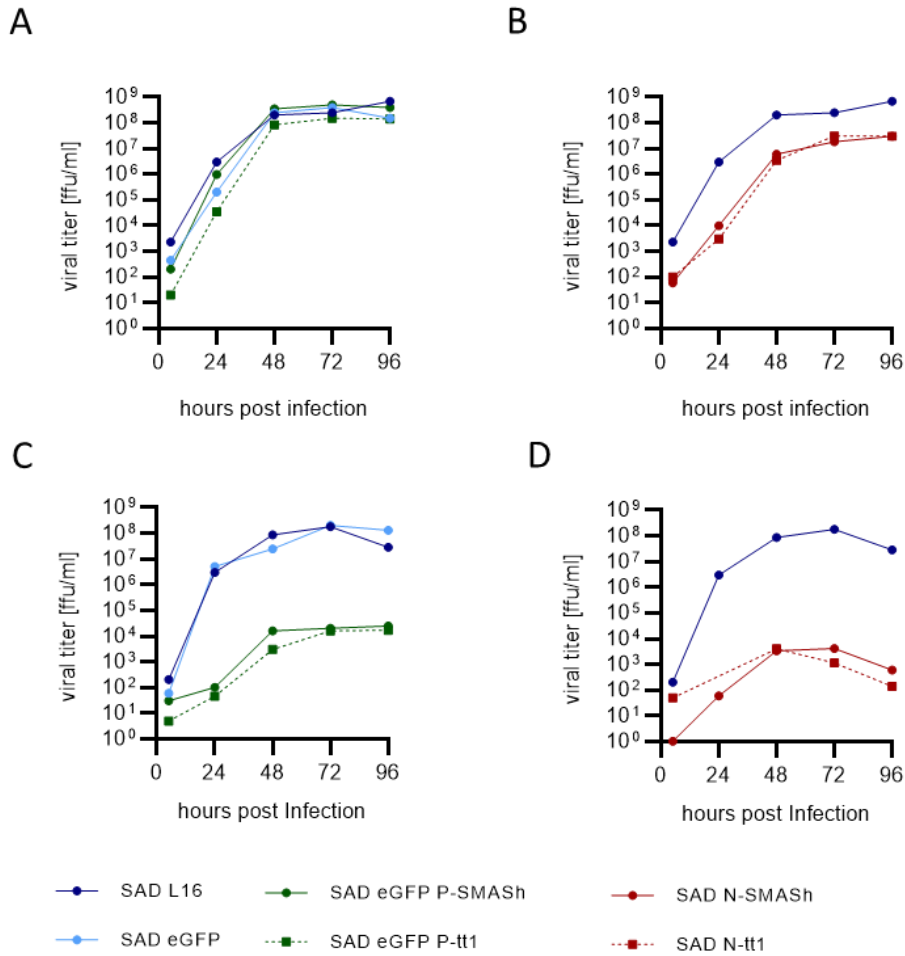
Figure 39: Terminator tag viruses display similar growth kinetic as SMASh viruses.
Multistep growth curves were performed on BSR T7 cells with SAD L16, SAD eGFP, SAD eGFP P-SMASh, SAD eGFP P-tt1, SAD N-SMASh and SAD N-tt1. Cells were infected (MOI=0.01), followed by a media exchange 5 hours later. Then, supernatant samples were harvested at the indicated time points. Respective titers (ffu/mL) were determined by titration on BSR T7 cells. (A, B) Growth kinetic without inhibitor. (C, D) Growth kinetic with 3 µM DNV addition after media exchange.

3.2.4   Establishment of tt1-virus infection can be prevented

During previous growth curve analysis DNV was added 5 hours post infection in order to initiate infection beforehand. This led the question open whether an establishment of infection of tt1 viruses can be prevented with the protease inhibitor. To examine this, BSR T7 cells were infected with a high MOI of three and treated at the same time with DNV or DMSO for 4 days. As before, SAD N-tt1 and SAD eGFP P-tt1 were compared with SAD N-SMASh and SAD eGFP P-SMASh, respectively.

As expected, protein levels of SMASh viruses and respective tt1 viruses were similar in each condition. In SAD eGFP P-tt1 infected cells RABV P was almost not detectable and also RABV N levels were slightly reduced. Strikingly, SAD N-tt1 infected cells display not only complete absence of RABV N, but also RABV P was almost not detectable as well (Figure 40). We concluded that protein control of P-tt1 and N-tt1 is possible in both cases. However, tagging the nucleoprotein might enable a faster virus control because inactivation or degradation of newly made RABV N had an enormous effect on other viral proteins (see Discussion).
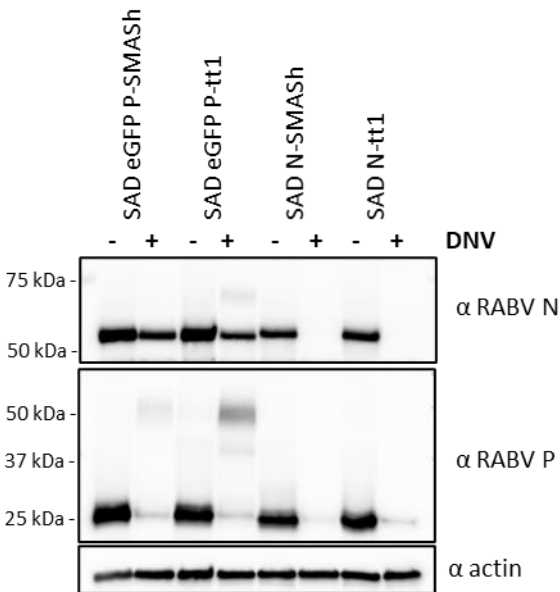
Figure 40: Establishment of SAD N-tt11 and SAD eGFP P-tt1 infection can be prevented.
BSR T7 cells were infected with SAD eGFP P-SMASh, SAD eGFP P-tt1, SAD N-SMASh or SAD N-tt1 (MOI=3) and directly treated with 3 µM DNV (+) or DMSO (-). 96 hours later cells were lysed and subjected to Western blot analysis.

3.2.5 Curing of tt1-virus infection

Next, we aimed to investigate the possibility of curing of cell cultures after infection by SAD N-tt1 or SAD eGFP P-tt1. This is of particular interest as it would allow a longer duration for analysis in neuronal tracing approaches with similar experimental settings as before. For this experiment, neuronal cells were not available. Instead hIPSC derived astrocytes (kindly provided by Giovanna Sonsalla from AG Götz) were infected with SAD N-tt1 or SAD eGFP P-tt1 with a MOI of 1 for 3 days. Non-tagged SAD eGFP served as control. After 3 days, media were replaced with fresh ones supplemented with DNV or DMSO. Since regular media exchange was necessary every 3 to 4 days, these timepoints were used for collecting supernatant samples to determine viral titers. After 18 days the experiment was stopped due to degeneration of cells.

A schematic representation of the experimental setup is depicted in Figure 41A. Of note, viral titers represent virus production of previous 3 or 4 days, depending on the beforehand media exchange. This is in contrast to growth kinetics, where media was only exchanged after infection initiation and total virus accumulation was determined afterwards at each timepoint.

As expected, SAD eGFP P-tt1 control display equal titers as SAD eGFP, whereas treatment with the protease inhibitor caused diminished virus production. This effect was even more strikingly in case of SAD N-tt1, where viral production was completely blocked after 10 days post drug treatment. As seen in other experiments, SAD N-tt1 was attenuated showing lower virus production as the other viruses (Figure **41**B, C). All in all, these results fit very well to previous experiments. Thus, SAD eGFP P-tt1 can be regulated, but virus production last longer after infection and inhibitor treatment than in case of SAD N-tt1. In contrast, virus control of SAD N-tt1 is relatively rapid.
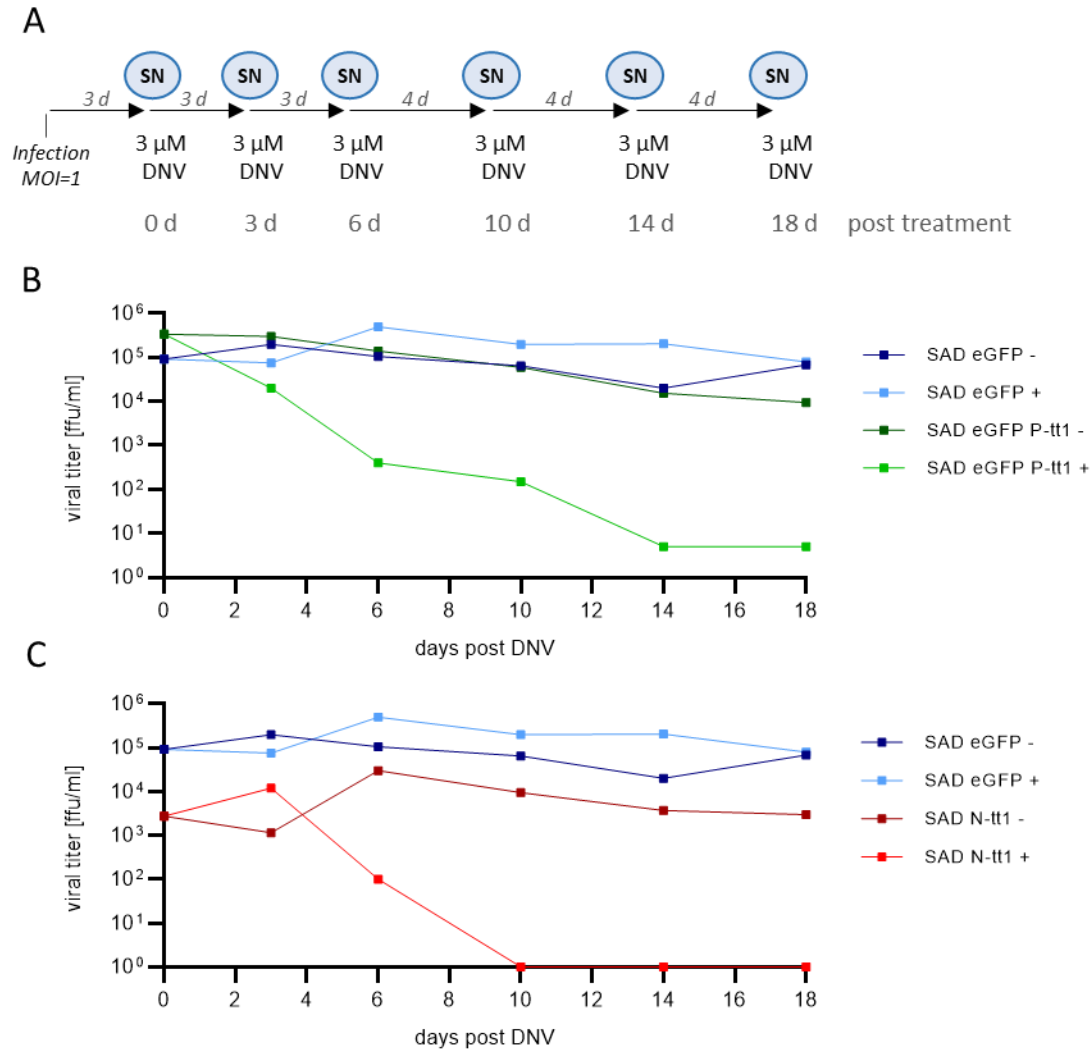
Figure 41: Curing hIPSC derived astrocytes of SAD N-tt1 is possible.
(A) Schematic representation of experimental setup. hIPSC-derived astrocytes were infected with SAD eGFP, SAD eGFP P-tt1 or SAD N-tt1 (MOI=1) for three days. Then, media was exchanged and fresh one supplemented with 3 µM DNV or DMSO. Thereby, supernatant (SN) was collected for later titration on BSR T7 cells. As indicated this step was repeated every 3 to 4 days until day 18. (A) Viral titer of SAD eGFP and SAD eGFP P-tt1. (B) viral titer of SAD eGFP and (C) SAD N-tt1.

3.2.6   Generation of SAD ΔG Cre-T2A-eGFP N-tt1

Since previous experiment revealed tt1 fusion to the nucleoprotein as most efficient regarding virus regulation, we generated a respective SAD ΔG virus expressing a Cre recombinase linked via T2A to eGFP. The so-called SAD ΔG Cre-T2A-eGFP N-tt1 was successfully rescued and pseudotyped with SAD-G for first experiments. In order to validate whether Cre recombination functions accurately, HEK 293T cells were

transfected with the reporter plasmid pCDH-EF1-DOI-tdTomato containing a floxed tdTomato followed by media exchange and infection with SAD ΔG Cre-T2A-eGFP N-tt1 (MOI=1) 10 h. p. t.. For control only transfection and only infection, respectively, was done. Two days later, cells were analyzed via microscope. Hence, red fluorescence should only appear after successful recombination. As expected we could not see any red cells in the control cultures. Only when cells were transfected with the reporter plasmid and infected with SAD ΔG Cre-T2A-eGFP N-tt1 (SAD-G) at the same time, a red fluorescent signal was detectable (Figure 42). This indicates a successful recombination, which is indeed Cre dependent. In conclusion, SAD ΔG Cre-T2A-eGFP N-tt1 appears to be a perfect candidate for long term neuronal tracing approaches allowing virus shutdown after non-toxic staining with the help of the virus-encoded Cre recombinase. For monosynaptic tracing, viruses pseudotyped with EnvA as described previously, can be provided.
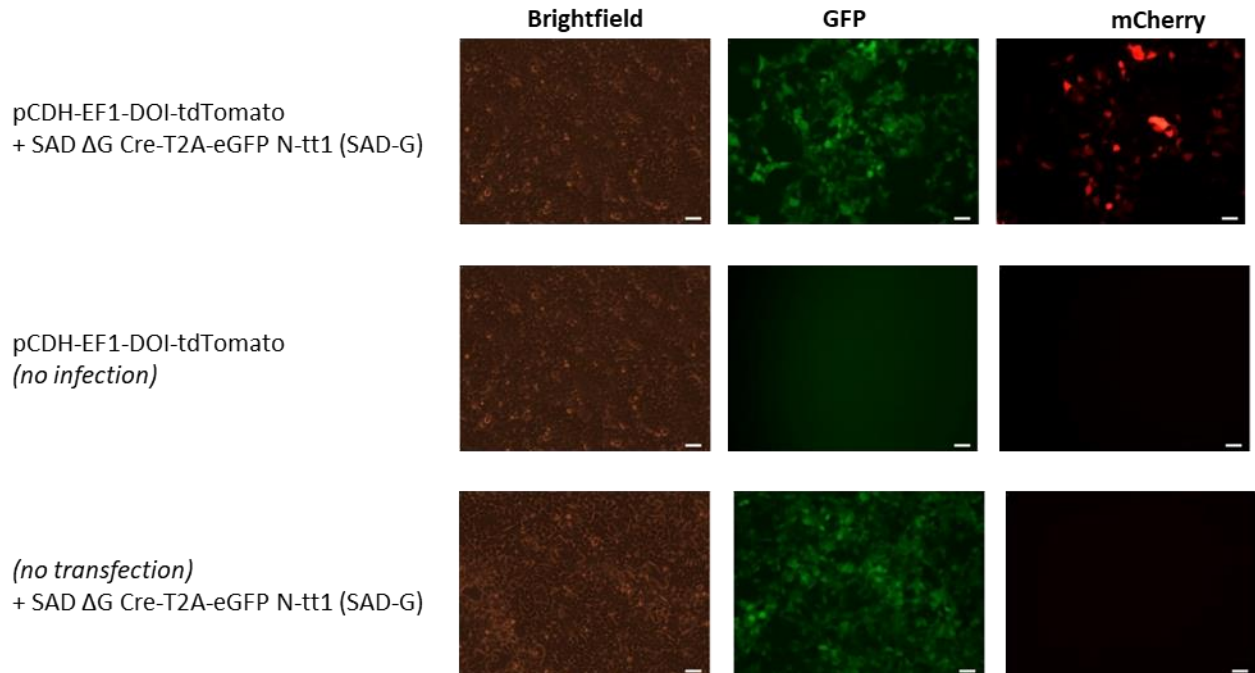
Figure 42: Cre recombinase in SAD ΔG eGFP-Cre N-tt1 (SAD-G) is functional.
HEK 293T cells were transfected with 500 ng of the reporter plasmid pCDH-EF1-DOI-tdTomato. A media exchange was performed 10 h. p. t. and cells infected with SAD ΔG Cre-T2A-eGFP N-tt1 (MOI=1). Two days later, cells were analyzed via microscope. Scale bar: 100 μm.

4 Discussion

4.1 Induction of apoptosis by SMASh

Apoptosis as a highly regulated form of cell death is an important process within multicellular organisms to ensure normal homeostasis, physiology, and tissue function. With this process, the organism is able to remove damaged or malfunctional cells, or cells that are no longer needed. Furthermore, organisms use apoptosis to eliminate spread of pathogens by depletion of infested cells. For this reason, apoptosis often plays a crucial role during infection. To evade those host defense mechanisms or to retard them viruses have evolved different strategies to inhibit the fatal outcome. However, some viruses are known to even induce apoptosis. In fact, in many cases viruses exhibit both pro- and anti-apoptotic activity.

For example, HCV was shown to inhibit as well as induce apoptosis. Especially the role of the core (Chou et al. 2005; Saito et al. 2006), E2 (Lee et al. 2005; Chiou et al. 2006), NS3 (Prikhod'ko et al. 2004; Tanaka et al. 2006) and NS5A (Siavoshian et al. 2005; Wang et al. 2006) protein is controversially discussed and function either pro- or anti-apoptotically depending on the experimental setting.

Based on HCV NS3/4A, Chung and colleagues invented the SMASh protein degradation tag (Chung et al. 2015). We found that the SMASh-tag alone is not toxic but induces apoptosis after addition of a NS3 inhibitor, most strikingly in case of SAD P-SMASh (Figure 12). Interestingly, a cytotoxic effect of SMASh was not found by the inventors. Chung and colleagues engineered Measles virus (MeV) and replaced the MeV P Protein by MeV P-SMASh. (Chung et al. 2015). However, MeV is naturally cytopathic in cell culture (Griffin et al. 2012; Guillerme et al. 2013), which could be the reason why a SMASh-induced toxicity was not noticed.

Although a specific host cell protein that is responsible for cell death could not be found in the scope of this thesis, analysis of different cells as well as different virus constructs gave new insights on SMASh-induced cytotoxicity. Those will be discussed in the following.

4.1.1 Expression levels are important

Previously, we could identify the induction of apoptosis upon NS3 inhibitor treatment after establishment of an infection with a SMASh-tagged RABV. Within this thesis one aim was to further characterize cell death induced by SMASh and inhibitor treatment. Experiments in our group showed already that for SAD P-SMASh a time duration of 8 hours is needed until cytotoxicity can be induced by DNV. However,

more time between infection and inhibitor treatment led to higher levels of cell death (Masterthesis V. Pfaffinger 2016). Therefore, we assumed that expression levels might play an important role for the cytotoxicity levels.

To further investigate this hypothesis, real time viability experiments were performed with different SMASh-tagged viruses. SAD P-SMASh killed HEK293T at fasted speed and highest rate, followed by SAD N-SMASh and SAD YFP-SMASh (Figure 12). Interestingly, this does not correspond to the transcriptional gradient, that is usually generated by RABV resulting in most abundant N protein levels, followed by P, M, G and L (Albertini et al. 2011; Fodor 2020). Following this, one would expect SAD N-SMASh to be the most cytotoxic virus upon drug treatment. However, SAD P-SMASh was found to be significantly more cytotoxic. Reasons for this observation could be the following: as observed in growth curve analysis, SAD N-SMASh appears to be slightly attenuated (Figure 11). This attenuation might be caused by the few extra amino acids, namely DEMMEC, remaining at the C-terminus after cleavage interfering with proper encapsidation of the viral genome. In contrast, the functionality of RABV P does not seem to be affected these extra amino acids at its C-terminus. Additionally, SAD L-SMASh and SAD SMASh-L, which naturally only express low levels of L, did not become cytotoxic upon inhibitor treatment. In any case, no cytotoxicity was observed when inhibitor was added before infection, as this prevented virus replication and accumulation of SMASh-fusion proteins.

In contrast to SAD N-, P-, and L-SMASh, respectively, SAD YFP-SMASh represents a special case because the SMASh is not fused to a viral protein. Thus, viral growth was not affected by inhibitor addition at any time, leading to constant accumulation of fusion protein (Figure 11). YFP-SMASh was introduced between the genes G and L. Due to the start stop mechanism during gene expression, a lower expression of YFP-SMASh than of P-SMASh can be expected at similar time points after infection. This might be the explanation for the fact that only a low cytotoxicity was observed after a few hours of inhibitor treatment, which increased significantly over time (Figure 12). Thus, the reason why the inventor of the SMASh-tag did not observe a cytotoxic effect of SMASh could also be due to low expression levels of SMASh in their case. Moreover, the establishment of infection before inhibitor treatment seems to be crucial. This fits also to the fact, that SAD N-SMASh and SAD P-SMASh were not toxic at all, when inhibitor is added at infection, whereas SAD YFP-SMASh needed a certain time to become cytotoxic in this scenario (Figure 13).

Importantly, we could demonstrate that SMASh was not only toxic when expressed in the viral context, but also after plasmid transfection revealing that viral trigger is not needed for SMASh-related cytotoxicity. Moreover, similar expression levels led to similar cytotoxicity within a killing assay. Only P-SMASh was

higher expressed by SAD which might be the reason for higher toxicity upon DNV addition (Figure 14). As mentioned before, viruses with tagged viral proteins did not become toxic when inhibitor was applied directly at infection (Figure 12). All together, these data strongly indicate, that a certain level of expression level of respective SMASh-tagged protein is indeed essential in order to induce apoptosis upon inhibitor treatment. Indeed, lower expression levels might also be the reason, why the inventors of the SMASh-tag did not report any cytotoxicity (Chung et al. 2015). Additionally, Chung generated not RABV, but SMASh-tagged MeVs, which are naturally cytopathic in cell culture (Griffin et al. 2012; Guillerme et al. 2013).

As mentioned before, the greatest cytotoxicity levels were observed with SAD P-SMASh. Therefore, standard killing assay included this virus and were performed 24 hours of infection, followed by addition of 3 µM NS3 inhibitor. Microscopic analysis indicated already a fast induction of apoptosis (Figure 9). Nevertheless, we were further interested in the exact timing. To this end, a real time Annexin V binding assay was performed. Annexin V binding to a cell happens during apoptosis due to the exposure of phosphatidylserine (PS) on the outer leaflet of the membrane. Strikingly, Annexin V bound already after 1 hour of DNV treatment to the SAD P-SMASh infected cells (Figure 15), indicating an instant induction of apoptosis by the inhibitor binding. Of note, Annexin V is also able to bind PS during necrosis. However, we excluded this lytic cell death because we could not detect any significant LDH release (Figure 15). Interestingly, Annexin V binding could also be observed in SAD L16 infected HEK 293T cells as well as in SAD P-SMASh infected control cells after 24 hours post treatment (Figure 15). We could see this repeatedly also in other experiments suggesting that wildtype RABV is cytotoxic to some extent independently of SMASh. Usually, RABV is known to effectively evade the host immune system to silently reach the CNS. Nevertheless, in the present thesis the attenuated vaccine strain SAD L16 was used, which has been shown to be slightly cytotoxic. The exact mechanism how RABV induces apoptosis still remains unclear. It could be shown that cytotoxicity correlates with higher expression levels of RABV G (Finke and Conzelmann 2005; Jackson et al. 2006; Suja et al. 2011). To clarify the induction of apoptosis in the context of RABV infection particularly in human cells more studies are necessary in the future.

In case of SAD eGFP P-SMASh and DNV, Annexin V binding could be verified by flow cytometry showing more than 75 % Annexin V positive cells (Figure 16). In fact, not only Annexin V binding could be detected very early after inhibitor addition. Additional kinetic experiments with subsequent Western blot analysis using a PARP antibody indicated PARP cleavage already one hour after drug treatment (Figure 17). PARP is specifically cleaved into two distinct fragments at the late stage of apoptosis and serves therefore commonly as marker for respective cell death (Gobeil et al. 2001). Altogether, cell death occurred very

rapidly. This led us to the assumption that activation of a factor directly involved in apoptosis execution is very likely.

4.1.2 Intracellular induction of apoptosis by SMASh

Many viral proteases cleave cellular factors and thereby modulate immune response. For example, the Human Rhinovirus 3C protease interacts with cellular pro-survival and apoptotic pathways by cleaving RIPK1 (Croft et al. 2018). Coxsackievirus protease 3Cpro cleaves the inhibitor of κBα and triggers thereby apoptosis (Zaragoza et al. 2006). Furthermore, the HCV NS3 protease is known to prevent innate immune response by cleaving the two cellular adaptor proteins MAVS and TRIF (Li et al. 2005a; Li et al. 2005b). Previously, we could show that MAVS is cleaved by NS3/NS4A in context of SMASh but, as revealed in MAVS-KO cells, does not play a role in killing (Masterthesis V. Pfaffinger 2016). By using constructs with disrupted catalytic center (S139A) we could further confirm that the NS3 protease activity is not important at all for apoptosis induction (Figure 32, Figure 33). This also fits with the findings showing cytotoxicity of SAD YFP-SMASh despite complete inhibition which is indicated by the lack of cleaved proteins throughout the duration of infection (Figure 13). Therefore, we concluded that the protease activity of SMASh is not the reason for killing. This makes sense because the SMASh-tag only becomes cytotoxic once the protease is inhibited.

In fact, apoptosis is directly induced by several viruses through various mechanisms. The PB1-F2 of influenza A virus is one example for a protein, that is able to directly induce apoptosis. Forming pores by PB1-F2 within the outer mitochondrial membrane in similar manner as by Bak and Bax leads to MOMP, cytochrome c release and further activation of apoptosis (Chanturiya et al. 2004). Indeed, also indirect activation by modulation of certain protein levels is possible. The Human Immunodeficiency virus type 1 Tat protein for example upregulates procaspase-8 levels, which leads to increasing apoptosis levels and higher sensitivity to apoptotic stimuli (Bartz and Emerman 1999). Another example is viral dsRNA binding to the cellular serine/threonine-protein kinase PKR. PKR activation leads to a shutdown of the cellular translation machinery and apoptosis. Beside dsRNA, the PKR pathway is induced due to other stress conditions like ER stress (Lee et al. 2007).

During the HCV life cycle proteins are synthesized at the ER (Moradpour et al. 2007). There, the NS3/4A protease, beside other HCV proteins, is known to induce oxidative and ER stress (Bureau et al. 2001; Choi et al. 2004; Ríos-Ocampo et al. 2019). Interestingly, induction of PKR was observed during HCV infection (Kang et al. 2009). Therefore, PKR appeared to be an interesting candidate for triggering SMASh related

apoptosis. In order to analyze whether PKR also plays a role during SMASh killing, we generated HEK 293T PKR$^{-/-}$ cells. However, we could not detect any difference compared to wildtype cells (Figure 21). As a consequence, we excluded PKR as key element of cell death triggered by SMASh. This fits also to the fact, that PKR is unlikely to be triggered by expression plasmid, which led to a similar degree of cytotoxicity as SMASh viruses (Figure 14).

Interestingly, the flaviviruses West Nile virus, Langat virus and HCV were shown to induce apoptosis *in vitro* by binding and activating caspase-8 through the NS3 protease (Prikhod'ko et al. 2002; Prikhod'ko et al. 2004; Ramanathan et al. 2006). In case of HCV NS3, four amino acids, which can be found also within the SMASh-tag, played thereby a crucial role: LTHP. In consequence, we hypothesized that direct binding of caspase-8 by NS3 could be also the reason for cell death induction by SMASh. However, different mutations disrupting this motif had no influence on cytotoxicity (Figure 30). As the mutants in this thesis were confined to SMASh-tag, i.e. a small part of the NS3 protease, a role of this motif in the context of the full-length proteins, as published, remains possible.

By conducting caspase activation experiments, we could confirm that the initiator caspases -8, -9 and as well as the effector caspase-3/-7 are activated (Figure 18). Involvement of those caspases, together with caspase-10 was already previously identified by Western blot analysis (Masterthesis V. Pfaffinger 2016). Furthermore, experiments with individual caspase inhibitors suggested a substantial role of caspase-8 and -10 and a minor role of caspase-9 in first place (Figure 19). Although those caspase inhibitors are widely used, there are concerns regarding their specificity (Pereira and Song 2008; Pop and Salvesen 2009). Indeed, we could not verify the major role of caspase-8 and -10 by using inhibitors. In contrast, experiments with individual caspase-8, and -10 knockouts indicated that the presence of both caspases is not essential for SMASh related killing (Figure 23, Figure 24, Figure 26). Notably, the caspase-10 antibody used in this thesis was able to detect a band of about 58 kDa, which indeed corresponds to the size of caspase-10, not only in wildtype HeLa and HeLa CASP8$^{-/-}$ cells, but also in HeLA CASP10$^{-/-}$ cells. Interestingly, the band disappeared upon treatment with DNV (Figure 23). Since this antibody is a polyclonal antibody and caspase-8 and -10 are closely related, it is very likely that this caspase-10 antibody crossreacts with the 55 kDa procaspase-8.

Infection of HeLa CASP8$^{-/-}$ cells led to reduced viability even without SMASh (Figure 23). This was unexpected and was not observed in HEK 293T CASP8$^{-/-}$. Caspase-8 plays a crucial role in the fate of a cell as it is an important element of extrinsic apoptosis and suppresses the induction of necroptosis once it is active. Thus, in absence of active Caspase-8, RIPK1 and RIPK3 are able to mediate necroptosis. However,

this would require the activation of the death receptors by stress molecules such as pathogen-associated molecular patterns (PAMPS) and danger-associated molecular patterns (DAMPS) (Yan et al. 2020; Bertheloot et al. 2021), which was so far not shown for RABV. In addition to apoptotic and necroptotic cell death, caspase-8 also influences inflammatory pathways such as IFN and NF-κB signaling. For instance, caspase-8 was shown to negatively regulate viral RNA-triggered type I IFN signaling by cleaving RIPK1. (Rajput et al. 2011). Furthermore, cleavage of RIPK1 by Caspase-8 prevents induction of the NF-κB pathway (Rébé et al. 2007; Bertheloot et al. 2021). In conclusion, Caspase-8 deficiency may lead to impaired antiviral response. If this is the case in HeLa CASP8$^{-/-}$ cells, and which signaling is affected specifically needs to be determined.

Besides individual CASP8 and CASP10 knockout cells, HEK 293T CASP8/10 double knockouts were generated. Although genomic sequence exhibited mainly out of frame mutations (data not shown), complete CASP8/10 double knockout could not be ensured. In consequence, there is a certain probability that both caspases can substitute each other. In fact, there are studies suggesting that caspase 10 is able to functionally replace caspase-8 (Kischkel et al. 2001; Wang et al. 2001). However, the ability to substitute caspase-8 is controversially discussed, as others report that caspase-10 lacks this ability (Sprick et al. 2002). Interestingly, the group of Leverkus observed an inhibitory role of caspase-10 in regard of caspase-8 (Horn et al. 2017). Nevertheless, we assumed a pro-apoptotic role for both caspases during SMASh related apoptosis as both were cleaved during cell death.

Although caspase-8 and -10 are typically associated with extrinsic apoptosis involving ligand binding to a death receptor (Bodmer et al. 2000; Kuang et al. 2000; Sprick et al. 2000), their activation upon SMASh and NS3 inhibitor is not of extracellular nature. This could be already shown in previous work, where real time microscopy with SAD ΔG eGFP P-SMASh revealed that SMASh related apoptosis is only induced in infected cells, whereas bystander cells are not affected (Masterthesis V. Pfaffinger 2016). Here, we could further confirm these findings by additional experiments with ΔG viruses that were unable to spread (Figure 20). In addition, the hypothesis of an exclusive intracellular induction of apoptosis is supported by the fact that HEK 293T FADD$^{-/-}$ cells are still killable (Figure 22). FADD is a key adaptor protein during extrinsic apoptosis and essential for apoptotic signal transmission from external ligands (Tourneur and Chiocchia 2010). In conclusion, extracellular initiation of apoptosis as well as initiation by FADD were excluded.

In order to receive more insights in SMASh induced apoptosis, we performed a whole genome knockout screen. However, all knockout cells died upon SMASh and inhibitor treatment (data not shown). For this

reason, we assumed that not an exclusive single trigger is responsible for cell death, but rather multiple pathways might be activated. This is also in line with the instant cell death that could be observed. However, we could not exclude a major contribution of direct activation of the downstream caspase-3 in first place leading to further activation of caspase-8, -10 and -9. To clarify this, experiments with CASP3 knockout cells would be required. Moreover, the screen was performed with SAD P-SMASh. As mentioned above, SAD L16 as well as SAD P-SMASh alone led to slight cytotoxicity, which could be measured two days post infection (Figure 15). Thus, there is the possibility, that survivors of SMASh were missed due to the intrinsic cytotoxicity of viral infection.

How exactly SMASh induces apoptosis is still unclear. Co-immunoprecipitation using SAD P-SMASh failed to determine a direct interaction partner for SMASh (data not shown). Fast degradation of the SMASh fusion protein after inhibitor treatment might be one reason for this failure. In fact, there was no fusion protein detectable in case of P-SMASh and N-SMASh and only minor levels of YFP-SMASh could be observed. Proteasomal overload is one possibility for apoptosis induction. However, previous experiments with the proteasomal inhibitor MG132 did not support this hypothesis (Masterthesis V. Pfaffinger 2016).

Moreover, the SMASh-tag is constantly degraded in absence of the inhibitor. In case of YFP-SMASh, SMASh-tag and YFP have similar molecular weight. If proteasomal overload is the reason for cell death, SAD YFP-SMASh should induce apoptosis also in absence of inhibitor, when reaching high viral titers and therefore a certain expression level. However, we could not detect any cytotoxic effect in the absence of DNV or ASV (Figure 12, Figure 13). For this reason, we discarded the hypothesis of proteasomal overload as trigger for cell death.

Unfortunately, the levels of the different SMASh-tags could not be determined, even in the presence of proteasome inhibitors. Thus, besides the proteasomal degradation, other pathways such as endolysosomal or autophagosomal degradation might be involved. The fact that degradation of the SMASh-tag appears to be fast led us to the assumption that only short binding or interaction is needed for triggering apoptosis. As high expression is needed for cytotoxicity in addition, it might be that respective binding is rather unspecific or weak.

4.1.3   Alterations of the SMASh-tag influencing its cytotoxicity

To gain further insights into how inhibition of SMASh activity induces apoptosis, we wanted to know which parts of the tag are necessary for induction. For this purpose, mutants were generated that contain a stop codon downstream of the protease domain or the helicase domain, respectively. Strikingly, SMASh lost its

ability to induce cytotoxicity as soon as NS4A, or NS4A together with the helicase domain were removed (Figure 34). Similar effect, however, could be observed by depleting the helicase, with the NS4A remaining (Figure 38), indicating a combined activity. Together, we were not able to find a specific domain which is responsible for the cytotoxicity. In contrast, the SMASh-tag as a whole appears to be necessary. In consequence, it might be that NS3 inhibitor leads to a conformational change within the SMASh-tag to achieve a "toxic conformation". As soon as alterations are made, conformational change differs, which seems to influence cytotoxicity. However, small modifications like mutations within the LTHP motif, as mentioned before, might not influence conformation or its change upon inhibitor treatment.

Conformational changes of NS3/NS4A protease occur naturally during HCV life cycle. There, conformational state is dependent on the pH modulating the ATPase and helicase activity of NS3 (Ventura et al. 2014). During allosteric inhibitor binding, NS3 changes its conformation towards an inactive state, as shown for HCV and other flaviviruses (Erbel et al. 2006; Wichapong et al. 2010; La Cruz et al. 2011; Xue et al. 2014). The hypothesis of changed conformation after inhibitor treatment fits also to the fact, that slight cytotoxicity was observed without NS3 inhibitor, when SMASh-tag was fused to the N-terminus of a protein (Figure 35). Thus, it might be, that in the case of N-terminal fusion, the SMASh-tag takes already a conformation which allows binding of certain proteins with low affinity inducing thereby apoptosis. However, cytotoxicity was significantly enhanced by inhibitor addition. In consequence, inhibitor binding could further alter the conformation of the SMASh-tag which allows binding of respective proteins with higher affinity enabling more effective killing. Again, it has to be mentioned that we could not identify a binding partner for SMASh so far.

Although SMASh is also toxic without fusion protein, the cleavage site seems to be important for conditional cytotoxicity. Strikingly, deletion the cleavage site resulted in induction of high cytotoxicity, independent of inhibitor treatment. However, no apoptotic markers such as cleaved PARP could be detected (Figure 31). Thus, it remains unclear, whether another mode of regulated cell death is induced in this case. To clarify this issue, further research is necessary in the future.

By analyzing the sequence of the SMASh-tag, we found an insert within the helicase domain containing the four amino acids KIDT. Of note, this KIDT insertion was not further discussed by the inventors of SMASh (Chung et al. 2015). Nevertheless, we assumed that this could serve as a linker, implemented to ensure the correct cofactor function of NS4A or to enhance degradation efficiency of SMASh. Interestingly, a mutant with KIDT replaced by four alanines showed slightly enhanced constitutive cytotoxicity, which was detectable even before addition of any NS3 inhibitor (Figure 30).

Altogether, there are various lines of evidence, that inhibitor treatment leads to a conformational change of the SMASh-tag, which subsequently becomes cytotoxic. Mutations within the inhibitor binding site could further clarify whether inhibitor binding is required. Thus, R155K and D168A mutations within the binding pocket of the HCV NS3 protease were shown to lead to multi-drug resistance (Romano et al. 2012; Soumana et al. 2014). Both amino acids appear in the SMASh-tag (see Figure 43) and might therefore affect SMASh cytotoxicity. Hence, analyzing these mutations could be interesting in the future.

Figure 43: ASV resistance mutations of HCV NS3 within the SMASh-tag.
HCV NS3 R155K and D168A mutations were shown to result in ASV resistance. R155 and D168 are indicated within the SMASh sequence by red asterisks. Black asterisks indicate catalytic triad of the NS3 protease (modified from Chung et al. 2015).

4.1.4 Model of SMASh induced apoptosis

Taken all findings together, we developed a model, how apoptosis might be induced by SMASh and inhibitor treatment. As mentioned before, there are several indications that the NS3 inhibitor triggers a conformational change of SMASh. Alteration in the conformation might allow binding of certain proteins which are responsible for apoptotic fate. Which proteins are activated upon SMASh and inhibitor treatment is still not clear. However, experiments with various cells including knockout cells as well as the whole genome knockout screen indicated induction of multiple apoptotic pathways. Moreover, the need of high expression levels might suggest a non-specific or low affinity binding or interaction. In consequence, it could be speculated that several caspases are bound directly or via caspase interacting proteins to SMASh after inhibitor treatment and induced simultaneously. Rapid induction of cell death corroborates this theory of direct caspase activation. Once, caspases -8, -10, -9, -3 and-7 are activated, cross activation of caspases and further progress of apoptosis could occur. This includes induction of the effector caspase-3 and -7 by the initiator caspases -8, -10, -9, and vice versa.

Additionally, Bid might be cleaved by caspase-8, which then forms pores in the outer mitochondrial membrane and induces thereby so called mitochondrial outer membrane permeabilization (MOMP). As consequence, cytochrome c would be released into the cytoplasm, where it promotes the formation of the apoptosome including heptamerized APAF-1 as well as pro-caspase-9. Within the apoptosome dimerization and auto-catalytic cleavage of pro-caspase-9 and thus activation of caspase-9 could occur, leading to further activation of caspase-3 and -7. As one substrate PARP is cleaved by the effector caspases representing a hallmark of apoptosis (Figure 44).

Furthermore, it could be that caspase-3 is activated in first place and activates caspase-8, -9 and -10 later on. Usually, the effector caspase is activated downstream of the initiator caspases -8, -9 and -10. After activation caspase-3 cleavages further substrates such as PARP, but also amplifies the signal via a feedback loop. Thereby, it further activates caspase -8, -9 and -10. With this amplification loop other caspase molecules become activated at a certain time accelerating the apoptotic fate (Fujita et al. 2001; Twiddy and Cain 2007; Ferreira et al. 2012). In consequence, it might be that caspase-3 is activated directly by SMASh upon inhibitor binding and is therefore necessary to activate all other caspases. To test this hypothesis, HEK 293T CASP3 knockout cells could be generated and used in killing assays. If caspase-3 is directly and exclusively activated by SMASh, those cells should be resistant to cell death induced by SMASh.

Indeed, another possibility is the induction of caspase-9 alone, which in turn activates extrinsic caspases as well as effector caspases leading to final cell death. The activation of the mitochondrial apoptotic pathway and induction of caspase-9 by HCV NS3/4A was already observed by Deng and colleagues (Deng et al. 2008). In addition, other members of the *Flaviviridae* like the Japanese encephalitis virus induce caspase-9 dependent apoptosis by NS3 (Yiang et al. 2013). Nevertheless, experiments with caspase inhibitors support the first hypothesis involving induction of various caspases at the same time, as caspase-9 inhibitor alone could not prevent cell death. This theory matches the results of the whole genome knockout screen revealing no survivors.

In addition to caspase activation, cleavage of RIPK1, a key regulator of TNF-mediated apoptosis, necroptosis and inflammatory pathways, upon addition of the protease inhibitor was already observed during the master thesis (Masterthesis V. Pfaffinger 2016). RIPK1 mediates between pro- and anti-survival pathways and is a natural substrate of caspase-8. Upon its cleavage, apoptotic fate is favored, whereas necrosis or induction of pro-survival NF-κB is inhibited (Festjens et al. 2007). After activation of caspase-3 and -7, PARP is cleaved, and final cell death initiated.
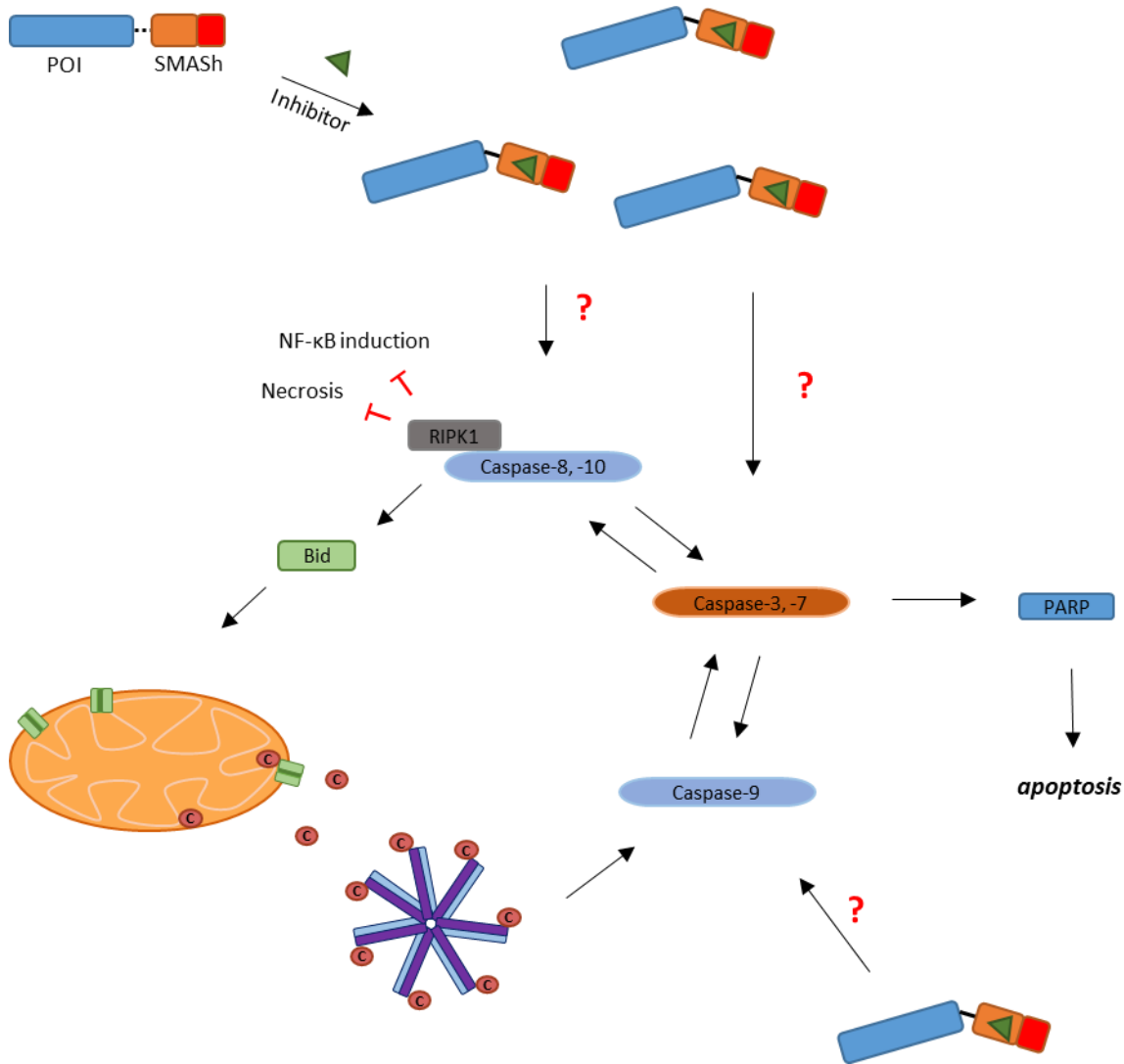
Figure 44: Model of apoptosis induction by SMASh upon inhibitor treatment.
After expression of the protein of interest (POI) fused to the SMASh-tag, addition of the NS3 inhibitor prevents auto-cleavage and induces a conformational change of the fusion protein. This conformational change possibly enables direct activation of several caspases such as the initiator caspases -8, -10, -9, as well as the effector caspases -3 and -7. Active caspase-8 prevents NF-κB as well as necrosis induction. In addition, it is able to amplify the apoptotic signal by cleaving Bid, which then forms pores in the outer mitochondrial membrane, thereby permeabilizing it. In consequence, cytochrome c (C) is released into the cytoplasm, where it leads to the formation of the so-called apoptosome including APAF-1 and pro-caspase-9 and thus activation of caspase-9. Active caspase– 9 can further activate effector caspases -3 and -7, which in turn are also able to activate initiator caspases. Moreover, effector caspases cleave other substrates such as PARP and cause final cell death.
C: cytochrome c; POI: protein of interest

4.1.5   Potential of RABV expressing SMASh as oncolytic virus

Beside the previously mentioned knockout cells, several other cells were tested with the idea to find cell death resistant cells. Those cells would have been interesting for further investigations in order to clarify the exact pathway triggered by SMASh. To this end, different cell lines from different hosts were analyzed including human, mouse, hamster, and monkey cells. Strikingly, all cells could be killed upon SMASh and inhibitor treatment. Interestingly, cytotoxicity was even in primary HFF cells induced.

A list of all tested and killable cells is presented in Table 21, including also tested cell lines from previous work (Masterthesis V. Pfaffinger 2016).

Table 21: Cell Lines that are killable by SMASh and inhibitor treatment

Species	Cell line	Description
Homo sapiens	HEK 293T	Human embryonic kidney cells expressing SV40 T-antigen
	HEK 293T MAVS -/-	HEK 293T containing MAVS Knockout
	HEK 293T FADD -/-	HEK 293T containing FADD Knockout
	HEK 293T Casp8 -/-	HEK 293T containing Caspase-8 Knockout
	HEK 293T Casp8/Casp10 -/-	HEK 293T containing Caspase-8/-10 double Knockout*
	HEK 293	Human embryonic kidney 293, provided by Arnd Kieser
	HEK 293 TRADD-/-	HEK 293 cells containing TRADD Knockout, provided by Arnd Kieser
	HeLa	Human cervix carcinoma cells
	HeLa Casp8 -/-	HeLa containing Caspase-8 Knockout
	HeLa Casp10 -/-	HeLa containing Caspase-10 Knockout
	DG75	Human DG75 B lymphocytes, provided by Arnd Kieser
	DG75 TRADD KO	Human DG75 B lymphocytes containing TRADD Knockout, provided by Arnd Kieser
	Huh 7	Hepatocarcinoma cell line
	Huh 7.5	Hepatocarcinoma cell line clone 7.5 (RIG-I deficient)
	U3A-LC3-GFP	U3A cell line (derived from human sarcoma cells HT1080) expressing an LC3-GFP fusion protein
	hIPSC derived astrocytes	Human induced pluripotent stem cell derived astrocytes
	U-87 MG	Human glioblastoma cells
	U-251 MG	Human glioblastoma cells
	HFF	Human foreskin fibroblasts (primary isolate)
Mus musculus	N2A	Mouse neuroblastoma cell line
	MEF	Mouse embryonic fibroblasts
	mESC derived neurons	Mouse embryonic stem cell derived neurons
	GL261 new	Mouse glioblastoma cells

Species	Cell line	Description
	GL261 moko	Mouse glioblastoma cells
	B16	Mouse melanoma cells
	MC38	Mouse colon carcinoma cells
Mesocricetus auratus	BHK21	Baby hamster kidney cells
	BSR T7/5	BHK-21-derived cells expressing T7-pol
Cercopithecus aethiops	Vero	African green monkey cells

*in-frame deletions in caspase 8 and caspase 10

Since we could so far not find any resistant cells, we assumed that multiple pathways or caspases might be triggered by SMASh inhibition. This fits also to the finding that no survivors were found in the whole genome knockout screen.

Because many of the listed (killable) cells are derived from cancers cells, SMASh-tagged viruses might be especially interesting as oncolytic virus. First analysis revealed a cytotoxic effect already of RABV in different cancer cell lines, which could be enhanced by SMASh and inhibitor treatment (Figure 27, Figure 28, Table 20). Additionally, we could observe a slight release of LDH after inhibitor treatment in some cancer cells like B16 melanoma cells for example. Often, tumor cells have defects in apoptotic signaling pathways preventing them from apoptotic death. Hence, the *p53* apoptosis suppressor gene is often affected (Kandoth et al. 2013; Roberts and Huang 2017; Aubrey et al. 2018). In mouse B16 melanoma cell line loss of the p16Ink4a and p19Arf tumor suppressor expression could be shown, which are usually responsible for cell cycle arrest and p53 regulation, respectively (Weitzman 2001; Melnikova et al. 2004; Ozenne et al. 2010). In case of mouse glioma GL261, cells carry point mutations in the *K-ras* as well as the *p53* gene (Szatmári et al. 2006). In contrast to *p53* which is directly invovled in apoptosis, mutations in K-ras often results in its constant activation leading to cell aberrant signaling such as the excessive transmission of growth signals (Jinesh et al. 2018). In this thesis GL261 new and GL261 moko cells were used. Both are original GL261 cells, but grow at different rates with GL261 new growing faster (both cell lines were kindly provided by C. Engeland). As they were originally obtained from different sources, it might be that additional mutations affecting growth could manifest as a result of numerous passaging. Nevertheless, both cell lines were susceptible to SMASh-inhibition dependent killing.

Although different tumor cell models with different mutations were selected, RABV and SMASh were able to kill all different cancer cells. Indeed, this makes RABV SMASh an interesting tool for viral cancer therapy. Attenuated RABV was already shown to induce anti-tumor immune response and was already discussed as possible immune adjuvant for cancer treatment (Altinoz et al. 2017; Bongiorno et al. 2017). Beside

RABV, many other viruses show natural cancer killing phenotype, for example VSV or measles virus (Cattaneo et al. 2008; Cattaneo and Russell 2017). Often, those viruses naturally replicate better in cancer cells due to the high expression of receptors or defective antiviral signaling pathways such as PKR or STING signaling (Masemann et al. 2017; Queiroz et al. 2019). So far, clinical studies mainly focused on oncolytic herpesviruses, adenoviruses, measles viruses and reoviruses (Mondal et al. 2020). However, only very few oncolytic virus have been approved to date: as first oncolytic virus an Enterovirus was approved in Lativa already in 2004 under the tradename Rigvir to treat melanoma (Tilgase et al. 2018; Alberts et al. 2018). In 2005, Oncorine, an oncolytic adenovirus was approved in China for nasopharyngeal carcinoma in combination with chemotherapy (Liang 2018). Furthermore, the genetically modified herpes simplex virus I named Talimogen laherparepvec (T-VEC) expresses the granulocyte-macrophage colony-stimulating factor (GM-CSF) and was the first approved oncolytic virus in the US and Europe to treat advanced melanoma (Conry et al. 2018; Hemminki et al. 2020). Recently, Teserpaturev (G47Δ) was conditionally approved for malignant glioma in June 2021 by the Japanese Health Authority. It belongs to the third generation of oncolytic herpes simplex virus I and carries three mutations within the genome to enhance antitumor efficacy (Fukuhara et al. 2016; Rahman and McFadden 2021).

In contrast to many DNA viruses such as retroviruses or herpesviruses, RNA viruses are not able to integrate their viral genome into the host genome, which reduces safety concerns. Moreover, RABV and other rhabdoviruses allow possible delivery of multiple proteins in an easy and straightforward manner. Simple cloning enables the additional delivery of tumor antigens or immune modulators. Furthermore, SMASh fused to a viral protein like RABV P or N facilitate control of viral spread. In addition to that, a single-round virus lacking the glycoprotein could be a possible approach for a safe oncolytic treatment. Indeed, modifying the glycoprotein could enhance efficacy in regard of tumor selectivity. Muik and coworkers engineered VSV with a variant glycoprotein of the lymphocytic choriomeningitis virus (LCMV) allowing the targeted replication in glioblastoma cells, while sparing normal neurons (Muik et al. 2011; Muik et al. 2014).

In the end, oncolytic RABV could be applied as follows: Injection of the recombinant RABV expressing SMASh into the tumor could allow effective infection of the cancer cells. Then, oral application or on-site injection of the already approved NS3 inhibitor ASV could induce high cytotoxicity leading to tumor destruction. However, so far, only *in vitro* studies have been performed. How strong SMASh cytotoxicity appears *in vivo* has to be further investigated. For this purpose, collaborations with C. Engeland (DKFZ, Heidelberg) were started. The focus in this collaboration is on experiments targeting glioblastoma in mice.

As deletion of SAD-G of RABV allows studies under laboratory S1 conditions, SAD ΔG eGFP P-SMASh will be used for those studies. Thus, the SMASh virus will be injected into the tumor with a high MOI to infect a high number of tumor cells, followed by the direct injection of the protease inhibitor later on. Then, tumor progression/regression will be analyzed.

In case of brain tumors, direct injection of the protease inhibitor into the brain is necessary, since NS3 inhibitors are not able to cross the blood–brain barrier (BBB) representing a huge obstacle for brain applications.

Nevertheless, as SMASh was able to induce cytotoxicity in different cancer cell lines, the application is not limited to one specific cancer type. Additionally, since SMASh cytotoxicity is independent of the delivering vector, the system could be also established within VSV or other oncolytic viruses.

4.2 Non-toxic controllable rabies viruses

RABV is a highly neurotropic virus that spreads from neuron to neuron in an exclusively retrograde manner. Thus, only pre-synaptically connected neurons are infected. Because of this specific feature, RABV is widely used as tool for mapping neuronal connections. Thereby, mostly G deleted viruses are used that allow monosynaptic tracing after infection of a distinct starter cell. However, slight cytotoxicity of RABV like SAD limits the time frame for studies (Ghanem and Conzelmann 2016). To circumvent this cytotoxicity, controllable viruses might be useful. Thus, a major goal of this thesis was to investigate and establish non-cytotoxic controllable viruses.

4.2.1 Terminator-tag1 as non-toxic tag

To allow switch-off approaches, we aimed to develop a non-toxic tag which still would be suitable to control RABV replication by degradation of fused proteins. The SMASh-tag served as a starting point. First, we deleted the helicase domain, which is a part of the degron within the SMASh-tag. In order to compensate the impaired ability for degradation, a PEST sequence was further included. A PEST sequence is rich in proline (P), glutamic acid (E), serine (S), and threonine (T) and functions as signal for rapid intracellular degradation (Rogers et al. 1986; Rechsteiner and Rogers 1996).

In addition to this terminator-tag1 (tt1), we analyzed a variant similar to tt1, that contains the minimal NS4A lacking the membrane anchor domain (tt2) and other constructs with the minimal NS4A N-terminally of the normal and minimal SMASh NS3 protease (tt3and tt4, respectively). As mentioned above, larger alterations like deleting the helicase domain resulted already in loss of cytotoxicity (Figure 34). However,

NS4 on the N-terminal side of the NS3 protease domain like in case of YFP-tt3 and YFT-tt4 resulted in drastically impaired protease activity. In contrast, tt1 and tt2 were able to cleave the tag from the fusion protein but showed impaired protein degradation, which was still better for tt1 than for tt2 (Figure 37). Viruses with tt1-tags showed similar growth kinetics as respective SMASh-viruses (Figure 39). In fact, RABV with P or N protein fused to the tt1 replicate as efficient as the corresponding SMASh-tagged viruses (Figure 39). Experiments analyzing the prevention of infection by direct addition of DNV, as well as curing after infection suggested that virus control by tt1 fusion to P or N is possible. Particularly, in case of SAD N-tt1 we could only detect minor detect any P protein levels when DNV was added at timepoint of infection. In contrast, DNV treatment of SAD eGFP P-tt1 at infection affected only slightly nucleoprotein production (Figure 40). Moreover, while curing of hIPSC derived astrocyte cultures of RABV was possible in case of both SAD N-tt1 and SAD P-tt1 infections, this occurred faster in case of SAD N-tt1 than in case of SAD eGFP P-tt1 (Figure 41). Altogether, these findings strongly indicate that tt1 fused to the RABV nucleoprotein is most efficient in regard of virus control. One reason therefore could be because one RABV N molecule is needed to enwrap 9 ribonucleotides leading to the formation of the typical helical structure (Iseni et al. 1998) and too low N levels prevent replication. Additionally, the nucleoprotein plays an important role for the transition from primary transcription to replication. Thus, a high copy number of newly produced soluble N is essential for binding the nascent leader RNA (Albertini et al. 2011). In consequence, a significant reduction of N levels might be sufficient to block replication completely. On the other hand, RABV P serves as cofactor for the RNA-dependent RNA polymerase L. Already existing copies of P allow replication in first place. However, new RNPs cannot be formed due to the lack of newly generated P in case of SAD eGFP P-tt1 and DNV treatment. At the end, fast virus control is desirable for various approaches including neurotracing. For this reason, we continued virus generation with tt1 fusion to the nucleoprotein.

Notably, during the duration of this thesis, other groups reported engineering controllable negative stand RNA viruses as well. A self-inactivating RABV (SiR) with a PEST sequence on each viral protein, with a Tobacco Etch Virus (TEV) cleavage site in between, was developed by Ciabatti and colleagues. Only the addition of a TEV protease separates the PEST sequence and prevents degradation of the respective proteins (Ciabatti et al. 2017). However, the validity of this approach was challenged, as the C-terminal degradation tags were found to be removed by introduction of stop codons (Matsuyama et al. 2019). Furthermore, the group of Wickersham reported that actual introduction of the SIR destabilization domain to the C-terminus of the RABV Nucleoprotein prevented viral spread, contrary to the claims of Ciabatti and

colleagues. In fact, this engineered RABV did only spread between neurons if the domain was removed (Jin et al. 2019).

Other scientists applied different strategies to generate controllable viruses. The group of Takeda used so called Magnet proteins. Those are paired photoswitchable proteins that heterodimerize upon blue light illumination. By the insertion of the Magnet proteins into the flexible domain of the viral polymerase photocontrollable measles and rabies viruses were generated. The resulting viruses showed strong replication and oncolytic activity when activated by blue light illumination (Tahara et al. 2019). Furthermore, Leber and colleagues integrated microRNA target sites into the measles virus genome allowing control of viral replication (Leber et al. 2018). Multiple strategies including inducible expression of glycoproteins were used by Gao et al. for virus control. One of the approaches targeting viral replication was similar to the SMASh-derived tt1-tag that was developed in this thesis: namely, use of a linker containing the HCV NS3 protease and its cleavage site. In this case, the NS3 protease was flanked by the cleavage site on both sides and incorporated between P and L of RABV. Only in absence of the protease inhibitor ASV, P and L were separated by proteolytic activity allowing replication, whereas inhibition leads to loss of functionality of both proteins (Gao et al. 2020). Another linker was generated by Heilmann and colleagues using a dimeric HIV protease, cleavage site and inhibitor inserted into the P or L gene of VSV. Thereby, viral replication could be reversibly switched off and on by using HIV protease inhibitors (Heilmann et al. 2021).

The tt1-tag that was engineered in this thesis functions comparable to the two latter strategies allowing virus control by addition of a small molecule inhibitor. However, it has to be mentioned that C-terminal fusion of the tt1-tag to a viral protein in context of a full-length virus might favor the production of escape mutants having a stop codon before the tag. To circumvent this potential problem an N-terminal tt1 should be generated similar to the N-terminal SMASh-tag in the future.

4.2.2 SAD ΔG Cre-T2A-eGFP N-tt1 for long term monosynaptic neuronal tracing approaches

As mentioned before, fusion of the tt1-tag to the RABV nucleoprotein allowed most effective virus control. Therefore, a G deleted N-tt1 virus was generated expressing a Cre recombinase linked via T2A to eGFP and named SAD ΔG Cre-T2A-eGFP N-tt1. As controllability was shown already before for SAD N-tt1 viruses (Figure 40, Figure 41), we performed one experiment analyzing the functionality of the Cre recombinase using a reporter plasmid. In fact, red fluorescence appearing exclusively in case of plasmid transfection and additional SAD ΔG Cre-T2A-eGFP N-tt1 virus infection suggested an intact Cre recombination system

(Figure 42). Therefore, this controllable virus pseudotyped with EnvA can be used for future *in vivo* long term monosynaptic tracing experiments. Various reporter mice are available expressing floxed fluorescent proteins already (Madisen et al. 2010; Li et al. 2018). Thus, a possible approach could look like following: the starter cells are provided with TVA for viral entry, RABV G for single-round spread and an additional fluorescent protein such as DsRed2. Of note, virally expressed, starter cell, and Cre dependent floxed fluorescent protein should be different in their fluorescence excitation spectrum. For example, virally expressed eGFP, DsRed2 provided within the starter cell and floxed BFP could be one possible combination. Infection of the starter cells by SAD ΔG Cre-T2A-eGFP N-tt1 (EnvA) leads to their additional staining due to the virally expressed eGFP and the recombination of fluorescent floxed BFP. As a result of the presence of SAD G within the starter cell, RABV can move to second-order neurons and also stain them in a similar manner as before. Then, virus can be shut down by addition of NS3 inhibitor such as ASV or DNV. As transport across blood brain barrier has not yet been elucidated for these molecules, local inhibitor treatment by injection to the brain might be the first choice. Notably, while cells are cured of viral infection to prevent long term cytopathic effects, Cre dependent BFP staining is preserved while eGFP fluorescence diminishes. In consequence, staining can be maintained without permanent virus infection. Using this system neurotracing experiments that require longer duration can be performed that were not feasible until now. Indeed, even reprogramming experiments may be possible using this controllable N-tt1 virus. As RABV is able to deliver expression of various additional proteins, different reprogramming factors could be included in the controllable SAD ΔG N-tt1 vector.

4.3   Conclusion and future perspectives

Apoptosis is induced by the SMASh-tag in combination with NS3 inhibitors like ASV and DNV. In the present thesis, new insight could be gained in regard of SMASh-mediated cell death induction. We could determine that the combination of all at least two domains within the SMASh-tag is required for the conditional cell death in addition to a high expression level of the SMASh-tag. In fact, all domains of the SMASh-tag might contribute to the conformation adopted after binding of the inhibitor. It is very likely that a conformational change provides access for interaction with a yet unknown death protein. To clarify this further, mutations within the inhibitor binding pocket could be introduced and analyzed. Moreover, ASV resistance mutations R155K and D168A (both annotations refer to the original HCV NS3 protease) could be analyzed regarding SMASh induced apoptosis in the future.

Various gene knockout and caspase inhibitor treatment experiments suggested the intracellular induction of multiple pathways that lead to apoptosis. This special feature makes RABV SMASh a potential candidate

for oncolytic approaches. Nevertheless, it remains unclear how exactly SMASh triggers apoptosis upon inhibitor treatment. Unfortunately, we were not able to prove a specific interaction partner of SMASh, and to produce clean CASP8/10$^{-/-}$ cells to check the importance of the most probable causal interaction partner. Induction of several caspases in parallel might be one possibility. In order to confirm this hypothesis, optimized immunoprecipitation experiments using proteasomal inhibitors could be done in future studies. As we could observe repeatedly YFP-SMASh fusion protein bands in Western blots, but not P-SMASh or N-SMASh, SAD YFP-SMASh might be the most suitable candidate for this purpose. Nevertheless, as direct binding of caspases is still speculative, a high-throughput screen might be interesting to find interaction partners of SMASh. Since the interaction partner of SMASh has not yet been elucidated, it is still unclear whether a strong or weak, transient, or permanent interaction is involved. For this reason, immunoprecipitation using chemical crosslinking to freeze transient interactions could be performed in the future. Tandem affinity purification with subsequent mass spectrometry analysis could therefore identify one or more interaction partners of SMASh. Additionally, not only stable but also transient protein-protein interactions could be analyzed by Blue Native PAGE, followed by Mass Spectrometry as done by Darie and colleagues (Darie et al. 2011). This approach could either validate direct induction of caspases or identify other binding partners of SMASh. Altogether, focusing on interaction studies should shed more light on the exact apoptosis inducing protein, that is triggered by SMASh and the NS3 inhibitor. Although in cancer cells apoptotic pathways are often silenced, RABV SMASh might be a promising oncolytic virus for cancer treatment. In particular, a RABV lacking the glycoprotein to enhance safety might be interesting for this approach. To analyze RABV SMASh in regard of possible cancer treatment, studies in mice are inevitable. Additionally, integration of SMASh within other viruses such as VSV or measles, that are already extensively used as oncolytic viruses, might increase the acceptability for cancer treatment in humans in future.

As an alternative to the cytotoxic SMASh-tag, a non-cytotoxic, but controllable tag was engineered within this thesis to allow virus control without harming infected cells. The newly generated tag called terminator-tag1, was most efficient in regard of virus control when fused to the RABV nucleoprotein. Although tt1 functions already very well in regard of virus controllability, the tag might be optimized in the future allowing N-terminal fusion to a protein of choice in order to circumvent the generation of escape mutants. Additionally, tt1 degradation could be improved. To this end, an additional or stronger degradation sequence could be implemented. Nevertheless, tt1 as we have generated it in this thesis allows already a wide range of new experimental approaches.

A RABV SMASh construct encoding a Cre recombinase as well as the tt1-tag at the nucleoprotein was shown to be a suitable candidate for future *in vivo* neurotracing experiments. Indeed, monosynaptic neuronal tracing is not the only interesting application of tt1. In addition to analyzing the half-life of different proteins, tt1 could be used for studying protein function. In particular, tt1 fused to viral proteins such as the phosphoprotein could allow further insights in regard of interferon signaling modulation by RABV P or its cofactor function for RABV L. Of course, the tt1-tag could not only be used to control RABV spread but allows shutoff of other RNA viruses as well. In particular, live attenuated vaccine viruses, viral vectors or oncolytic viruses could be shutoff for the purpose of improved safety. Importantly, this can be achieved with an already approved drug for HCV, namely asunaprevir (ASV).

Furthermore, not only viral proteins, but also cellular proteins could be studied by using tt1. Specifically, essential proteins, which are not possible to be studied in knockout cells, could be investigated in the future using the tt1-tag. This could be achieved by tagging the protein of interest via genetic knock-in using the CRISPR/Cas9 system. After transfection of a plasmid containing the mutant protein, the native tt-1 tagged protein could be shutoff and effects of respective mutations could be analyzed. In summary, the non-toxic terminator tag1 can be used in a variety of experimental settings and has the potential to increase safety of viruses used in patients.

5   References

Albertini, A. A. V.; Schoehn, G.; Weissenhorn, W.; Ruigrok, R. W. H. (2008): Structural aspects of rabies virus replication. In *Cellular and molecular life sciences : CMLS* 65 (2), pp. 282–294. DOI: 10.1007/s00018-007-7298-1.

Albertini, Aurélie A. V.; Ruigrok, Rob W. H.; Blondel, Danielle (2011): Rabies virus transcription and replication. In *Advances in virus research* 79, pp. 1–22. DOI: 10.1016/b978-0-12-387040-7.00001-9.

Albertini, Aurélie A. V.; Wernimont, Amy K.; Muziol, Tadeusz; Ravelli, Raimond B. G.; Clapier, Cedric R.; Schoehn, Guy et al. (2006): Crystal structure of the rabies virus nucleoprotein-RNA complex. In *Science (New York, N.Y.)* 313 (5785), pp. 360–363. DOI: 10.1126/science.1125280.

Alberts, Pēteris; Tilgase, Andra; Rasa, Agnija; Bandere, Katrīna; Venskus, Dite (2018): The advent of oncolytic virotherapy in oncology: The Rigvir® story. In *European journal of pharmacology* 837, pp. 117–126. DOI: 10.1016/j.ejphar.2018.08.042.

Altinoz, M. A.; Guloksuz, S.; Elmaci, I. (2017): Rabies virus vaccine as an immune adjuvant against cancers and glioblastoma: new studies may resurrect a neglected potential. In *Clinical & translational oncology : official publication of the Federation of Spanish Oncology Societies and of the National Cancer Institute of Mexico* 19 (7), pp. 785–792. DOI: 10.1007/s12094-017-1613-6.

Astic, Liliane; Saucier, Diane; Coulon, Patrice; Lafay, Florence; Flamand, Anne (1993): The CVS strain of rabies virus as transneuronal tracer in the olfactory system of mice. In *Brain Research* 619 (1-2), pp. 146–156. DOI: 10.1016/0006-8993(93)91606-S.

Aubrey, Brandon J.; Kelly, Gemma L.; Janic, Ana; Herold, Marco J.; Strasser, Andreas (2018): How does p53 induce apoptosis and how does this relate to p53-mediated tumour suppression? In *Cell death and differentiation* 25 (1), pp. 104–113. DOI: 10.1038/cdd.2017.169.

Baer, George M. (2007): The History of Rabies, pp. 1–22.

Balachandran, S.; Kim, C. N.; Yeh, W. C.; Mak, T. W.; Bhalla, K.; Barber, G. N. (1998): Activation of the dsRNA-dependent protein kinase, PKR, induces apoptosis through FADD-mediated death signaling. In *The EMBO journal* 17 (23), pp. 6888–6902. DOI: 10.1093/emboj/17.23.6888.

Bartenschlager, R.; Lohmann, V.; Wilkinson, T.; Koch, J. O. (1995): Complex formation between the NS3 serine-type proteinase of the hepatitis C virus and NS4A and its importance for polyprotein maturation. In *Journal of Virology* 69 (12), pp. 7519–7528. DOI: 10.1128/JVI.69.12.7519-7528.1995.

Bartz, S. R.; Emerman, M. (1999): Human immunodeficiency virus type 1 Tat induces apoptosis and increases sensitivity to apoptotic signals by up-regulating FLICE/caspase-8. In *Journal of Virology* 73 (3), pp. 1956–1963. DOI: 10.1128/JVI.73.3.1956-1963.1999.

Bertheloot, Damien; Latz, Eicke; Franklin, Bernardo S. (2021): Necroptosis, pyroptosis and apoptosis: an intricate game of cell death. In *Cellular & molecular immunology* 18 (5), pp. 1106–1121. DOI: 10.1038/s41423-020-00630-3.

Bodmer, J. L.; Holler, N.; Reynard, S.; Vinciguerra, P.; Schneider, P.; Juo, P. et al. (2000): TRAIL receptor-2 signals apoptosis through FADD and caspase-8. In *Nature cell biology* 2 (4), pp. 241–243. DOI: 10.1038/35008667.

Bongiorno, Emily K.; Garcia, Samantha A.; Sauma, Sami; Hooper, D. Craig (2017): Type 1 Immune Mechanisms Driven by the Response to Infection with Attenuated Rabies Virus Result in Changes in the Immune Bias of the Tumor Microenvironment and Necrosis of Mouse GL261 Brain Tumors. In *Journal of immunology (Baltimore, Md. : 1950)* 198 (11), pp. 4513–4523. DOI: 10.4049/jimmunol.1601444.

Brenndörfer, Erwin Daniel; Karthe, Juliane; Frelin, Lars; Cebula, Patricia; Erhardt, Andreas; Am Schulte Esch, Jan et al. (2009): Nonstructural 3/4A protease of hepatitis C virus activates epithelial growth factor-induced signal transduction by cleavage of the T-cell protein tyrosine phosphatase. In *Hepatology (Baltimore, Md.)* 49 (6), pp. 1810–1820. DOI: 10.1002/hep.22857.

Brzózka, Krzysztof; Finke, Stefan; Conzelmann, Karl-Klaus (2005): Identification of the rabies virus alpha/beta interferon antagonist: phosphoprotein P interferes with phosphorylation of interferon regulatory factor 3. In *Journal of Virology* 79 (12), pp. 7673–7681. DOI: 10.1128/JVI.79.12.7673-7681.2005.

Buchholz, U. J.; Finke, S.; Conzelmann, K. K. (1999): Generation of bovine respiratory syncytial virus (BRSV) from cDNA: BRSV NS2 is not essential for virus replication in tissue culture, and the human RSV leader region acts as a functional BRSV genome promoter. In *Journal of Virology* 73 (1), pp. 251–259. DOI: 10.1128/JVI.73.1.251-259.1999.

Bureau, C.; Bernad, J.; Chaouche, N.; Orfila, C.; Béraud, M.; Gonindard, C. et al. (2001): Nonstructural 3 protein of hepatitis C virus triggers an oxidative burst in human monocytes via activation of NADPH

oxidase. In *The Journal of biological chemistry* 276 (25), pp. 23077–23083. DOI: 10.1074/jbc.M100698200.

Butkiewicz, N. J.; Wendel, M.; Zhang, R.; Jubin, R.; Pichardo, J.; Smith, E. B. et al. (1996): Enhancement of hepatitis C virus NS3 proteinase activity by association with NS4A-specific synthetic peptides: identification of sequence and critical residues of NS4A for the cofactor activity. In *Virology* 225 (2), pp. 328–338. DOI: 10.1006/viro.1996.0607.

Cattaneo, Roberto; Miest, Tanner; Shashkova, Elena V.; Barry, Michael A. (2008): Reprogrammed viruses as cancer therapeutics: targeted, armed and shielded. In *Nature reviews. Microbiology* 6 (7), pp. 529–540. DOI: 10.1038/nrmicro1927.

Cattaneo, Roberto; Russell, Stephen J. (2017): How to develop viruses into anticancer weapons. In *PLoS pathogens* 13 (3), e1006190. DOI: 10.1371/journal.ppat.1006190.

Chanturiya, A. N.; Basañez, G.; Schubert, U.; Henklein, P.; Yewdell, J. W.; Zimmerberg, J. (2004): PB1-F2, an influenza A virus-encoded proapoptotic mitochondrial protein, creates variably sized pores in planar lipid membranes. In *Journal of Virology* 78 (12), pp. 6304–6312. DOI: 10.1128/JVI.78.12.6304-6312.2004.

Chaurio, Ricardo A.; Janko, Christina; Muñoz, Luis E.; Frey, Benjamin; Herrmann, Martin; Gaipl, Udo S. (2009): Phospholipids: key players in apoptosis and immune regulation. In *Molecules (Basel, Switzerland)* 14 (12), pp. 4892–4914. DOI: 10.3390/molecules14124892.

Chiou, Hui-Ling; Hsieh, Yih-Shou; Hsieh, Ming-Ru; Chen, Tzy-Yen (2006): HCV E2 may induce apoptosis of Huh-7 cells via a mitochondrial-related caspase pathway. In *Biochemical and biophysical research communications* 345 (1), pp. 453–458. DOI: 10.1016/j.bbrc.2006.04.118.

Choi, Jinah; Lee, Ki Jeong; Zheng, Yanyan; Yamaga, Ardath K.; Lai, Michael M. C.; Ou, Jing-Hsiung (2004): Reactive oxygen species suppress hepatitis C virus RNA replication in human hepatoma cells. In *Hepatology (Baltimore, Md.)* 39 (1), pp. 81–89. DOI: 10.1002/hep.20001.

Chong, Hui Ying; Leow, Chiuan Yee; Abdul Majeed, Abu Bakar; Leow, Chiuan Herng (2019): Flavivirus infection-A review of immunopathogenesis, immunological response, and immunodiagnosis. In *Virus research* 274, p. 197770. DOI: 10.1016/j.virusres.2019.197770.

Chou, Ai-Hsiang; Tsai, Hwei-Fang; Wu, Yi-Ying; Hu, Chung-Yi; Hwang, Lih-Hwa; Hsu, Ping-I; Hsu, Ping-Ning (2005): Hepatitis C virus core protein modulates TRAIL-mediated apoptosis by enhancing Bid cleavage

and activation of mitochondria apoptosis signaling pathway. In *Journal of immunology (Baltimore, Md. : 1950)* 174 (4), pp. 2160–2166. DOI: 10.4049/jimmunol.174.4.2160.

Chung, Hokyung K.; Jacobs, Conor L.; Huo, Yunwen; Yang, Jin; Krumm, Stefanie A.; Plemper, Richard K. et al. (2015): Tunable and reversible drug control of protein production via a self-excising degron. In *Nature chemical biology* 11 (9), pp. 713–720. DOI: 10.1038/nchembio.1869.

Ciabatti, Ernesto; González-Rueda, Ana; Mariotti, Letizia; Morgese, Fabio; Tripodi, Marco (2017): Life-Long Genetic and Functional Access to Neural Circuits Using Self-Inactivating Rabies Virus. In *Cell* 170 (2), 382-392.e14. DOI: 10.1016/j.cell.2017.06.014.

Conry, Robert M.; Westbrook, Brian; McKee, Svetlana; Norwood, Timothy Graham (2018): Talimogene laherparepvec: First in class oncolytic virotherapy. In *Human vaccines & immunotherapeutics* 14 (4), pp. 839–846. DOI: 10.1080/21645515.2017.1412896.

Croft, Sarah N.; Walker, Erin J.; Ghildyal, Reena (2018): Human Rhinovirus 3C protease cleaves RIPK1, concurrent with caspase 8 activation. In *Scientific reports* 8 (1), p. 1569. DOI: 10.1038/s41598-018-19839-4.

Daniel, P. T.; Wieder, T.; Sturm, I.; Schulze-Osthoff, K. (2001): The kiss of death: promises and failures of death receptors and ligands in cancer therapy. In *Leukemia* 15 (7), pp. 1022–1032. DOI: 10.1038/sj.leu.2402169.

D'Arcy, Mark S. (2019): Cell death: a review of the major forms of apoptosis, necrosis and autophagy. In *Cell biology international* 43 (6), pp. 582–592. DOI: 10.1002/cbin.11137.

Darie, Costel C.; Deinhardt, Katrin; Zhang, Guoan; Cardasis, Helene S.; Chao, Moses V.; Neubert, Thomas A. (2011): Identifying transient protein-protein interactions in EphB2 signaling by blue native PAGE and mass spectrometry. In *Proteomics* 11 (23), pp. 4514–4528. DOI: 10.1002/pmic.201000819.

Davis, Benjamin M.; Rall, Glenn F.; Schnell, Matthias J. (2015): Everything You Always Wanted to Know About Rabies Virus (But Were Afraid to Ask). In *Annual review of virology* 2 (1), pp. 451–471. DOI: 10.1146/annurev-virology-100114-055157.

Degli Esposti, M. (2002): The roles of Bid. In *Apoptosis : an international journal on programmed cell death* 7 (5), pp. 433–440. DOI: 10.1023/a:1020035124855.

Deng, Lin; Adachi, Tetsuya; Kitayama, Kikumi; Bungyoku, Yasuaki; Kitazawa, Sohei; Ishido, Satoshi et al. (2008): Hepatitis C virus infection induces apoptosis through a Bax-triggered, mitochondrion-mediated,

caspase 3-dependent pathway. In *Journal of Virology* 82 (21), pp. 10375–10385. DOI: 10.1128/JVI.00395-08.

Dietzgen, Ralf G.; Kondo, Hideki; Goodin, Michael M.; Kurath, Gael; Vasilakis, Nikos (2017): The family Rhabdoviridae: mono- and bipartite negative-sense RNA viruses with diverse genome organization and common evolutionary origins. In *Virus research* 227, pp. 158–170. DOI: 10.1016/j.virusres.2016.10.010.

Erbel, Paul; Schiering, Nikolaus; D'Arcy, Allan; Renatus, Martin; Kroemer, Markus; Lim, Siew Pheng et al. (2006): Structural basis for the activation of flaviviral NS3 proteases from dengue and West Nile virus. In *Nature structural & molecular biology* 13 (4), pp. 372–373. DOI: 10.1038/nsmb1073.

Etessami, Réza; Conzelmann, Karl-Klaus; Fadai-Ghotbi, Babak; Natelson, Benjamin; Tsiang, Henri; Ceccaldi, Pierre-Emmanuel (2000): Spread and pathogenic characteristics of a G-deficient rabies virus recombinant: an in vitro and in vivo study. In *The Journal of general virology* 81 (Pt 9), pp. 2147–2153. DOI: 10.1099/0022-1317-81-9-2147.

Falschlehner, Christina; Schaefer, Uta; Walczak, Henning (2009): Following TRAIL's path in the immune system. In *Immunology* 127 (2), pp. 145–154. DOI: 10.1111/j.1365-2567.2009.03058.x.

Fay, Elizabeth J.; Aron, Stephanie L.; Stone, Ian A.; Waring, Barbara M.; Plemper, Richard K.; Langlois, Ryan A. (2018): Engineered Small-Molecule Control of Influenza A Virus Replication. In *Journal of Virology* 93 (1). DOI: 10.1128/JVI.01677-18.

Ferrao, Ryan; Wu, Hao (2012): Helical assembly in the death domain (DD) superfamily. In *Current opinion in structural biology* 22 (2), pp. 241–247. DOI: 10.1016/j.sbi.2012.02.006.

Ferreira, Karine Sá; Kreutz, Clemens; Macnelly, Sabine; Neubert, Karin; Haber, Angelika; Bogyo, Matthew et al. (2012): Caspase-3 feeds back on caspase-8, Bid and XIAP in type I Fas signaling in primary mouse hepatocytes. In *Apoptosis : an international journal on programmed cell death* 17 (5), pp. 503–515. DOI: 10.1007/s10495-011-0691-0.

Festjens, N.; Vanden Berghe, T.; Cornelis, S.; Vandenabeele, P. (2007): RIP1, a kinase on the crossroads of a cell's decision to live or die. In *Cell death and differentiation* 14 (3), pp. 400–410. DOI: 10.1038/sj.cdd.4402085.

Finke, S.; Conzelmann, K. K. (1997): Ambisense gene expression from recombinant rabies virus: random packaging of positive- and negative-strand ribonucleoprotein complexes into rabies virions. In *Journal of Virology* 71 (10), pp. 7281–7288. DOI: 10.1128/JVI.71.10.7281-7288.1997.

Finke, Stefan; Conzelmann, Karl-Klaus (2005): Replication strategies of rabies virus. In *Virus research* 111 (2), pp. 120–131. DOI: 10.1016/j.virusres.2005.04.004.

Finke, Stefan; Mueller-Waldeck, Roland; Conzelmann, Karl-Klaus (2003): Rabies virus matrix protein regulates the balance of virus transcription and replication. In *The Journal of general virology* 84 (Pt 6), pp. 1613–1621. DOI: 10.1099/vir.0.19128-0.

Fodor, Ervin (2020): Insight into the multifunctional RNA synthesis machine of rabies virus. In *Proceedings of the National Academy of Sciences of the United States of America* 117 (8), pp. 3895–3897. DOI: 10.1073/pnas.2000120117.

Fooks, Anthony R.; Cliquet, Florence; Finke, Stefan; Freuling, Conrad; Hemachudha, Thiravat; Mani, Reeta S. et al. (2017): Rabies. In *Nature reviews. Disease primers* 3, p. 17091. DOI: 10.1038/nrdp.2017.91.

Fu, Tian-Min; Li, Yang; Lu, Alvin; Li, Zongli; Vajjhala, Parimala R.; Cruz, Anthony C. et al. (2016): Cryo-EM Structure of Caspase-8 Tandem DED Filament Reveals Assembly and Regulation Mechanisms of the Death-Inducing Signaling Complex. In *Molecular cell* 64 (2), pp. 236–250. DOI: 10.1016/j.molcel.2016.09.009.

Fujita, E.; Egashira, J.; Urase, K.; Kuida, K.; Momoi, T. (2001): Caspase-9 processing by caspase-3 via a feedback amplification loop in vivo. In *Cell death and differentiation* 8 (4), pp. 335–344. DOI: 10.1038/sj.cdd.4400824.

Fukuhara, Hiroshi; Ino, Yasushi; Todo, Tomoki (2016): Oncolytic virus therapy: A new era of cancer treatment at dawn. In *Cancer science* 107 (10), pp. 1373–1379. DOI: 10.1111/cas.13027.

Fulda, S.; Debatin, K-M (2006): Extrinsic versus intrinsic apoptosis pathways in anticancer chemotherapy. In *Oncogene* 25 (34), pp. 4798–4811. DOI: 10.1038/sj.onc.1209608.

Gal-Ben-Ari, Shunit; Barrera, Iliana; Ehrlich, Marcelo; Rosenblum, Kobi (2019): PKR: A Kinase to Remember. In *Frontiers in molecular neuroscience* 11, p. 480. DOI: 10.3389/fnmol.2018.00480.

Galluzzi, L.; Maiuri, M. C.; Vitale, I.; Zischka, H.; Castedo, M.; Zitvogel, L.; Kroemer, G. (2007): Cell death modalities: classification and pathophysiological implications. In *Cell death and differentiation* 14 (7), pp. 1237–1243. DOI: 10.1038/sj.cdd.4402148.

Galluzzi, Lorenzo; Vitale, Ilio; Aaronson, Stuart A.; Abrams, John M.; Adam, Dieter; Agostinis, Patrizia et al. (2018): Molecular mechanisms of cell death: recommendations of the Nomenclature Committee on Cell Death 2018. In *Cell death and differentiation* 25 (3), pp. 486–541. DOI: 10.1038/s41418-017-0012-4.

Gao, Xiaojing J.; Chong, Lucy S.; Ince, Michaela H.; Kim, Matthew S.; Elowitz, Michael B. (2020): Engineering multiple levels of specificity in an RNA viral vector. DOI: 10.1101/2020.05.27.119909.

García, M. A.; Meurs, E. F.; Esteban, M. (2007): The dsRNA protein kinase PKR: virus and cell control. In *Biochimie* 89 (6-7), pp. 799–811. DOI: 10.1016/j.biochi.2007.03.001.

Garcia-Ortega, M. B.; Lopez, G. J.; Jimenez, G.; Garcia-Garcia, J. A.; Conde, V.; Boulaiz, H. et al. (2017): Clinical and therapeutic potential of protein kinase PKR in cancer and metabolism. In *Expert reviews in molecular medicine* 19, e9. DOI: 10.1017/erm.2017.11.

Ghanem, Alexander; Conzelmann, Karl-Klaus (2016): G gene-deficient single-round rabies viruses for neuronal circuit analysis. In *Virus research* 216, pp. 41–54. DOI: 10.1016/j.virusres.2015.05.023.

Ghanem, Alexander; Kern, Anika; Conzelmann, Karl-Klaus (2012): Significantly improved rescue of rabies virus from cDNA plasmids. In *European journal of cell biology* 91 (1), pp. 10–16. DOI: 10.1016/j.ejcb.2011.01.008.

Gil, J.; Esteban, M. (2000a): Induction of apoptosis by the dsRNA-dependent protein kinase (PKR): mechanism of action. In *Apoptosis : an international journal on programmed cell death* 5 (2), pp. 107–114. DOI: 10.1023/a:1009664109241.

Gil, J.; Esteban, M. (2000b): The interferon-induced protein kinase (PKR), triggers apoptosis through FADD-mediated activation of caspase 8 in a manner independent of Fas and TNF-alpha receptors. In *Oncogene* 19 (32), pp. 3665–3674. DOI: 10.1038/sj.onc.1203710.

Gobeil, S.; Boucher, C. C.; Nadeau, D.; Poirier, G. G. (2001): Characterization of the necrotic cleavage of poly(ADP-ribose) polymerase (PARP-1): implication of lysosomal proteases. In *Cell death and differentiation* 8 (6), pp. 588–594. DOI: 10.1038/sj.cdd.4400851.

Griffin, Diane E.; Lin, Wen-Hsuan; Pan, Chien-Hsiung (2012): Measles virus, immune control, and persistence. In *FEMS microbiology reviews* 36 (3), pp. 649–662. DOI: 10.1111/j.1574-6976.2012.00330.x.

Guicciardi, Maria Eugenia; Gores, Gregory J. (2009): Life and death by death receptors. In *FASEB journal : official publication of the Federation of American Societies for Experimental Biology* 23 (6), pp. 1625–1637. DOI: 10.1096/fj.08-111005.

Guichard, Paul; Krell, Tino; Chevalier, Michel; Vaysse, Carole; Adam, Olivier; Ronzon, Frédéric; Marco, Sergio (2011): Three dimensional morphology of rabies virus studied by cryo-electron tomography. In *Journal of structural biology* 176 (1), pp. 32–40. DOI: 10.1016/j.jsb.2011.07.003.

Guillerme, Jean-Baptiste; Gregoire, Marc; Tangy, Frédéric; Fonteneau, Jean-François (2013): Antitumor Virotherapy by Attenuated Measles Virus (MV). In *Biology* 2 (2), pp. 587–602. DOI: 10.3390/biology2020587.

Häcker, G. (2000): The morphology of apoptosis. In *Cell and tissue research* 301 (1), pp. 5–17. DOI: 10.1007/s004410000193.

Hamad, Hamzah A.; Thurston, Jeremy; Teague, Thomas; Ackad, Edward; Yousef, Mohammad S. (2016): The NS4A Cofactor Dependent Enhancement of HCV NS3 Protease Activity Correlates with a 4D Geometrical Measure of the Catalytic Triad Region. In *PloS one* 11 (12), e0168002. DOI: 10.1371/journal.pone.0168002.

Hamamoto, Noriko; Uda, Akihiko; Tobiume, Minoru; Park, Chun-Ho; Noguchi, Akira; Kaku, Yoshihiro et al. (2015): Association between RABV G Proteins Transported from the Perinuclear Space to the Cell Surface Membrane and N-Glycosylation of the Sequon Asn(204). In *Japanese journal of infectious diseases* 68 (5), pp. 387–393. DOI: 10.7883/yoken.JJID.2014.533.

Hampson, Katie; Coudeville, Laurent; Lembo, Tiziana; Sambo, Maganga; Kieffer, Alexia; Attlan, Michaël et al. (2015): Correction: Estimating the global burden of endemic canine rabies. In *PLoS neglected tropical diseases* 9 (5), e0003786. DOI: 10.1371/journal.pntd.0003786.

Hannah, Jeffrey; Zhou, Pengbo (2015): Methods: A small-molecule SMASh hit. In *Nature chemical biology* 11 (9), pp. 637–638. DOI: 10.1038/nchembio.1886.

Heilmann, E.; Kimpel, J.; Hofer, B.; Rössler, A.; Blaas, I.; Egerer, L. et al. (2021): Chemogenetic ON and OFF switches for RNA virus replication. In *Nature communications* 12 (1), p. 1362. DOI: 10.1038/s41467-021-21630-5.

Hemachudha, Thiravat; Laothamatas, Jiraporn; Rupprecht, Charles E. (2002): Human rabies: a disease of complex neuropathogenetic mechanisms and diagnostic challenges. In *The Lancet Neurology* 1 (2), pp. 101–109. DOI: 10.1016/s1474-4422(02)00041-8.

Hemminki, Otto; Dos Santos, João Manuel; Hemminki, Akseli (2020): Oncolytic viruses for cancer immunotherapy. In *Journal of hematology & oncology* 13 (1), p. 84. DOI: 10.1186/s13045-020-00922-1.

Hengartner, M. O. (2000): The biochemistry of apoptosis. In *Nature* 407 (6805), pp. 770–776. DOI: 10.1038/35037710.

Horn, Sebastian; Hughes, Michelle A.; Schilling, Ramon; Sticht, Carsten; Tenev, Tencho; Ploesser, Michaela et al. (2017): Caspase-10 Negatively Regulates Caspase-8-Mediated Cell Death, Switching the Response to CD95L in Favor of NF-κB Activation and Cell Survival. In *Cell reports* 19 (4), pp. 785–797. DOI: 10.1016/j.celrep.2017.04.010.

Hu, Hai; Tian, Mingxing; Ding, Chan; Yu, Shengqing (2018): The C/EBP Homologous Protein (CHOP) Transcription Factor Functions in Endoplasmic Reticulum Stress-Induced Apoptosis and Microbial Infection. In *Frontiers in immunology* 9, p. 3083. DOI: 10.3389/fimmu.2018.03083.

Huber, Kristen L.; Serrano, Banyuhay P.; Hardy, Jeanne A. (2018): Caspase-9 CARD : core domain interactions require a properly formed active site. In *The Biochemical journal* 475 (6), pp. 1177–1196. DOI: 10.1042/BCJ20170913.

Hudacek, Andrew W.; Schnell, Matthias J. (2014): Rabies Virus Replication and Pathogenesis, pp. 335–351. DOI: 10.1142/9789814635349_0014.

Hüttemann, Maik; Pecina, Petr; Rainbolt, Matthew; Sanderson, Thomas H.; Kagan, Valerian E.; Samavati, Lobelia et al. (2011): The multiple functions of cytochrome c and their regulation in life and death decisions of the mammalian cell: From respiration to apoptosis. In *Mitochondrion* 11 (3), pp. 369–381. DOI: 10.1016/j.mito.2011.01.010.

Iseni, F.; Barge, A.; Baudin, F.; Blondel, D.; Ruigrok, R. W. (1998): Characterization of rabies virus nucleocapsids and recombinant nucleocapsid-like structures. In *The Journal of general virology* 79 (Pt 12), pp. 2909–2919. DOI: 10.1099/0022-1317-79-12-2909.

Ito, Naoto; Moseley, Gregory W.; Blondel, Danielle; Shimizu, Kenta; Rowe, Caitlin L.; Ito, Yuki et al. (2010): Role of interferon antagonist activity of rabies virus phosphoprotein in viral pathogenicity. In *Journal of Virology* 84 (13), pp. 6699–6710. DOI: 10.1128/JVI.00011-10.

Ito, Naoto; Moseley, Gregory W.; Sugiyama, Makoto (2016): The importance of immune evasion in the pathogenesis of rabies virus. In *The Journal of veterinary medical science* 78 (7), pp. 1089–1098. DOI: 10.1292/jvms.16-0092.

Jackson, Alan C. (2013): Current and future approaches to the therapy of human rabies. In *Antiviral research* 99 (1), pp. 61–67. DOI: 10.1016/j.antiviral.2013.01.003.

Jackson, Alan C.; Rasalingam, Pamini; Weli, Simon C. (2006): Comparative pathogenesis of recombinant rabies vaccine strain SAD-L16 and SAD-D29 with replacement of Arg333 in the glycoprotein after

peripheral inoculation of neonatal mice: less neurovirulent strain is a stronger inducer of neuronal apoptosis. In *Acta neuropathologica* 111 (4), pp. 372–378. DOI: 10.1007/s00401-005-0006-z.

Jayakar, Himangi R.; Jeetendra, E.; Whitt, Michael A. (2004): Rhabdovirus assembly and budding. In *Virus research* 106 (2), pp. 117–132. DOI: 10.1016/j.virusres.2004.08.009.

Jin, Lei; Matsuyama, Makoto; Sullivan, Heather A.; Zhu, Mulangma; Lavin, Thomas K.; Hou, YuanYuan et al. (2019): Rabies virus with a destabilization domain added to its nucleoprotein spreads between neurons only if the domain is removed. In *bioRxiv*. DOI: 10.1101/550640.

Jinesh, G. G.; Sambandam, V.; Vijayaraghavan, S.; Balaji, K.; Mukherjee, S. (2018): Molecular genetics and cellular events of K-Ras-driven tumorigenesis. In *Oncogene* 37 (7), pp. 839–846. DOI: 10.1038/onc.2017.377.

Kale, Justin; Osterlund, Elizabeth J.; Andrews, David W. (2018): BCL-2 family proteins: changing partners in the dance towards death. In *Cell death and differentiation* 25 (1), pp. 65–80. DOI: 10.1038/cdd.2017.186.

Kandoth, Cyriac; McLellan, Michael D.; Vandin, Fabio; Ye, Kai; Niu, Beifang; Lu, Charles et al. (2013): Mutational landscape and significance across 12 major cancer types. In *Nature* 502 (7471), pp. 333–339. DOI: 10.1038/nature12634.

Kang, Ju-Il; Kwon, Shi-Nae; Park, Se-Hoon; Kim, Yun Ki; Choi, Sang-Yun; Kim, Jungsuh P.; Ahn, Byung-Yoon (2009): PKR protein kinase is activated by hepatitis C virus and inhibits viral replication through translational control. In *Virus research* 142 (1-2), pp. 51–56. DOI: 10.1016/j.virusres.2009.01.007.

Kantari, Chahrazade; Walczak, Henning (2011): Caspase-8 and bid: caught in the act between death receptors and mitochondria. In *Biochimica et biophysica acta* 1813 (4), pp. 558–563. DOI: 10.1016/j.bbamcr.2011.01.026.

Kerr, J. F.; Wyllie, A. H.; Currie, A. R. (1972): Apoptosis: a basic biological phenomenon with wide-ranging implications in tissue kinetics. In *British journal of cancer* 26 (4), pp. 239–257. DOI: 10.1038/bjc.1972.33.

Kischkel, F. C.; Lawrence, D. A.; Tinel, A.; LeBlanc, H.; Virmani, A.; Schow, P. et al. (2001): Death receptor recruitment of endogenous caspase-10 and apoptosis initiation in the absence of caspase-8. In *The Journal of biological chemistry* 276 (49), pp. 46639–46646. DOI: 10.1074/jbc.M105102200.

Knobel, Darryn L.; Cleaveland, Sarah; Coleman, Paul G.; Fèvre, Eric M.; Meltzer, Martin I.; Miranda, M. Elizabeth G. et al. (2005): Re-evaluating the burden of rabies in Africa and Asia. In *Bulletin of the World Health Organization* 83 (5), pp. 360–368.

Korsmeyer, S. J.; Wei, M. C.; Saito, M.; Weiler, S.; Oh, K. J.; Schlesinger, P. H. (2000): Pro-apoptotic cascade activates BID, which oligomerizes BAK or BAX into pores that result in the release of cytochrome c. In *Cell death and differentiation* 7 (12), pp. 1166–1173. DOI: 10.1038/sj.cdd.4400783.

Koyuncu, Orkide O.; Hogue, Ian B.; Enquist, Lynn W. (2013): Virus infections in the nervous system. In *Cell host & microbe* 13 (4), pp. 379–393. DOI: 10.1016/j.chom.2013.03.010.

Kramer, Mitchell; Halleran, Daniel; Rahman, Moazur; Iqbal, Mazhar; Anwar, Muhammad Ikram; Anwar, Muhmad Ikram et al. (2014): Comparative molecular dynamics simulation of Hepatitis C Virus NS3/4A protease (Genotypes 1b, 3a and 4b) predicts conformational instability of the catalytic triad in drug resistant strains. In *PloS one* 9 (8), e104425. DOI: 10.1371/journal.pone.0104425.

Krueger, A.; Schmitz, I.; Baumann, S.; Krammer, P. H.; Kirchhoff, S. (2001): Cellular FLICE-inhibitory protein splice variants inhibit different steps of caspase-8 activation at the CD95 death-inducing signaling complex. In *The Journal of biological chemistry* 276 (23), pp. 20633–20640. DOI: 10.1074/jbc.M101780200.

Kuang, A. A.; Diehl, G. E.; Zhang, J.; Winoto, A. (2000): FADD is required for DR4- and DR5-mediated apoptosis: lack of trail-induced apoptosis in FADD-deficient mouse embryonic fibroblasts. In *The Journal of biological chemistry* 275 (33), pp. 25065–25068. DOI: 10.1074/jbc.C000284200.

Kumar, A.; Haque, J.; Lacoste, J.; Hiscott, J.; Williams, B. R. (1994): Double-stranded RNA-dependent protein kinase activates transcription factor NF-kappa B by phosphorylating I kappa B. In *Proceedings of the National Academy of Sciences of the United States of America* 91 (14), pp. 6288–6292. DOI: 10.1073/pnas.91.14.6288.

La Cruz, Laura de; Nguyen, Thi Hoang Duong; Ozawa, Kiyoshi; Shin, James; Graham, Bim; Huber, Thomas; Otting, Gottfried (2011): Binding of low molecular weight inhibitors promotes large conformational changes in the dengue virus NS2B-NS3 protease: fold analysis by pseudocontact shifts. In *Journal of the American Chemical Society* 133 (47), pp. 19205–19215. DOI: 10.1021/ja208435s.

Lafon, M. (2008): Immune evasion, a critical strategy for rabies virus. In *Developments in biologicals* 131, pp. 413–419.

Lafon, Monique (2005): Rabies virus receptors. In *Journal of neurovirology* 11 (1), pp. 82–87. DOI: 10.1080/13550280590900427.

Lahaye, Xavier; Vidy, Aurore; Pomier, Carole; Obiang, Linda; Harper, Francis; Gaudin, Yves; Blondel, Danielle (2009): Functional characterization of Negri bodies (NBs) in rabies virus-infected cells: Evidence that NBs are sites of viral transcription and replication. In *Journal of Virology* 83 (16), pp. 7948–7958. DOI: 10.1128/JVI.00554-09.

Leber, Mathias Felix; Baertsch, Marc-Andrea; Anker, Sophie Caroline; Henkel, Luisa; Singh, Hans Martin; Bossow, Sascha et al. (2018): Enhanced Control of Oncolytic Measles Virus Using MicroRNA Target Sites. In *Molecular therapy oncolytics* 9, pp. 30–40. DOI: 10.1016/j.omto.2018.04.002.

Lee, Eun-Soo; Yoon, Cheol-Hee; Kim, Yeon-Soo; Bae, Yong-Soo (2007): The double-strand RNA-dependent protein kinase PKR plays a significant role in a sustained ER stress-induced apoptosis. In *FEBS letters* 581 (22), pp. 4325–4332. DOI: 10.1016/j.febslet.2007.08.001.

Lee, Song Hee; Kim, Yoon Ki; Kim, Chon Saeng; Seol, Su Kyoung; Kim, Joonhyun; Cho, Sungchan et al. (2005): E2 of hepatitis C virus inhibits apoptosis. In *Journal of immunology (Baltimore, Md. : 1950)* 175 (12), pp. 8226–8235. DOI: 10.4049/jimmunol.175.12.8226.

Li, Honglin; Zhu, Hong; Xu, Chi-jie; Yuan, Junying (1998): Cleavage of BID by Caspase 8 Mediates the Mitochondrial Damage in the Fas Pathway of Apoptosis. In *Cell* 94 (4), pp. 491–501. DOI: 10.1016/S0092-8674(00)81590-1.

Li, Kui; Foy, Eileen; Ferreon, Josephine C.; Nakamura, Mitsuyasu; Ferreon, Allan C. M.; Ikeda, Masanori et al. (2005a): Immune evasion by hepatitis C virus NS3/4A protease-mediated cleavage of the Toll-like receptor 3 adaptor protein TRIF. In *Proceedings of the National Academy of Sciences of the United States of America* 102 (8), pp. 2992–2997. DOI: 10.1073/pnas.0408824102.

Li, Shun; Chen, Li-Xiang; Peng, Xiu-Hua; Wang, Chao; Qin, Bo-Yin; Tan, Dan et al. (2018): Overview of the reporter genes and reporter mouse models. In *Animal models and experimental medicine* 1 (1), pp. 29–35. DOI: 10.1002/ame2.12008.

Li, Xiao-Dong; Sun, Lijun; Seth, Rashu B.; Pineda, Gabriel; Chen, Zhijian J. (2005b): Hepatitis C virus protease NS3/4A cleaves mitochondrial antiviral signaling protein off the mitochondria to evade innate immunity. In *Proceedings of the National Academy of Sciences of the United States of America* 102 (49), pp. 17717–17722. DOI: 10.1073/pnas.0508531102.

Liang, Min (2018): Oncorine, the World First Oncolytic Virus Medicine and its Update in China. In *Current cancer drug targets* 18 (2), pp. 171–176. DOI: 10.2174/1568009618666171129221503.

Lin, C. (2006): Hepatitis C Viruses: Genomes and Molecular Biology. HCV NS3-4A Serine Protease (Chapter 6).

Luo, Xu; Budihardjo, Imawati; Zou, Hua; Slaughter, Clive; Wang, Xiaodong (1998): Bid, a Bcl2 Interacting Protein, Mediates Cytochrome c Release from Mitochondria in Response to Activation of Cell Surface Death Receptors. In *Cell* 94 (4), pp. 481–490. DOI: 10.1016/S0092-8674(00)81589-5.

Madisen, Linda; Zwingman, Theresa A.; Sunkin, Susan M.; Oh, Seung Wook; Zariwala, Hatim A.; Gu, Hong et al. (2010): A robust and high-throughput Cre reporting and characterization system for the whole mouse brain. In *Nature neuroscience* 13 (1), pp. 133–140. DOI: 10.1038/nn.2467.

Manning, Susan E.; Rupprecht, Charles E.; Fishbein, Daniel; Hanlon, Cathleen A.; Lumlertdacha, Boonlert; Guerra, Marta et al. (2008): Human rabies prevention--United States, 2008: recommendations of the Advisory Committee on Immunization Practices. In *MMWR. Recommendations and reports : Morbidity and mortality weekly report. Recommendations and reports* 57 (RR-3), pp. 1–28.

Manns, Michael P.; Buti, Maria; Gane, Ed; Pawlotsky, Jean-Michel; Razavi, Homie; Terrault, Norah; Younossi, Zobair (2017): Hepatitis C virus infection. In *Nature reviews. Disease primers* 3, p. 17006. DOI: 10.1038/nrdp.2017.6.

Marques, Joao T.; White, Christine L.; Peters, Gregory A.; Williams, Bryan R.G.; Sen, Ganes C. (2008): The Role of PACT in Mediating Gene Induction, PKR Activation, and Apoptosis in Response to Diverse Stimuli. In *Journal of interferon & cytokine research : the official journal of the International Society for Interferon and Cytokine Research* 28 (8), pp. 469–475. DOI: 10.1089/jir.2007.0006.

Masemann, Dörthe; Boergeling, Yvonne; Ludwig, Stephan (2017): Employing RNA viruses to fight cancer: novel insights into oncolytic virotherapy. In *Biological chemistry* 398 (8), pp. 891–909. DOI: 10.1515/hsz-2017-0103.

Matsuyama, Makoto; Jin, Lei; Lavin, Thomas K.; Sullivan, Heather A.; Hou, YuanYuan; Lea, Nicholas E. et al. (2019): "Self-inactivating" rabies viruses are susceptible to loss of their intended attenuating modification. DOI: 10.1101/550640.

Mavrakis, Manos; McCarthy, Andrew A.; Roche, Stéphane; Blondel, Danielle; Ruigrok, Rob W. H. (2004): Structure and function of the C-terminal domain of the polymerase cofactor of rabies virus. In *Journal of molecular biology* 343 (4), pp. 819–831. DOI: 10.1016/j.jmb.2004.08.071.

Mazarakis, N. D.; Azzouz, M.; Rohll, J. B.; Ellard, F. M.; Wilkes, F. J.; Olsen, A. L. et al. (2001): Rabies virus glycoprotein pseudotyping of lentiviral vectors enables retrograde axonal transport and access to the nervous system after peripheral delivery. In *Human molecular genetics* 10 (19), pp. 2109–2121. DOI: 10.1093/hmg/10.19.2109.

Mebatsion, T.; Weiland, F.; Conzelmann, K. K. (1999): Matrix protein of rabies virus is responsible for the assembly and budding of bullet-shaped particles and interacts with the transmembrane spike glycoprotein G. In *Journal of Virology* 73 (1), pp. 242–250. DOI: 10.1128/JVI.73.1.242-250.1999.

Mebatsion, Teshome; König, Matthias; Conzelmann, Karl-Klaus (1996): Budding of Rabies Virus Particles in the Absence of the Spike Glycoprotein. In *Cell* 84 (6), pp. 941–951. DOI: 10.1016/S0092-8674(00)81072-7.

Melnikova, Vladislava O.; Bolshakov, Svetlana V.; Walker, Christopher; Ananthaswamy, Honnavara N. (2004): Genomic alterations in spontaneous and carcinogen-induced murine melanoma cell lines. In *Oncogene* 23 (13), pp. 2347–2356. DOI: 10.1038/sj.onc.1207405.

Meylan, Etienne; Curran, Joseph; Hofmann, Kay; Moradpour, Darius; Binder, Marco; Bartenschlager, Ralf; Tschopp, Jürg (2005): Cardif is an adaptor protein in the RIG-I antiviral pathway and is targeted by hepatitis C virus. In *Nature* 437 (7062), pp. 1167–1172. DOI: 10.1038/nature04193.

Micheau, Olivier; Thome, Margot; Schneider, Pascal; Holler, Nils; Tschopp, Jürg; Nicholson, Donald W. et al. (2002): The long form of FLIP is an activator of caspase-8 at the Fas death-inducing signaling complex. In *The Journal of biological chemistry* 277 (47), pp. 45162–45171. DOI: 10.1074/jbc.M206882200.

Micheau, Olivier; Tschopp, Jürg (2003): Induction of TNF Receptor I-Mediated Apoptosis via Two Sequential Signaling Complexes. In *Cell* 114 (2), pp. 181–190. DOI: 10.1016/S0092-8674(03)00521-X.

Mondal, Moumita; Guo, Jingao; He, Ping; Zhou, Dongming (2020): Recent advances of oncolytic virus in cancer therapy. In *Human vaccines & immunotherapeutics* 16 (10), pp. 2389–2402. DOI: 10.1080/21645515.2020.1723363.

Moradpour, Darius; Penin, François; Rice, Charles M. (2007): Replication of hepatitis C virus. In *Nature reviews. Microbiology* 5 (6), pp. 453–463. DOI: 10.1038/nrmicro1645.

Morales, Julio C.; Li, Longshan; Fattah, Farjana J.; Dong, Ying; Bey, Erik A.; Patel, Malina et al. (2014): Review of Poly (ADP-ribose) Polymerase (PARP) Mechanisms of Action and Rationale for Targeting in Cancer and Other Diseases. In *Critical reviews in eukaryotic gene expression* 24 (1), pp. 15–28.

Morozov, Vladimir Alexei; Lagaye, Sylvie (2018): Hepatitis C virus: Morphogenesis, infection and therapy. In *World journal of hepatology* 10 (2), pp. 186–212. DOI: 10.4254/wjh.v10.i2.186.

Muik, Alexander; Kneiske, Inna; Werbizki, Marina; Wilflingseder, Doris; Giroglou, Tsanan; Ebert, Oliver et al. (2011): Pseudotyping vesicular stomatitis virus with lymphocytic choriomeningitis virus glycoproteins enhances infectivity for glioma cells and minimizes neurotropism. In *Journal of Virology* 85 (11), pp. 5679–5684. DOI: 10.1128/JVI.02511-10.

Muik, Alexander; Stubbert, Lawton J.; Jahedi, Roza Z.; Geiβ, Yvonne; Kimpel, Janine; Dold, Catherine et al. (2014): Re-engineering vesicular stomatitis virus to abrogate neurotoxicity, circumvent humoral immunity, and enhance oncolytic potency. In *Cancer research* 74 (13), pp. 3567–3578. DOI: 10.1158/0008-5472.CAN-13-3306.

Nagata, Shigekazu; Tanaka, Masato (2017): Programmed cell death and the immune system. In *Nature reviews. Immunology* 17 (5), pp. 333–340. DOI: 10.1038/nri.2016.153.

Natsume, Toyoaki; Kanemaki, Masato T. (2017): Conditional Degrons for Controlling Protein Expression at the Protein Level. In *Annual review of genetics* 51, pp. 83–102. DOI: 10.1146/annurev-genet-120116-024656.

Neumeier, Julia; Meister, Gunter (2020): siRNA Specificity: RNAi Mechanisms and Strategies to Reduce Off-Target Effects. In *Frontiers in plant science* 11, p. 526455. DOI: 10.3389/fpls.2020.526455.

Nevers, Quentin; Albertini, Aurélie A.; Lagaudrière-Gesbert, Cécile; Gaudin, Yves (2020): Negri bodies and other virus membrane-less replication compartments. In *Biochimica et biophysica acta. Molecular cell research* 1867 (12), p. 118831. DOI: 10.1016/j.bbamcr.2020.118831.

Nikolic, Jovan; Le Bars, Romain; Lama, Zoé; Scrima, Nathalie; Lagaudrière-Gesbert, Cécile; Gaudin, Yves; Blondel, Danielle (2017): Negri bodies are viral factories with properties of liquid organelles. In *Nature communications* 8 (1), p. 58. DOI: 10.1038/s41467-017-00102-9.

Niwa, H.; Yamamura; K.; Miyazaki, J. (1991): Efficient selection for high-expression transfectants with a novel eukaryotic vector. In *Gene* 108 (2), pp. 193–199. DOI: 10.1016/0378-1119(91)90434-d.

Ogino, Tomoaki; Green, Todd J. (2019): RNA Synthesis and Capping by Non-segmented Negative Strand RNA Viral Polymerases: Lessons From a Prototypic Virus. In *Frontiers in microbiology* 10, p. 1490. DOI: 10.3389/fmicb.2019.01490.

Okumura, Atsushi; Harty, Ronald N. (2011): Rabies virus assembly and budding. In *Advances in virus research* 79, pp. 23–32. DOI: 10.1016/B978-0-12-387040-7.00002-0.

Ozenne, Peggy; Eymin, Beatrice; Brambilla, Elisabeth; Gazzeri, Sylvie (2010): The ARF tumor suppressor: structure, functions and status in cancer. In *International journal of cancer* 127 (10), pp. 2239–2247. DOI: 10.1002/ijc.25511.

Pasparakis, Manolis; Vandenabeele, Peter (2015): Necroptosis and its role in inflammation. In *Nature* 517 (7534), pp. 311–320. DOI: 10.1038/nature14191.

Pereira, Natasha Ann; Song, Zhiwei (2008): Some commonly used caspase substrates and inhibitors lack the specificity required to monitor individual caspase activity. In *Biochemical and biophysical research communications* 377 (3), pp. 873–877. DOI: 10.1016/j.bbrc.2008.10.101.

Perez, D.; White, E. (1998): E1B 19K inhibits Fas-mediated apoptosis through FADD-dependent sequestration of FLICE. In *The Journal of cell biology* 141 (5), pp. 1255–1266. DOI: 10.1083/jcb.141.5.1255.

Pfaffinger, V. (2016): Induction of cell death by small molecule–assisted shutoff (SMASh). In *Master thesis*.

Pop, Cristina; Oberst, Andrew; Drag, Marcin; van Raam, Bram J.; Riedl, Stefan J.; Green, Douglas R.; Salvesen, Guy S. (2011): FLIP(L) induces caspase 8 activity in the absence of interdomain caspase 8 cleavage and alters substrate specificity. In *The Biochemical journal* 433 (3), pp. 447–457. DOI: 10.1042/BJ20101738.

Pop, Cristina; Salvesen, Guy S. (2009): Human caspases: activation, specificity, and regulation. In *The Journal of biological chemistry* 284 (33), pp. 21777–21781. DOI: 10.1074/jbc.R800084200.

Prikhod'ko, Elena A.; Prikhod'ko, Grigori G.; Siegel, Richard M.; Thompson, Peter; Major, Marian E.; Cohen, Jeffrey I. (2004): The NS3 protein of hepatitis C virus induces caspase-8-mediated apoptosis independent of its protease or helicase activities. In *Virology* 329 (1), pp. 53–67. DOI: 10.1016/j.virol.2004.08.012.

Prikhod'ko, Grigori G.; Prikhod'ko, Elena A.; Pletnev, Alexander G.; Cohen, Jeffrey I. (2002): Langat flavivirus protease NS3 binds caspase-8 and induces apoptosis. In *Journal of Virology* 76 (11), pp. 5701–5710. DOI: 10.1128/JVI.76.11.5701-5710.2002.

Queiroz, Nina Marí Gual Pimenta de; Xia, Tianli; Konno, Hiroyasu; Barber, Glen N. (2019): Ovarian Cancer Cells Commonly Exhibit Defective STING Signaling Which Affects Sensitivity to Viral Oncolysis. In *Molecular cancer research : MCR* 17 (4), pp. 974–986. DOI: 10.1158/1541-7786.MCR-18-0504.

Rabaan, Ali A.; Al-Ahmed, Shamsah H.; Bazzi, Ali M.; Alfouzan, Wadha A.; Alsuliman, Shahab A.; Aldrazi, Fatimah A.; Haque, Shafiul (2020): Overview of hepatitis C infection, molecular biology, and new treatment. In *Journal of infection and public health* 13 (5), pp. 773–783. DOI: 10.1016/j.jiph.2019.11.015.

Rahman, Masmudur M.; McFadden, Grant (2021): Oncolytic Viruses: Newest Frontier for Cancer Immunotherapy. In *Cancers* 13 (21). DOI: 10.3390/cancers13215452.

Rajput, Akhil; Kovalenko, Andrew; Bogdanov, Konstantin; Yang, Seung-Hoon; Kang, Tae-Bong; Kim, Jin-Chul et al. (2011): RIG-I RNA helicase activation of IRF3 transcription factor is negatively regulated by caspase-8-mediated cleavage of the RIP1 protein. In *Immunity* 34 (3), pp. 340–351. DOI: 10.1016/j.immuni.2010.12.018.

Ramanathan, Mathura P.; Chambers, Jerome A.; Pankhong, Panyupa; Chattergoon, Michael; Attatippaholkun, Watcharee; Dang, Kesen et al. (2006): Host cell killing by the West Nile Virus NS2B-NS3 proteolytic complex: NS3 alone is sufficient to recruit caspase-8-based apoptotic pathway. In *Virology* 345 (1), pp. 56–72. DOI: 10.1016/j.virol.2005.08.043.

Rébé, Cédric; Cathelin, Séverine; Launay, Sophie; Filomenko, Rodolphe; Prévotat, Laurent; L'Ollivier, Coralie et al. (2007): Caspase-8 prevents sustained activation of NF-kappaB in monocytes undergoing macrophagic differentiation. In *Blood* 109 (4), pp. 1442–1450. DOI: 10.1182/blood-2006-03-011585.

Rechsteiner, Martin; Rogers, Scott W. (1996): PEST sequences and regulation by proteolysis. In *Trends in Biochemical Sciences* 21 (7), pp. 267–271. DOI: 10.1016/s0968-0004(96)10031-1.

Rieder, Martina; Brzózka, Krzysztof; Pfaller, Christian K.; Cox, James H.; Stitz, Lothar; Conzelmann, Karl-Klaus (2011): Genetic dissection of interferon-antagonistic functions of rabies virus phosphoprotein: inhibition of interferon regulatory factor 3 activation is important for pathogenicity. In *Journal of Virology* 85 (2), pp. 842–852. DOI: 10.1128/JVI.01427-10.

Riley, J. S.; Malik, A.; Holohan, C.; Longley, D. B. (2015): DED or alive: assembly and regulation of the death effector domain complexes. In *Cell death & disease* 6, e1866. DOI: 10.1038/cddis.2015.213.

Ríos-Ocampo, W. Alfredo; Daemen, Toos; Buist-Homan, Manon; Faber, Klaas Nico; Navas, María-Cristina; Moshage, Han (2019): Hepatitis C virus core or NS3/4A protein expression preconditions hepatocytes against oxidative stress and endoplasmic reticulum stress. In *Redox report : communications in free radical research* 24 (1), pp. 17–26. DOI: 10.1080/13510002.2019.1596431.

Roberts, A. W.; Huang, Dcs (2017): Targeting BCL2 With BH3 Mimetics: Basic Science and Clinical Application of Venetoclax in Chronic Lymphocytic Leukemia and Related B Cell Malignancies. In *Clinical pharmacology and therapeutics* 101 (1), pp. 89–98. DOI: 10.1002/cpt.553.

Roder, Allison E.; Vazquez, Christine; Horner, Stacy M. (2019): The acidic domain of the hepatitis C virus NS4A protein is required for viral assembly and envelopment through interactions with the viral E1 glycoprotein. In *PLoS pathogens* 15 (2), e1007163. DOI: 10.1371/journal.ppat.1007163.

Rogers, S.; Wells, R.; Rechsteiner, M. (1986): Amino acid sequences common to rapidly degraded proteins: the PEST hypothesis. In *Science (New York, N.Y.)* 234 (4774), pp. 364–368. DOI: 10.1126/science.2876518.

Romano, Keith P.; Ali, Akbar; Aydin, Cihan; Soumana, Djade; Ozen, Ayşegül; Deveau, Laura M. et al. (2012): The molecular basis of drug resistance against hepatitis C virus NS3/4A protease inhibitors. In *PLoS pathogens* 8 (7), e1002832. DOI: 10.1371/journal.ppat.1002832.

Rosatte, R. C. (2013): Rabies Control in Wild Carnivores, pp. 617–670. DOI: 10.1016/B978-0-12-396547-9.00018-3.

Röth, Sascha; Fulcher, Luke J.; Sapkota, Gopal P. (2019): Advances in targeted degradation of endogenous proteins. In *Cellular and molecular life sciences : CMLS* 76 (14), pp. 2761–2777. DOI: 10.1007/s00018-019-03112-6.

Saito, Kousuke; Meyer, Keith; Warner, Rebecca; Basu, Arnab; Ray, Ratna B.; Ray, Ranjit (2006): Hepatitis C virus core protein inhibits tumor necrosis factor alpha-mediated apoptosis by a protective effect involving cellular FLICE inhibitory protein. In *Journal of Virology* 80 (9), pp. 4372–4379. DOI: 10.1128/JVI.80.9.4372-4379.2006.

Sanjana, Neville E.; Shalem, Ophir; Zhang, Feng (2014): Improved vectors and genome-wide libraries for CRISPR screening. In *Nature methods* 11 (8), pp. 783–784. DOI: 10.1038/nmeth.3047.

Saraste, A. (2000): Morphologic and biochemical hallmarks of apoptosis. In *Cardiovascular Research* 45 (3), pp. 528–537. DOI: 10.1016/S0008-6363(99)00384-3.

Scheuner, Donalyn; Patel, Rupali; Wang, Feng; Lee, Kuei; Kumar, Kotlo; Wu, Jun et al. (2006): Double-stranded RNA-dependent protein kinase phosphorylation of the alpha-subunit of eukaryotic translation initiation factor 2 mediates apoptosis. In *The Journal of biological chemistry* 281 (30), pp. 21458–21468. DOI: 10.1074/jbc.M603784200.

Schmidt, Tobias; Schmid-Burgk, Jonathan L.; Hornung, Veit (2015): Synthesis of an arrayed sgRNA library targeting the human genome. In *Scientific reports* 5, p. 14987. DOI: 10.1038/srep14987.

Schneider, L. G. (1995): Rabies virus vaccines. In *Developments in biological standardization* 84, pp. 49–54.

Schnell, M. J.; Mebatsion, T.; Conzelmann, K. K. (1994): Infectious rabies viruses from cloned cDNA. In *The EMBO journal* 13 (18), pp. 4195–4203.

Schug, Z. T.; Gonzalvez, F.; Houtkooper, R. H.; Vaz, F. M.; Gottlieb, E. (2011): BID is cleaved by caspase-8 within a native complex on the mitochondrial membrane. In *Cell death and differentiation* 18 (3), pp. 538–548. DOI: 10.1038/cdd.2010.135.

Siavoshian, Samila; Abraham, Jean Daniel; Thumann, Christine; Kieny, Marie Paule; Schuster, Catherine (2005): Hepatitis C virus core, NS3, NS5A, NS5B proteins induce apoptosis in mature dendritic cells. In *Journal of medical virology* 75 (3), pp. 402–411. DOI: 10.1002/jmv.20283.

Siegel, R. M.; Martin, D. A.; Zheng, L.; Ng, S. Y.; Bertin, J.; Cohen, J.; Lenardo, M. J. (1998): Death-effector filaments: novel cytoplasmic structures that recruit caspases and trigger apoptosis. In *The Journal of cell biology* 141 (5), pp. 1243–1253. DOI: 10.1083/jcb.141.5.1243.

Silva, Manuel T. (2010): Secondary necrosis: the natural outcome of the complete apoptotic program. In *FEBS letters* 584 (22), pp. 4491–4499. DOI: 10.1016/j.febslet.2010.10.046.

Soumana, Djadé I.; Ali, Akbar; Schiffer, Celia A. (2014): Structural analysis of asunaprevir resistance in HCV NS3/4A protease. In *ACS chemical biology* 9 (11), pp. 2485–2490. DOI: 10.1021/cb5006118.

Sprick, Martin R.; Rieser, Eva; Stahl, Heiko; Grosse-Wilde, Anne; Weigand, Markus A.; Walczak, Henning (2002): Caspase-10 is recruited to and activated at the native TRAIL and CD95 death-inducing signalling complexes in a FADD-dependent manner but can not functionally substitute caspase-8. In *The EMBO journal* 21 (17), pp. 4520–4530. DOI: 10.1093/emboj/cdf441.

Sprick, Martin R.; Weigand, Markus A.; Rieser, Eva; Rauch, Charles T.; Juo, Peter; Blenis, John et al. (2000): FADD/MORT1 and Caspase-8 Are Recruited to TRAIL // FADD/MORT1 and Caspase-8 Are Recruited to TRAIL Receptors 1 and 2 and Are Essential for Apoptosis Mediated by TRAIL Receptor 2. In *Immunity* 12 (6), pp. 599–609. DOI: 10.1016/s1074-7613(00)80211-3.

Su, Justin M.; Wilson, Maxwell Z.; Samuel, Charles E.; Ma, Dzwokai (2021): Formation and Function of Liquid-Like Viral Factories in Negative-Sense Single-Stranded RNA Virus Infections. In *Viruses* 13 (1). DOI: 10.3390/v13010126.

Suja, M. S.; Mahadevan, Anita; Madhusudana, S. N.; Shankar, S. K. (2011): Role of apoptosis in rabies viral encephalitis: a comparative study in mice, canine, and human brain with a review of literature. In *Pathology research international* 2011, p. 374286. DOI: 10.4061/2011/374286.

Szatmári, Tünde; Lumniczky, Katalin; Désaknai, Szilvia; Trajcevski, Stéphane; Hídvégi, Egon J.; Hamada, Hirofumi; Sáfrány, Géza (2006): Detailed characterization of the mouse glioma 261 tumor model for experimental glioblastoma therapy. In *Cancer science* 97 (6), pp. 546–553. DOI: 10.1111/j.1349-7006.2006.00208.x.

Tahara, Maino; Takishima, Yuto; Miyamoto, Shohei; Nakatsu, Yuichiro; Someya, Kenji; Sato, Moritoshi et al. (2019): Photocontrollable mononegaviruses. In *Proceedings of the National Academy of Sciences of the United States of America* 116 (24), pp. 11587–11589. DOI: 10.1073/pnas.1906531116.

Tanaka, Motofumi; Nagano-Fujii, Motoko; Deng, Lin; Ishido, Satoshi; Sada, Kiyonao; Hotta, Hak (2006): Single-point mutations of hepatitis C virus NS3 that impair p53 interaction and anti-apoptotic activity of NS3. In *Biochemical and biophysical research communications* 340 (3), pp. 792–799. DOI: 10.1016/j.bbrc.2005.12.076.

Tang, Daolin; Kang, Rui; Berghe, Tom Vanden; Vandenabeele, Peter; Kroemer, Guido (2019): The molecular machinery of regulated cell death. In *Cell research* 29 (5), pp. 347–364. DOI: 10.1038/s41422-019-0164-5.

Taylor, Emma; Del Rio Vilas, Victor; Scott, Terence; Coetzer, Andre; Prada, Joaquin M.; Alireza, Gholami et al. (2021): Rabies in the Middle East, Eastern Europe, Central Asia and North Africa: Building evidence and delivering a regional approach to rabies elimination. In *Journal of infection and public health* 14 (6), pp. 787–794. DOI: 10.1016/j.jiph.2021.02.009.

Tilgase, Andra; Patetko, Liene; Blāķe, Ilze; Ramata-Stunda, Anna; Boroduškis, Mārtiņš; Alberts, Pēteris (2018): Effect of the oncolytic ECHO-7 virus Rigvir® on the viability of cell lines of human origin in vitro. In *Journal of Cancer* 9 (6), pp. 1033–1049. DOI: 10.7150/jca.23242.

Tourneur, Léa; Chiocchia, Gilles (2010): FADD: a regulator of life and death. In *Trends in immunology* 31 (7), pp. 260–269. DOI: 10.1016/j.it.2010.05.005.

Twiddy, Davina; Cain, Kelvin (2007): Caspase-9 cleavage, do you need it? In *The Biochemical journal* 405 (1), e1-2. DOI: 10.1042/BJ20070617.

Ugolini, G. (1995): Specificity of rabies virus as a transneuronal tracer of motor networks: transfer from hypoglossal motoneurons to connected second-order and higher order central nervous system cell groups. In *The Journal of comparative neurology* 356 (3), pp. 457–480. DOI: 10.1002/cne.903560312.

Ugolini, Gabriella (2011): Rabies virus as a transneuronal tracer of neuronal connections. In *Advances in virus research* 79, pp. 165–202. DOI: 10.1016/b978-0-12-387040-7.00010-x.

Vanden Berghe, T.; Vanlangenakker, N.; Parthoens, E.; Deckers, W.; Devos, M.; Festjens, N. et al. (2010): Necroptosis, necrosis and secondary necrosis converge on similar cellular disintegration features. In *Cell death and differentiation* 17 (6), pp. 922–930. DOI: 10.1038/cdd.2009.184.

Velasco-Villa, Andres; Mauldin, Matthew R.; Shi, Mang; Escobar, Luis E.; Gallardo-Romero, Nadia F.; Damon, Inger et al. (2017): The history of rabies in the Western Hemisphere. In *Antiviral research* 146, pp. 221–232. DOI: 10.1016/j.antiviral.2017.03.013.

Ventura, Gustavo Tavares; Da Costa, Emmerson Corrêa Brasil; Capaccia, Anne Miranda; Mohana-Borges, Ronaldo (2014): pH-dependent conformational changes in the HCV NS3 protein modulate its ATPase and helicase activities. In *PloS one* 9 (12), e115941. DOI: 10.1371/journal.pone.0115941.

Vora, Neil M.; Basavaraju, Sridhar V.; Feldman, Katherine A.; Paddock, Christopher D.; Orciari, Lillian; Gitterman, Steven et al. (2013): Raccoon rabies virus variant transmission through solid organ transplantation. In *JAMA* 310 (4), pp. 398–407. DOI: 10.1001/jama.2013.7986.

Vos, A.; Neubert, A.; Aylan, O.; Schuster, P.; Pommerening, E.; Müller, T.; Chivatsi, D. C. (1999): An update on safety studies of SAD B19 rabies virus vaccine in target and non-target species. In *Epidemiology and infection* 123 (1), pp. 165–175. DOI: 10.1017/s0950268899002666.

Wachowius, M. (2016): The Rabies Virus Phosphoprotein: Novel Targets and Functions Involved in Interferon Antagonism. In *Dissertation*.

Wang, J.; Chun, H. J.; Wong, W.; Spencer, D. M.; Lenardo, M. J. (2001): Caspase-10 is an initiator caspase in death receptor signaling. In *Proceedings of the National Academy of Sciences of the United States of America* 98 (24), pp. 13884–13888. DOI: 10.1073/pnas.241358198.

Wang, Jiadong; Tong, Wenyan; Zhang, Xiaonan; Chen, Li; Yi, Zhigang; Pan, Tingting et al. (2006): Hepatitis C virus non-structural protein NS5A interacts with FKBP38 and inhibits apoptosis in Huh7 hepatoma cells. In *FEBS letters* 580 (18), pp. 4392–4400. DOI: 10.1016/j.febslet.2006.07.002.

Wang, Jinliang; Wang, Zilong; Liu, Renqiang; Shuai, Lei; Wang, Xinxin; Luo, Jie et al. (2018): Metabotropic glutamate receptor subtype 2 is a cellular receptor for rabies virus. In *PLoS pathogens* 14 (7), e1007189. DOI: 10.1371/journal.ppat.1007189.

Weitzman, Jonathan B. (2001): p16Ink4a and p19Arf: terrible twins. In *Trends in Molecular Medicine* 7 (11), p. 489. DOI: 10.1016/s1471-4914(01)02190-6.

Wessels, Hans-Hermann; Méndez-Mancilla, Alejandro; Guo, Xinyi; Legut, Mateusz; Daniloski, Zharko; Sanjana, Neville E. (2020): Massively parallel Cas13 screens reveal principles for guide RNA design. In *Nature biotechnology* 38 (6), pp. 722–727. DOI: 10.1038/s41587-020-0456-9.

Westphal, Dana; Dewson, Grant; Czabotar, Peter E.; Kluck, Ruth M. (2011): Molecular biology of Bax and Bak activation and action. In *Biochimica et biophysica acta* 1813 (4), pp. 521–531. DOI: 10.1016/j.bbamcr.2010.12.019.

Whelan, S. P. J.; Barr, J. N.; Wertz, G. W. (2004): Transcription and replication of nonsegmented negative-strand RNA viruses. In *Current topics in microbiology and immunology* 283, pp. 61–119. DOI: 10.1007/978-3-662-06099-5_3.

WHO (2018): Zero by 30: the global strategic plan to end human deaths from dog-mediated rabies by 2030.

WHO (2020): Ending the neglect to attain the Sustainable Development Goals: a road map for neglected tropical diseases 2021–2030.

WHO (2021): Fact Sheet.

Wichapong, Kanin; Pianwanit, Somsak; Sippl, Wolfgang; Kokpol, Sirirat (2010): Homology modeling and molecular dynamics simulations of Dengue virus NS2B/NS3 protease: insight into molecular interaction. In *Journal of molecular recognition : JMR* 23 (3), pp. 283–300. DOI: 10.1002/jmr.977.

Wickersham, Ian R.; Finke, Stefan; Conzelmann, Karl-Klaus; Callaway, Edward M. (2007a): Retrograde neuronal tracing with a deletion-mutant rabies virus. In *Nature methods* 4 (1), pp. 47–49. DOI: 10.1038/nmeth999.

Wickersham, Ian R.; Lyon, David C.; Barnard, Richard J. O.; Mori, Takuma; Finke, Stefan; Conzelmann, Karl-Klaus et al. (2007b): Monosynaptic restriction of transsynaptic tracing from single, genetically targeted neurons. In *Neuron* 53 (5), pp. 639–647. DOI: 10.1016/j.neuron.2007.01.033.

Willoughby, Rodney E. (2012): Rabies Virus, 1145-1149.e2. DOI: 10.1016/B978-1-4377-2702-9.00230-0.

Willoughby, Rodney E.; Tieves, Kelly S.; Hoffman, George M.; Ghanayem, Nancy S.; Amlie-Lefond, Catherine M.; Schwabe, Michael J. et al. (2005): Survival after treatment of rabies with induction of coma. In *The New England journal of medicine* 352 (24), pp. 2508–2514. DOI: 10.1056/NEJMoa050382.

Wilson, Ross C.; Doudna, Jennifer A. (2013): Molecular mechanisms of RNA interference. In *Annual review of biophysics* 42, pp. 217–239. DOI: 10.1146/annurev-biophys-083012-130404.

Wiltzer, Linda; Okada, Kazuma; Yamaoka, Satoko; Larrous, Florence; Kuusisto, Henna Veera; Sugiyama, Makoto et al. (2014): Interaction of rabies virus P-protein with STAT proteins is critical to lethal rabies disease. In *The Journal of infectious diseases* 209 (11), pp. 1744–1753. DOI: 10.1093/infdis/jit829.

Wu, Hao; Lo, Yu-Chih (2009): Structures, Domains and Functions in Cell Death (DD, DED, CARD, PYD). In *Encyclopedia of Life Sciences*. DOI: 10.1002/9780470015902.a0021579.

Wu, X.; Molinaro, C.; Johnson, N.; Casiano, C. A. (2001): Secondary necrosis is a source of proteolytically modified forms of specific intracellular autoantigens: implications for systemic autoimmunity. In *Arthritis and rheumatism* 44 (11), pp. 2642–2652. DOI: 10.1002/1529-0131(200111)44:11<2642::aid-art444>3.0.co;2-8.

Wu, Youjun; Yang, Lu; Chang, Tammy; Kandeel, Fouad; Yee, Jiing-Kuan (2020): A Small Molecule-Controlled Cas9 Repressible System. In *Molecular therapy. Nucleic acids* 19, pp. 922–932. DOI: 10.1016/j.omtn.2019.12.026.

Wunner, William H.; Conzelmann, Karl-Klaus (2013): Rabies Virus, pp. 17–60. DOI: 10.1016/B978-0-12-396547-9.00002-X.

Xu, Cheng; Gamil, Amr A. A.; Munang'andu, Hetron Mweemba; Evensen, Øystein (2018): Apoptosis Induction by dsRNA-Dependent Protein Kinase R (PKR) in EPC Cells via Caspase 8 and 9 Pathways. In *Viruses* 10 (10). DOI: 10.3390/v10100526.

Xue, Weiwei; Yang, Ying; Wang, Xiaoting; Liu, Huanxiang; Yao, Xiaojun (2014): Computational study on the inhibitor binding mode and allosteric regulation mechanism in hepatitis C virus NS3/4A protein. In *PloS one* 9 (2), e87077. DOI: 10.1371/journal.pone.0087077.

Yan, Ge; Elbadawi, Mohamed; Efferth, Thomas (2020): Multiple cell death modalities and their key features (Review). In *World Acad Sci J*. DOI: 10.3892/wasj.2020.40.

Yiang, Giou-Teng; Chen, Yen-Hsieh; Chou, Pei-Lun; Chang, Wei-Jung; Wei, Chyou-Wei; Yu, Yung-Luen (2013): The NS3 protease and helicase domains of Japanese encephalitis virus trigger cell death via caspase-dependent and -independent pathways. In *Molecular medicine reports* 7 (3), pp. 826–830. DOI: 10.3892/mmr.2013.1261.

Yoneyama, M.; Suhara, W.; Fukuhara, Y.; Fukuda, M.; Nishida, E.; Fujita, T. (1998): Direct triggering of the type I interferon system by virus infection: activation of a transcription factor complex containing IRF-3 and CBP/p300. In *The EMBO journal* 17 (4), pp. 1087–1095. DOI: 10.1093/emboj/17.4.1087.

Zaragoza, Carlos; Saura, Marta; Padalko, Elizaveta Y.; Lopez-Rivera, Ester; Lizarbe, Tania R.; Lamas, Santiago; Lowenstein, Charles J. (2006): Viral protease cleavage of inhibitor of kappaBalpha triggers host cell apoptosis. In *Proceedings of the National Academy of Sciences of the United States of America* 103 (50), pp. 19051–19056. DOI: 10.1073/pnas.0606019103.

Zhang, Lidong; Zhu, Hongbo; Teraishi, Fuminori; Davis, John J.; Guo, Wei; Fan, Zhen; Fang, Bingliang (2005): Accelerated degradation of caspase-8 protein correlates with TRAIL resistance in a DLD1 human colon cancer cell line. In *Neoplasia (New York, N.Y.)* 7 (6), pp. 594–602. DOI: 10.1593/neo.04688.

Zhu, Shimao; Guo, Caiping (2016): Rabies Control and Treatment: From Prophylaxis to Strategies with Curative Potential. In *Viruses* 8 (11). DOI: 10.3390/v8110279.

Zhu, Wenliang; Zhang, Boya; Li, Mengqi; Mo, Fan; Mi, Tingwei; Wu, Yihui et al. (2019): Precisely controlling endogenous protein dosage in hPSCs and derivatives to model FOXG1 syndrome. In *Nature communications* 10 (1), p. 928. DOI: 10.1038/s41467-019-08841-7.Klicken oder tippen Sie hier, um Text einzugeben.

6 Appendix

6.1 List of Oligonucleotides

Table 22: List of Oligonucleotides.

VP-Nr.	Name	Sequence (5´- 3´)
1	032_f	caccgGCTCTTCCGAATTAATAGAC
2	032_r	aaacGCTCTTCCGAATTAATAGACc
3	033_f	caccgAGTCGTTGATTATCTTCAGC
4	033_r	aaacAGTCGTTGATTATCTTCAGCc
5	034_f	caccgTCCTTTGCGGAATGTAGTCC
6	034_r	aaacGGACTACATTCCGCAAAGGAc
7	Smash_BglII_R	ATATAGATCTTCAGTAGAGAACCTCCCTG
85	SacI_yfp_f	ATATgagctcGCCACCATGGTGAGCAAGGG
10	NS3_S139A_F	CTACTTGAAAGGCTCCGCCGGGGGTCCGCTGTTG
11	NS3_S139A_R	CAACAGCGGACCCCCGGCGGAGCCTTTCAAGTAG
12	SMASh_prot_stop_NheI_R	TATAGCTAGCTCAGTCCGTGAACACCGGGGAT
13	Smash_heli_stop_NheI_R	TATAGCTAGCTCACGTGACGACCTCCAGGTCG
14	035_f	caccgGGGGGTCCAAGATGTGGAGA
15	035_r	aaacTCTCCACATCTTGGACCCCCc
16	036_f	caccgGAGCAGCTCGCGCAGGAGCT
17	036_r	aaacAGCTCCTGCGCGAGCTGCTCc
	PKR_iluseq_R	TGACTGGAGTTCAGACGTGTGCTCTTCCGATCTACTCGTCATGTTAGCATTAGGTAT
	PKR_iluseq_F	ACACTCTTTCCCTACACGACGCTCTTCCGATCTGAAGAAGAAATGGCTGGTGATCT
	Casp8_032_iluseq_F	ACACTCTTTCCCTACACGACGCTCTTCCGATCTtcaaggatgccttgatgttattcc
	Casp8_032_iluseq_R	TGACTGGAGTTCAGACGTGTGCTCTTCCGATCTaatttcttaatctggctccggtgggacatct
18	037_f	caccgGTTCTGGGGCCAAGTAGCCC
19	037_r	aaacGGGCTACTTGGCCCCAGAACc
20	038_f	caccgGCTCCTGGGCGTCATCATAG
21	038_r	aaacCTATGATGACGCCCAGGAGCc
	FADD_iluseq_F	ACACTCTTTCCCTACACGACGCTCTTCCGATCTaagcgcaagctggagcgcgtgcaga
	FADD_iluseq_R	TGACTGGAGTTCAGACGTGTGCTCTTCCGATCTactgaatgctagtattactctcagac
	Casp10_iluseq_F	ACACTCTTTCCCTACACGACGCTCTTCCGATCTgctggccatgaaatctcaaggtcaa
	Casp10_iluseq_R	TGACTGGAGTTCAGACGTGTGCTCTTCCGATCTctgccacactgaggtgggcttcact
22	SMASh-prot-NS4A_R	GCACCCAGGTGCTGTCCGTGAACACCGGGGATCTCATGGTTGTCTCTAG

VP-Nr.	Name	Sequence (5´- 3´)
23	SMASh_prot-NS4A_F	GGTGTTCACGGACAGCACCTGGGTGCTCGTTGGCGGCGTCCTGGCTG
24	SMASh-NS4A-PEST_R	gggaagccatgGTAGAGAACCTCCCTGTCAGGTATAATTG
25	SMASh-NS4A-PEST_F	GAGGTTCTCTACcatggcttcccgccggcggtggc
26	PEST-stop_NheI_R	TATAGCTAGCTCAgtgacggtccatcccgctctcctgg
27	TautzNS3aa180-PEST_F	agacactcgacgttgttacaaggcatggcttcccgccggcggtg
28	Tautz-NS3aa213-PEST_F	tggcagtggaaagagcaccaagcatggcttcccgccggcggtg
29	Tautz-NS3aa213-PEST_R	caccgccggcgggaagccatgcttggtgctctttccactgcca
30	TautzNS3aa180-PEST-R	caccgccggcgggaagccatgccttgtaacaacgtcgagtgtct
31	YFP-TautzNS4Aaa21_F	GCTCCGGATCCGGCACTAGTggatgcgtttccatcatcgg
32	YFP-TautzNS4Aaa21_R	ccgatgatggaaacgcatccACTAGTGCCGGATCCGGAGC
33	SMASh-prot-NS4A-21-R	GACCACGCAGCCGTCCGTGAACACCGGGGATCTCATGGTTGTCTCTAG
34	SMASh-prot-NS4A-21_F	GGTGTTCACGGACGGCTGCGTGGTCATAGTGGGCAGGATC
	Casp8_034_iluseq_F	ACACTCTTTCCCTACACGACGCTCTTCCGATCTgccttttaaaaagatggacttca
	Casp8_034_iluseq_R	TGACTGGAGTTCAGACGTGTGCTCTTCCGATCTtagaattgtggcactgctgggt
	Casp8_033_iluseq_F	ACACTCTTTCCCTACACGACGCTCTTCCGATCTggatattttcatagagatggaga
	Casp8_033_iluseq_R	TGACTGGAGTTCAGACGTGTGCTCTTCCGATCTagaaaaagtagagcaggcacgtta
35	PEST-stop_NheI_R2	TATAGCTAGCTCAgtgacggtccatcccgctctcctgggcacaagacatgggcagcgtgccatcatcctgcgccgccaccgccggcgggaagccatg
36	SMASh-prot-NS4A-21_F2	CAACCATGAGATCCCCGGTGTTCACGGACGGCTGCGTGGTCATAGTGGGCAGG
37	SMASh-prot-NS4A-21-R2	CCTGCCCACTATGACCACGCAGCCGTCCGTGAACACCGGGGATCTCATGGTTG
38	SMASh-NS4A-PEST_F2	ATTATACCTGACAGGGAGGTTCTCTACcatggcttcccgccggcggtggc
39	SMASh-NS4A-PEST_R2	gccaccgccggcgggaagccatgGTAGAGAACCTCCCTGTCAGGTATAAT
40	SMASh_prot-NS4A_F2	TGAGATCCCCGGTGTTCACGGACAGCACCTGGGTGCTCGTTGGCGGCGTCCTGGCTG

VP-Nr.	Name	Sequence (5´- 3´)
41	SMASh_prot-NS4A_R2	CAGCCAGGACGCCGCCAACGAGCACCCAGGTGCTGTCCGTGAACACCGGGGATCTCA
42	041_f	caccgGACTGCTGCCCACCCGACAA
43	042_f	caccgTCTTCTGCCGTATGATATAG
44	043_f	caccgGTAGACCTCCCTAAGTTTCC
45	041_r	aaacTTGTCGGGTGGGCAGCAGTCc
46	042_r	aaacCTATATCATACGGCAGAAGAc
47	043_r	aaacGGAAACTTAGGGAGGTCTACc
55	BstBI_Nsmash_F	atatTTCGAAttgccaccATGGAGCCCGGGCCCATGGATTAC
58	mP-NcoI_R	tataCATGGTTGGGCGATTTTCCATCATCCAGG
59	ClaI-NS3heli_F	tataATCGATACCAAATACATCATGACA
60	P-aa150_R	TGTTGTCTCCTTCTTGAGCTCTC
61	N-aa285_F	TATCTGGGAGAGGAATTCTTCGG
62	N/P-border-NSMASh-F	CTCCTTTCGAACCATCCCAAACatggagcccgggcccatggattac
63	N/P-border-NSMASh-R	gtaatccatgggcccgggctccatGTTTGGGATGGTTCGAAAGGAG
64	Pend_C-SMASh_F	CTTGAATCGCTATACATCTTGCGATGAGATGGAAGAGTGCTCTCA
65	C-PEST_stop_P3UTR_xbaI_R	TTGTCTAGAGGGACTGAGGGGAGAGGTTCGGTCAgtgacggtccatcccgctctcct
66	Pend_C-SMASh_R	TGAGAGCACTCTTCCATCTCATCGCAAGATGTATAGCGATTCAAG
67	PEST-stop-NotI-R	TATAGCGGCCGCTCAgtgacggtccatcccgctctcctgg
68	Sac1_mCherry_f	TATAgagctcGCCACCATGgtgagcaagggcgaggaggat
69	PEST_stop_NheI_r	TATAGCTAGCtcacacattgatcctagcaga
70	N-P-seq-F	AAAATGCTTTATTTGTGAA
71	N-P-seq-R	ATTATGCCCAGTACATGACCTT
73	C-PEST_stop_N3utr_bstBI_R	ATGGTTCGAAAGGAGGGGTGTTAGTTTTTTTCATGATGGATATACACAATCCGTAGATTTCCGGCATTTTGTTATTCAACTTCTCAgtgacggtccatcccgctctcct
74	Nend_nostop_C-SMASh_F	CAAGACATATTCGAGTGACTCAGATGAGATGGAAGAGTGCTCTCA
75	Nend_nostop_C-SMASh_R	TGAGAGCACTCTTCCATCTCATCTGAGTCACTCGAATATGTCTTG
76	mCherry-R	TTGGTCACCTTCAGCTTGG
77	SnaBI_N_R	ACATCTACGTAGGAGGTTCATTTTAT
78	N-aa54_F	ACGTACTGATGTAGAAGGGAATTG
79	N_aa295_F	AGGCTTGAGTGGGAAATCTCC
80	M_aa15_R	GGATTTTTGAGTGTCCTCGTCC
81	EcoRI_SMAShNterm_F	ATATGAATTCGCCACCATGgagcccgggcccatgga
82	P_stop_SphI_R	ATATGCATGCTTAGCAAGATGTATAGCGAT

VP-Nr.	Name	Sequence (5´- 3´)
83	PEST-stop_NheI_R	TATAGCTAGCTCAgtgacggtcca
88	NheI_cleave_F	ATATgctagcGCCACCATGGATGAGATGGAAGAGTGCT
89	NheI_ATG_Flag_F	ATATgctagcGCCACCATGGATTACAAGGATGACGACGATAAG
90	N/P-border_F	GGATTGTGTATATCCATCATGAA
96	SacI-ATG-Flag_F	ATATGAGCTcGCCACCATGgattacaaggatga
97	YFP-stop-BglII_R	tataAGATCTtcacttgtacagctcgtccatgccgagagtgat
98	HCV-NS3-P1640A_F	CTGACGCACGCAATCACCAA
99	HCV-NS3-P1640A_R	TTGGTGATTGCGTGCGTCAG
100	HCV-NS3-KIDT-AAAA_F	ACGCACCCAATCACCGCAGCCGCTGCCAAATACATCATGACATGCA
101	HCV-NS3-KIDT-AAAA_R	TGCATGTCATGATGTATTTGGCAGCGGCTGCGGTGATTGGGTGCGT
104	HCV-NS3-LTHP-AAHP_F	CAGCAGTCACCGCGGCGCACCCAATCACCAA
105	HCV-NS3-LTHP-AAHP_R	TTGGTGATTGGGTGCGCCGCGGTGACTGCTG
106	HCV-NS3-LTHP-LTAA-F	CAGCAGTCACCCTGACGGCCGCAATCACCAA
107	HCV-NS3-LTHP-LTAA_R	TTGGTGATTGCGGCCGTCAGGGTGACTGCTG
108	HCV-NS3-LTHP-LTAHP_F	CAGCAGTCACCCTGACGGCACACCCAATCACCAA
109	HCV-NS3-LTHP-LTAHP_R	TTGGTGATTGGGTGTGCCGTCAGGGTGACTGCTG
110	NheI-ATG-Flag_F	ATATGCTAGCGCCACCATGgattacaaggatga
111	YFP-stop_NotI_R	tataGCGGCCGCtcacttgtacagctcgtccatgccgagagtgat
112	HCV-NS3-LTHP-AAAA-F2	CACCAGCAGTCACCGCGGCGGCAGCAATCACCAAAATC
113	HCV-NS3-LTHP-AAAA-R2	GATTTTGGTGATTGCTGCCGCCGCGGTGACTGCTGGTG
114	Gend_seq_R	CTGGTCTCACCCCCACTCTTGTGTGATTCCCATGAA
115	Lend_seq_F	CGATCCTGGAGAGGTCTATGATGACCCTATTGACC
136	HCV-NS3-LTHP-AAAA-F_2	GAGAACCTAGAGACAACCATGAGATCCCCGGTGTTCACGGACAACTCCTCTCCACCAGCAGTCACCGCGGCGGCCGCAATCACCAAAATC
137	HCV-NS3-LTHP-AAHP_F2	GAGAACCTAGAGACAACCATGAGATCCCCGGTGTTCACGGACAACTCCTCTCCACCAGCAGTCACCGCGGCGCACCCAATCACCAA
138	HCV-NS3-P1640A_F2	GAGAACCTAGAGACAACCATGAGATCCCCGGTGTTCACGGACAACTCCTCTCCACCAGCAGTCACCCTGACGCACGCAATCACCAA
139	Nhe-YFP-F2	TAACACCCCTCCTTTCGGATCTGgctagcGCCACCATGGTGAGCAAGGGCGAGGA
140	SMASh_NotI_R2	AGCTAGGTCCGCGGTGGCGGCCgcTCAGTAGAGAACCTCCCTGTC

VP-Nr.	Name	Sequence (5´- 3´)
142	KS-primer_Seq_F	atcgataccgtcgacctcga
145	L_end_seq_F2	AGAGGATATCAGATCTAGATCA
146	M_end_seq2	TGTCAACTATGGTCTGAC

6.2 Abbreviations

Table 23:List of Abbreviations.

Abbreviation	Description
µM	micromolar
µm	Micrometers
AAV	Adeno-Associated virus
ANOVA	Analysis of Variance
APAF-1	Apoptotic Protease Activating Factor-1
ASLV	Avian Sarcoma leukosis virus
ASV	Asunaprevir
ATP	Adenosine Triphosphate
Bak	Bcl-2 homologous Antagonist/Killer
Bax	Bcl-2-like Protein 4
BBB	Blood–Brain Barrier
BCL-2	B-cell Lymphoma 2
BHK	Baby Hamster Kidney
Bid	BH3 Interacting Domain Death Agonist
CARD	Caspase Activation and Recruitment Domain
CASP10	Caspase-10
CASP3	Caspase-3
CASP8	Caspase-8
CASP9	Caspase-9
cDNA	copy DNA
CHOP	CCAAT-Enhancer-Binding Protein Homologos Protein
CIP	Calf Intestine Phosphatase
CIP	Calf Intestine Phosphatase
CNS	Central Nervous System
CRISPR	Clustered Regularly Interspaced Short Palindromic Repeats
DD	Death Domain
ddH$_2$O	Bidestilled Water
DED	Death Effector Domains
DISC	Death-inducing Signaling Complex
DMSO	Dimethyl Sulfoxide
DNA	Deoxyribonucleic Acid
DNV	Danoprevir

Abbreviation	Description
dsRNA	Double Stranded RNA
eGFP	enhanced Green Fluorescent Protein
eIF2α	Eukaryotic Initiation Factor-2α
ER	Endoplasmic Reticulum
FADD	Fas-associated Protein with Death Domain
ffu	Focus Forming Units
h	Hours
h. p. DNV	Hours Post DNV
h. p. i.	Hours Post Infection
HCV	Hepatitis C Virus
IFN	Interferon
IGR	Intergenic Region
ISG	Interferon-Stimulated Gene
kDa	kilo Dalton
KO	Knockout
LCMV	Lymphocytic choriomeningitis virus
LDH	Lactatdehydrogenase
MAVS	Mitochondrial antiviral-signaling protein
MeV	Measles virus
min	Minutes
ml	Milliliter
mM	millimolar
MOI	Multiplicity of Infection
MOM	Mitochondrial Outer Membrane
MOMP	Mitochondrial Outer Membrane Permeabilization
nAChR	Nicotinic Acetylcholine Receptor
NCAM	Neuronal Cell Adhesion Molecule
NF-κB	Nuclear Factor κB
NNSV	Non-segmented Negative Strand RNA Viruses
NS3	Non-Structural Protein 3
NS4	Non-Structural Protein 4
p75NTR	p75 Neurotrophin Receptor
PARP	Poly (ADP-ribose) Polymerase
PCR	Polymerase Chain Reaction
PEP	Post-Exposure Prophylaxis
PKR	Protein Kinase R
POI	Protein of Interest
Puma	P53 Upregulated Modulator of Apoptosis
RABV	Rabies virus
RIP	Receptor-interacting Protein

Abbreviation	Description
RIPK1	Receptor-Interacting Serine/Threonine-Protein Kinase 1
RNAi	RNA interference
RNP	Ribonucleoprotein
ROS	Reactive Oxygen Species
RT	Room Temperature
SAD	Street Alabama Dufferin
SDS	Sodium Dodecyl Aulfate
SDS-PAGE	Sodium Dodecyl Sulfate Polyacrylamide Gel Electrophoresis
sec	Seconds
SMASh	Small Molecule–Assisted Shutoff
TIS	Transcription Initiation Signal
TNF	Tumor Necrosis Factor
TRADD	Tumor Necrosis Factor Receptor type 1-associated Death Domain Protein
TRAF2	TNF Receptor Associated Factor 2
TRAIL	Tumor Necrosis Factor Related Apoptosis Inducing Ligand
tt	Terminator tag
TTP	Transcription Termination and Polyadenylation
TVA	Tumor Virus A
T-VEC	Talimogen Laherparepvec
wt	Wildtype
YFP	Yellow Fluorescent Protein

6.3   List of Figures

6.4   List of Tables

7 Curriculum vitae

EDUCATION

02/2017 – 06/2022	**Max von Pettenkofer-Institute, Virology/**
	Ludwig-Maximilians-Universität, Munich
	AG Conzelmann
	Doctoral thesis
	Conditionally cytotoxic and drug-controllable non-cytotoxic
	rabies viruses
10/2014 - 12/2016	**Ludwig-Maximilians-Universität, Munich**
	Biology; Master of Science (grade: 1.27)
10/2011 - 09/2014	**Ludwig-Maximilians-Universität, Munich**
	Biology; Bachelor of Science (grade: 2.32)

CONFERENCES

04/2019	**7th European Congress of Virology, Rotterdam, Netherlands**
	Oral presentation
03/2019	**29th Annual Meeting of the Society for Virology, Düsseldorf, Germany**
	Oral presentation

PUBLICATIONS

Hennrich AA, Sawatsky B, Santos-Mandujano R, Banda DH, Oberhuber M, Schopf A, **Pfaffinger V**., Wittwer K, Riedel C, Pfaller CK, Conzelmann KK. Safe and effective two-in-one replicon-and-VLP minispike vaccine for COVID-19: Protection of mice after a single immunization. PLoS Pathog. 2021 Apr 21;17(4):e1009064. doi: 10.1371/journal.ppat.1009064